Alma Mater Studiorum – Università di Bologna

DOTTORATO DI RICERCA IN

CHIMICA

Ciclo XXVII

Settore Concorsuale di afferenza: 03/D1

Settore Scientifico disciplinare: CHIM/08

Design and Synthesis of Naphthalene Diimides Based Small Molecules as Anticancer Agents: Targeting the Polyamine Transporter, G-quadruplex Structures and HDAC

Presentata da: Chiara Marchetti

Coordinatore Dottorato	**Relatore**
Prof. Aldo Roda	**Prof.ssa Anna Minarini**

Esame finale anno 2015

Contents

Preface

This PhD thesis has been carried out at the Department of Pharmacy and Biotechnology, Alma Mater Studiorum-University of Bologna (Italy), under the supervision of Prof. Anna Minarini.

The whole PhD thesis is devoted to the study of new naphthalene diimide derivatives for the treatment of cancer.

This thesis describes four main projects: the first project is focused on the development of naphthalene diimide-polyamine conjugates with the aim of obtaining a selective delivery to the cancer cells, while the second one concerns the development of new MTDLs acting also as epigenetic modulators. The third project regards the synthesis of naphthalene diimide macrocyclic derivatives targeting the quadruplex structures, and the fourth one the development of trisubstituted naphthalene diimides for the treatment of pancreatic cancer.

The thesis is organized in different chapters: the first chapter is a brief introduction about the physiopathological aspects and the current approaches for the treatment of cancer. Chapters 2, 3 and 4 describe the main targets involved in cancer that constitute the drug discovery basis for the design of the new synthesized molecules.

Chapter 5, 6, 7 and 8 contain the drug design approaches used in each project, the synthetic methods and the biological evaluation assays of the new synthesized compounds. Results and discussions section and experimental procedures are also reported.

I would like to thanks other researchers involved in the present investigation:

✓ Prof. Vincenzo Tumiatti and Dr. Andrea Milelli, Department for Life Quality Studies, University of Bologna;
✓ Prof. Michela Rosini and Dr. Elena Simoni, Department of Pharmacy and Biotechnology, University of Bologna:
✓ Prof. Stephen Neidle, Dr. Stephan Ohnmacht and Dr. Mekala Gunaratnam, School of Pharmacy, University College London;
✓ Prof. Stefano Alcaro and his group, Dipartimento di Scienze della Salute, "Magna Græcia" Catanzaro University;
✓ Prof. Heather Wallace and her group, Kosterlitz Centre for Therapeutics Division of Applied Medicine, University of Aberdeen;
✓ Prof. Claudia Sissi and her group, Dept. of Pharmaceutical Sciences, University of Padova.

In addition, I wish to thank MIUR (Rome) and University of Bologna for their financial support.

Abstract

Cancer is a multifactorial disease characterized by a very complex etiology and several biochemical targets have been recognized to play a fundamental role in its development. Basing on its complex nature, a promising therapeutic strategy could be based by the "Multi-Target-Directed Ligand" (MTDL) approach. This new strategy stands on the assumption that a single molecule could hit several targets responsible for the onset and/or progression of the pathology.

In particular, in cancer therapy, in the last years G-quadruplex structures and epigenetic enzymes have raised much interest as potential anticancer targets.

Several agents acting on DNA are clinically used, but the severe deriving side effects limit their therapeutic application. G-quadruplex structures are DNA secondary structures that are located in key zones of human genome, such as oncogene promoters and telomeres. Targeting quadruplex structures could allow obtaining an anticancer therapy more free from side effects.

On the other end, in the last years it has been proved that epigenetic modulation can control the expression of human genes, thus allowing the presence of different variants determining the disease. The epigenetic regulation of gene expressions plays a crucial role in carcinogenesis and, in particular, an abnormal expression of histone deacetylase enzymes (HDACs) are related to tumor onset and progression, making them attractive candidate targets for new anticancer drugs and therapies.

This thesis deals with the design and synthesis of new naphthalene diimide (NDI) derivatives endowed with anticancer activity, interacting with DNA together with other targets implicated in cancer development, such as HDACs.

It has been proved that NDI derivatives display anticancer properties as intercalators and G-quadruplex-binding ligands, leading to DNA damage, senescence and down-regulation of oncogene expression.

NDI-polyamine and NDI-polyamine-hydroxamic acid conjugates have been designed with the aim to provide potential MTDLs, in order to create molecules able simultaneously to interact with different targets involved in this pathology, specifically the G-quadruplex structures and HDAC, and to exploit the polyamine transport system to get selectively into cancer cells. The most active compound among the polyamine derivatives, displayed antiproliferative activity in submicromolar range, the ability to bind duplex and quadruplex DNA, to inhibit Taq polymerase and topoisomerase, while the most promising in the hydroxamic acid series proved to be able to selectively induce HDAC inhibition in cancer cells.

Macrocyclic NDIs have been designed with the aim to improve the quadruplex targeting profile of the disubstituted NDIs. These compounds proved the ability to induce a high and selective stabilization of the quadruplex structures, together with cytotoxic activities in the micromolar range.

Finally, trisubstituted NDIs have been developed as G-quadruplex-binders, potentially effective against pancreatic adenocarcinoma. In order to improve the cellular uptake of the tetrasubstituted lead compound, one of the substituents in the bay position has been removed. The most interesting compound, which was able to interact with a wide range of G-quadruplex structures, showed antiproliferative activity in the low nanomolar range mainly in pancreatic and cancer cell lines and was tested in an *in vivo* model of human pancreatic adenocarcinoma, presenting an improved biological profile in comparison with that of the lead compound.

In conclusion, all these studies may represent a promising starting point for the development of new interesting molecules useful for the treatment of cancer, underlining the versatility of the NDI scaffold.

Chapter 1. Introduction to cancer therapy

Cancer is a term used for diseases characterized by out of control cell-growth: the principal feature of cancer is the rapid creation of abnormal cells able to grow beyond their usual boundaries, invading adjoining parts of the body and spreading to other organs. Cancer can develop in different tissues of the body and can have different forms, so there are more than a hundred distinct types of cancer differing substantially in their behavior and response to treatments. The incidence of this disease is different within the different genders: skin cancer is the most common type of malignancy for both men and women, the second most common type in men is prostate cancer, while in women is breast cancer. Not all cancer forms lead to death: during the most recent 5 years for which there are data (2004-2008), overall cancer incidence rates declined slightly in men (by 0.6% per year) and were stable in women, while cancer death rates decreased by 1.8% per year in men and by 1.6% per year in women.[1] Despite that, the number of global cancer deaths is projected to increase of 45% from 2007 to 2030 (from 7.9 million to 11.5 million deaths), influenced in part by the increase in aging of the global population.
Cancer, by definition, is a disease of genes. Throughout people's lives, cells are growing, dividing and replacing themselves. Many genes produce proteins that are involved in controlling the processes of cell growth and division. An alteration (called mutation) of DNA can disrupt these genes and produce faulty proteins; in this case the cell becomes abnormal and loses its restraints on growth. The abnormal cell begins to divide uncontrollably and eventually forms a new growth known as a "tumor" or neoplasm (medical term for cancer meaning "new growth"). There are two different types of tumor:

- benign tumors, which can form in different part of the body but remain confined in the initial location. This type of tumors grows slowly and cannot invade other tissues.
- malignant tumors (also called cancers), which are able to spread in other part of the body different from the original site (the primary tumor) in order to give origin to a secondary tumor, or metastases. Malignant cells are much “nimbler” than non-malignant ones, they can pass more easily through smaller gaps, as well as apply a much greater force on their environment compared to other cells, and through bloodstream or lymphatic channels can reach other tissues. These secondary tumors may grow, invade and damage nearby tissues, and spread again; this is why whereas benign tumors can usually be removed surgically, the spread of malignant tumors to distant body sites frequently makes them resistant to such localized treatment.[2]

1.1 Cancer therapy

In order to decrease the mortality rate due to cancer, in the last years a lot of efforts were spent in the research of new therapies, searching for treatments able to remove all or as much of the tumor as possible and to prevent the recurrence or spread of the primary tumor. While devising a treatment plan for cancer, the likelihood of curing the cancer has to be weighed against the possible side effects caused by the treatment itself. If the cancer is very aggressive and a cure is not possible, then the treatment should be aimed at relieving the symptoms and controlling the cancer as long as possible. There are different type of cancer treatments, depending on the type and the localization of the disease, the presence of metastases, the age

and the health of the patient. The major types of treatment are: surgery, radiation, chemotherapy, immunotherapy, hormone therapy, and bone-marrow transplantation.

Among them, chemotherapy is the most common form of cancer treatment and involves the use of chemical entities capable to interfere with the cell division process, through the infliction of damages to DNA or proteins. After this treatment, cancer cells go through apoptosis (if the compound is cytotoxic) or stop their proliferation (if the compound is cytostatic). The majority of chemotherapeutic drugs can be classified into alkylating agents, antimetabolites, anthracyclines, plant alkaloids, topoisomerase inhibitors, and other antitumor agents. All of these drugs affect cell division or the synthesis and function of DNA in different ways. These treatments target any rapidly dividing cells and not necessarily just cancer cells, so chemotherapy brings a lot of side effects like nausea, vomiting, tiredness, pain and hair loss.

A novel approach in the chemotherapy field is the molecular targeted therapy. Molecular targeted therapy represents an attempt to achieve antitumor effects by selectively targeting the differences in the biological features between normal and cancer cells or between normal and cancer tissues, providing a broader therapeutic window with less toxicity. An ideal molecular targeted therapeutic treatment should satisfy the following three pre-requisites: the treatment should be directed at the target, the treatment itself should have an antitumor effect and the antitumor effect should be explicable in terms of modification of the target. Molecular-targeted agents now account for >70% of all anticancer agents currently under development. Further, the great majority of recent standard therapies for cancers of various organs include molecular-targeted therapies.[3] There are multiple types of targeted therapies available, including monoclonal antibodies, tyrosine kinase inhibitors, and antisense inhibitors of growth factor receptors. Some targeted therapies block specific enzymes and growth factor receptors involved in cancer cell proliferation. These drugs are sometimes called signal transduction inhibitors. For example, Erlotinib (Tarceva) is used in the treatment of non-small lung cell cancer and it is an epidermal growth factor receptor inhibitor (EGFRi)[4].

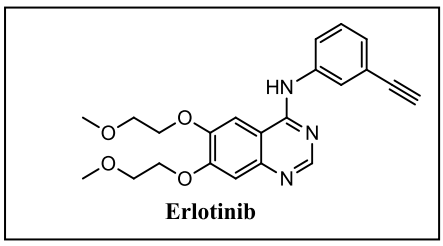

Erlotinib

A new approach for the treatment of diseases with complex etiology is the Multi-Target-Directed Ligand approach. Drug research was always addressed to the discovery of small molecules able to modulate the biological function of a single target (a protein or another macromolecule), thought to be fully responsible for a certain disease. The most important thing for a chemical entity to be developed as a drug was its selectivity towards a single target, and indeed, nowadays, many ligands endowed with outstanding *in vitro* selectivity are available. This paradigm is based on the assumption of the presence of a direct cause-effect relationship between the activity of a gene product and a particular phenotype. This one-molecule, one-target paradigm brought to the discovery of some important drugs, and it will probably remain the principal approach for drug discovery in some fields.[5] Drugs directed to single target might not always modify complex systems, even if they act in the way they are expected to proceed. It is very common in the cell to have ‘‘back-up’’ systems yielding the same effect such as gene expression, protein synthesis, receptors response, and protein degradation. Proteins and intermediates involved in these back-up systems can be completely different and therefore, drugs targeting primary pathways will have no effect over those back-up pathways, an effect known as redundancy.[6] Complex disorders, such as cancer, cardiovascular disease, depression, and neurodegenerative diseases, arise from multiple molecular abnormalities and not from a single defect, so the use of target-directed drugs may not ensure that the effect will modify the

evolution of the illness. There are alternative ways to overcome the limitation due to the use of a single drug.[7] It is possible to employ a multiple-medication therapy (MMT) (also referred to as a "cocktail" or "combination of drugs") that is made up of two or three different drugs that combine different therapeutic mechanisms. This approach may be limited by the lack of compliance and the adverse reactions due to the interaction between different drugs. A second approach might be the use of a multiple-compound medication (MCM) (also referred to as a "single-pill drug combination"), which implies the incorporation of different drugs into the same formulation in order to simplify dosing regimens and improve patient compliance. Nowadays, designing a single drug molecule able to simultaneously and specifically interact with multiple targets is gaining major consideration in drug discovery. This approach is usually referred to as "polypharmacology" or "Multi Target Directed Ligand" strategy to distinguish the approach from combination therapy in which two or more drugs are typically used in combination (Figure 1.1). It is by now generally recognized that several approved drugs elicit their therapeutic effect through complex polypharmacology.[8]

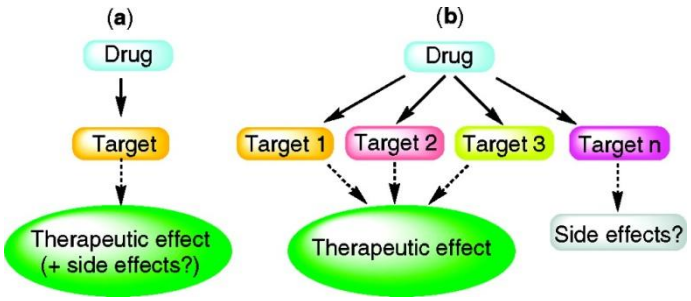

Figure 1.1. "One molecule, one target" paradigm *vs* MTDLs approach.[6]

This approach requires the use of a single chemical entity able to hit multiple targets; this therapy regimen provides a lot of advantages respect to the MMT or MCM strategies:

- a single drug displays a more simple and predictable pharmacokinetic and safety profile. Indeed, considering the complexity of the ADMET profile, an MMT/MCM approach might be untenable for some molecules;
- the combination of multiple entities can cause positive and negative synergistic effects, determining a limit in the use of some combinations;
- the insurgence of resistance is more probable towards separate molecular entities respect to a single one;
- the administration of a single compound guarantees the simultaneous presence of all the pharmacophoric groups in the tissue where the drug is supposed to work;
- a MTDL regimen, simpler that a MMT or MCM one, limits the risk of drug-drug interactions, simplifies the regimen itself and increases the compliance;
- further, in terms of pharmacokinetic and ADMET optimization, the clinical development of a drug able to hit multiple targets should not, in principle, be different from the development of any other single lead molecule.

According to that, the development of MTDLs may offer an appealing and cost-effective complement or an alternative strategy for the treatment of complex diseases such as

neurodegenerative disorders or cancer, for which an effective cure is an urgent need.[9] Nevertheless, very few, among designed MTDLs, reached the market. A problem in the drug discovery process of MTDLs is that the different pharmacophores that made up the singular entity have to act with a similar potency on different targets, moreover designing multi-target drugs can be challenging for medicinal chemists, with current lead-discovery strategies often producing large, complex molecules with low ligand efficiency and poor oral bioavailability.[10] Polypharmacology is mostly relevant for diseases involving wide target networks and cellular pathways, such as cancer. Cancer cells present a transformed phenotype that allows them to proliferate uncontrollably. This abnormal cellular activity is due to the deregulation in the expression or activity of different proteins that cause a modification of the normal survival pathways. In this scenario, protein kinases play a very important role: these proteins belong to a family of over 500 members in humans and are involved in multiple cellular pathways and networks. An example of MTDL as anticancer agent is the clinically used tyrosine kinase inhibitors Lapatinib, that was rationally designed as a MTDL targeting EGFR and ErbB2.[11, 12] It shows good selectivity for these two kinases from a panel of 317 enzymes of the same family, thus it can be considered a MTDL in the purest form of the definition.

1.2 Pancreatic adenocarcinoma

Pancreatic ductal adenocarcinoma is the most common type of pancreatic cancer and is the most lethal kind of cancer, with a 5-year survival rate of only 5% and a survival expectation of 6 months after the diagnosys.[13] Despite decades of efforts, actually, a cure does not exist and also the causes of the disease remain mostly unknown, with only cigarette smoking showing some evidence to be linked to the pathology. For smokers, the risk is about 2.5 times higher than for non-smokers and it is correlated with the use and the time of exposure.[14] Also the genetic factor plays an important role in the rise of the disease: individual with a pancreatic cancer family history have more probability to develop the tumor respect to people without affected family members.[15] Tackling this devastating cancer has been a major challenge to the scientific and medical communities, in part due to its intense therapeutic resistance.

The principal genetic mutations involved in the etiology happen in KRAS, BRCA2, PALB2, BRCA1, CDKN2A, TP53 and SMAD4 genes.[16] Studies have highlighted that these genetic lesions are at the base of the development of pancreatic cancer, but it is not known how these mutations exactly contribute to the cancer evolution.

Particularly, Kras mutations are found in advanced tumors and their presence is a hallmark of cancer progression. The activation of Kras oncogene, that is usually concomitant with the inactivation of the tumor suppressor gene CDKN2A, determines a wide range of cellular effects such as increasing levels of proliferation, survival and invasion through the activation of the autocrine EGFR signaling, that determines the stimulation of the phosphatidylinositol 3-kinase (PI3K) pathway.[17] The pancreatic tissue is also able to produce high levels of EGF family ligands and receptors.[18, 19] In pancreatic cancer, Kras is usually mutated at a specific residue (the G12 residue) and this modification can alter the interaction site with GAPs (GTPase activating proteins), and therefore mutant proteins are GTP hydrolysis impaired, resulting in a constitutively active (GTP-bound) form of Kras. Kras mutations drive many metabolic alterations in this type of cancer, endowing it with a unique metabolism that allows the uncontrolled growth. Ras is able to promote autophagy and macropinocytosis in cancer cells, that are essential for tumor development because the cells are more efficient in recycling and scavenging molecules to promote their own survival.[20, 21] Kras mutations appear to drive these mechanisms in the tumor, allowing tumor cells to adapt to environments where the

access to nutrients can be diminished. Kras is also able to increase the expression of the glucose transporter 1 (GLUT1), leading to increasing level of glucose and stimulating the anabolic glucose metabolism.[22]

Germline mutations in CDKN2A tumor-suppressor gene, BRCA2, PALB2 and BRCA1 are associated with the increasing risk of pancreatic carcinoma. The CDKN2A modification is able to determine a loss of p16 protein with concomitant increasing level of cell proliferation.[23]

The TP53 gene is responsible for the production of the p53 protein that controls the cellular responses to exogenous stimuli, such as DNA repair and apoptosis.[24] If this gene is compromised, the cell loses the ability to control the proliferation and is more likely to become a cancer cell.

Another important gene in the onset of pancreatic cancer is SMAD4 that encodes for a protein that participate in the transforming growth factor beta (TGFb) cell signaling pathway.[25]

The genetic modifications causing this type of cancer are well studied, but little is known about their implication in the biological features of the disease. The aggressive behavior of the pathology is probably due to the alteration at the oncogene and tumor-suppressor gene levels, as well to the increased production of growth receptors and their correlated factors. Together, these events allow the cell to escape from the growing control mechanisms.

Pancreatic cancer is classified using the American Joint Committee on Cancer (AJCC) system, which classifies the tumors based on their resectability. AJCC resectable stages are the stages I and II, while stage III is defined as borderline resectable. The advanced stage III and stage IV are defined unresectable. Stage I and II are usually treated with surgical resection and some therapy as help, resectable stage III tumors are treated with surgical resection after neoadjuvant therapy while unresectable stage III and stage IV neoplasms are treated with chemotherapy and are characterized by a low survival expectation.[26]

The principal agent used for the treatment of the disease is Gemcitabine, used alone or in combination with other chemotherapeutic agents. A lot of drugs were tested in combination with Gemcitabine, without any significant improvement except for Erlotinib,[27] an EGFR inhibitor, although this benefit is limited to the presence of the Kras mutation in the advanced cancer stages. Furthermore, the improved toxicity of the combination therapy has limited its use until now. Other possible combinations are 5-flurouracil (5-FU), Leucovorin, Irinotecan, and Oxaliplatin (a regimen referred to as Folfirinox) or the combination of Gemcitabine, Docetaxel and Capecitabine (a regimen referred to as GTX).

The increasing understanding of the molecular biology of pancreatic cancer can open a new landscape of possibilities for the treatment of the disease with some misregulated proteins in the disease, such as Kras and EGF, representing potential targets.

A common characteristic of almost all cancer cells is the up-regulation of hTERT, the catalytic component of the telomerase enzyme complex, contributing in this way to cell immortalization.

In order to evaluate the importance of the telomerase activity for pancreatic cancer, a study of the genomic status of patients with pancreatic adenocarcinoma has been done and has showed that telomerase expression is low in the early phase of the disease, while the protein is more expressed in the late phases, when the cancer is able to give metastasis.[28]

Telomerase is becoming a potential target for pancreatic cancer, and that has been confirmed by the use of antibodies targeting hTERT.[29]

Chapter 2. DNA as target: G-quadruplex structures

DNA is the molecular target for many of the drugs that are used in cancer therapy, and is viewed as a non-specific target for cytotoxic agents. Anticancer agents targeting this macromolecule are some of the most effective agents in clinical use and have produced significant increases in the survival rate of patients, especially when used in combination with drugs acting through different mechanisms. A large percentage of chemotherapeutic anticancer drugs are compounds that interact with DNA directly or prevent the proper relaxation of DNA (through the inhibition of topoisomerases). In addition, DNA-targeting anticancer drugs continue to be developed, as evidenced by the recent approval of belotecan.[30] Drugs active at the DNA level can be classified in four different groups:

- alkylating agents, highly electrophilic compounds which react with nucleophiles to form strong covalent bonds. There are several nucleophilic groups in DNA, in particular the 7-nitrogen of guanine. Drugs with two alkylating groups could therefore react with a guanine on each chain and cross-link the strands in order to prevent the unravelling during replication or transcription. Alternatively, the drug could link two guanine groups on the same chain, thus being attached like a limpet to the side of the DNA helix, masking a portion of DNA and blocking the access to the enzymes required for DNA function. Since alkylating agents are very reactive, they react with any good nucleophile and so they are not very selective; in fact they have the ability to alkylate proteins and other macromolecules as well as DNA. Eg, Mechlorethamine or Cisplatin;

- intercalating agents are compounds capable of slipping between the layers of nucleic acid base pairs and disrupting the shape of the double helix. This disruption prevents replication and transcription. Drugs exploiting this mechanism should be flat in order to fit between the base pairs, so they must be aromatic or heteroaromatic. Some drugs prefer to approach the helix via the major groove, whereas others prefer access via the minor groove. Several antibiotics such as the antitumor agents Actinomycin D and Adriamycin operate by intercalating into the DNA;

- antimetabolites are compounds able to interfere with DNA production and to stop cell division and the growth of tumors, these substances are often similar in structure to the metabolite they interfere with, such as the antifolates able to block with the synthesis of folic acid;

- drugs interacting with protein-DNA complexes, for example Topoisomerase I and II (Topo I and II) poisons, such as Etoposide.

2.1 DNA intercalation

DNA intercalation consists in the insertion of a small ligand or fragment between two adjacent base pairs in the DNA strand, forming stable sandwich-like structures. As a result, intercalation leads to significant perturbations to the DNA double helix, causing the opening of a space between base pairs and the unwinding of the helical twist (Fig. 2.1).[31]

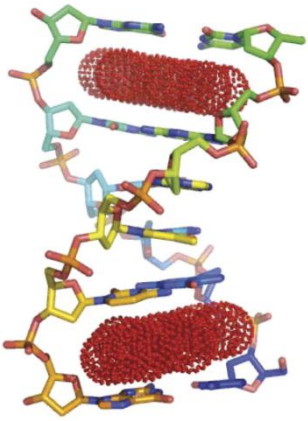

Figure 2.1 Mechanism of action of an intercalator.[32]

The changes in the DNA structure disturb the biological functions, such as transcription, replication and the DNA repair processes. DNA intercalators are mostly polycyclic, aromatic, and planar compounds, indeed their intercalation can be considered as a specific case of aromatic stacking interactions, where the dispersion of energy plays an important role.[33]

Intercalators can be divided into three main groups (Fig. 2.2): [32]

a) typical intercalators consisting of fused rings, e.g. 9-aminoacridine;[34,35]

b) atypical intercalators, containing non fused ring systems, e.g. Chlorpheniramine;

c) bis-intercalators, molecules consisting of two intercalating heterocyclic moieties usually linked together with an alkyl chain. Linker can be based on different structural motifs like a polyamine, which is capable to create multiple hydrogen bonds with the DNA structure, as in elinafide.

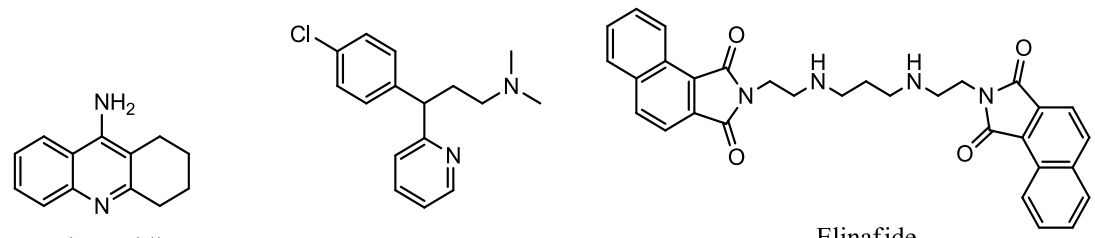

9- aminoacridine Chlorpheniramine Elinafide

Figure 2.2 Example of the different class of intercalating agents.

In the recent years, with the advent of new molecular targets such as kinases and cell surface receptors that can achieve selectivity for cancer cells, the interest in DNA-targeted drugs has decreased, even though they are still the mainstay of most treatment regimens.[36] The first glimpse of a new era for DNA-targeted therapeutics came through the realization that telomeres can form four-stranded DNA structures that are termed G-quadruplex.[37] Intramolecular G-quadruplex are very interesting due to their potential formation in telomeres

and oncogene promoter regions, so they have recently emerged as a new class of novel molecular targets for anticancer drugs.

2.2 G-quadruplex structures

G-quadruplexes are four-stranded DNA secondary structures that deviate from the normal duplex form of DNA and occur in guanine-rich DNA sequences. The basic element of a G-quadruplex is the G-quartet or G-tetrad, a substructure made up by four guanines connected by cyclic Hoogsteen hydrogen bonding (Fig.2.3).

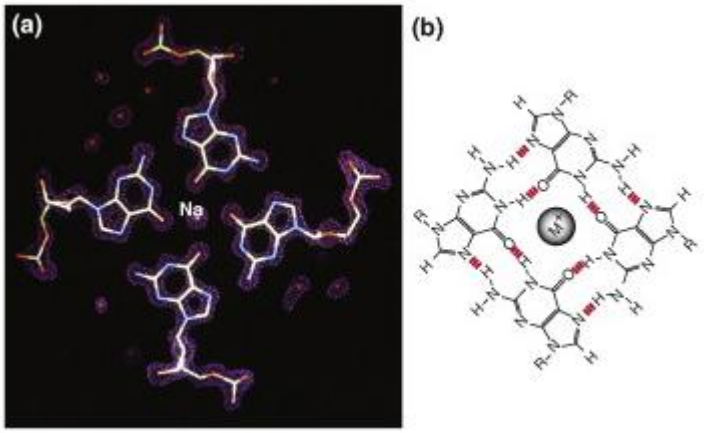

Figure 2.3. Structure of G-quartet, the basic unit of the G-quadruplex structures.[38]

The crystal structure of a G-quadruplex shows that the G-quartet can be considered as an aromatic square whose dimensions are much larger than those of the base pair of the Watson-Crick double DNA model and this difference constitutes the basis for the design of specific ligands.[39] G-quartets are stacked one above the other to form four propellers G-quadruplex. These structures have a wider diversity and structural polymorphism respect to the double helix DNA; this polymorphism deriving mostly from the nature of the cycle, such as variations in the stoichiometry of the chain, the polarity, the angle of twist of glycosides, and the position of the rings connecting the filament of guanine. Furthermore, in physiological conditions, the presence of metal ions, molecules that interact with the DNA or molecular crowding conditions, can affect the topology of the G-quadruplex. The G-quadruplex can be made up by a single sequence of guanine that forms intramolecular interactions or by intermolecular association of two (dimeric) or four (tetrameric) separated strands. Even the arrangement of the filament, depending on the different variations of polarity, can give rise to structural polymorphism. For example, the polarities of the four strands in a G-quadruplex can be parallel, three parallel and one antiparallel, adjacent parallel, alternating or antiparallel, resulting in different conformations denominated as parallel and antiparallel G-quadruplex. Adjacent linked parallel strands require a connecting loop to link the bottom G-tetrad with the top G-tetrad, leading to propeller type loops; in parallel quadruplexes all the guanines have glycosidic angles in an *anti* conformation. Quadruplexes are designated as anti-parallel when at least one of the four strands is anti-parallel to the others and in these structure it is possible to have lateral or edge-wise loops join adjacent G-strands or diagonal loop joins opposite G-

strands. Anti-parallel quadruplexes have both *syn* and *anti* guanines, arranged in a way that is particular for a given topology and for each different set of strand orientations, since different topologies have the four strands in differing positions relative to each other. Even the same sequence can assume different conformations depending on the environment (Fig. 2.4).[40]

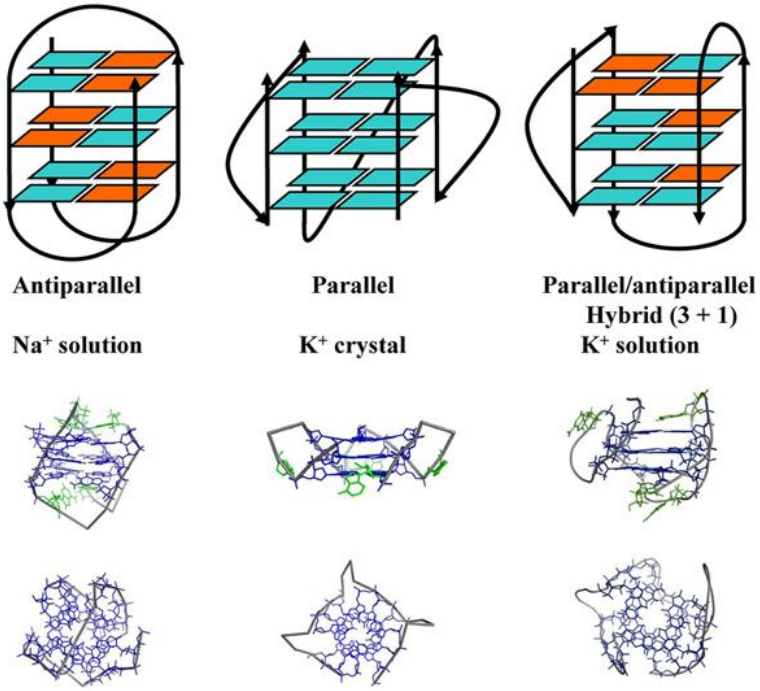

Figure 2.4. The structures observed for the intramolecular quadruplex formed by the human telomeric repeat sequence in different conditions: solution structure in Na^+, crystal structure in the presence of K^+ and solution structure in K^+.[41]

The sequence and the size of the rings play an important role in determining the topology of G-quadruplex. Moreover, the residues of the loop can give additional interactions, in fact they can form hydrogen bonds that can further stabilize (or destabilize) the structures and the folding of the G-quadruplex. A recent molecular dynamics simulation revealed that the sequences of the loops connecting the structures of the G-quadruplex represent the major contributors to the flexibility and may be potential binding sites for drugs.[26]

G-quadruplex structures can coordinate cations such as K^+ and Na^+. The cavity between the four G-tetrads is well suited to coordinating cations of these dimensions because the two floors of the tetrads are surrounded by eight oxygen atoms characterized by a strong negative electrostatic potential and these origin a center of negative charge within the channel of the two tetrads in which the positive ion is well fitted.[42]

The conformation of G-quadruplexes depends from all of these structural elements, as a consequence these secondary structures of DNA are characterized by a high degree of complexity. This complexity suggests that quadruplex might have a functional and regulatory significance for the cell, playing an important role in certain biological events, as many regulatory regions rich in guanine possess the potential to adopt the G-quadruplex conformation. The different possible G-quadruplex conformations provide numerous specific recognition sites for small molecules. As discussed above, it is evident that the area of the G-quartets, the loop regions, the size of the grooves, the negative electrostatic potential of the

anionic skeleton and the central channel, as well as the flexibility and dynamics of the structure itself are critical elements that must be considered in order to improve the selectivity of the binding of potential drugs. Following, will be argued localization and function of G-quadruplex structures in human DNA that give account of their importance as a target for the development of anticancer drugs.

2.3 G-quadruplex location and functions

The efforts spent for the structural characterization of G-quadruplexes are closely related to the fact that they are located in key regions of the human genome. These regions include the telomeres, regulatory elements as oncogene promoters, ribosomal DNA, minisatellites, the switch region for the immunoglobulin heavy chain and mutational hot spots.[43] The main role of G-quadruplex may be the ability to "turn on" or "off" some physiological events through the regulation of gene transcription or telomere length.

2.3.1 G-quadruplex in gene promoters

G-quadruplexes are present in oncogene promoter regions and, due to this localization, are viewed as emerging therapeutic targets in oncology, both as through the stabilization or the repression of oncogenes. Many G-quadruplex gene promoters have physicochemical properties and structural characteristics that make them druggable and their complexity may allow achieving selectivity, as a consequence G-quadruplexes can be important therapeutic targets. The structure of gene promoter sequences was studied and it was discovered that it contains a continuous stretch of a G-quadruplex sequence with four or more G-tracts folded into an intramolecular G-quadruplex, but other conformations are possible, such as bimolecular G-quadruplexes.[44, 45] G-quadruplex structures in gene promoters can be studied through NMR and crystallographic techniques, circular dichroism and chemical footprinting.[46] Quadruplex structures in promoters are constrained by the duplex nature of DNA so they have to compete with this most common structure; while the telomeric quadruplexes are easily formed because of the presence of the single-stranded DNA template at the 3′ end of human telomeres.

Intriguingly, bioinformatics show that the promoters of human oncogenes and regulatory genes (for example, transcription factors) are more likely than the average gene to contain quadruplex motifs, whereas these structures are less represented in the promoters of housekeeping and tumor suppressor genes.[48]

It is well known that supercoiling can influence the transcription either positively or negatively and quadruplex structures are considered a result of supercoiling induced stress during transcription, indeed their creation can compensate for the negative supercoiling.[49] These secondary structures of DNA can enhance or inhibit the transcription. The transcriptional event can be blocked if the quadruplex is on the template strand, blocking the access to polymerase; while it can be enhanced if the quadruplex is on the non-template strand, helping in this way the transcribed strand in a single strand conformation and facilitating the access to polymerase. Furthermore G-qudruplexes can bind proteins such as transcriptional enhancers or receptors, indirectly influencing the transcription (Fig. 2.5).[47]

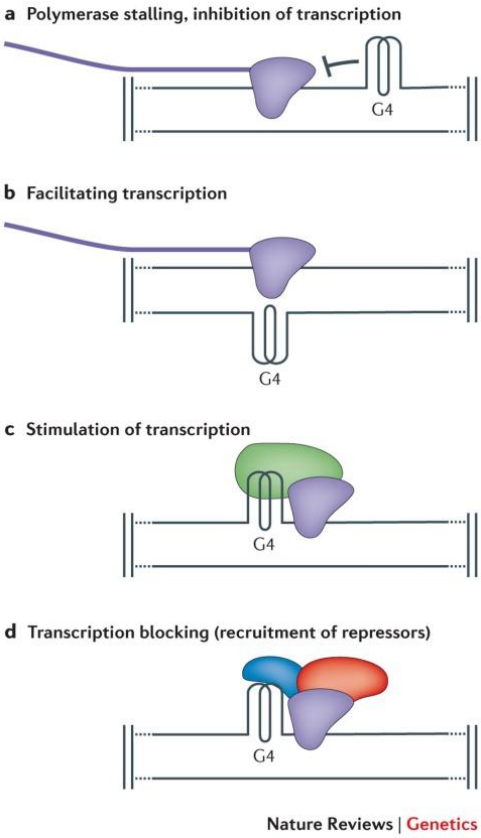

Figure 2.5. Putative functional roles of G-quadruplex structures during transcription. [47]

- *C-Myc*. C-Myc is a regulator gene that codes for a transcription factor. The finding that human cancers frequently display altered expression of human c-Myc underscores the importance of this gene in causing human cancers. Significant progress has been made over the last two decades in our understanding of the function of c-Myc in normal cells and in cancer cells. This gene is highly regulated in normal cells and it is only expressed when cells actively divide, while cancer cells may express the gene in an uncontrolled way as the result of genetic aberrations. It is now well-established that the deregulated expression of c-Myc plays a significant role in human cancer development, it is overexpressed in a wide variety of human cancers with 80% of breast cancers, 70% of colon cancer, 90% of gynecological cancers, 50% of hepatocellular carcinomas and a variety of hematological tumors.[50] The transcriptional regulation of c-Myc is mainly due to the nuclease hypersensitivity element (NHE)III1 of the c-Myc promoter that controls 85–90% of c-Myc transcription and has been the subject of considerable research over the past two decades.[51] The purine-rich strand of the NHEIII1 sequence is a guanine-rich segment and because of this feature it can fold into a G-quadruplex structure which is in equilibrium with the double strand DNA.[52] The protruding G-quadruplex structure and the I-motif formed on the opposite strand keep the two DNA strands separated and prevent the formation of the basal transcriptional complex. When this promoter region is in duplex form the transcription can be initiated.[53] Specific G-A mutations that decrease the number of guanines in this region destabilizing the quadruplex structure, are known to enhance the transcription of c-Myc.[54] Ligands able to stabilize the quadruplex form of the silencer element can decrease the oncogene overexpression and reduce its activity in the progress of the tumor, so a lot of efforts are spent in the research of c-Myc silencer element ligands.[55]

- *C-Kit*. The proto-oncogene c-Kit encodes for a 145-kDa transmembrane tyrosine kinase receptor (kit) that has the same structure of other tyrosine kinase receptors, and it is expressed in hematopoietic stem cells, mast cells, gametocytes and melanocytes; its overexpression can induce the development of cancer in these tissues; in particular it is a validated target in gastrointestinal stromal tumors (GIST).[56, 57] The kit protein has become a major molecular target of focus for GIST therapy, as exemplified by the multitarget kinase inhibitors Imatinib (Glivec/Gleevec; Novartis) and, more recently, Sunitinib (Sutent; Pfizer).[58] However, the onset of drug resistance makes it necessary to search a new approach for the treatment of this disease with a new generation of c-Kit inhibitors. It has been shown that the c-Kit promoter contains two G-quadruplex-forming sequences, positioned between -12 and -33 bp (c-kit1), and -64 and -83 bp (c-kit2).[59, 60] The development of new c-Kit inhibitors different from TKis able to act at the transcriptional level rather than at the protein level could offer a lot of therapeutic advantages.

- *KRAS*. KRAS gene encodes for the homonym protein that is a member of the small GTPase superfamily. The protein product of the normal KRAS gene performs an essential function in normal tissue signaling, and the mutation of KRAS gene that determines a single amino acid substitution is responsible for an activating mutation and is an essential step in the development of many cancers. The chronological order of the mutations is important in the impact of KRAS mutations in regard to colorectal cancer, with a primary KRAS mutation generally leading to a self-limiting hyperplastic or borderline lesion, but if occurring after a previous APC mutation, it often causes the progression to cancer.[61] KRAS mutation is a genetic biomarker that allows to predict the patient's response to a given treatment. KRAS test is the first genetic test that allows to determine, at the time of diagnosis, the normal or mutated state of the gene encoding the protein KRAS in patients with colorectal cancer, and can be predictable about the response to a treatment with EGFRi. KRAS promoter contains a nuclease hypersensitive element (NHE) with a polypurine–polypyrimidine motif able to form a G-quadruplex suspected to be involved in transcription regulation.[62] NHE, which is conserved both in human and mouse, is located upstream of the main transcription start site and controls most of the transcriptional activity of KRAS. The purine rich strand of the NHE forms a very stable G-quadruplex structure that is able to arrest DNA polymerase I in primer extension experiments. In the context of transcription, a G-quadruplex at NHE behaves as a repressor element. In fact, specific G-to-A or G-to-T mutations in the promoter abolishing the G-quadruplex structure result in an increase of the basal transcription activity, up to 4 times compared to the transcription of the wild type promoter. Moreover, the basal KRAS transcription in Panc-1 cells is strongly repressed when they are treated with TMPyP4, a cationic porphyrin that stabilizes G-quadruplex DNA, but not with TMPyP2 which does not bind to quadruplex DNA.

- *Bcl-2*. Bcl-2 is a gene that is aberrantly overexpressed in a wide range of tumors and plays an important role in the control of cell proliferation. Bcl-2 is also involved in the chemotherapeutic response of the ill tissues, in fact its inhibition has proved to enhance the effect of chemotherapeutic drugs, leading to a decrease in the proliferation rate.[63] Bcl-2 can be defined as a proto-oncogene, because it is not able to promote cell proliferation, but it explains its activity by reducing the rate of cell death. Its broad expression in a variety of tumors, together with its function in the resistance to chemotherapy-induced apoptosis, makes Bcl-2 a rational target for anticancer therapy.
Two main promoters are responsible for Bcl-2 expression: P1 is the major promoter and is a G-rich promoter located 1386−1423 base pairs upstream of the translation start site.[64] This

promoter is also preceded by a 39 bp G-rich sequence able to form quadruplex structures. This region can be found 57-19 bp upstream the promoter region and is constituted by six runs of 3-5 consecutive guanines, giving it the potential to assume 15 different intramolecular G-quadruplex structures by combining differently the guanine rich tracts. Studies have demonstrated that the main adopted conformation is the one in which the quadruplex is formed on the central four G-runs, because of its higher stability respect to the other possible conformations. That structure is a three tetrad mixed parallel/antiparallel G-quadruplex with three loops of 1, 7, and 3 nt.[65] More recent studies have also pointed out that the sequence can also assume another stable conformation, that is a parallel structure involving the four non successive G-runs I, II, IV and V. This structure contains also a 1nt loop and a 13nt loop. Parallel-stranded structures with two 1-nt loops and one variable-length middle loop are found to be prevalent in the G-quadruplex promoters; the length of the middle one can determine the overall structure and the potential ligand's recognition sites. The length of the middle loop is usually about 7 nt, the extraordinary 13 nt loop found in Bcl-2 suggests a different behaviour for this quadruplex structure. The presence of these two different folding quadruplexes in the Bcl-2 promoter is very interesting: both the structures could be important for the regulation. It is highly intriguing that both of them are able to regulate gene transcription, as different proteins preferably bind each G-quadruplex. Furthermore the two interchangeable G-quadruplexes can be separately targeted with small molecules, allowing us to modulate in different ways the gene transcription.[66]
Some well known G-quadruplex ligands, i.e. Telomestatin, TMPyP4 and Se2SAP (a synthetic, core-modified, expanded porphyrin) were used to test their ability to selectively target these different conformations of the G-rich sequence in the Bcl-2 promoter. While Telomestatin has not shown any selectivity, TMPyP4 and Se2SAP were able to selectively stabilize the parallel form and the mixed form respectively, demonstrating that is possible to target the different foldings of the sequence of the Bcl-2 promoter.[67] This possibility might help to reach different biological activities.

2.3.2 G-quadruplex and telomerase

Linear DNA fragments are toxic to mammalian cells so many mechanisms such as degradation or reparation of the fragments, cell cycle arrest or death are used to deal with them. The natural ends of linear chromosomes resemble DNA breaks and their repair would lead to deleterious chromosome fusions and therefore has to be avoided. This is prevented thanks to the presence of telomeres, specialized ribonuclein proteins able to cap both ends of the chromosome. Telomeres are made up of long, repetitive TTAGGG sequences which extend for 9-15 kb in humans, associated with a variety of telomere-binding proteins known as shelterins.[68] The repetitive and G-rich nature of telomeric DNA allows the ends of the chromosomes to form higher order DNA secondary structures, such as G-quadruplexes that can help to regulate the replication of cells.[69] The telomeres are fragile structure of DNA, in order to protect them the shelterin six proteins complex has evolved (Fig. 2.6). Three of its components bind in a sequence-specific manner to the TTAGGG repeats, specifically TRF1 and TRF2 bind the duplex repeat regions and POT1 binds the single-stranded overhangs.[70] The other proteins bind the first three component of the shelterin through protein-protein interactions: RAP1 binds TRF2, TPP1 binds POT1, and TIN2 binds TRF1, TRF2, and TPP1 simultaneously, thus playing an essential role in stabilizing the shelterin complex and linking the single- and double-stranded binding components of shelterin.[71] Each shelterin has a particular role in telomere maintenance. TRF1 and TRF2 are constitutively present at telomeres and their proportion norms the telomere length: TRF1 has DNA remodelling activity and promote the efficient replication of telomeres.[72] TRF2 primarily prevents end to

end telomere fusions and is associated with RAP1, which function is not well established.[73] POT1 contributes to telomere protection by binding single stranded telomeric DNA, it can displace the quadruplex structure in this site and "close" the end of the telomere. Its interaction with TPP1 is very important; in fact, this complex binds the single stranded DNA with a higher affinity compared to POT1 and TPP1 alone. Furthermore, an *in vitro* assay showed that the TPP1/POT1 complex enables the increasing in telomerase processivity.[74] Taken together, the shelterin complex, despite consisting of only six proteins, has an immensely complex role in telomere length regulation, protection from enzymatic attack and recruitment of required enzymatic activities, and in the control of signaling cascades from the natural chromosome ends.

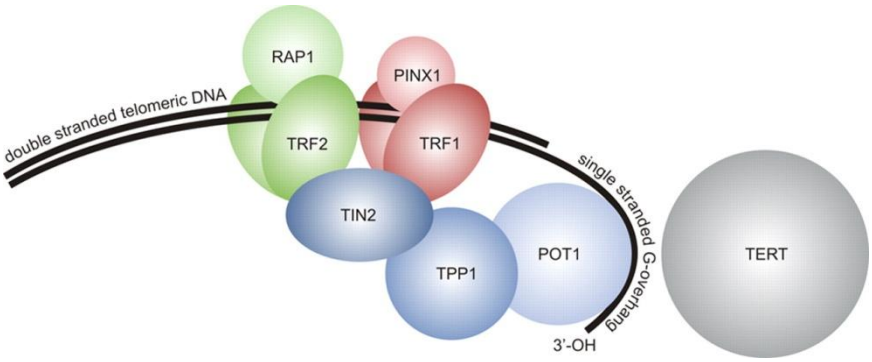

Figure 2.6. The shelterin complex.[75]

In addition to the shelterin complex, numerous other factors critically contribute to telomere integrity. The telomeric ribonucleoprotein complex (TeRRA) is a telomeric repeat-containing RNA, originated by the activity on the C-strand of RNA polymerase II and made up by UUAGGG containing transcripts.[76] TeRRA displays a strong inverse correlation with telomerase activity, acting as a potent telomerase inhibitor.[77]

In addition to avoiding the inappropriate reparation of single strand DNA, another function of telomeres is to prevent the loss of genetic information by providing a means for telomere-length maintenance in replicating cells. Telomere length is maintained thanks to the telomerase enzyme, a reverse transcriptase complex that uses a short segment of its RNA subunit as a template to direct the addition of telomeric repeats onto chromosome ends. In somatic cells every cell division causes a loss of 100-200 bp of telomeric sequence, and because these cells lack of a high telomerase activity, they enter in a phase called replicative senescence. After few replications, the telomere becomes critically short and the cell undergoes to apoptosis, a form of cell death. This mechanism allows to check the replicative lifespan of individual cells and probably of some cellular compartments in organisms and acts as a tumor suppressive pathway preventing cells from becoming immortal.[78] Telomerase is normally active in human stem/progenitor cells and germ-line cells, as well as in a subset of somatic cells (e.g., activated lymphocytes) but it is almost completely inactive in somatic cells.

The telomerase enzyme is a ribonucleoprotein functioning as a reverse transcriptase and is the main positive regulator of telomere length. The particular property distinguishing telomerase from different RNA-dependent DNA polymerases is the use of a fixed region of special telomerase RNA as template for telomere elongation. This enzyme consists of two main

components, a telomere RNA component (hTR) and a telomere reverse transcriptase (hTERT).[79]

The RNA component (hTR) of telomerase provides the template for the synthesis of the telomeric repeat, it derives from the activity of RNA polymerase II and is processed at its 3' end to produce a mature transcript of 451 nucleotides.[80] The template used by the enzyme for telomere elongation lies near the 5' end of the molecule (nucleotides 46 to 53) and contains the code of the telomeric DNA sequence. Despite divergences of the primary sequences among telomerase RNAs, hTR has a conserved secondary structure within telomerase RNAs from a variety of vertebrate species, indicating an important role for RNA structure in telomerase function. A number of RNA binding proteins, that are species-specific proteins such as hGAR, dyskerin, hNOP10, hNHP2, hStau, L22, hnRNP C1/C1, La, and hTERT bind hTR and are involved in hTR stability, maturation, accumulation and in the functional assembly of the telomerase ribonucleoprotein complex.[81]

The telomerase catalytic subunits (hTERT) are highly conserved in different species, but are very different than other reverse transcriptases and therefore form a distinct subgroup within the reverse transcriptase family.[82] hTERT is different from other reverse transcriptase because of some different features:

- all of the reverse transcriptase motifs are located in the C-terminal half of the proteins;
- a conserved telomerase-specific region, termed the T motif, is located just N-terminal to the reverse transcriptase motifs;
- a large N-terminal region contains conserved, functionally important domains.

HTERT is made up by three distinct domains: an N-terminal extension, the RT domain and a C-terminal extension (CTE) (Fig.2.7).

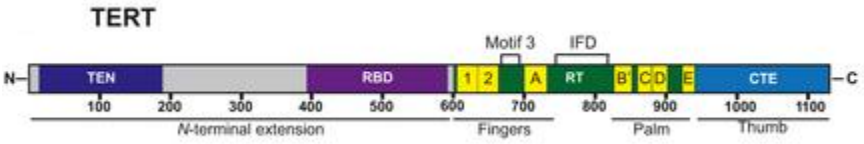

Figure 2.7. Structure of hTERT.[83]

The N-terminus of hTERT consists of 400 amino acids, and may be divided into two functionally important domains: the telomerase essential N-terminal domain (TEN) and the telomerase RNA-binding domain (TRBD). The TRBD domain is able to bind hTR thanks to its RNA recognition motif,[84] while the TEN domain ensures the maintenance of the binding with the single strand DNA during catalysis.[85] Furthermore the TEN domain contains a DAT (dissociates activities of telomerase) region that directs telomerase to the telomeric substrate in cells and allows the correct location of the enzyme on the telomeric DNA.[86] The RT domain of hTERT is the reverse transcriptase domain and is constituted by seven universally conserved RT motifs, whose mutations cause a complete loss of telomerase activity.[87] The RT domain is organized in two sub-domains, the 'fingers' which comprise motifs 1 to A, and the 'palm', comprising motifs B' to E.[64] The fingers domain interacts with the nucleic acid substrate, while the palm domain contains the catalytic site.[88] These two domains are linked with a 'primer grip' region, which is implicated in the binding with the single stranded DNA, the RT domain also contains another region called 'insertion in fingers' domain (IFD), which is not

present in other transcriptase and is important in the stabilization of protein-protein interactions.[89] The RT domain contains three critical amino acids that are critical for its polymerase activity: motifs A and C comprehend a conserved triad of aspartic acid residues.[90] The CTE region contains the "thumb" domain, not highly conserved among different species.[91] Telomerase, like all polymerase enzymes, use a two-metal mechanism to mediate the chemistry of nucleotide transfer and in the catalytic process an important role is accomplished by the Asp residues. There are essentially three catalysis steps in telomerase-mediated DNA synthesis: DNA binding and positioning, synthesis of the telomeric sequence to the end of the hTR template, and translocation and realignment of the catalytic site with the 3' end of the substrate (Fig. 2.8).

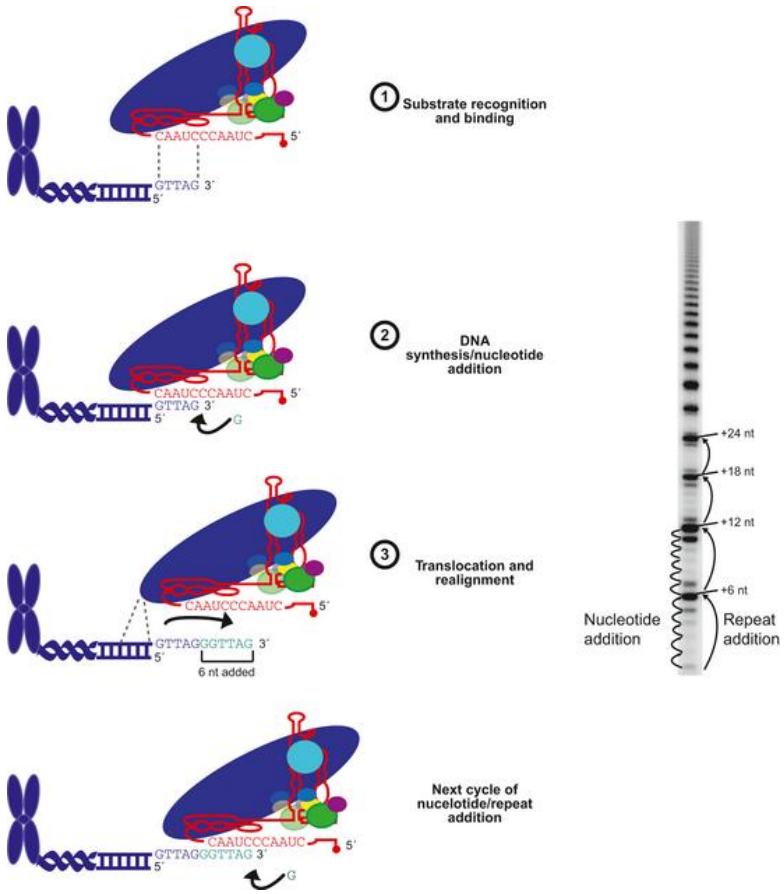

Figure 2.8. Telomere synthesis by telomerase.[92]

In this process, the TEN domain allows the correct binding of the DNA at the 5′ end of the substrate, while the "thumb" domain stabilizes the DNA/RNA hybrid, the "finger" and "palm" domains interact with the incoming deoxynucleotide triphosphates (dNTPs) and the correct position of 3' end in the active site is guaranteed by the E motif of the palm domain.[92] As telomerase catalyses the addition of consecutive dNTPs to the free 3′ OH of its primer substrate, a constant number of base-paired nucleotides are maintained between the template region of hTR and the primer substrate. This means that, as dNTPs are added at the 3′end, base-pair interactions at the 5′ end are disrupted. Telomerase adds dNTPs until the 5′ end within hTR is reached, after this event the translocation of the enzyme occurs with the repositions near a new 3′end in the catalytic site, and the cycle of nucleotide addition and

translocation resumes. The incorporation of individual dNTPs by telomerase is called nucleotide addition processivity (or type I processivity). After the synthesis of the first repeat, telomerase can move onto the DNA substrate and re-align hTR in order to do a second synthesis of the six-nucleotide repeat, or dissociate from the substrate completely. This second event is called repeat addition processivity (RAP, or type II processivity) and this feature is different for telomerase among other reverse transcriptase.[93]

In normal human cells, telomerase activity is highly regulated during development, and it is very low in somatic cells while is kept in some tissues, such as male germ cells, activated lymphocytes, and certain types of stem cell populations.[94] Probably the high replication rate of these kind of cells justifies a special need for telomerase activity in order to maintain telomere length and genetic stability.

Despite that, a lot of human diseases are linked to telomerase dysfunction: human dyskeratosis congenital is a multiple-systems disease resulting from proliferative deficiencies that affects tissues such as skin, gut, and bone marrow, all of which require constant renewal and are normally highly regenerative and it is due to mutations in either hTR or the telomerase RNA-associated protein dyskerin.[95]

In 1967 Hayflick & Moorhead discovered that cancer development is blocked by a natural mechanism, the replicative senescence and that every cell has a limited replication capacity.[96] This replicative capacity is linked to the age of the cells, thus indicating that every cell has a specific molecular mechanism able to limit its replicative life span. Particularly in somatic cells, every replication cycle is characterized by the loss of 100-200 bp at the telomere end and this process is unavoidable because of the lack of telomerase activity. Accordingly, after a defined number of replications (called Hayflick limit) the telomeres become critically short and the cell goes into replicative senescence, leading to activation of the apoptosis pathway. Replicative senescence is a way to avoid the immortalization and the onset of cancer.[78] On the other hand it was showed that fibroblasts in which hTERT is introduced are able to prevent cell death and become immortal.[97]

During normal human growth and development, telomerase activity is regulated to meet the proliferative demand of specific cellular functions while at the same time preserving proliferative barriers (senescence) against tumorigenesis. Telomerase is overexpress in 90% of tumor samples, demonstrating that telomerase activity is the cause for the escape of cells from the barriers to proliferation and for the immortalization of cells.[94] By telomere elongation, the enzyme allows the cells to avoid replicative senescence and provides an unlimited replicative potential; hence, its inhibition in cancer cells leads to apoptotic death through telomeres shortening.

Given its involvement in the onset of cancer, telomerase represents a compelling therapeutic target. Different strategies were studied in the past years to develop therapeutics against this target.

The first approach used was the direct inhibition of the enzyme. This method can allow to achieve selectivity: as normal cells do not have telomerase activity, this strategy can affect cancer cells without severely affecting normal ones. This approach however presents several potential issues. The use of a telomerase inhibitor can damage telomerase positive high-turnover cell populations, such as hematopoietic, bone marrow and stem cells.[98] A second problem is that cancer cells treated with telomerase inhibitor can escape treatment through the activation of other pathways, e.g. ALT pathway. In this case, the treatment inducing telomere dysfunction might cause genomic changes and enhance the tumor evolution and progression, analogous to what is proposed to occur during early tumor development. In addition telomerase direct inhibition may affect differently on different types of tumors; for example in tumors characterized by long telomeres there may be a significant delay from treatment onset

to the induction of tumor proliferative inhibition. The only telomerase inhibitor in clinical trials is GRN163L, called Imetelstat, that is a 13-mer oligonucleotide N3'→P5' thio-phosphoramidate lipid conjugate that is complementary to the template region of the human functional telomerase RNA (hTR) subunit. Imetelstat binds and blocks the active site of the enzyme acting as a competitive enzyme inhibitor.[99] This drug is currently undergoing under phase I/II clinical trials alone and in combination with Paclitaxel and Bevacizumab for the treatment of different cancers.[100] It was demonstrated that Imetelstat is able to remove cancer stem cells, that have a critical role in tumor progression and resistance, indicating that telomerase inhibitors could be very useful to treat this peculiar subset of cells.[101]

Another approach against telomerase is the use of RNA interference to deplete hTR and hTERT, this approach gives a rapid response both *in vitro* and *in vivo* suggesting that the depletion of the telomerase ribonucleoproteins may abrogate a telomere-independent function of telomerase, but this hypothesis has not yet been proven. The limit of this kind of therapy is that the delivery of inhibitory RNAs to cancer cells is difficult to achieve.[102]

Another possibility against telomerase is the use of Telomerase-Targeted Immunotherapy. Cancer immunotherapy consists in the use of the immune system to reject cancer. This can be obtained, either through immunization of the patient or through the administration of therapeutic antibodies as drugs, e.g. by administering a cancer vaccine. In the first case the patient's own immune system is trained to recognize tumor cells as targets to be destroyed, in the second case the patient's immune system is recruited to destroy tumor cells by the therapeutic antibodies. The principle limit to cancer immunotherapy is the heterogeneous expression of tumor antigen within a tumor and lack of antigens that can be widely used to target different tumors that is why telomerase that is highly expressed in many tumors, can be an optimal target for cancer immunotherapy. The most advanced TERT-directed vaccines are GemVax's GV1001 and Geron's GRNVAC1.[103,104]

One of the principal approach to telomerase inhibition was the use of (mostly backbone modified) antisense oligonucleotides that are complementary to the 11-base-pair RNA template sequence.[105] Under favorable circumstances, inhibition can be achieved at the nanomolar level.

An additional method to achieve telomerase inhibition is the use of G-quadruplex ligands. The telomerase enzyme complex requires the telomeric DNA primer to be in a single stranded form for the effective hybridization to the RNA template to occur. Recently it was showed that potassium ions, by inducing the formation of quadruplexes, are able to inhibit the enzime.[106] Given the G-rich nature of the telomeric sequence, folding the telomeric repeats at and close to the 3′ end into a higher-order DNA structure is a way to block the activity of the enzime.[107]

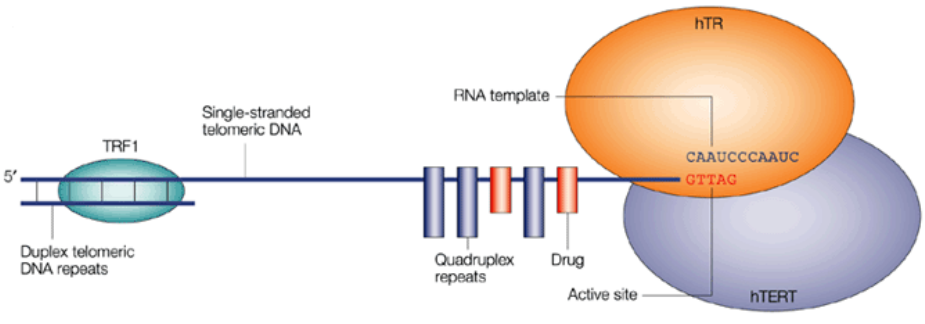

Figure 2.9. Telomerase inhibition being produced by folding of the end telomere primer strand into G-quadruplex units.[87]

Stabilization of G-quadruplexes at the single-stranded G-rich telomere overhang by G-quadruplex ligands can displace telomere-binding proteins, including POT1, and can inhibit telomere elongation by telomerase, thereby causing rapid tumor growth inhibition both *in vitro* and *in vivo*.
Furthermore, in this case lengthy telomere attrition is not necessarily a requirement for the onset of a biological response to quadruplex-binding ligands and this approach may be useful both in cells with short or long telomeres, though it was demonstrated that the shortest telomeres within a population are especially sensitive to these agents.[108] However, a problem arises by the lack of specificity of G-quadruplex ligands, given that G-quadruplex structures are also present at many other genomic loci such as gene promoters.

2.3.3 G-quadruplex ligands

According to what previously stated, stabilization of quadruplex structure that are able to interfere with oncogene expression and to block telomerase activity by small molecules is emerging as a potential anticancer approach.[109] The ligands can interact with G-quadruplex trough different binding mode: external stacking, intercalation, or groove binding (Fig. 2.10). However, the intercalation between G-tetrads inside the quadruplex is very difficult to achieve, since the G-quadruplex is an extremely stable and rigid structure, so the distortion of quadruplex integrity requires a very high energy cost.[110]

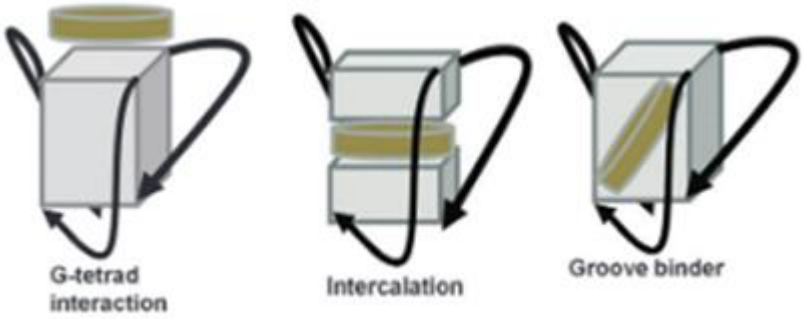

Figure 2.10. Representations of ligand-G-quadruplex possible binding modes.[111]

Although G-quadruplexes are characterized by a high polymorphism, in these structures some common features can be exploited to develop small molecules able to interact with them. One aspect common to all G-quadruplexes is the large planar surface of the terminal G-quartet, so the quadruplex-stabilization can occur through π- π interactions between the ligand and the external G-quartet. This binding mode (external stacking) has been thoroughly discussed since it allows to distinguish quadruplex structures compared to duplex DNA.[112] An efficient G-quadruplex ligand must have a large aromatic surface, much larger than a duplex binder to improve the aromatic-aromatic overlap and provide selectivity. Furthermore, the presence of cationic charges promotes the electrostatic interactions with the negatively charged biopolymer.
Another binding mode is the intercalation, widely studied for duplex DNA. The intercalators fit between two pairs of axially contiguous bases in a conformation generally perpendicular to the axis of the helix. The structural requirement for this type of interaction is a planar geometry. However, these features alone are not sufficient to ensure high affinity and selectivity. Affinity and greater selectivity can be achieved in several ways, for example by

restricting access to the terminal G-quartet as a result of a steric hindrance imposed on it by the loop, or by exploiting the possibility of additional interactions with the negative electrostatic potential of the central channel and anion skeleton of the grooves and loops.
Another chance to interact with the quadruplex structure is the groove binding mode.
In order to achieve selectivity in the design of quadruplex ligands is important to consider the differences in these structures, both in the sequences of the loops and in the characteristics of the grooves. Unfortunately, this approach has not yet been undertaken in a systematic manner, mainly for the insufficiency of solid structural information.
A lot of different classes of molecules have been developed that efficiently target G-quadruplex DNA and, among them, macrocycles rapidly became popular.[113, 114] They are particularly interesting for the interaction within G-quadruplex structures for two reasons: on one hand they show low affinity for DNA in duplex form, since for steric reasons have more difficulty to intercalate between base pairs, and on the other, in contrast, they adapt very well to stacking on the terminal G-quartet of the G-quadruplex that is a site accessible to large planar aromatic nuclei.

- *Antraquinone and fluorenone derivatives.* The first found G-quadruplex ligand able to inhibit telomerase was the 2,6-disubstituted amminoalchilamidoantrachinone BSU-1051, a symmetrical molecule possessing an IC_{50} of 23 μM towards telomerase (Fig. 2.11).[115] Later, in order to improve its activity, studies of structure-activity relationship (SAR) were performed for a wide range of antraquinones (AQ), obtaining the 1,4- 1,5- 1,8- 2,6- 2,7-disubstituted derivatives by modifying the substituents' position on the chromophore.[116, 117] The AQ-DNA complex has been studied by molecular modeling and has emerged that the overlap of the ligand on the G-quartet through external stacking is plausible and that any flexible side chain can be positioned in the wider groove. To reduce the cytotoxicity caused by the redox cycles, the quinone moiety has been removed and a series of 2,7-fluorenones (FO) was synthesized (Fig. 2.11).[118]

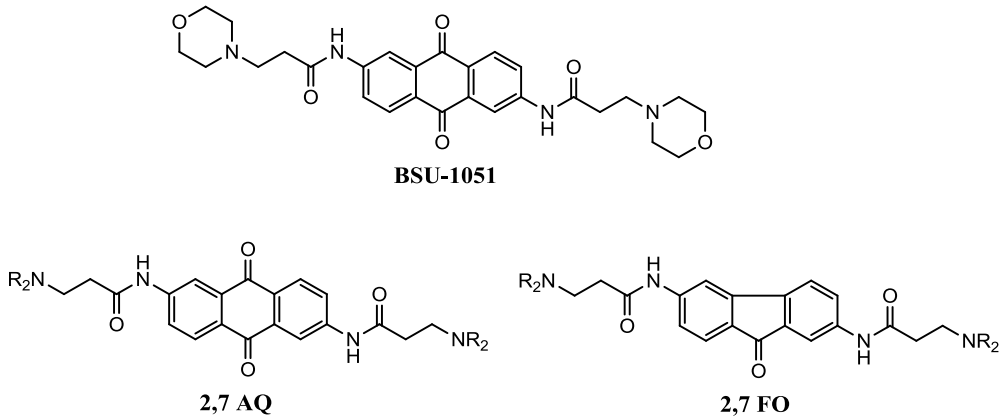

Figure 2.11. Structures of BSU-1051 and 2,7-AQ/FO.

The most potent compound in this series (R_2 = 1-(2-methyl)piperidinyl)) presents an IC_{50} of 12 μM, with a 2-10 fold reduction in toxicity compared to the corresponding anthraquinone. In general among the FOs, the observed effect of the substituents on the telomerase inhibition is similar to the one reported for anthraquinones. The comparison between 2,7-disubstituted FOs and 2,7-disubstituted AQs demonstrates that FOs are slightly less active in inhibiting

telomerase, probably because they are less planar then AQs and their chromophore is more electron-poor, thus decreasing the stacking with the G-quadruplex structure.

- *Acridine derivatives.* A library of 3,6-disubstituted acridinium salts was synthesized with the aim to investigate the importance of the introduction of a positive charge onto the aromatic planar chromophore (Fig. 2.12). In these molecules the protonated nitrogen atom might give additional interactions with the negative electrostatic potential of the channel between the stacked tetrads of G-quadruplexes.[119] Compared to the 2,7-AQs, these compounds do not have a more pronounced ability to inhibit telomerase, probably because of the low basicity of the nitrogen atom in the ring and because the substituents have no electron-donor effect. Hence the electronic properties of the acridinine ring are similar to those of the anthraquinone fragment.[120] In order to obtain more selective derivatives towards G-quadruplex DNA, a series of 3,6,9-trisubstituted acridine was designed (Fig. 2.12).[121]

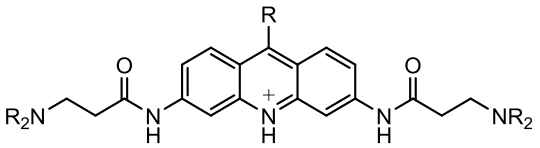

3,6- Bisamidoacridine R= H
3,6,9- Bisamidoacridine R≠ H

Figure 2.12. General structure of 3,6-bis-amidoacridinium and 3,6,9-bis-amidoacridinium salts.

In this series the most interesting compounds are those with an aniline group in 9: for such molecules the two amide substituents are positioned in the two wider grooves, while the aniline moiety lies in a third groove.[94] Moreover the latter substituent increases the basicity of the nitrogen atom of the aromatic ring. Through SPR and computational studies it was determined that 3,6,9-trisubstituted derivatives increase their inhibitory activity towards telomerase respect to the 3,6-disubstituted acridines, a direct result of a 30-40 times higher affinity for the G-quadruplex DNA compared to the duplex form DNA.

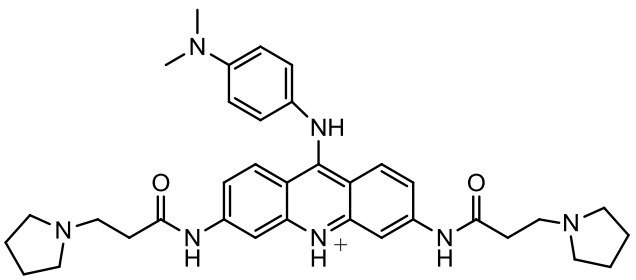

BRACO-19

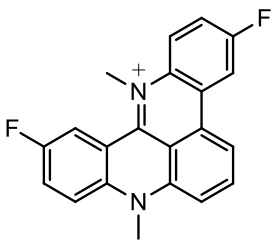

RHPS4

Figure 2.13. Structure of BRACO-19 and RHPS4.

Recently some members of the family of the 3,6,9-trisubstituted acridines with an IC_{50} in the range of 10-20 nM towards telomerase entered in preclinical studies.[122] Particularly BRACO-

19 showed significant telomerase inhibitory activity, with an IC_{50} value of 6.3 μM (Fig.2.13).[123] *In vitro* it was able to inhibit cell growth at sub-cytotoxic concentrations in a number of cancer cell lines, to induce senescence, telomere shortening, telomere end-to-end fusions and displacement of the protein POT1 from telomeres of treated cells.[124, 125, 126, 127]
In vivo, BRACO-19 has been evaluated in xenograft models of the vulvar carcinoma cell line A431 in combination with Paclitaxel, showing a major antitumor effect than paclitaxel alone. As single agent, BRACO-19 was tested in uterine carcinoma xenograft UXF1138L, showing high activity against early-stage tumors.[102] Despite all its favorable characteristics, the major limitations of BRACO-19 are its lack of membrane permeability and a small therapeutic window.
Another compound belonging to the acridine derivatives is RHPS4: this pentacyclic compound has been identified as a potent inhibitor of telomerase, with an IC_{50} value of 0.33 μM (Fig.2.13). This compound inhibits proliferation of cells within 2-3 weeks at non-cytotoxic concentrations.[128]

- *Chindoline derivatives*. Molecular modeling studies and the SAR on the anthraquinone and acridine compounds previously described revealed that tricyclic systems are not expected to be sufficient to give good stacking interactions on the surface of the terminal G-quartet. Therefore, two classes of compounds with tetracyclic chromophores were designed.
Among the benzo[*b*]naphtho[2,3-*d*]furanoid derivatives, the monosubstituted compound **I** has an IC_{50} of 7.0 μM (Fig. 2.14).[129]
Among the chindoline derivatives, the disubstituted compounds show IC_{50} values in the range of 6-16 μM (Fig. 2.14).[130, 131] It is interesting to note that the 11-monosubstituted compounds show a higher inhibitory activity towards telomerase than the disubstituted derivatives, with IC_{50} values between 0.44-12.3 μM (Fig. 2.14).[132, 133] This can be explained considering that the electron-donor substituents in position 11 can increase the basicity of the nitrogen atom of the pyridine ring of quinoline, normally protonated at physiological pH. This results in an increase of the magnitude of electrostatic interactions between the protonated nitrogen of the chindoline derivatives and the negative electrostatic potential of the central canal of the G-quadruplex. Recent studies have shown that these compounds are not only able to stabilize G-quadruplexes, but also to induce their formation, for example in c-Myc.[134]

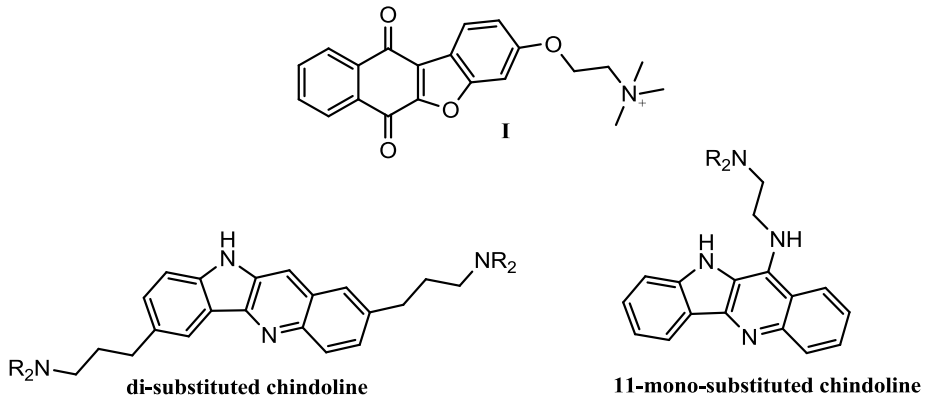

Figure 2.14. Structure of **I** and general structure of mono and disubstituted chindoline.

- *Quinacridine derivatives.* As demonstrated with FRET assay, pentacyclic compounds such as quinacridine are able to stabilize G-quadruplexes. Five aromatic rings fused together in a non-linear arrangement constitute the chromophores of these compounds. These compounds have a good ability to bind G-quadruplexes, as evidenced by the increase in melting temperature ΔTm, to which is associated an increase in telomerase inhibition.

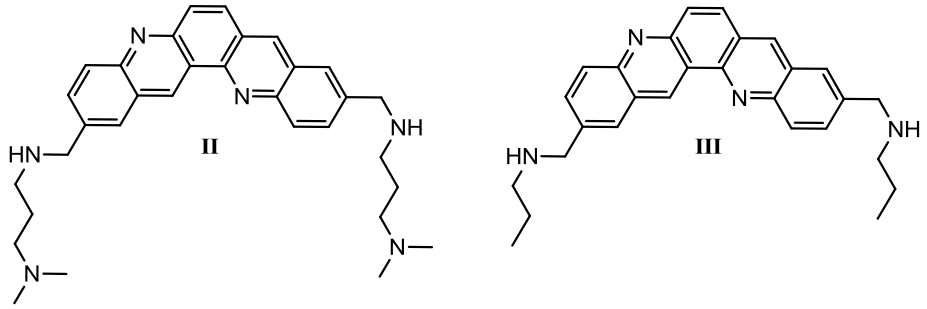

Figure 2.15. Structure of **II** and **III**.

For the two most active compounds of this series **II** and **III** the ΔTm is of 19.7 and 12.5 °C, while the IC_{50} values are 0.028 and 0.5 μM, respectively (Fig. 2.15).[135]
More recently, a quinacridine-Pt hybrid compound (Pt-MPQ), made up by a monosubstituted quinacridine core and a group containing Pt, has been shown to interact with the G-quadruplex structures of DNA through a dual binding mode: stacking interaction mediated by the quinacridine fragment and covalent bond between Pt and bases (platination). PT-MPQ is the first prototype of the hybrid G-quadruplex ligand class (Fig. 2.16).[136]

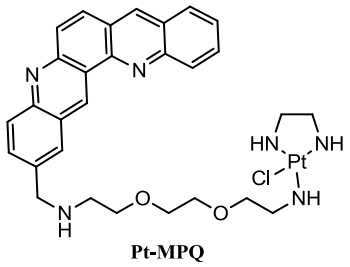

Pt-MPQ

Figure 2.16. Structure of Pt-MPQ.

- *Perilene derivatives.* In order to increase the size of the chromophore and improve the stacking interactions, a serie of perylene derivatives has been developed. Within this class a very promising compound is PIPER, that is able to induce and stabilize the formation of G-quadruplexes in the promoter region of c-Myc , as well as to inhibit telomerase activity with an IC_{50} value in the low μM range (Fig. 2.17).[137]
SAR studies have been made on this compound regarding both the amino side chains and the size of the central intercalating core. The chemical nature of the basic side chain and its pKa, its length and the position of the protonated nitrogen atoms influence the amount of electrostatic interactions with the phosphate groups in the grooves, thus the stability of the G-quadruplex-ligand complex and the telomerase inhibition properties.[138]

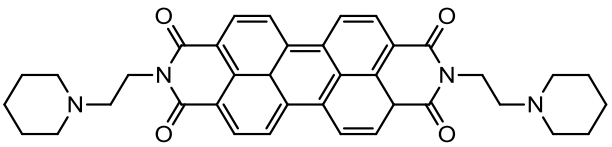

PIPER

Figure 2.17. Structure of PIPER.

Particularly the size of the planar core has been widely studied and it was showed that compounds resulting from a decrease in the number of condensed aromatic rings such as naphthalene diimides are still able to interact with G-quadruplexes.

- *Naphthalene imides and diimides derivatives.* The naphthalene diimides derivatives were developed starting from naphthalene imides (NI) compounds, among which the most important ones are Mitonafide and Amonafide (Fig. 2.18); these compounds show excellent antineoplastic activity due to their ability to intercalate into DNA, but they have not passed the phase II of clinical trials because of the important side effects associated with their administration.[138] In order to overcome the toxicity of these compounds, their pharmacophore was modified, passing from NI to NDI compounds with a 1,4,5,8-tetracarboxynaphthalene diimide core. The prototype of this class of compounds is N-BDMPrNDI, which shows an increased capacity to intercalate between the bases of the duplex DNA and, for the first time, the ability to stabilize the triplex form of DNA (Fig. 2.18).[139]

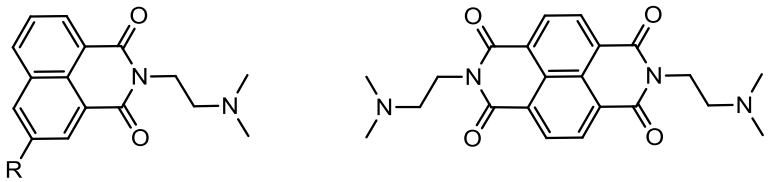

Mitonafide R= NO_2
Amonafide R= NH_2

N-BDMPrNDI

Figure 2.18. Structure of Mitonafide, Amonafide and N-BDMPrNDI.

Since several years, my research group has been involved in the research of new G-quadruplex ligand based on a NDI scaffold. They developed a series of compounds bearing two basic polymethylene chains linked to the NDI core, the length of which has been the subject of SAR studies. In all the compounds of this series, the two nitrogen atoms of the linker are protonated at physiological pH, increasing the interaction with the DNA due to the formation of electrostatic bonds with the phosphate groups. The basicity of these nitrogen atoms is also increased by the 2-methoxybenzyl substituent present in all the derivatives. The more active compounds are **IV** and **V**, presenting a linker of two and three methylenes between the NDI core and the basic nitrogen atom respectively (Fig. 2.19).[140, 141]

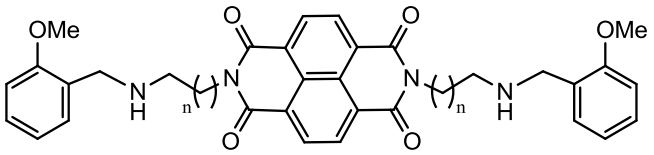

Figure 2.19 Structure of compound **IV** (n = 1) and **V** (n = 2).

These compounds show an interesting antiproliferative activity in the μM range in several cancer cell lines, due to an effective interaction with the DNA, preferentially with the quadruplex respect to the duplex form, the activation of caspases, the accumulation of the p53 protein, the downregulation of AKT, and ultimately to the inhibition of phosphorylation of ERK. Considering their wide range of activities, **IV** and **V** can be considered as Multi-Target-Directed Ligands. The two lead compounds were the subject of SAR studies with the aim to evaluate the importance of the nature and the position of the substituent on the aromatic ring. It was found that derivative **VI** with side chains of three methylene groups and 2,3,4-trimethoxybenzyl substituents is the most powerful compound within the series (Fig. 2.20).

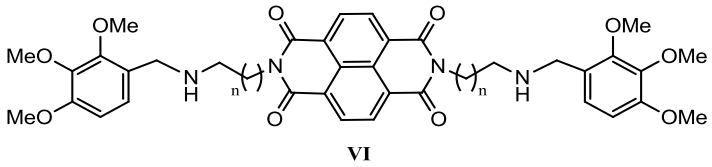

VI

Figure 2.20. Structure of **VI** (n = 2).

Many disubstituted NDIs have been screened for their ability to bind G-quadruplex, but all of them have showed poor selectivity for quadruplex versus duplex DNA. Starting from this consideration and with the aim to improve the selectivity for the quadruplex DNA, Neidle and coworkers developed more complex molecules, i.e. tri- and tetrasubstituted NDIs, by adding two more chains able to target the four grooves of the parallel telomeric G-quadruplex structures (Fig.2.21). The major complexity of these molecules allows also adding chemical variability in one single entity that can be exploited to discriminate between different quadruplexes.

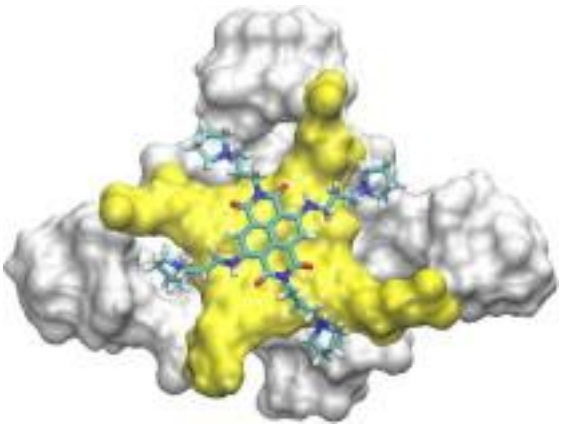

Figure 2.21. Molecular model of a tetrasubstituted NDI bound to a G-quadruplex structure.[142]

The ability of these derivatives to bind the quadruplex DNA was assessed through the FRET assay. The data obtained from that analysis showed that the tetrasubstituted NDIs have a higher capacity to stabilize the quadruplex DNA respect to the trisubstituted NDI, that are better than the disubstituted ones as well. The stability inducted depends on the nature of the different groups linked to the aromatic core: compounds bearing basic groups, due to their ability to interact with the phosphate groups of DNA, are more active than the others in the FRET assay. The tri- and tetrasubstituted derivatives are also more selective, in fact they bind the duplex DNA less than the disubstituted NDIs, and in particular the tetrasubstituted ones are more selective for the quadruplex structures than the trisubstituted, probably due to steric reasons.[143] The initial hypothesis about the ability of these compounds to target the four loops of the quadruplex DNA was also supported by molecular modelling studies and by crystallographic analyses on several quadruplex-NDI complexes. To better understand the binding mode of NDIs, a tetrasubstituted derivative of this series has been co-crystallized with an intramolecular human telomeric 23-mer G-quadruplex DNA. As shown in Figure 2.22, the terminal G-tetrads are coordinated by one NDI core each while four NDI molecules coordinate the G-tetrads of two G-quadruplexes, and two NDI molecules display external interactions with the loops at the sides of the G-quadruplexes.

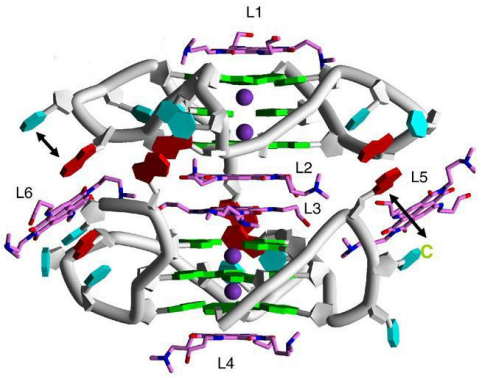

Figure 2.22. The 23-mer crystal structure of the intramolecular quadruplex of the sequence d[TAGGG(TTAGGG)3] complexed with tetrasubstituted NDI ligand.[121]

This kind of derivatives demonstrated the capacity to inhibit telomerase in the TRAP assay and a correlation has been proved between the FRET and the TRAP data: the compounds that are more active in the FRET are also the more active *in vitro* in inhibiting the telomerase activity. The interference with telomerase activity is also due to the possibility to displace the human protection of telomeres protein (POT1) from the single-stranded telomeric DNA overhang, that is considered to be a consequence of quadruplex formation, induced by the NDI compounds.[144] The cytotoxicity of this library is also very high; they reach nanomolar level in a wide range of cancer cell line, and are particularly active towards pancreatic cancer cytotypes. The intrinsic fluorescence of these compounds permitted to visualize them into the cell and, through confocal microscopy, it was shown that the derivatives are rapidly internalized into the cell and they localize exclusively in the nucleus, with a preference for the nucleolus that is connected to telomerase activity. Some of these molecules were also evaluated *in vivo* for their anticancer activity: they displayed significant antitumor activity in a

pancreatic cancer xenograft model, with a 50% reduction in tumor volume on intraperitoneal administration.[145]

Neidle and coworkers also used structure-based design methods to optimize the pharmacological properties of several analogues with four side-chains each terminating in an *N*-methyl-piperazine group. They noticed that compounds with di-*N*-methyl-piperazine and di-morpholine end groups have superior (by up to 10-fold) cellular potency, especially against a panel of pancreatic and non-small-cell lung cancer cell lines. From this further study, they identified Endamine as a potent inhibitor of cell growth in pancreatic and lung cancer cell lines, with IC_{50} values against the chemo-resistant Panc1 cell line of 3 nM (Fig. 2.23). The study of the telomere elongation in presence of Endamine showed no change in mean telomere length, so it is possible to say that inhibition of telomerase is not responsible for the antiproliferative activity of the compound that is indeed responsible for the change in the expression of a number of cellular stress/DNA damage response genes.[146]

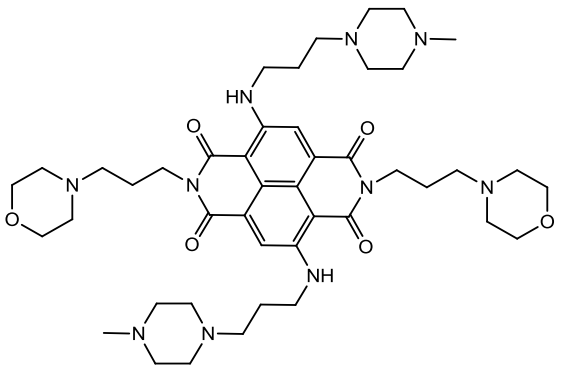

Figure 2.23. Structure of Endamine.

-*Telomestatin analogues.* As previously explained, macrocyclic compounds are particularly interesting for the interaction with G-quadruplex structures. Telomestatin is a macrocyclic natural compound isolated for the first time in 2001 from *Streptomyces anulatus*, whose structure presents five oxazole rings, two methyloxazole rings and a thiazoline ring (Fig 2.24).[147] It has been extensively studied due to its outstanding selectivity for G-quadruplex and highly promising biological properties.

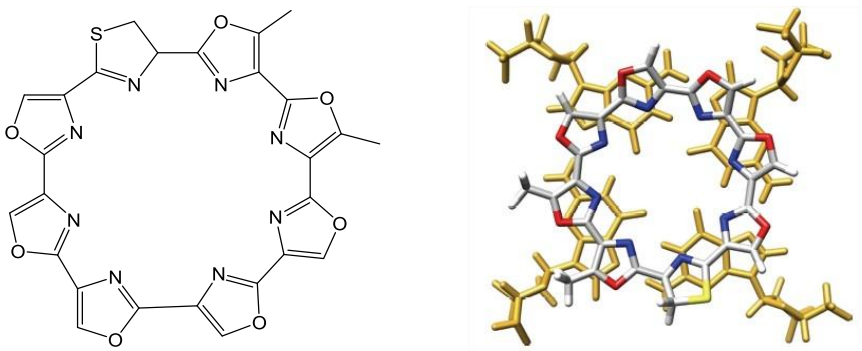

Figure 2.24 Structure of Telomestatin and its binding mode with G-quartet.

The quadruplex overduplex-DNA selectivity of this compound was established via competitive FRET melting which is carried out in presence of competitive duplex DNA. In the presence of telomestatin, the increase in melting temperature is very large (ΔTm = 24 °C), and since this value is unaffected by the presence of up to 50 equivalents of competitive duplex DNA, telomestatin is one of the most selective G-quadruplex ligands. Telomestatin is also able to inhibit telomerase with an IC_{50} in the nanomolar range (IC_{50} = 5 nM).[148]
The exceptional effectiveness in G-quadruplexes binding is attributable to the high hydrophobic nature of the molecule, which strengthens the stacking on the external G-quartet, and to the perfect adaptation of the shape of the molecule with the G-quartet, as demonstrated by computational studies (Fig. 2.23).[149]
The reason at the base of telomestatin selectivity for cancer cell lines is not clear yet. Probably, this is due to the differences in plasmic membrane permeability between normal and cancer cells or to modifications in the shelterin complex.
The complexity of telomestatin makes its synthesis a hard goal. For this reason, more synthetically accessible telomestatin analogs were synthesized: HXDV and S2A2-6OTD are hexaoxazole macrocyclic ligands obtained by the association of two symmetrical tri-oxazole fragments with an amino acidic bridge such as protected valine or serine (Fig. 2.25).[150, 151]
HXDV has been widely investigated and found to profoundly stabilize the telomeric G-quadruplex structure by UV-melting assay (ΔTm = 24 °C), without any significant binding to duplex DNA. In order to avoid its solubility problems, various analogs of HXDV have been prepared by modifying the nature of the side chain and among these the most interesting derivative is HXDL, presenting two lysine residues (Fig. 2.25).[152]

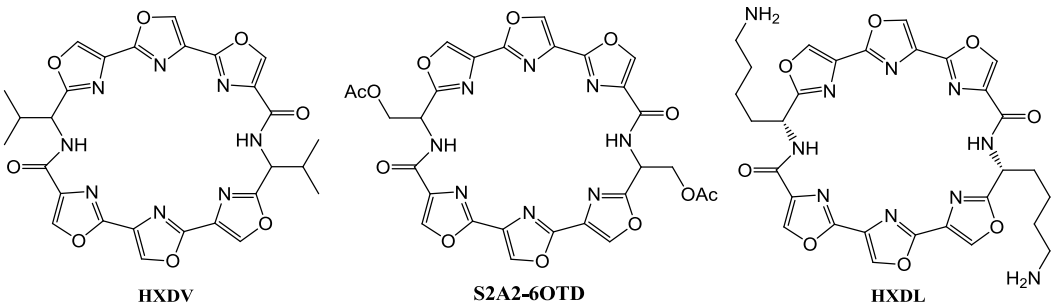

Figure 2.25. Structure of HXDV, S2A2-6OTD and HXDL.

This compound is more affine and selective towards G-quadruplexes, probably due to the presence of the two primary amino groups of the leucine linker, protonated at physiological pH. These features determine an increase of the solubility in aqueous environment and confer the possibility of adding, besides the stacking interaction with the G-quartet, some electrostatic interactions with the negative charges of the phosphate groups of the DNA skeleton.

- *Porphyrin-like macrocycles.* Along with neutral and cationic cyclic polyheteroarenes, cationic porphyrins are probably the most widely used macrocyclic G-quadruplex ligands. TMPyP4 (5,10,15,20-tetra(*N*-methyl-4-pyridyl)porphyrin) is a reference compound, representative of the family of the G-quadruplex ligands characterized by the porphyrin core (Fig. 2.26). Its ability to bind DNA was known for a long time, but its capacity to bind G-quadruplexes was discovered approximately twenty years ago.

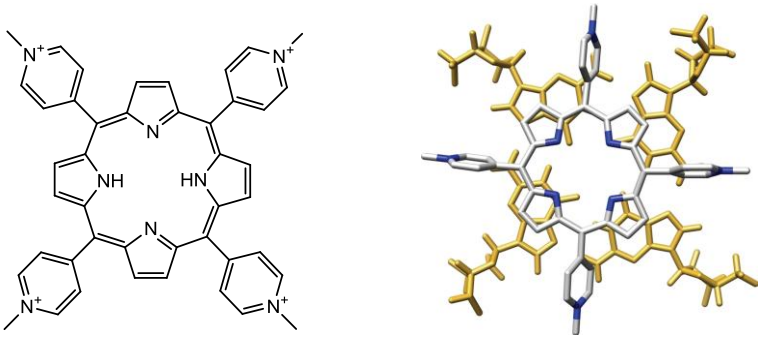

Figure 2.26. Structure of TMPyP4 and its binding mode to G-quartet.[130]

This tetracationic porphyrin has shown high affinity for G-quadruplex DNA (as proved through FRET melting assay, ΔTm = 17 °C), but it does not possess any kind of selectivity.[153] Despite this, it was particularly used as a tool to investigate its ability in downregulating the oncogene expression, due to quadruplex formation or induction (like c-myc, c-kit, and hTERT genes). [54, 154, 155] The binding mode between TMPyP4 and quadruplex structures have been widely studied in the last years. Interestingly, this compound displays various quadruplex-interactions, ranging from intercalation between adjacent G-quartets, to the stacking on the external G-quartet, passing by a mode totally devoid of direct contacts with G-quartets and through the possibility of combining several binding modes during a single recognition process.[156, 157, 158]

Given the known modulation of G-quadruplex structures by metal and the capacity of the porphyrin structures to coordinate metals in their internal cavity, TMPyP4 complexes with various metals have been developed. Among Pt (II), Cu (II), In (III), Zn (II), Co (II), Fe (III), Ni (II), Mn (III), Mg (II), and Pd (II) complexes, the most interesting resulted Mn-TMPyP4, displaying an affinity ten times higher for quadruplex DNA compared to the duplex DNA (Fig. 2.27).[54]

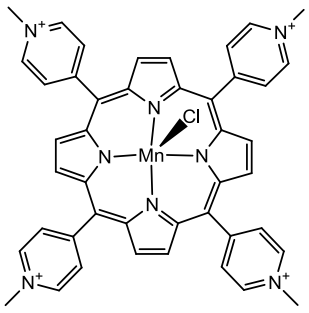

Figure 2.27. Structure of Mn-TMPyP4.

In this class of compounds, the nature of the side arms surrounding the porphyrin core is very important in order to achieve selectivity. Indeed, while the above mentioned Mn-TMPyP4 was able to interact with G-quadruplex 10 times faster than with duplex DNA, the shift of the *N*-methylpyridinium moieties from the proximity of the porphyrin core gives a 10000-fold difference.[159] This modification improves the electrostatic interactions with the quadruplex grooves, preventing at the same time the intercalation into DNA duplex. The same result was

obtained through the substitution of the *N*-methylpyridinium moieties with (trimethylammonium)methylphenol arms.[160]

Despite these encouraging results, the development of TMPyP4 porphyrin derivatives has stopped. The difficulty of obtaining selectivity towards G-quadruplex structures and the evidences that tetrapyrrolic structures are not geometrically optimal for the interaction with the G-quartets have prompted to explore new structures. For example, compound 3,4-TMPyPz, deriving from the fusion of pyridinium groups directly to the porphyrin skeleton leads to a planar, electron-deficient and structurally frozen porfirazine structure, which allows an excellent overlap on the G-quartet (Fig. 2.27). 3,4-TMPyPz, both in complexed and not complexed form, shows a high affinity for G-quadruplexes.

Structurally related to porfirazine, phthalocyanines present a benzene ring fused to the porphirin nucleus instead of the pyridine. Two compounds representatives of this class are ZnPc and ZnDIGP, with quaternary ammonium groups and guanidine fragments in the side chains, respectively (Fig. 2.28).[161, 162] These compounds show improved affinity and selectivity through SPR studies and CDs.

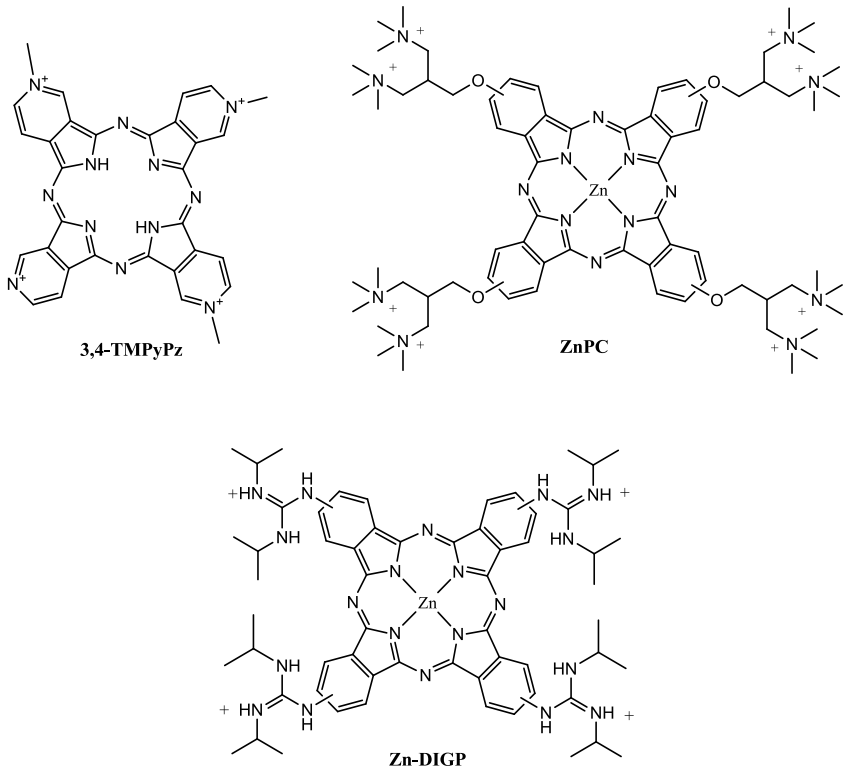

Figure 2.28. Structure of 3,4-TMPyPz, ZnPc and ZnDIGP.

Another family of porphyrins is represented by Hemin and related compounds. Hemin is a Fe(III)-protoporphyrin IX, known to be the cofactor of Hemoglobin and Myoglobin (Fig. 2.28).[163] This compound binds tightly the quadruplex structures, but despite that, it has not been studied as a ligand, but rather as an investigative tool for G-quadruplex. In fact, the Hemin-G-quadruplex complex acquires the ability to catalyze the H_2O_2-mediated oxidation of certain precursors, such as luminol, useful to see where they form G-quadruplex in the human genome and then investigate the potential ligands. A porphyrin related to Hemin, NMM (N-methylmesoporphyrin IX), is the only G-quadruplex macrocyclic ligand negatively charged,

thanks to the presence of two carboxyl groups deprotonated at physiological pH (Fig. 2.29). NMM is moderately affine to G-quadruplex, despite an excellent overlap in the G-quartet, but highly selective. Even NMM is mainly used as an investigative tool to evaluate the formation of G-quadruplex *in vivo* and to determine whether the sequences capable of forming G-quadruplex identified through computational studies actually exist in that form in a cellular context.

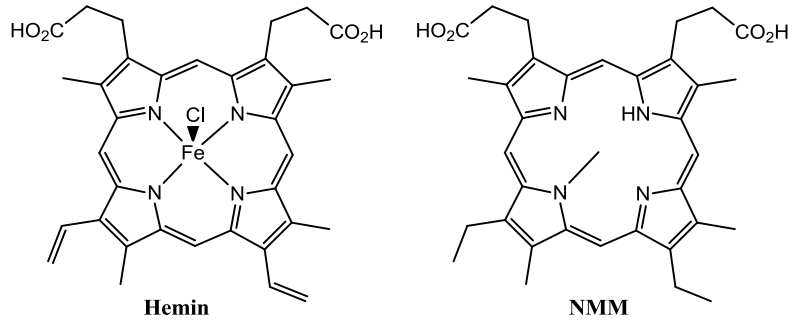

Figure 2.29. Structure of Hemin and NMM.

- *Polyammonium Cyclophane-Type macrocycles.* The only two groups of molecules belonging to this category are the cyclo bis-intercalator family (CBI) and the neomycin-capped aromatic platforms. The CBI are made up of two aromatic chromophores linked through polyamine chains; because of the presence of protonated nitrogen atoms these molecules are less hydrophobic than the previously discussed macrocycles and are highly soluble. Only two compounds of this family have been tested towards G-quadruplex: BOQ1 and BisA (Fig. 2.30).

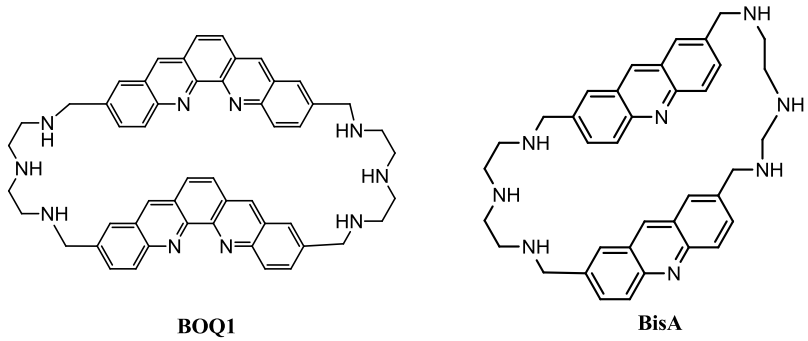

Figure 2.30. Structure of BOQ1 and BisA.

BOQ1 is composed of two acridine rings bound with polyamine linkers, while BisA contains two quinacridine rings as aromatic scaffold.[164, 165] This molecules bind the quadruplex DNA much stronger than their acyclic analogues and they both efficiently induce thermal stabilization of the human telomeric quadruplex (ΔTm = 28 °C and 15 °C, respectively), indicating that the size of the aromatic core is very important for the interaction.

The two compounds are also very selective towards quadruplex DNA and this feature may be due to their particular topology. While the macrocycles previously described have very planar and rigid conformation, CBIs show a particular arrangement, called semiclosed conformation, in which the two aromatic rings face each other in parallel planes.[125] As a result, these molecules cannot bind duplex DNA: steric reasons and the restricted length of the linkers prevent the bis-intercalation between contiguous bases.[166] The binding mode of BOQ1 has been long studied, for this molecule the semiclosed conformation occurs both in the free state and in the complex with quadruplex structure at telomeric ends (Fig. 2.31).[167]

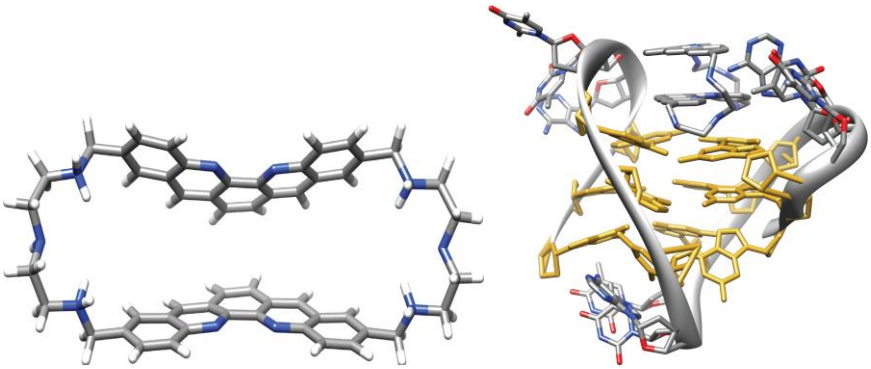

Figure 2.31. Structure of BOQ1 in the free state and during the molecular dynamic simulation between BOQ1 and the human telomeric quadruplex.[168]

Other studies revealed that BOQ1 in this conformation interacts not only through π-π stacking with the G-quartets, but also H-bonding interactions between the linkers and the loop backbone occur to stabilize the complex.
The promising results obtained with BOQ1 in terms of affinity and selectivity, have pushed the researchers to synthesize new series of analogous compounds, whose members differ in the nature and the number of aromatic nuclei, as well as in the nature and derivatization of spacer chains(Fig. 2.32).[169]

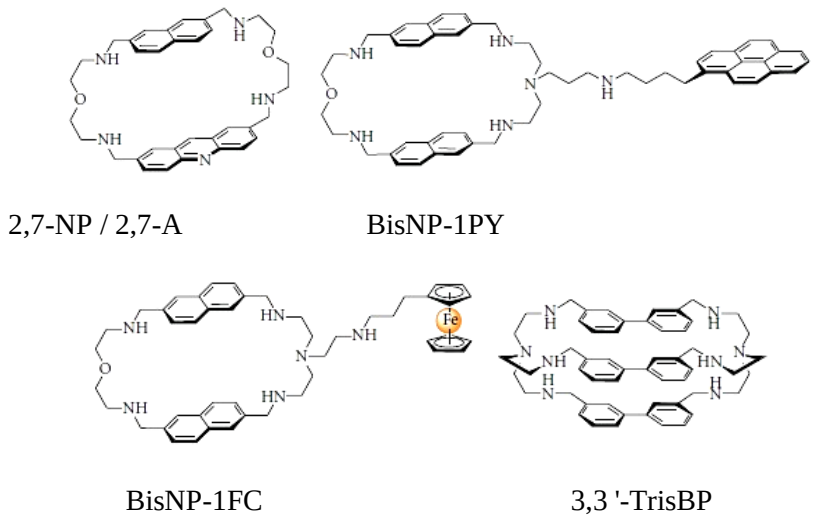

Figure 2.32. Structure of 2,7-NP/2,7-A, BisNP-1PY, BisNP-1FC, 3,3 '-TrisBP.

In particular, the aromatic nucleus can be a naphthalene, anthracene, biphenyl, acridine, quinacridinine, phenazine and bipyridine or ferrocene ring. In the same molecule, two or three equal or diverse nuclei differently linked can be present. Chains spacer can be a polyamine presenting secondary or tertiary nitrogens, functionalized with side chains, and the nitrogen atoms of the chain can be replaced with oxygen or sulfur atoms. These series were subjected to screening using FRET techniques from which emerged four highly promising compounds 2,7-NP/2,7-A, BisNP-1PY, BisNP-1FC, 3,3'-TrisBP endowed with an interesting biological profile (Fig. 2.32).[170]

The second category of polyammonium cyclophane-type macrocycles are the neomycin-capped macrocycles, in which the aminoglycoside neomycin is linked to three different planar cores, such as acridine, phenanthroline, and quinacridine. The most active molecule within this series is the quinacridine derivative NCQ, a highly flexible molecule that strongly binds the telomeric G-quadruplex, while showing low affinity for the duplex DNA (Fig 2.33).[171] NCQ is selective for the intramolecular G-quadruplex conformations, such as the telomeric one, because they have numerous loops with which the fragment of Neomycin may establish strong and specific interactions with; these loops are instead absent in tetrameric G-quadruplexes. This strategy could be useful and innovative to develop selective ligands for the various G-quadruplex forms.

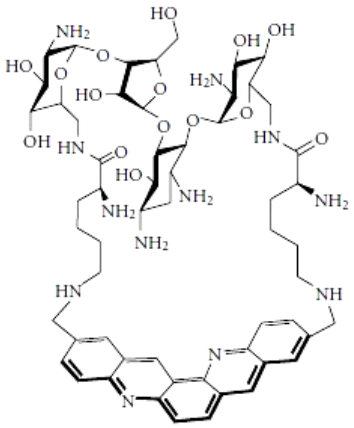

Figure 2.33. Structure of NCQ.

Chapter 3. Epigenetic and cancer

In the cells, DNA can exist in various forms and these different conformations are closely related with the different phases of the cell cycle. The macromolecule is usually packaged as chromatin, that is a highly organized and dynamic protein-DNA complex whose roles are to reduce DNA volume, allow mitosis, control replication and transcription processes, and prevent DNA damage. The nucleosome, the basic unit of chromatin, is made up of a segment of DNA wound in sequence around eight histone proteins. The nucleosome core particle consists of an H3 and H4 tetramer and two H2A and H2B dimers, surrounded by 146 bp of DNA (Fig. 3.1).[172]

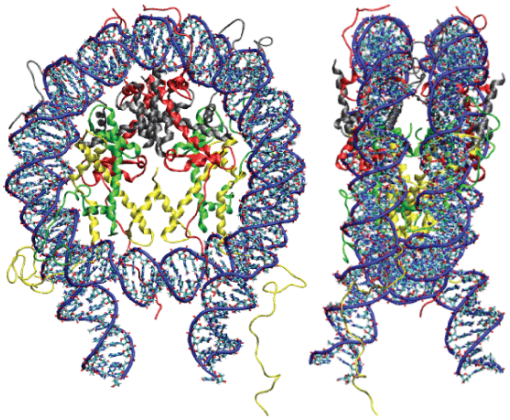

Figure 3.1. Structure of the nucleosome core particle consisting of histones H2A in red, H2B in grey, H3 in yellow and H4 in green, and DNA (http://malone.bioquant.uni-heidelberg.de/methods/modeling/modeling.html).

The organization of the DNA that is achieved by the nucleosome cannot fully explain the packaging of the nucleic acid observed in the cell nucleus. Further compaction of chromatin into the cell nucleus is necessary, but that is not well understood yet; it is known that a chain of nucleosomes can be arranged in a 30 nm fiber, depending on the presence of the H1 histone.[173] These fibers can create loops along a central protein in order to give euchromatin, the transcriptionally active form of DNA, while further compaction generates the transcriptionally inactive form heterochromatin. Local chromatin architecture is now generally recognized as an important factor in the regulation of gene expression.

The term “epigenetic” literally means “in addition to changes in genetic sequence”. Epigenetic studies any process that alters gene expression without changing the DNA sequence, and leads to heritable modifications (although experiments show that some epigenetic changes can be reversed).[174] Many types of epigenetic processes have been identified and some of them are natural in cells and lead to the expression only of the genes that are necessary for their own activity, while other genes are silenciated. However when epigenetic changes occur improperly, they can give origin to diseases. For example, epigenetic changes in histone acetylation cause lupus-like symptoms in mice, and that was confirmed by the fact that the treatment with the well known histone deacetylase inhibitor Trichostatin A can reverse these modifications.[175]

Among all the research in the epigenetic field conducted so far, the most extensively studied disease is cancer and the evidence linking epigenetic processes with cancer is becoming "extremely compelling". For a long time, cancer has been considered to be the result of a wide variety of genetic and genomic alterations, such as amplifications, translocations, deletions, and point mutations of proto-oncogenes and tumor suppressor genes (Fig. 3.2).

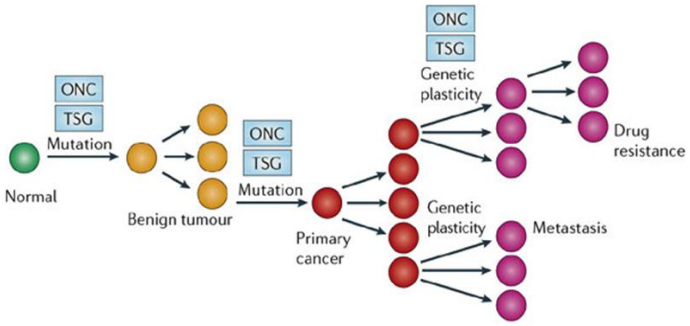

Figure 3.2. The genetic model of cancer.[176]

This picture presents, however, significant limitations: it remains unclear what is the engine at the base of the progressive stage, the role of the environment in the development of the pathology and the age and the long latency period that characterizes the majority of tumors.[177]
Cancer can also be considered an epigenetic disease, since a tumor originates from an alteration of the genetic material, which leads to an increase of the cell turnover, to an alteration of the cellular functions and cell invasiveness. An alteration of the DNA structures that reduces or increases the accessibility to the transcription and translation of genes is configured as an epigenetic event that alters the cellular balance and leads to the disease. Epigenetic alterations are able to influence the penetrance of the variants of a particular gene, and can help to understand these issues. A gene, in fact, can have one or multiple variants determining the disease, but their expression is epigenetically controlled. It is becoming clear that gene expression regulated by epigenetic changes plays a crucial role in carcinogenesis. The epigenetic alterations are responsible for the uncontrolled growth of the tumor size.
According to this epigenetic perspective, cancer develops in three stages (Fig. 3.3):

• alteration of epigenetic progenitor cell, that is a stem cell not yet differentiated into a specific tissue. This alteration is caused by an aberrant regulation of a tumor progenitor gene;
• mutation of proto-oncogenes and tumor suppressor genes that leads to the development of a benign tumor;
• genetics and epigenetics instability responsible for the progression that results in the appearance of metastasis and drug resistance.[178]

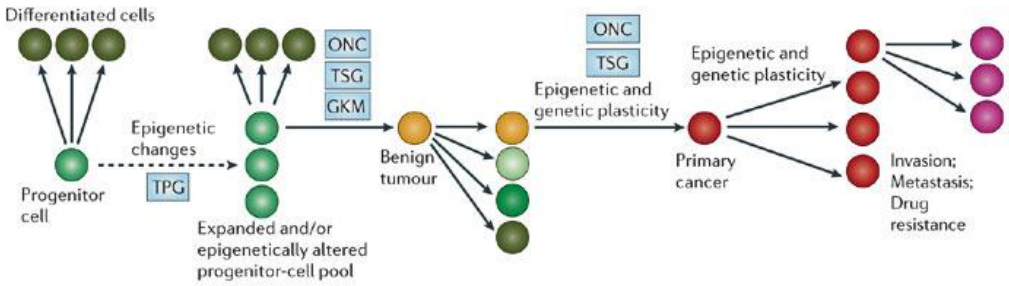

Figure 3.3. Epigentic model of cancer.[176]

To date, a wide range of post-translational enzyme-catalyzed modifications have been reported, most of them affecting the N-terminal tail of histone, such as acetylation, methylation, ubiquination and sumoylation. Furthermore, ADP-ribosylation can occur to the residues of lysine and glutamate in the histone tail and also methylation of dinucleotides CpG in 5' position that leads to gene silencing. The two major post-translational histone modifications consist in the addition or removal of acetyl and methyl groups. Acetylation/deacetylation, methylation/demethylation are the two most studied epigenetic alterations regulated by a wide range of proteins. The presence of acetylated lysine in the histone tails gives the transcriptionally active euchromatin structure, while deacetylation of lysine residues is associated with heterochromatin and transcriptional gene silencing.[179] Methylated histones can positively or negatively affect transcription, according to the site affected and the degree of methylation. Until now DNA methylation, and in particular silencing of tumor-suppressor genes by promoter hypermethylation, has been the most widely studied epigenetic modification in human tumors.[180] Lately another modification has been deeply studied, i.e. the acetylation of lysine residues of histones.
Among the epigenetic enzymes, proteins such as histone acetyltransferase and histone methyltransferase, respectively responsible for the addition of acetyl and methyl groups, are called writers. Proteins that recognize and bind these groups are referred to as readers and they include bromodomines, cromodomines and etc. Most of the writers, in addition to the catalytic domain responsible for the epigenetic alterations, possess a reader domain that recognizes and binds modified histones or interacts with DNA and other proteins. Enzymes like lysine demethylases and histone deacetylases, responsible for the removal of methyl and acetyl groups, are called erasers.
Readers, writers and erasers can lead to the onset of diseases like cancer through two different mechanisms:

• alteration of gene expression and cellular determinants of the variants of the disease;
• cooperation with other cellular proteins and with tissue-specific transcription factors sensitive to environmental stimuli.

Since cancer is a disease with epigenetics bases, epigenetic enzymes are very important targets for the treatment of these diseases; among them HDAC and LSD1 are very promising.

3.1 HDAC: structure and functions

HDACs are a family of evolutionarily conserved metalloproteases, able to catalyze the removal of acetyl groups from lysine residues of proteins such as histones.[181] HDACs are classifies into four different classes according to their catalytic mechanism and domain organization. Class I, II and IV are Zinc-dependent enzymes, while class III are nicotinamide adenine dinucleotide (NAD) dependent amidohydrolases, these latter are also called sirtuins.

The Zn dipendent HDACs require a single transition metal ion and the catalytic process proceeds through the polarization of the carbonyl substrate by Zn^{2+} coordination, which allows the general base-promoted nucleophilic attack of a water molecule also coordinated by the metal ion (Fig. 3.4).[182] The Zn^{2+} is usually pentacoordinate, in HDACs' catalytic site is coordinated by two water molecules, two aspartic acid residues and one histidine residue. The acetylated lysine can displace a water molecule and coordinate the Zn^{2+} ion, it also accepts a hydrogen bond from a tyrosine residue.[183] This interaction promotes the nucleophilic attack by polarizing the carbonyl substrate. The H142 is very important in the catalytic process and is used as a base in this step, its basicity is increased thanks to the H-bond that it forms with the aspartate residues.[184] The tetrahedral intermediate and its transition states are stabilized by coordination to Zn^{2+} and hydrogen bonds with Y306, H142, and H143. H143, lying near the leaving amino group of lysine, offers the proton that allows the collapse of the tetrahedral intermediate, serving as a general base- general acid catalyst. Lysine exits immediately from the catalytic site, while the acetate ion is slowly released, in fact it is initially coordinated by the metal ion.[185]

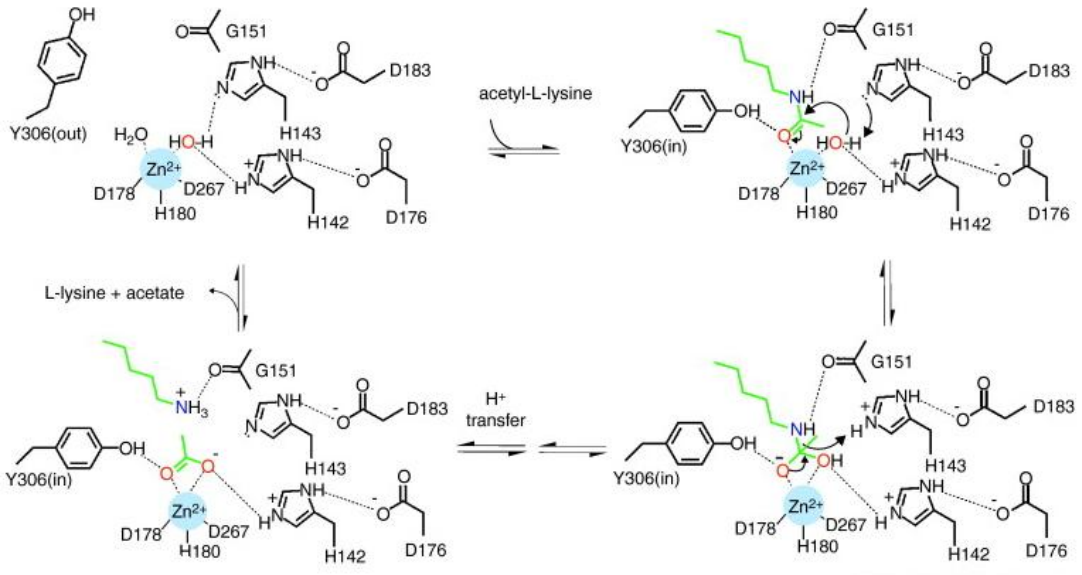

Figure 3.4. Proposed mechanism of HDACs and HDAC-related enzymes.[186]

The Zn-dependent HDACs differ in structure, enzymatic function, subcellular localization and expression patterns.

Class I HDACs consists of HDAC 1, 2, 3 and 8 and are mainly present in nucleus. This class is characterized by a relative simple structure; they consist in the deacethylase domain and short N- and C-terminal extensions and display high enzymatic activity toward histone

substrates. HDAC 1, 2 and 3 are generally found in complexes with other proteins, while no complex has been shown for HDAC8.

Class II HDACs can be divided into two different subtypes, depending on structure organization and sequence homology, HDAC IIa (consisting of HDAC 4, 5, 7 and 9) and HDAC IIb (consisting of HDAC 6 and 10). Class IIa HDACs present large N-terminal extensions with conserved binding sites for the transcription factor myocyte enhancer factor 2 (meF2) and the chaperone protein 14-3-3, which render HDACs signal responsive. These enzymes go from the nucleus to the cytoplasm using the 14-3-3 shuttle, as a consequence of a phosporilation.[187] The dissociation of class IIa HDACs from meF2 allows the HAT p300 to associate with meF2 via the HDAC docking site, thereby converting meF2 from a transcriptional repressor to a transcriptional activator.[188] The HDAC IIa members are very localized in the organism: HDAC 5 and 9 are mainly present in muscles, heart and brain, HDAC 4 is usually localized in brain; while HDAC 7 is expressed in Lymphocyte T precursor and endothelial cells.[189, 190, 191] Class IIa HDACs have mainly a repressor activity on transcription and that probably derives by their interaction with class I HDACs and other transcriptional repressor such as heterochromatin protein 1 (HP1) and C-terminal-binding protein (CTBP).[192, 193]

Class IIb consists of two members: HDAC6, which deacetylates mainly cytoskeletal proteins such as tubulin, cortactin and chaperones; and HDAC10 that is still not well known.[194]

Class IV is made up by one member, HDAC11. It is a special enzyme present in the nucleus of brain, heart, muscle, kidney and testis cells; this protein has an high homology with HDAC3 and 8, in fact it is composed of a deacetylase domain and small N-and C-terminal extensions.[195]

HDAC proteins are not alone in the cell, but associated with other proteins to give some complexes interacting with specific region of DNA through interaction with well defined DNA binding factors. There are different ways by which HDACs are recruited to gene promoters (Fig. 3.5).[196]

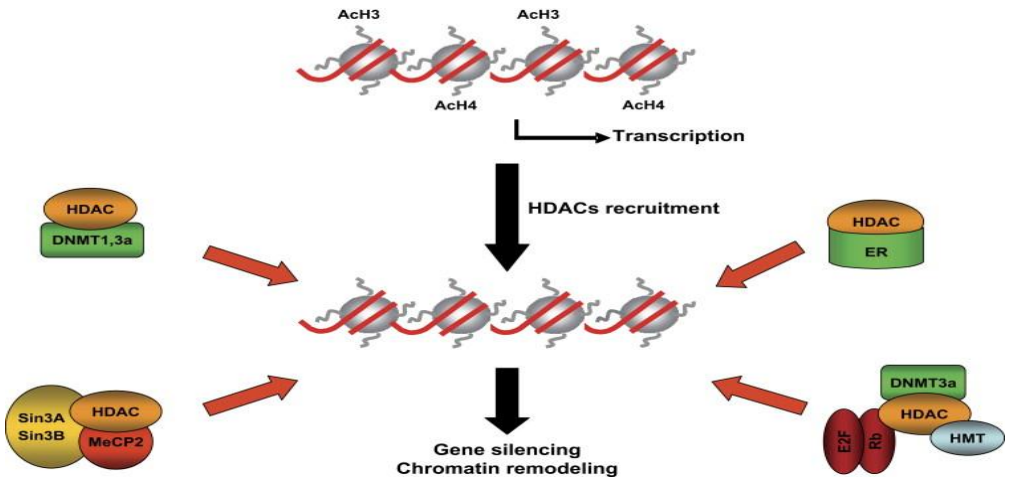

Figure 3.5. Different ways by which HDACs are recruited to gene promoters.[196]

The first interaction studied was the one that provides the interaction of HDACs with methylated DNA via methyl-binding proteins (MBDs). One example is the link with MeCP2, an MBD that recruits HDAC-containing complexes to methylated gene promoters as a mechanism for gene-transcription repression.[197] Deacetylases interact also with other

epigenetic enzymes, the methyltransferase proteins (DNMTs). HDACs interplay with DNMT1 causing an higher level of acetylated forms of histone H3 and at the same time a lower level of the methylated forms of histone H3, thus indicating that changes in DNA methylation also cause changes in histone proteins due to direct interactions between the two different classes of epigenetic enzymes.[198] Another DNMT protein linked to the deacetylase activity is DNMT3, interacting with HDAC2.[199] HDACs also participate in gene expression regulation thanks to the connection with estrogen nuclear receptors (ERs) and suppress its transcriptional activity. The interaction of HDAC1 with ER-α involves the activation function-2 (AF-2) domain, DNA-binding domain of ER-α and other proteins such as DNMTs, and retinoblastoma protein Rb.[200]

HDACs have a lot of substrates, not only the histones; as some studies have highlighted that these enzymes preceded the evolution of the histone proteins.[201] There are many non histone-proteins acting as substrates of this class of enzymes, such as transcription factors and regulators, chaperone proteins, structural proteins, signal transduction mediators, inflammation mediators, DNA repair enzymes (Fig. 3.6).

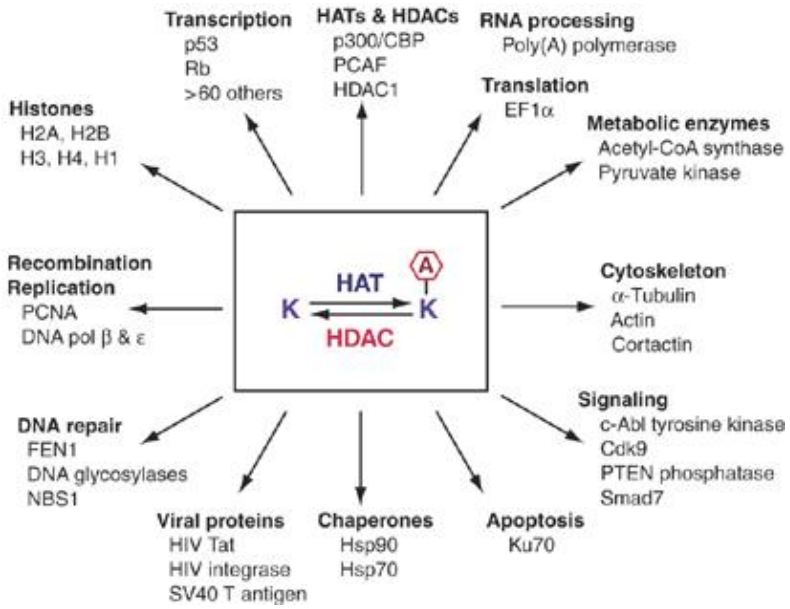

Figure 3.6. Example of reversible lysine acetylation in diverse cellular processes.[202]

In these proteins acetylation may cause different responses: it can either increase or decrease the function or stability of the proteins, or affect protein-protein interactions.[203] These HDAC substrates take part directly or indirectly in many biological processes that are involved in cellular cycle. As a consequence there is more than one mechanism by which HDACs function in cancer development.

The transcriptional repression of tumor-suppressor genes due to the overexpression and the aberrant recruitment of HDACs to their promoter region are some of the main causes of tumor onset and progression. As example, the cyclin-dependent kinase inhibitor p21 is able to block the cell cycle and it is downregulated in many different tumors; in some of these, p21 is epigenetically inactivated by hypoacetylation of its promoter. The use of HDAC inhibitors causes the inhibition of tumor-cell growth and an increase in both the acetylation levels of the promoter and gene expression.[204] The role of HDACs in cancer is not limited to their

deacetylase activity, but also to their role in the regulation of acetylation levels of non-histone proteins. The tumor suppressor protein p53 is a substrate of this class of epigenetic enzymes, and it is acetylated under stress conditions. When the protein is acetylated, these residues can overlap the ubiquitinated ones and cause the promotion of protein activation, influencing the cell cycle through the induction of checkpoints, the blockage of cellular division and of cell death.[205]

The wide range of proteins and processes regulated by HDACs described above demonstrates that these proteins are key elements in the regulation of gene expression, differentiation, development and maintenance of cellular homeostasis. Thus, an abnormal expression of HDACs might play an active role in tumor onset and progression, and make them attractive candidate targets for new anticancer drugs and therapies.

3.1.1 HDAC inhibitors: structure and functions

Based on the considerations made, HDAC appears to be a very promising target for therapeutic interventions designed to reverse aberrant epigenetic states associated with cancer. In many types of cancer is found altered expression of HDAC.[206] The HDACis do not cause direct damage to DNA, but the change of the conformation of chromatin exposes the DNA to cytotoxic agents that can cause breakage of the double helix. They have multiple biological effects as a result of the alteration of the acetylation pattern of both histone and non-histone proteins, and this wide range of biological events goes from growth cell arrest to terminal differentiation, angiogenesis and cell death (Fig. 3.7). Cell death can occur through apoptosis, through either the intrinsic or extrinsic pathway, or other mechanisms such as mitotic catastrophe, autophagy, senescence, reactive oxygen species (ROS) dependent death.

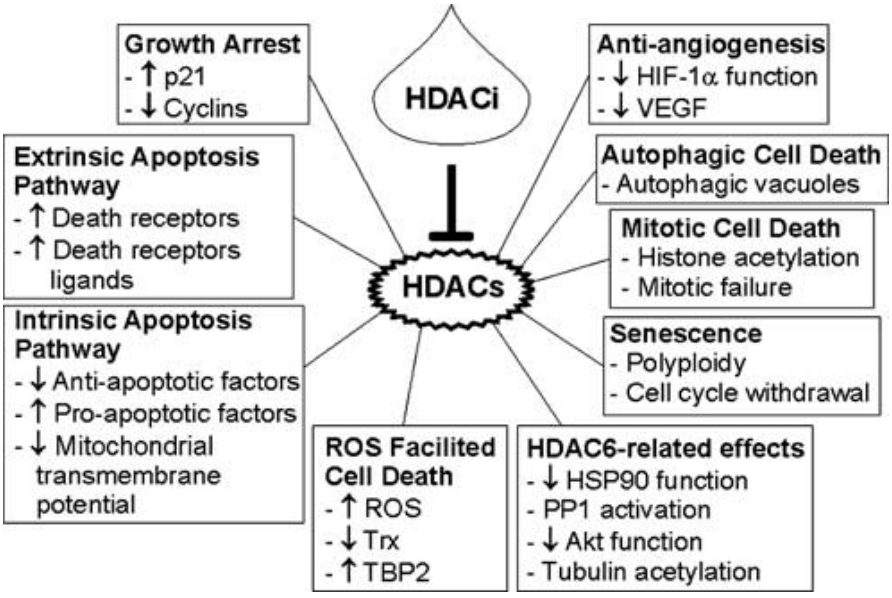

Figure 3.7. Multiple HDACi-activated antitumor pathways.[202]

- *Growth arrest*. HDACIs can affect the gene expression either directly through interaction with gene promoters and indirectly. Particularly these compounds are able to induce the cyclin-dependent kinase (CDK) inhibitor p21, this effect does not result from the interaction with p53 or from the acetylation of histones located in the promoter region of the p21 gene.[207, 204]

- *Cell cycle arrest*. The block of the cell cycle due to the administration of HDACIs occurs both in cancer and normal cells, the concentration of the compound is very important in order to determine in which phase of the cycle the arrest happens. G1 arrest derives from low concentration of HDACi, while higher levels of compound can give G1 or G2/M arrest.[208] p21 causes the arrest in G1 and G2 phase, mainly by the inhibition of CDKs that control G1 progression and G1/S transition; but the G1 blockade may be due to the activity of HDACIs against CDKs, by inducing their inhibitors.[209]
- *Activation of the extrinsic apoptotic pathway*. This mechanism of action is shown by HDACIs only in cancer cells and derives from the upregulation of the expression of death receptors and their ligands, such as Fas, tumor necrosis factor receptor 1 (TNFR-1), DR-3 and DR-6, TNF related apoptosis inducing ligand (TRAIL) ligand receptors (DR-4 and DR-5).[210, 211] The activation of the extrinsic pathway results in the activation of caspase 8 and 10 that leads to cell death.
- *Activation of the intrinsic apoptotic pathway*. The intrinsic apoptotic pathway involves some proteins like SMAC, cytochrome c, IAF that cause the activation of the caspase cascade. This pathway is one of the main causes of HDACIs induced cell death. These compounds cause the release of cytochrome c and the activation of caspase-9. Moreover they alter the factors that mediate or regulate the intrinsic apoptosis pathway; for example, they cause Bid cleavage starting the intrinsic pathway, increase the expression of proapoptotic Bcl-2 proteins such as Bim, Bmf, Bax, Bak and Bik, downregulate antiapoptotic Bcl-2 proteins such Bcl-2,Bcl-XL, Bcl-w and Mcl-1.[212]
- *Induction of mitotic catastrophe*. Histone acetylation damages the structure and functions of the centromere, as well as the pericentric heterochromatin, leading to a decrease in the binding of proteins to heterochromatin. Newly synthesized chromatin is acetylated, HDACIs act by maintaining the acetylation levels, thus disrupting the structure and function of the centromere and the pericentric heterochromatin. The increasing acetylation given by HDACIs, moreover, increases the phosphorylation of histones and alters the functions of the proteins of the mitotic spindle checkpoint (BubR1, hBUB1, CENP-F and CENP-E). As a consequence, HDACIs cause cell arrest at prometaphase, followed by aberrant mitosis and mitotic catastrophe.[213]
- *Induction of autophagy*. Another mechanism by which HDACIs induce cell death is autophagy. This membrane process regulates the delivery of cytoplasmic constituents to lysosomes for degradation and can be directly activated by p53. HDACIs are able to induce autophagy independently of caspases.[214]
- *Activation of ROS-induced cell death*. HDACIs induce the accumulation of ROS in treated cells in a very short time (2 hours).[215] The high level of this species leads to the disruption of mitochondria. HDACIs also increase the expression of the thioredoxin (Trx) binding protein-2 (TBP2), thus decreasing the level of Trx, a ROS scavenger, only in cancer cells.
- *Inhibition of HDAC6*. The specific inhibition of HDAC 6 or its down-regulation increases the accumulation of acetylated α-tubulin and cortactin, in association with inhibition of cell migration. The acetylation of HSP90 alters its function and chaperone proteins such as Akt, Bcr-Abl, c-Raf and Erb-2 can be poly-ubiquitinated and degraded by proteasomes associated with apoptosis.[216]
- *Induction of differentiation*. HDACIs can act in synergy with retinoic acid to induce differentiation in numerous cell types, although the mechanisms involved have not been clarified yet.
- *Immunomodulatory effects*. HDACIs can increase the immune response against the tumor mass, either acting directly on the malignant cells, in order to make them a more attractive

target for the immune system, either by altering the activity of immune cells and/or the production of cytokine. They cause, for example, an increased expression of proteins belonging to the major histocompatibility complex classes I and II and of CD40, CD80, CD86 and intercellular adhesion molecule-1 (ICAM1).

- *Angiogenesis inhibition*. HDACIs are able to block angiogenesis either by increasing the level of hypoxia inducible factors (HIF), either by reducing the expression of pro-angiogenic proteins. The expression of angiogenic genes is controlled by the transcription factors HIF1 and HIF2. Hypoxia, a recurrent event in tumors, leads to activation of HIF and to the promotion of angiogenesis. This pathway can be stopped by the administration of HDACIs.[217] HDACIs inhibit also the angiogenesis by preventing the endothelial cells from responding to the angiogenic stimulus generated by vascular endothelial growth factor (VEGF). Thricostatin A (TSA) and Vorinostat (SAHA) inhibit VEGF-induced expression of VEGF receptors and neuropilin-1, as well as the induction of emaphorine III expression in endothelial cells.[218]

In the recent years, a lot of synthetic molecules or natural products were identified as HDACi. In 2006, FDA approved Vorinostat for the treatment of cutaneous cell T lymphoma (CTCL) (http://www.fda.gov/cder/Offices/OODP/whats-new/vorinostat.htm) and, in 2009, Romidepsin was approved for the same disease, encouraging the development of new HDACIs.
From a structural point of view, a general pharmacophoric model for an HDACi requires the presence of some specific features: a zinc binding group (ZBG), a hydrophobic linker or connecting unit and a recognition cap group (CAP) (Fig. 3.8).

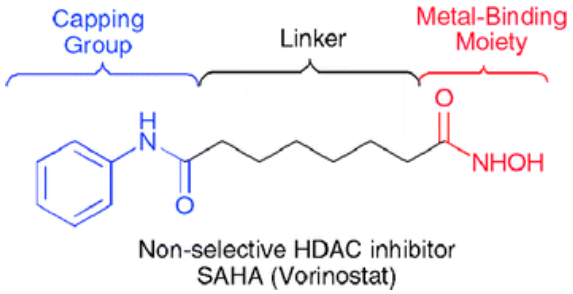

Figure 3.8. General structure of an hydroxamic acid based HDACi.[219]

Based on crystallographic studies of hydroxamic acid based inhibitors with HDAC 4, HDAC 8 and HDAC of an anaerobium bacterium (HDLP), it became evident that these structural motifs interact with three conserved regions in the active site (Fig. 3.9). The first recognition point for the inhibitor is the pocket that hosts the cation. As described before, Zn^{2+} facilitates the hydrolysis of the amide and is located on the bottom of the narrow catalytic pocket, it is pentacoordinated by two aspartic acids, a lysine residue and the remaining two bonds are provided by the substrate or by the inhibitor through its ZBG. The second zone of interaction is a hydrophobic channel, consisting of acetylated lysines, through which the inhibitor penetrates with the linker, and finally the third recognition site is constituted by the opening of the channel that contains a motif with a higher degree of diversity compared to the other two regions, that interacts with the hydrophobic CAP.

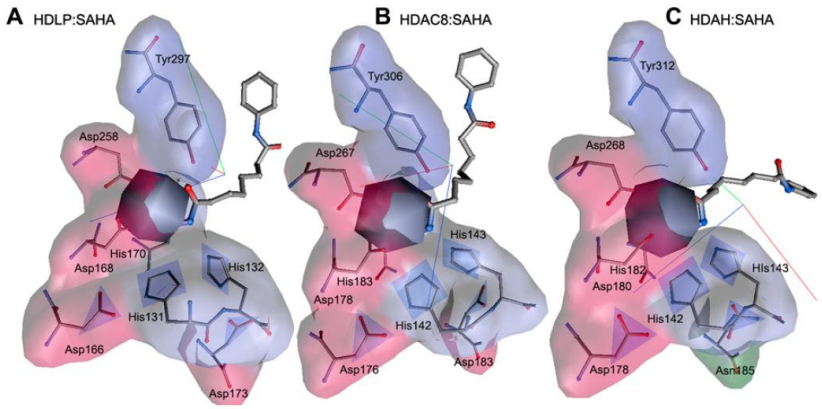

Figure 3.9. Binding mode of SAHA with the catalytic core of HDLP (A), HDAC8 (B) and the bacterial HDAC, HDAH (C).[220]

Several HDACIs have been designed based on a rational approach, starting from the knowledge of the structure of the catalytic site and changing the single motifs that make up the molecule.
HDACIs, according to their structure and to the nature of the ZBG, can be classified in four different groups:

1. Hydroxamates
2. Cyclic peptides
3. Aliphatic acids
4. Benzamides
5. Electrophilic ketones

1) Hydroxamates. Hydroxamate based compounds were among the first compounds to be identified as HDACIs, and these agents helped to define the pharmacophoric model for HDAC inhibitors. The bond with Zn^{2+}, which is essential for the activity, takes place thanks to the hydroxamic acid moiety. This was confirmed by the fact that, by replacing the hydroxamic acid with a carboxylic acid, the molecule becomes completely inactive.[221] Even methylation of the hydroxamic acid causes a drastic drop in activity, which suggests the rigidity of the active site.
In 1990, TSA, one of the major exponent of this class, was identified from a natural product isolated from a *Streptomyces hygroscopicus* strain by Yoshida and coworkers (Fig. 3.10).[221] It has a high activity, with a Ki against HDAC of 3.4 nM.

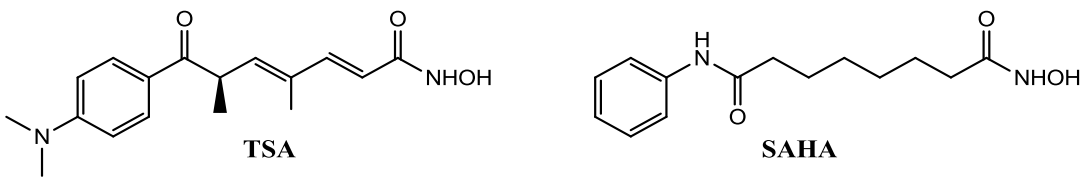

Figure 3.10. Structure of TSA and SAHA.

After that, SAHA was reported by Breslow and co-workers and it was the first HDACi approved by the FDA.[222] It showed an IC_{50} of about 1 nM and provided the binding mode model to the enzyme for this class of inhibitors (Fig. 3.11).

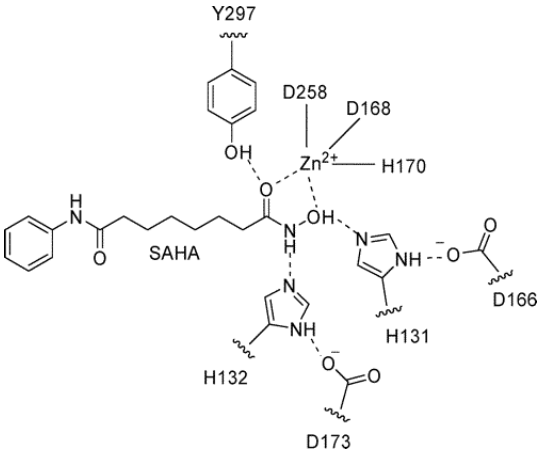

Figure 3.11. Binding mode of SAHA.[223]

From these starting compounds, the optimal length of the linker between the hydroxamic acid moiety and the aromatic nucleus was evaluated: the compound with greater activity appears to be the one with a six-methylene chain. A shorter chain entails a considerable decline of activity, being not sufficient to bring the hydroxamic acid close enough to the ion to be able to chelate it. The capping group, instead, can be modified by introducing different aryl substituents, without varying the activity.

A lot of studies were performed in order to understand the importance of the methyl-substituted olefinic linker in TSA derivatives, and it was shown that the addition of a methyl group and two double bonds caused a 2.3- and 33-fold reduction in activity, respectively, relative to the linear alkyl compounds.[224]

Among the inhibitors containing linear linker domain structures, Oxamflatin (Fig. 3.12), prepared by researchers at Shionogi Laboratories in 1996, is a potent inhibitor with an IC_{50} of 15.7 nM.[225]

Scriptaid was identified by Transcriptional High-Throughput Screening of a library of 16320 compounds. It owns a five methylene aliphatic chain bound to a naphthalene imide ring, which acts as linker between the bulky terminal group and the hydroxamic acid. Also in this case, the importance of the length of the linker was confirmed by the inactivity of Nullscript, which is the Scriptaid analogue with a three methylene shorter chain (Fig. 3.12).[226]

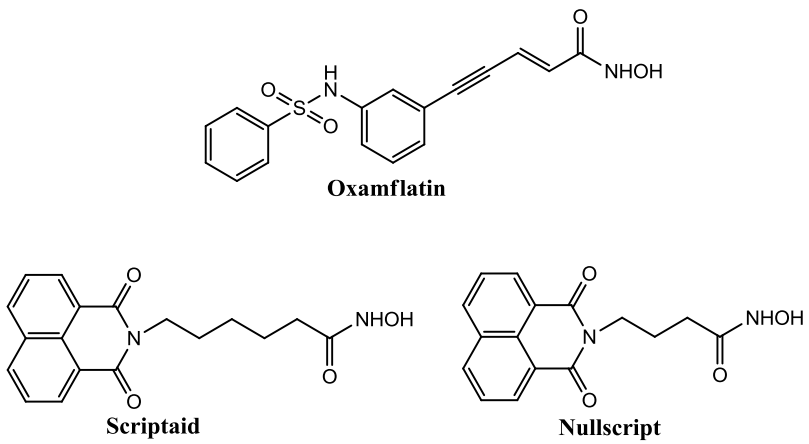

Figure 3.12. Structure of Oxamplatin, Scriptaid and Nullscript.

Taking Scriptaid as starting point and by modifying its capping group, a series of tricyclic derivatives was synthesized and among them, the most active one is compound **VII**, with an IC_{50} of 10 nM. Jung and coworkers also tried to improve SAHA activity through the synthesis of reverse amide SAHA derivatives of general structure **VIII** (Fig. 3.13). The benzene ring of SAHA was changed with substituted benzene rings, all the substituted derivatives show higher activity than the previous ones but that activity is not linked to the chemical features of the substituent.[227] The corresponding carboxylic acids were also tested and found to be inactive.

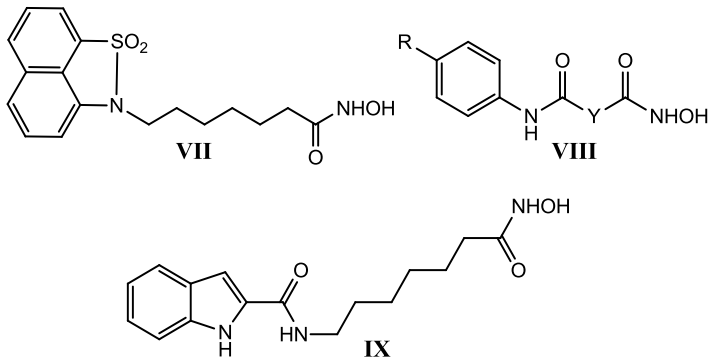

Figure 3.13. Structure of **VIII, IX** and **X**.

SAHA derivatives were obtained also by substituting the benzene capping group of the precursor with heterocyclic rings. Among this series the most interesting compound is compound **IX**, presenting an indole group (IC_{50} = 14 nM) (Fig. 3.13).[228]
Among the hydroxamate inhibitors containing cyclic linker domain substructures, the most famous is CBHA (Fig. 3.14).[198] CBHA demonstrated that is possible to introduce an aromatic ring in the linker maintaining the HDAC inhibitory activity. Starting from CBHA, some CBHA-Oxamflatin derivatives different for the nature and the length of the linker were synthesized; the most active are the compounds with a cinnamic **X** and hydrocinnamic **XI** linker respectively (Fig 3.14). This is probably due not only to the optimal length of the linker, but also to the geometries the compound can assume. The presence of the double bond does

not influence the activity, while the substitution of the α-position of the hydroxamate chain and the methylation of the sulfonamide group cause a loss of activity.[229].

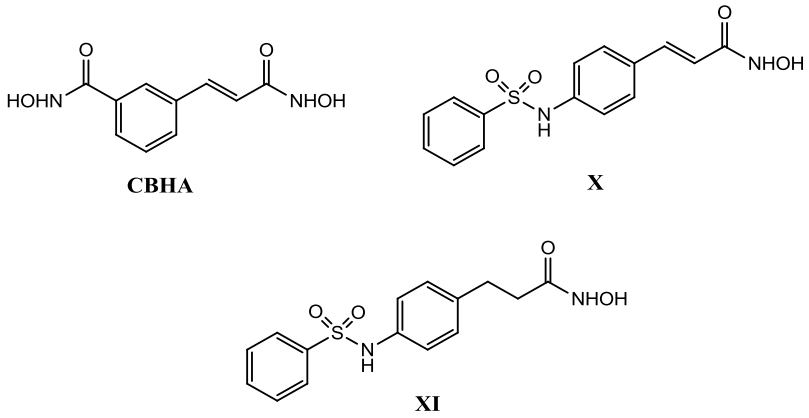

Figure 3.14. Structure of **CBHA**, **X** and **XI**.

Other oxamplatin-CBHA derivatives were designed and CBHA-derived ureas, sulfonamides and sulfonanilides were produced.[230]
Hydroxamic acids are the major class of HDACIs, they are endowed with a high activity (the most potent at nanomolar range) and many compounds are currently published both in patents and in literature. Hydroxamates are very interesting because they also have a great therapeutic potential, so that, some of them have been approved by FDA for the treatment of cancer.

2) Cyclic peptides. Cyclic peptides are the more complex class of HDACIs. They conform to the pharmacophoric model for HDACIs and possess a macrocycle containing hydrophobic amino acids acting as capping group that interacts at the enzyme surface, an alkyl chain as linker and a functional group able to chelate metals. The macrocycle in these agents is arranged with a D-amino acid and a cyclic amino acid (Pro or Pip) flanking the amino acid bearing the linker moiety, which generates a constrained 12-membered cyclic structure with extensive internal hydrogen bonding. The configuration of the amino acid must be the D-configuration, and it is the only case in which a strong association with the rim of the active site is obtained, thus allowing the linker to go through the groove of the enzyme.[231]
These molecules can be divided in two subclasses: inhibitors bearing a (*S*)-2-amino-9,10-epoxy-8-oxodecanoic acid (L-Aoe) moiety and inhibitors without the L-Aoe moiety. While these latter are reversible inhibitors, the cyclic peptides with L-Aoe moiety give an irreversible inhibition, but the binding mode of these compounds is not clear yet. It is possible that the interaction is either due to the formation of covalent bonds via nucleophilic attack of the reactive epoxy ketone in the active site or to the formation of non covalent interactions, not allowing the dissociation of the inhibitor from the active site.[232]
The first inhibitors belonging to this class were discovered through a natural product screening including HC-toxins, Cyl-1/2, WF-3161, chlamydocin and trapoxins A and B, all belonging to the L-Aloe subgroup (Fig 3.15).

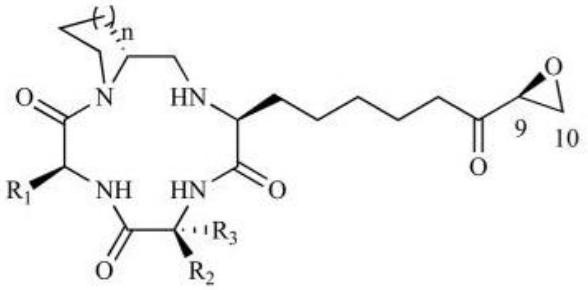

Trapoxin A (R_1=R_2= benzyl, R_3= H, n=2)
Trapoxin B (R_1=R_2= benzyl, R_3= H, n=1)
Chlamydocin (R_1 = benzyl, R_2=R_3= Me, n=1)
HC-Toxin (R_1= R_2 = Me, R_3 = H, n = 1)
Cyl-2 (R_1= ^{s}Bu, R_2= H, R_3= 4-MeObenzyl, n= 2)
WF-3161 (R_1= ^{s}Bu, R_2=H, R_3= benzyl, n= 2)

Figure 3.15. Structure of HC-toxins, Cyl-1/2, WF-3161, chlamydocin and trapoxins A and B.[233]

In these compounds the epoxyketone moiety is essential in order to give an irreversible inhibition; the replacement of that group with other chemical functionalities leads to a decrease in the activity.[234] These compounds are very interesting because, as well as showing a great inhibitory activity, they display a high selectivity: Chlamydocin, Cyl-2, trapoxin A and B show 640 to 57000-fold selectivity for HDAC1 versus HDAC6 with IC_{50} of 110 and 820pM respectively against HDAC1.[235]
The other subgroup of HDACIs with a peptide structure is the one of the molecules without the L-Aoe functionality. Among them Apicidin, a fungal metabolite, contains an (S)-2-amino-8-oxodecanyl side chain lacking of the epoxide functionality and acts as reversible HDACi. It has an IC_{50} = 1 nM, thus demonstrating that also the reversible inhibitor can be very powerful. In 2002, Apicidin analogs called Apicidin A, C, D1, D2 and D3 were isolated by Singh and coworkers (Fig. 3.16).[236] From the inhibitory activity of these molecules emerged that the carbonyl moiety at C8 is very important for the HDAC inhibition, since its removal or reduction cause a high increase in the IC_{50} values.

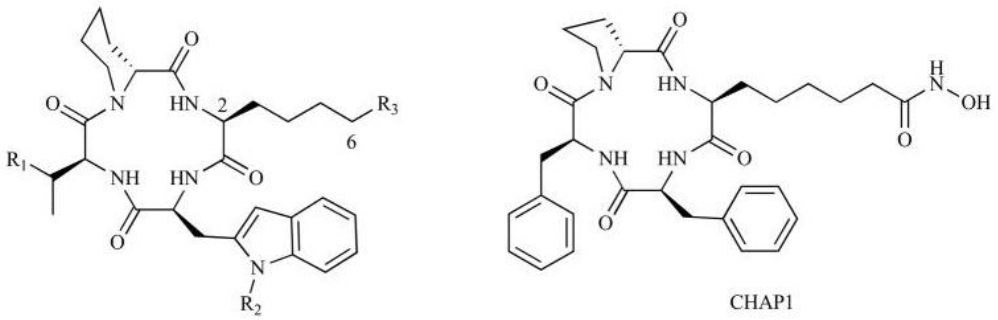

CHAP1

Apicidin (R_1= CH_2CH_3, R_2= OCH_3, R_3= $CH_2COCH_2CH_3$)
Apicidin A (R_1= CH_2CH_3, R_2= H, R_3= $CH_2COCH_2CH_3$)
Apicidin C (R_1= CH_3, R_2= OCH_3, R_3= $CH_2COCH_2CH_3$)
Apicidin D1 (R_1= CH_2CH_3, R_2= OCH_3, R_3= $CH_2COCH(OH)CH_3$
Apicidin D2 (R_1=CH_2CH_3, R_2= OCH_3, R_3= $CH_2CH(S\text{-}OH)CH_2CH_3$)
Apicidin D3 (R_1= CH_2CH_3, R_2= OCH_3, R_3= $CH_2CH_2CH(OH)CH_3$)

Figure 3.16. Structure of Apicidin, Apididin A, C, D1, D2, D3 and CHAP.[209]

That result conforms to the early observation by Colletti and coworkers who conducted SAR studies on the side chain of Apicidin. They found that the reduction of the keto group at C8 position to alcohol or methylene, as well as the conversion to olefin or epoxide, results in the attenuation of the anti-HDAC activity of Apicidin. However, substitution of the ethyl ketone moiety of the Apicidin side chain with a hydroxamic acid, epimeric epoxide or hydroxyketone group allows to obtain analogs with improved HDAC activity respect to Apicidin.[237]

Recently, a new group of cyclic peptides was obtained by substituting the epoxy ketone moiety of Trapoxine and derivatives with a metal binding group, i.e. a hydroxamic acid, to give the cyclic hydroxamic acid-containing peptides (CHAPs) (Fig. 3.14). All CHAPs are nanomolar HDAC inhibitors, particularly the chlamydocin-type CHAP possesses an IC_{50} = 0.44 nM. While Chlamidocin displays a high selectivity for HDAC1 rather than HDAC6 (640-5700 folds), the new molecule does not display the same trend (86 folds). Studies of the chain length between the macrocycle and the hydroxamic acid showed that the compounds that display the better activity are those with a five-methylene unit linker, respect to those with four- and seven-methylene unit linkers. In spite of their lower selectivity, all CHAPs are more drug-like than the parent compounds, in fact they have an improved half-life, due to the absence of the epoxy-ketone group.[235]

Among the cyclic peptides HDACIs, the only one under clinical investigation is FK228, or Romidepsin, a naturally occurring depsipeptide isolated from *Chromobacterium violaceum* (Fig. 3.17).[238, 239] FK228 possesses a bicyclic structure with four amino acids and a β-hydroxyamide moiety, which made up a 16-membered lactone with a disulfide bridge. The binding mode of FK228 was deeply studied and from those studies has emerged that the disulphide bridge is reduced *in vivo* by the glutathione reductase and the deriving butenyl thiol group is able to chelate the Zn^{2+} in the active site of the enzyme.[235] The presence of the thiol groups is crucial for HDAC inhibition, considering that the methylation of the two sulfhydryl groups leads to a high decrease of activity.

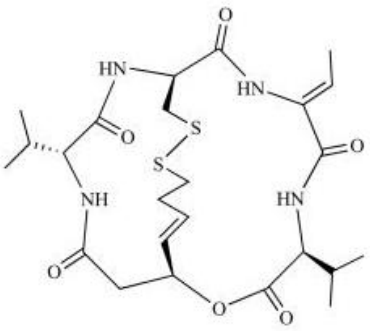

Figure 3.17. Structure of FK228 .

Furthermore, the conformational restriction given by the macrocyle is also important: the cleavage of the macrocyclic ester bond to give a linear peptide results in the complete loss of activity. FK228 is more active for HDAC1 and 2 with an IC_{50} of 36 nM and 47 nM respectively.

Cyclic peptides are very important HDACis either able of reversible and irreversible inhibition. These molecules have also helped in the understanding of the factors governing HDAC inhibitory activity and selectivity. Unfortunately, their druglikeness is poor, so a lot of

efforts have to be made in order to obtain inhibitors belonging to this class presenting an improved pharmacokinetic profile.

3) Aliphatic acids. As a general trend, most carboxylates presenting very simple aliphatic chains possess very low HDAC inhibitory activity, mainly in the millimolar range; but despite the poor activity, they were studied for the treatment of cancer. The carboxylic acid moiety is thought to be a metal-binding group, although the involved inhibition mechanism is not clear.[219] Some members of this class such as butyric acid (BA), phenylbutyric acid (PBA) and valproic acid (VPA) are in clinical trials for the treatment of cancer and spinal muscular atrophy (SMA) (Fig. 3.18). An advantage of these compounds is that, because of their common use as drugs, their toxicity has been extensively studied, thus allowing to shorten the time of the clinical trials.[240, 241]

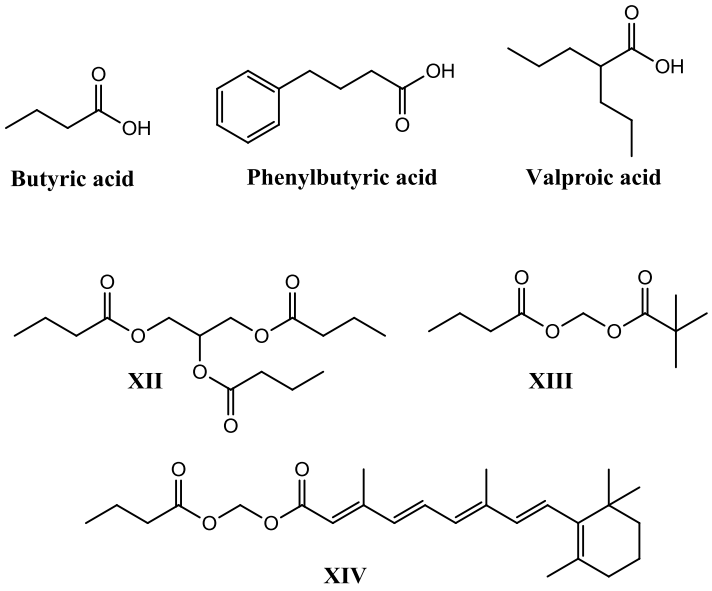

Figure 3.18. Structure of butyric acid, phenylbutyric acid and valproic acid and their derivatives **XII**, **XIII** and **XIV**.

In order to improve the activity of carboxylic acid inhibitors, ameliorate their bioavailability and avoid metabolic degradation, some prodrugs such as **XII**, **XIII** and **XIV** were developed (Fig. 3.18). **XIV** is a molecule combining the structure of BA and all-trans retinoic acid, the two precursors are already used in association for the treatment of highly resistant promyelocytic leukemia.[242,243]

4) Benzamides. The only group instead of the hydroxamic acid moiety that has allowed keeping the HDAC inhibitory activity so far is the benzanilide group. There are two hypothesized binding modes for the inhibition mechanism: the primary aniline group can form hydrogen bonds or other interactions with essential amino acids in the active site; alternatively, benzanilide can chelate Zn^{2+}. The finding that removing the primary aniline or its acetylation gives inactive derivatives supports the first hypothesis. Normally benzamides are less powerful than the corresponding hydroxamic acids; but MS-275 and CI-994, the most

active representatives of this class, have proved to be very interesting HDACIs (Fig. 3.19).[244, 245]

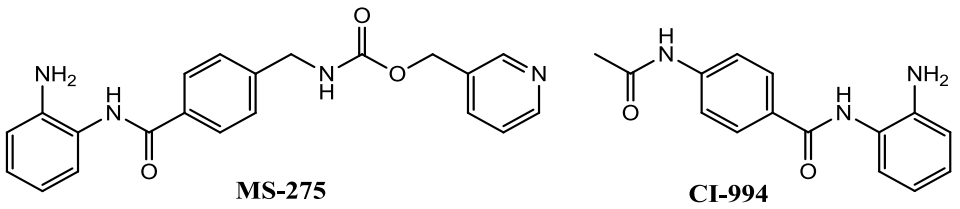

Figure 3.19. Structure of MS-275 and CI-994.

MS-275 is undergoing to clinical trials for the treatment of various cancers and inhibits class I HDACs, specifically the isoforms HDAC1 and HDAC3 with IC_{50} of 0.51 μM and 1.7 μM, respectively. Many SAR studies were performed on MS-275, from which emerged that substitution at the 3, 4, and 5 positions on the benzamide ring attenuates the activity because of steric hindrance. MS-275 inhibitory activity is associated with an increasing expression of p21 and accumulation of cells in G1 phase.[246]
CI-994 derives from the acetylation of dinaline and shows cytostatic effect with concomitant accumulation of cells in G0/G1 phase, a reduction of S phase level and increased apoptosis. It has an IC_{50} of 0.57 μM and exerts antitumor activity against solid tumors. The exact mechanism by which the benzamides exert their antiproliferative effects has not been fully elucidated. Additional studies will be required in order to understand the mechanistic differences between the benzamide and hydroxamic acid classes with regard to HDAC inhibition.

5) Electrophilic ketones. Recently, non-hydroxamate HDACIs containing electrophilic ketones such as trifluoromethyl ketones and α-keto amides, exemplified by trifluoromethyl ketone **XV,** have been reported (Fig. 3.20).[247] The inhibitory activity is due to the hydrated form of the ketone, that is able to coordinated the metal ion; this mechanism of action was demonstrated for carboxypeptidase A, but is probably used with HDAC too.[248] Compound **XV** has an IC_{50} of 2.6 mM and due to its interesting biological activity, SAR studies were performed in order to increase its potency. The connection of the linker with the aromatic rings can be obtained both with an ether or amide junctions; while the most active compounds are those with a linker made up by five or six methylene units. Unsaturations, a small ring (either aromatic or saturated) or heteroatoms such as S and O are also tolerated in the linker. The trifuoromethylketone group cannot be substituted because is essential for the activity. All the compounds derived from **XV** act against HDAC1 and HDAC2 with a high activity, in the low micromolar/high nanomolar range. Their antiproliferative properties occur *in vitro* through histone hyperacetylation and overexpression of p21 gene.

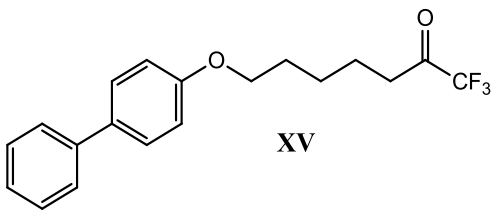

Figure 3.20. Structure of electrophilic ketone **XV**.

A limitation in the use of this class of molecules is due to their short half-life; in fact, they are fastly reduced to the corresponding alcohol. Despite that, these compounds retain high activity and *in vivo* efficacy, probably because also a brief exposure to HDAC inhibitors can induce a biological response. The interesting biological profile of the electrophilic ketone class leads to the search of new representatives with additional structural motifs deriving from other classes of HDACi. These efforts will allow finding optimal design parameters and tolerances and leading to the discovery of more stable molecules.

3.1.2 HDAC inhibitors in combination therapy

Cancer is a complex disease caused by insult to the normal genome and both genetic and epigenetic alterations are involved in tumor initiation and progression.[178] As monotherapies, HDACIs have proved to be effective against some well defined leukemia types but there are increasing evidences that they cannot be used as single agents for the treatment of solid tumors.[249] HDACIs have been used in combination with a lot of other anticancer agents, from cytotoxic drugs and irradiation to small molecule inhibitors of defined molecular cancer targets such as Topo II inhibitors, taxane, mitomycin and Imatinib.[250, 251, 252] Although it is difficult to provide a molecular rationale for combining an HDACi with another agent, it is possible to hypothesize one for cytotoxic agents acting on DNA. These agents act when the cell is in the S phase of the cell cycle that is when the double helix is less compact and not wrapped by histones. The binding of cytotoxic drugs acting on DNA is favored when the macromolecule is in the acetylated form, so a HDAC inhibitors will offer improved access for cytotoxic agents to the target DNA/protein complex through the decondensation of chromatin due to the increased level of acetylation of several histones (Fig. 3.21).[229]

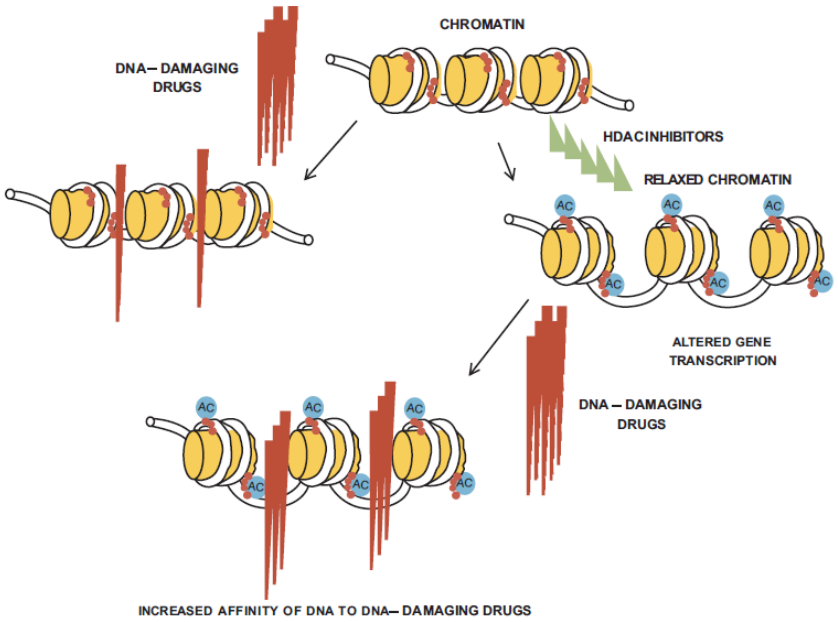

Figure 3.21. Mechanism of action of drugs acting on DNA in the presence and absence of HDACi.[253]

It is important that the treatment with HDACIs precedes or is simultaneous to the administration of the cytotoxic agent because it must make it more accessible to the drug and increase its potency. In addition to the synergistic effects, attributable to increased apoptotic

signals of both compounds, the traditional chemotherapy in combination with HDACIs increases its activity up to 10 times and the action is specific to cancer cells, without the involvement of healthy cells.

There are many example of combination therapy between HDACIs and cytotoxic agents.

Kurz and coworkers showed that the co-administration of Etoposide with sodium butyrate increased sensitivity of HL-60 myeloid leukemia or K562 erythroleukemia cells to etoposide-induced DNA damage and cell death;[254] also valproic acid can facilitate the cell cycle arrest and apoptosis if co-administered with this drug.[255] The administration of TSA with Etoposide increases the apoptosis levels in non-small cell lung carcinoma (NSCLC) and hepatocellular carcinoma cells too.[256, 257]

HDACIs increase the activity of melphalan, an alkylating agent belonging to the group of nitrogen mustards. Particularly its co-administration with Depsipeptide, Vorinostat and VPA leads to growth inhibition in multiple mieloma (MM) cells.[258, 259]

It has also been found an increased anticancer effect of Cisplatin in combination with HDACIs. The synergistic action is due to the changes in chromatin structure, which make DNA more accessible to the covalent modifications, to the changes in DNA interaction with transcriptional regulators, to the decrease of GSH inducted by cisplatin.[260]

Anthracyclines anticancer activity is enhanced by the co-administration with HDACIs. Several HDACis (i.e. TSA, VPA, Entinostat, Panobinostat, sodium butyrate, Vorinostat, Abexinostat) were shown to potentiate the effects of Doxorubicin in many cancer cell lines *in vitro*, *in vivo* and in clinical trials.

Because of the promising results found in preclinical studies utilizing HDAC in combination with other cytotoxic agent and in order to avoid the problems due to the co-administration of different drugs, it might be interesting to develop a MTDL; otherwise a single compound constructed by incorporation of HDACIs into other active agents. Because of the presence of large hydrophobic patches at the HDAC surface rim, it is conceivable that appropriate conjugation of the surface recognition group of a prototypical HDACi to other hydrophobic antitumor pharmacophores could furnish a new class of bifunctional agents. Guerrant et al., combining in one molecule SAHA and the fragment of the drug Daunorubicin, have realized an example of such MTDL design (Fig. 3.22).

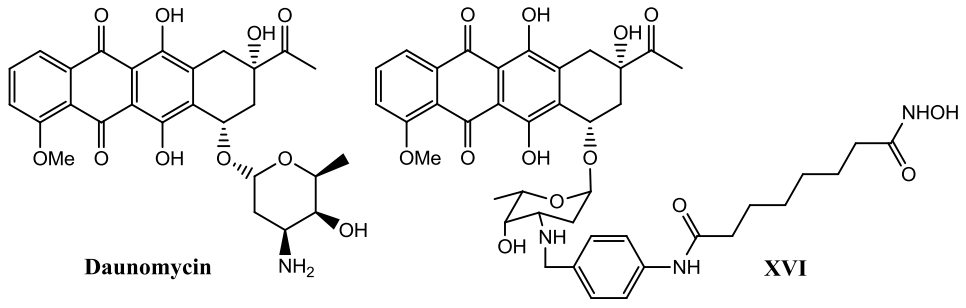

Figure 3.22. Structure of Daunomycin and the MTDL derivative **XVI**.

On this basis, also conjugates of Daunomycin and triazolaryl-hydroxamic acid were designed, considering that triazole may facilitate the recognition by the enzyme. The biological tests have shown that these hybrid molecules lead to an inhibition of the proliferation of some cancer cell lines at micromolar concentrations, thus confirming the compatibility of HDACi

with the Topo II inhibitor. Although their IC_{50} values are lower than those of SAHA and Daunorubicin administered alone, the bifunctional molecules synthesized are very promising, because they allow avoiding the adverse effects due to the pharmacokinetics interaction of two drugs administered separately. The best results were obtained with compound **XVI**, whose cytotoxic activity is in the submicromolar range.[261]

Chapter 4. Polyamine and cancer

Polyamines are basic natural compounds occurring *in vivo* as polycations. They are important cellular components with numerous functions, in particular cell growth. The polyamines physiologically present at the cellular level are the tetramine spermine, the triamine spermidine and the diamine putrescine (Fig. 4.1).

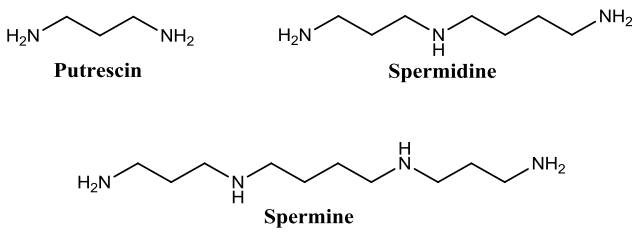

Figure 4.1. Structure of naturally occurring polyamines: putrescine, spermidine and spermine.

These molecules, positively charged at physiological pH, bind via ionic bonds and electrostatic interactions many negatively charged macromolecules such as nucleic acids, proteins, phospholipids and are able to modulate the activity of proteins and organelles. In particular, the charge distribution of spermine makes this polycation able to stabilize the DNA helix against thermal or radiation damage following the formation of bonds with the phosphate groups of the two strands of the macromolecule; spermine also favors the formation of DNA structures typical of mitosis which are characterized by a greater compactness. Thanks to their ability to establish links with DNA and modulate DNA-protein interaction, the polyamines are proposed as cell cycle modulators.

The role of these macromolecules on cell replication has been widely studied and, starting from assessments carried out on cell cultures, it was shown that the concentration of polyamines varies in the different phases of the cell cycle. In particular, in correspondence of the transition phase G1/S, the intracellular concentration of putrescine increases, causing the exit of the cell from the G1 phase prior to the DNA synthesis and promotes the cell incoming in the phase of DNA replication (S). Furthermore, a decrease in polyamine concentration during the G1 phase leads to an increased concentration of the cell cycle inhibitor proteins p21, p27 and p53, which results in the block of the cell cycle. The considerable importance of polyamines in the processes involved in cell proliferation has made clear the involvement of these molecules in carcinogenesis.[262]

4.1 Polyamine synthesis and transport

The polyamines are critical factors for growth regulation, differentiation and cell death: they are present in concentrations in the μM range and their concentration is finely regulated by different control mechanisms, such as the synthesis of precursors of amino acids or uptake of the cell. In cells polyamines are synthesized from the amino acids L-arginine and L-methionine via a series of six enzymatic reactions. Starting from arginine, the enzyme arginase

generates L-ornithine, precursor of putrescine, while for the biosynthesis of spermidine and spermine is critical methionine, which is capable of giving propyl-aminic groups (Fig. 4.2).
The first enzyme involved in the synthesis of these molecules is the ornithine decarboxylase (ODC), which, following the decarboxylation of ornithine, allows to obtain putrescine. Subsequently enzymes spermine and spermidine synthase form respectively spermine and spermidine.[263] The activity of these enzymes is strictly regulated by the availability of the substrate, i.e. the decarboxylated S-adenosylmethionine, which then serves as propyl-aminic group donor and is synthesized by the enzyme S-adenosylmethionine decarboxylase (SAM-DC). The decarboxylases ODC and SAM-DC remain active for a very short time and are highly inducible and, thanks to that, the biosynthesis of polyamines is tightly regulated. Despite the synthesis of polyamines is a non-reversible process, the cell has developed a mechanism to prevent the accumulation of spermine and spermidine involving the spermine/spermidine N1-acetyltransferase enzyme. This enzyme is able to convert the spermine and spermidine in putrescine. The activity of this enzyme is usually very low but it may increase in response to accumulation of polyamines, for example, following exogenous administration. The enzyme uses acetyl-CoA as cofactor to give acetylated spermine and spermidine, which become substrates of N1-acetyl polyaminoxidase (PAO) that is responsible for the conversion of spermine previously in spermidine and then in putrescine.

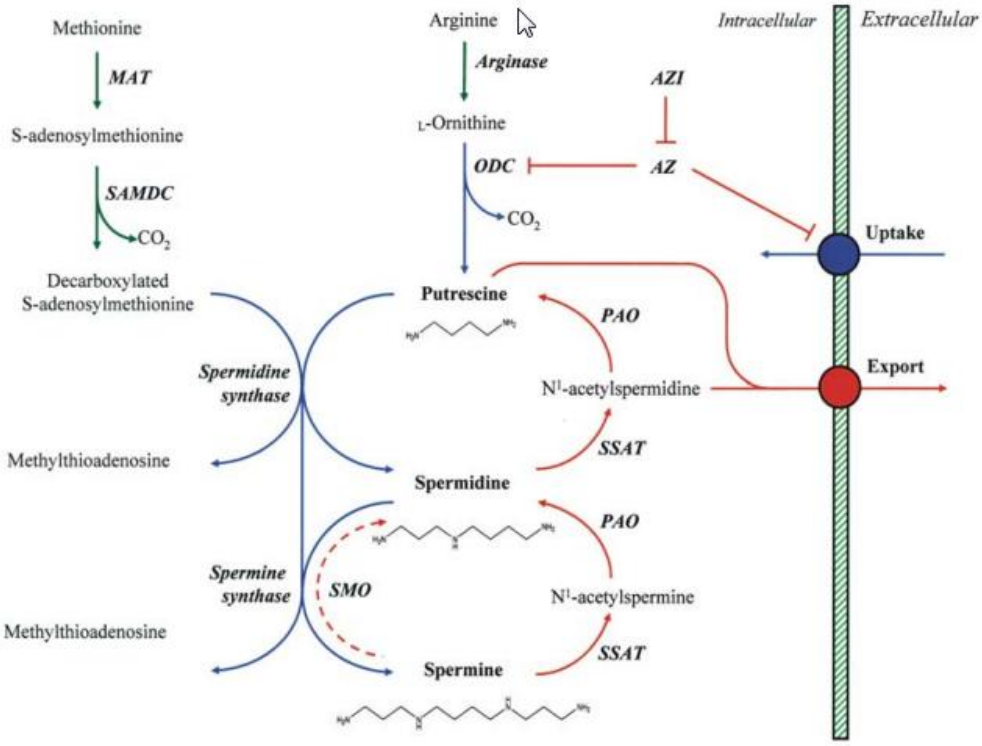

Figure 4.2. Synthesis and metabolism of natural polyamine.[263]

Acetylation leads to the loss of the positive charges of polyamines; furthermore the acetylated form of the molecules are able to permeate the membrane more easily, thus facilitating their removal from the intracellular compartment.
The metabolic pathway mediated by PAO leads to the formation of secondary products such as γ-aminobutyric acid, ammonia, 3-acetamidopropanale and hydrogen peroxide; which accumulation leads to programmed cell death because of their toxic properties.

The concentration of polyamines in cells is mainly due to their endogenous production, but also the transport between the inside and the outside of the cell contributes to their homeostasis. The process of influx of polyamines from the extracellular environment is done by the polyamine transporter system (PTS) in an energy-dependent manner. It is known that PTS acts in a time-, temperature-, concentration- dependent mode and that it is saturable. Although some cells have a single transport system for all the three major polyamines, most of the cells have two different types of carrier, one with affinity for putrescine, able to also transport the other polyamines and one for spermine and spermidine. The putrescine-PTS is a sodium dependent transporter, while the spermine/spermidine-PTS is sodium indipendent. Two different modes for the internalization of these macromolecules by the transporter have been hypothesized: the first model proposes that the polyamines are introduced into the cell through a receptor-mediated endocytosis after their binding to heparan sulphate on a molecule of glypican-1.[264] The second hypothesis describes the need of a negative membrane potential in order to have the transport.[265] The transport from inside to outside the cell instead is a process regulated by the state of cell growth, induced by the decrease of the rate of replication and inhibited by the opposite stimulus.

Cancer cells have a high demand for polyamines to support their rapid growth and, being the endogenous synthesis inadequate to their needs, use the polyamine transporter to import them from the extracellular environment. In contrast, normal cells synthesize individually polyamines for their needs and have a relatively low level of activity of the transporter. As a consequence, the PTS turns out to be overexpressed in cancer cells and that is demonstrated by the fact that radiolabelled putrescine accumulates in brain tumors much more than in the surrounding normal brain parenchyma.[266] More importantly, the PTS is promiscuous so it is able to transport various polyamine-like molecules. The differences in the level of transporter activity between normal and malignant cells provide a mechanism preferentially directing anti-cancer drugs (polyamine-drug conjugates) to cancer cells. The polyamine can be linked to the drug to provide a vector for delivery through the PTS, at the same time reducing the toxic effect on normal cells associated with conventional chemotherapy. In addition, the polyamine vector may increase the activity of cytotoxic drugs acting on DNA by increasing their binding due to the polyamine affinity for DNA.[267]

That approach has not proved to be not so simple as thought, since, as mentioned before, the uptake of polyamines is regulated not only by the PTS but also from other transport systems and the different analogs can bind to different carriers.[268] Moreover the cell itself possesses more systems responsible for the expulsion of these molecules from the cell, depending on the state of growth of the cell itself and therefore of its actual need. Unfortunately, although it has long been known that polyamines are essential in cancer and that their transporter is overexpressed in cancer cells, yet very little is known about the structure and functioning of the latter and the development of drugs that exploit PTS remains a hard goal.

4.2 Polyamine-drug conjugates

As previously stated, polyamines are able to interact with DNA by virtue of their charge distribution that allows the formation of ionic bonds with phosphates, and in particular are able to increase the stability of G-quadruplex structures. Thanks to those properties, polyamines have been used in the design of compounds with antitumor activity joined to other portions. The molecules obtained from this approach are internalized in tumor cells due to the presence of the PTS at the cell membrane level. Being PTS more expressed in the tumor cell types that strategy allows to decrease the side effects induced by the drugs in load of healthy

cells. One of the first synthesized compounds of this class was the Chlorambucil-spermidine conjugate developed by Cohen and coworkers (Fig. 4.3). Chlorambucil is a nitrogen mustard-alkylating agent used for the treatment of some types of leukemia, but its use is strongly limited by the induction of hematological suppression. Its polyamine derivative enters into the cell through the PTS, in fact, its co-administration with difluoromethylornithine (DFMO), an inhibitor of polyamine synthesis, causes an increase of cytotoxicity of 35 fold respect to chlorambucil alone. In addition, the conjugate successfully competed with spermidine for uptake and the presence of the polyamine moiety determines an increase of the affinity towards the DNA of 10000 times.[269]

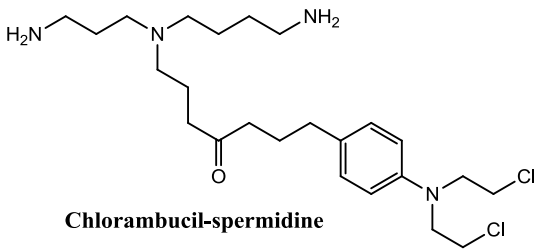

Figure 4.3. Structure of Chlorambucil-spermidine conjugate.

Later Phanstiel and coworkers created a series of polyamine-intercalator conjugates with the dual purpose of facilitating the entry of Topo II inhibitors via the PTS, and to increase the affinity of these agents for the DNA. Such compounds are made up by an aminoacridine (**XXXVI** and **XXXVII**) or anthracene (**XXXVIII** and **XXXIX)** nucleus, therefore able to intercalate, linked to the skeleton of the polyamine spermidine (Fig. 4.4).[270]

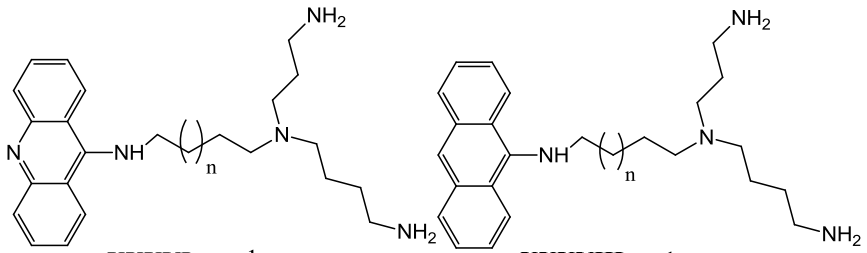

Figure 4.4. Structure of aminoacridine- and antracene-polyamine conjugates.

Further studies have led to affirm that the architecture itself of polyamines is toxic to the cell and the different scaffolds linked to them determine different cytotoxicity. In order to assess the importance of the polyamine structure, Phanstiel synthesized a series of anthracene conjugates in which the number of methylenes between the nitrogen atoms of natural polyamines was varied. The ability of such compounds to enter the cytoplasmic compartment via the PTS in comparison to the natural polyamines has been studied in a detailed manner together with their toxicity against tumor cells. Through cytotoxicity studies carried out on these compounds, it was found that triamine-conjugates have a greater toxicity and are more

internalized than tetramine-conjugates. From the study of the affinity of the different molecules for the PTS were obtained, however, lower Ki values for tetramines in competition experiments involving radiolabeled spermidine. Furthermore it was noted that the length of the methylene spacer between the amino groups has an important effect on the Ki values, with obvious preference by the carrier for the butyl spacer. It was possible to assume tetramines, having lower K_i values, should have been more toxic to malignant cells. Studies of IC_{50} give instead an opposite trend. Studies at the cellular level have shown that triamines bind the cell surface but are easily removed by means of washes because of their low affinity for the PTS. In contrast, the tetramine-conjugates with higher affinity (K_i in nM range) are irreversibly bound to the membrane and remain adherent to the cell surface even after several washings. Triamines, however, have a higher cytotoxicity because they are more internalized by tumor cells (low IC_{50} values). The internalization of polyamines was effectively studied by deconvolution microscopy: initially polyamines placed in contact with the cell surface bind the PTS and are subsequently subjected to endocytosis with the formation of vesicles rich in polyamines within the cell. Triamines have less affinity for the PTS than tetramines, so they can dissociate from the transporter and determine their toxic effects by acting in the cytoplasm, while the tetramines conjugates, tightly bound, can not do that.[271]
A very successful polyamine-drug conjugate is F14152, an etoposide-spermine conjugate synthesized by Barret and coll (Fig. 4.5). This molecule presents all the researched properties for polyamine conjugates: increased cytotoxicity and DNA binding affinity than eEtoposide, uptake through PTS and *in vivo* reduced toxicity. F14152 was 8 time more cytotoxic than the parent compound, due to increased DNA affinity and to its higher concentration in cancer cells and, thanks to its optimal anticancer profile, the compound is now ongoing in clinical trials.[272]

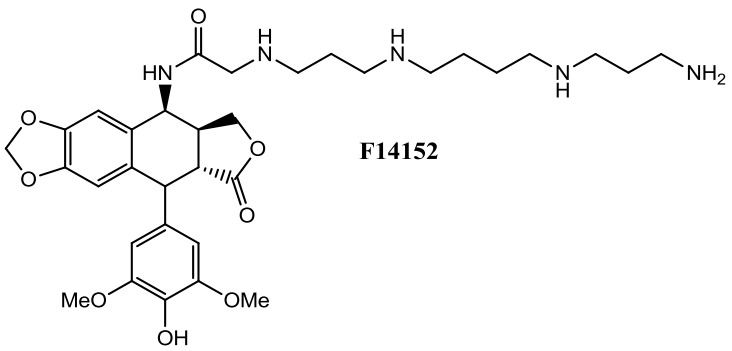

F14152

Figure 4.5. Structure of the Etoposide-spermine conjugate, F14152.

The identification of the mammalian PTS will greatly help in the development of polyamine drug conjugates in the future. Currently, the evidence for their uptake via PTS is obtained indirectly and it cannot be established with safety that these conjugates used the PTS for their internalization.
Despite the lack of knowledge about the structure of the transporter, some effective compounds like F14152 have been developed, thus allowing the identification of the structural requirements necessary for the use of the PTS.

Chapter 5. Naphthalene diimide-polyamine conjugates as Multi-Target-Directed Ligands

5.1 Drug design

The design and synthesis of novel anticancer agents is one of the most active research fields in medicinal chemistry. Many efforts have been spent in the last decades in order to find new potential candidates for the treatment of this complex pathology but, despite those, the drugs that are currently used are characterized by a multitude of side effects deriving from their lack of selectivity for cancer cells.

Particularly, one of the most important classes of cytotoxic agents is represented by molecules able to reversibly interact with DNA, since DNA is involved in cell proliferation and in the cancerogenetic process. Among them, intercalators constitute a large group: they are able to stabilize the double helix through the formation of non covalent bonds with adjacent base pairs. As a consequence, DNA cannot recognize associated proteins like transcription factors or polymerase, leading to replication problems and apoptosis.

As previously highlighted, NDI derivatives are able to act as intercalators and they also have demonstrated their ability to stabilize higher order DNA secondary structures, such as triplex and quadruplex DNAs.

Polyamines are naturally occurring compounds that, because of their protonation at physiological pH, are able to interact with the phosphate residues of the backbone of the DNA and are also involved in cell cycle regulation and apoptotic processes. It has been demonstrated that polyamines are able to interact with different biological counterparts, so that have been considered a "universal template" for the recognition of different targets.[273] Furthermore, polyamines have been studied to achieve the delivery of drugs through the PTS. Their structural diversity can be exploiting for the selective targeting, by varying their length, by inserting appropriate substituents and by varying the number of nitrogen atoms of the polyamine backbone.

My research group has long been involved in the design and synthesis of anticancer compounds based on a NDI scaffold. After the studies conducted by the National Cancer Institute (NCI) on a panel of 60 cell lines the most interesting compounds of our previous NDI series have proved to be **V** and its analogue **VI** in which the *o*-methoxy benzylic ring is replaced with the 2,3,4-trimethoxybenzylic one. In particular the interesting biological profile of symmetric derivatives **V** and **VI**, which makes them promising MTDLs, has stimulated further research in this field. For this reason, these two NDI derivatives were chosen as lead compounds for the structural modifications subject of this project, whose aim was to synthesize polyamine-NDI asymmetric conjugates. This was accomplished by replacing one of the two side chains of **V** and **VI** with a polyamine chain in order to increase, on one hand, the selective cytotoxic activity towards cancer cells thanks to the interaction with G-quadruplex structures and secondly to obtain a selective delivery exploiting the natural PTS (Fig. 5.1). The derivatives **1**-**13** have been obtained by varying the number of nitrogen atoms and the methylene chain length between them. In order to assess the importance of the terminal primary amine function for the recognition by PTS, derivatives **2** and **9**, in which primary amine is monomethylated to a secondary amine, and **13**, lacking of the terminal nitrogen group, were synthesized. Finally, to evaluate the importance of the secondary amine function of the spermine chain for the cell internalization through the PTS and for the

quadruplex targeting profile, compound **11**, in which the inner nitrogen atoms of spermine have been replaced with oxygen atoms, has been designed.

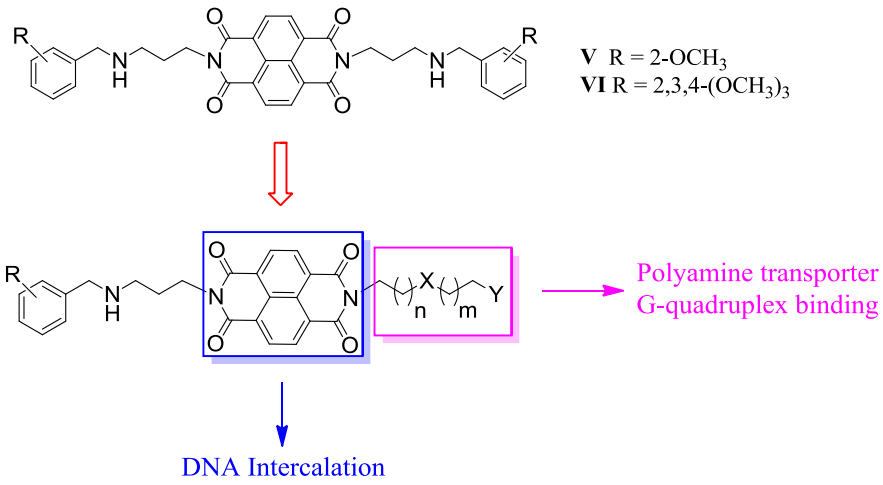

1 n = 2; m = 2; X = NH; Y = NH_2; R = 2-OCH_3
2 n = 2; m = 2; X = NH; Y = $NHCH_3$; R = 2-OCH_3
3 n = 2; m = 3; X = NH; Y = NH_2; R = 2-OCH_3
4 n = 3; m = 2; X = NH; Y = NH_2; R = 2-OCH_3
5 n = 2; m = 1; X = NH; Y = $NH(CH_2)_3NH_2$; R = 2-OCH_3
6 n = 2; m = 2; X = NH; Y = $NH(CH_2)_3NH_2$; R = 2-OCH_3
7 n = 2; m = 3; X = NH; Y = $NH(CH_2)_3NH_2$; R = 2-OCH_3
8 n = 2; m = 3; X = NH; Y = $NH(CH_2)_3NH_2$; R = 2,3,4-$(OCH_3)_3$
9 n = 2; m = 3; X = NH; Y = $NH(CH_2)_3NHCH_3$; R = 2-OCH_3
10 n = 2; m = 3; X = NH; Y = $NH(CH_2)_4NH_2$; R = 2-OCH_3
11 n = 2; m = 3; X = O; Y = $O(CH_2)_3NH_2$; R = 2-OCH_3
12 n = 2; X = NH_2; R = 2-OCH_3
13 n = 1; X = H; R = 2-OCH_3

Figure 5.1. Drug design of the NDI-polyamine conjugates.

5.2 Methods

5.2.1 Chemistry

Compound **1-13** were synthesized according to Schemes 5.3 and 5.4.
Intermediates **40** or **41** and the appropriate protected polyamines **23, 24, 27, 38, 39, 42-46, 18** and ethylamine **58** were condensed with 1,4,5,8-naphthalenetetracarboxylic dianhydride (NTCDA) to give the intermediates **47-57, 59** and **60**. The NDI intermediates were deprotected through acidic hydrolysis to give the final compounds **1-13**.
The diamines **40** and **41**, **18** and **19** and the protected polyamines **28, 29** and **42-46** were prepared according to literature procedures.[141, 274, 275] The protected polyamines **23, 24** and **27** were prepared following the procedure reported in scheme 5.1.
1,3-diaminopropane and 1,4-diaminobutane were selectively protected at one of the two basic functions using di-tert-butyl dicarbonate to give, respectively, the intermediates **18** and **19**. 3-amino-1-propanol and 4-amino-1-butanol were protected at the amino group as trifluoroacetic acid esters to give the intermediates **14** and **15**, respectively. After activation of the hydroxyl group of **14** and **15** with tosyl chloride, the corresponding tosylates **16** and **17** were condensed with **18** or **19** to provide the derivatives **20**, **21** and **22**. The basic hydrolysis of **20** and **21** led

to the removal of the trifluoroacetate protecting group giving the intermediates **23** and **24**. **22** was further reacted with di-tert-butyl dicarbonate to obtain the protected polyamine **25**, that underwent to condensation with **16** and then again to basic hydrolysis to afford **27**.
The protected polyamines **38** and **39** were obtained following the procedure reported in Scheme 5.2.
Polyamine **28** and **29** protected on the secondary basic groups, were treated with benzaldehyde to afford the corresponding Schiff bases, reduced *in situ* with sodium borohydride to obtain **30** and **31,** respectively. The latter were protected at the primary amine function as trifluoroacetic acid esters obtaining **32** and **33** that were converted in **34** and **35** through methylation of the benzyl amino group. The basic hydrolysis of the trifluoroacetic esters followed by removal of the benzylic protecting group through catalytic hydrogenation, allowed to obtain compounds **38** and **39**.

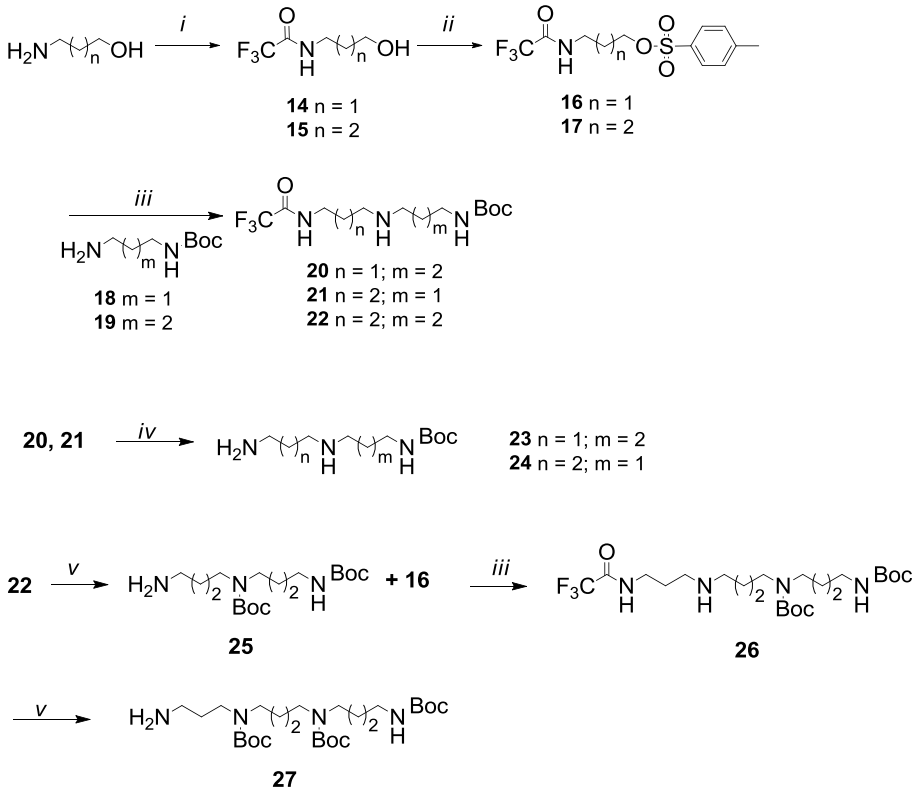

Scheme 5.1. (i) $EtOCOCF_3$, r.t., 1 h; (*ii*) Tosyl chloride, Et_3N, DIMAP, CH_2Cl_2, r.t., overnight; (*iii*) THF, r.t., 16 h; (*iv*) NaOH 40% p/p, MeOH, r.t., 16 h; (*v*) a) Boc_2O, MeOH, r.t., 16 h; b) NaOH 40% p/p, r.t., 12 h. Boc = $(CH_3)_3COCO$-

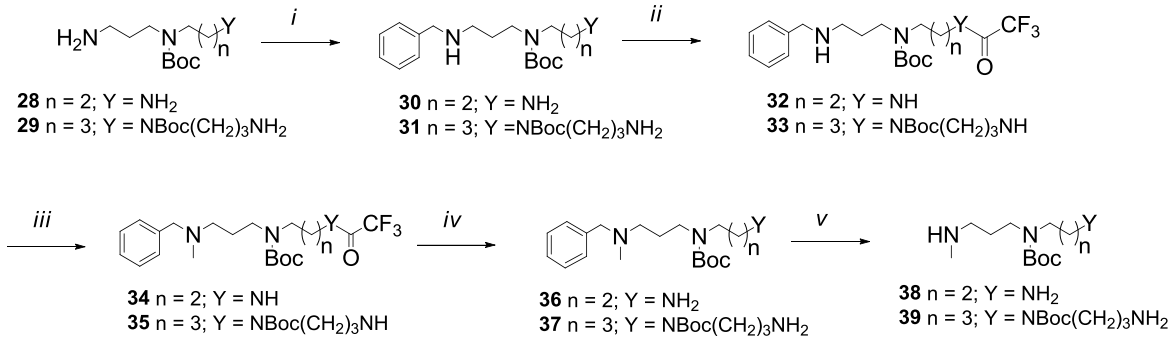

Scheme 5.2. (*i*) a) Benzaldehyde, MeOH, reflux, 5 h, b) $NaBH_4$, EtOH, r.t., 16 h; (*ii*) $EtOCOCF_3$, NEt3, r.t., 16 h; (*iii*) MeI, Et_3N, THF, r.t., 24 h; (*iv*) NaOH 40% p/p, MeOH, r.t., 16 h; (*v*) H_2/Pd, MeOH, r.t., 5 h.

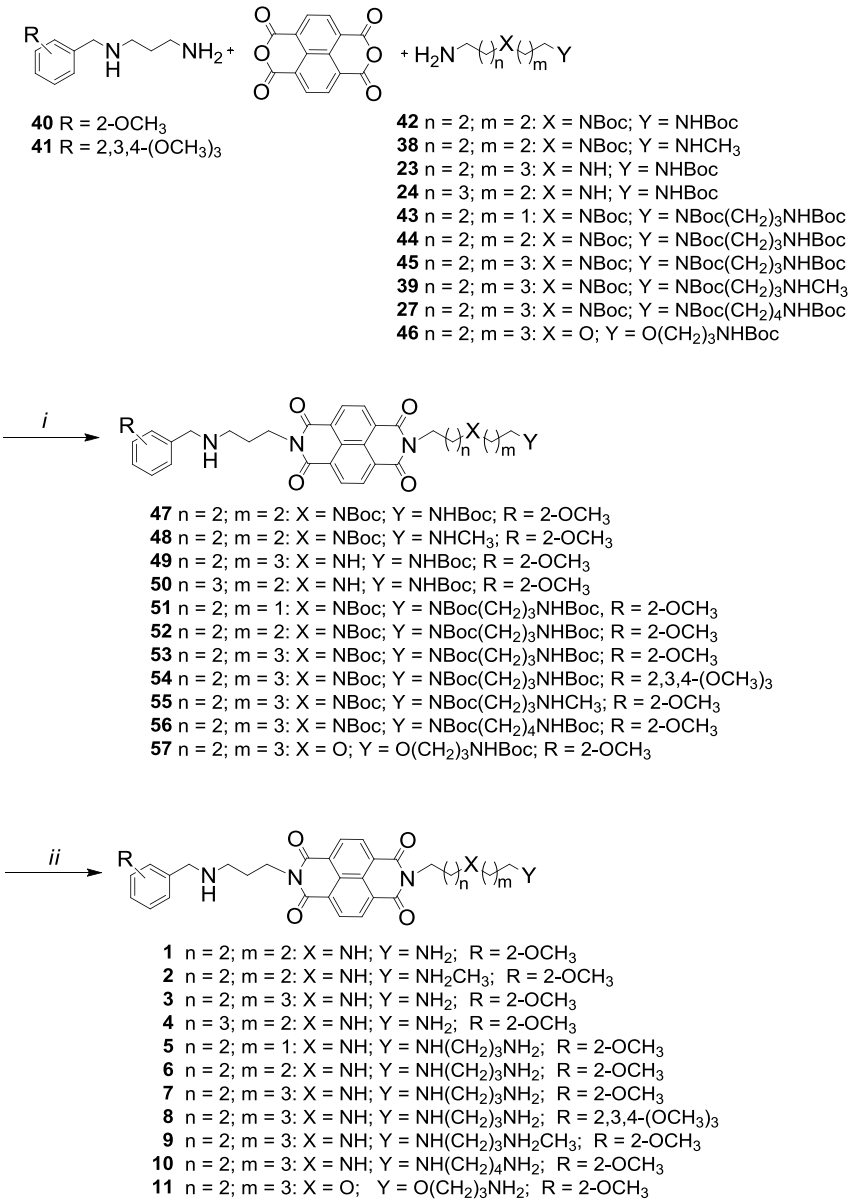

Scheme 5.3. (*i*) DMF, reflux, 3 h; (*ii*) HCl 3M, r.t., overnight.

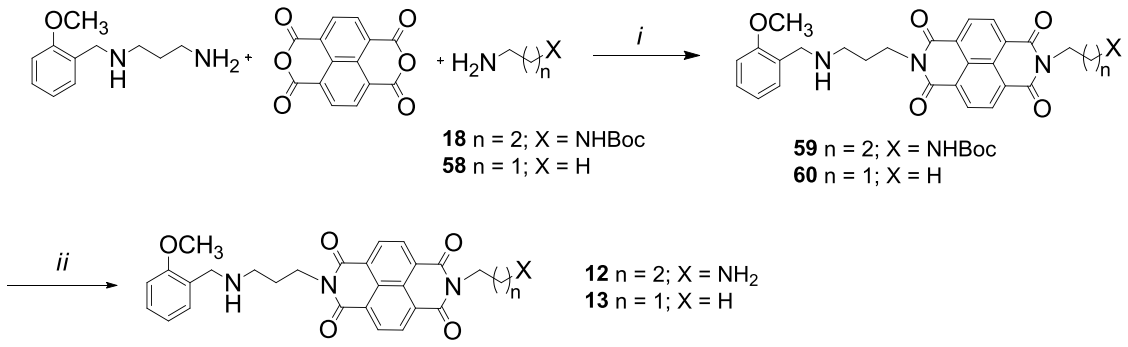

Scheme 5.4. (*i*) DMF, reflux, 3h; (*ii*) HCl 3M, r.t., overnight for **12**/ Et_2O/HCl for **13**.

5.2.2 Biophysical Evaluation

The G-quadruplex binding ability of compounds **1-13** was assessed by Fluorescence Resonance Energy Transfer (FRET) melting technique. Values are expressed as the melting temperature difference between the nucleotide with drug and the negative control (ΔTm).

5.2.3 Biology

Derivatives **1-13** were submitted to the Developmental Therapeutics Program (DTP) at National Cancer Institute (NCI) for evaluation of their antiproliferative activity against 60 human cancer cell lines derived from nine human cancer cell types, grouped in sub-panel disease including leukemia, non-small-cell lung, colon, central nervous system, melanoma, ovarian, renal, prostate, and breast cancer cell lines.
The derivatives were further tested to assess their ability to enter the cancer cells exploiting the PTS by evaluating the increase in the cytotoxic activity in presence of DFMO and aminoguanidine and for their ability to block Topo.

5.2.4 Computational studies

With the aim to investigate the binding mode of the most promisinng compounds **3**, **7**, **8**, **11** and **V** for duplex and G-quadruplex DNA, docking simulation were performed using the available crystallographic structures from the Protein Data Bank (PDB).

5.3 Results and discussion

As preliminary screening compounds **1-13** were submitted to the Developmental Therapeutics Program (DTP) at National Cancer Institute (NCI) for the evaluation of their anticancer activity against different cancer human cell lines, that have been grouped in disease sub-panels including leukemia, non-small-cell lung, colon, central nervous system, melanoma, ovarian, renal, prostate, and breast tumor cell lines. The compounds have been dissolved in dimethyl sulfoxide and evaluated at five concentrations at 10-fold dilution, the highest being 10^{-4} M. All the compounds were accepted except compound **6**, due to its low cytotoxicity in a preliminary assay. The results relative to the most promising cell lines are showed in Table 5.1 and are expressed as the negative log of the molar concentration at three assay end points: the 50%

growth inhibitory power (pGI_{50}), the cytostatic effect (pTGI = total growth inhibition) and the cytotoxic effect (pLC_{50}).

Table 5.1. Growth inhibition, cytostatic and cytotoxic activity of **1-5**, **7-13** and **V-VI** in the 60-Cell Panel.

	modes	Leukemia (SR)	NSCLC (NCI-H522)	Colon (COLO205)	CNS (SF-268)	Melanoma (SK-MEL-5)	Ovarian (OVCAR-4)	Renal (RXF393)	Prostate (PC-3)	Breast (MDA-MB-468)
1	pGI_{50}	7.49	6.05	6.37	6.39	6.28	6.18	6.64	6.07	6.24
	pTGI	4.57	5.56	5.75	5.12	5.72	5.68	5.73	5.20	5.46
	pLC_{50}	<4	5.11	5.31	4.42	5.33	5.33	5.29	<4	4.78
2	pGI_{50}	6.57	5.91	6.30	5.99	5.96	6.18	5.72	5.80	6.00
	pTGI	5.61	5.55	5.73	5.04	5.63	5.69	5.24	4.99	5.56
	pLC_{50}	<4	5.18	5.29	4.44	5.31	5.32	4.48	4.09	5.11
3	pGI_{50}	7.12	6.76	6.96	6.57	6.82	6.81	6.70	6.39	7.07
	pTGI	5.94	6.46	6.61	5.98	6.54	6.50	6.06	5.32	6.66
	pLC_{50}	<4	6.15	6.27	5.18	6.27	6.20	5.47	4.17	6.30
4	pGI_{50}	6.57	5.87	6.69	5.95	6.77	6.78	6.28	5.61	6.79
	pTGI	<4	5.49	6.40	5.14	6.45	6.45	5.69	4.84	6.44
	pLC_{50}	<4	5.11	6.11	4.34	6.13	6.13	5.24	<4	6.09
5	pGI_{50}	6.05	5.91	5.65	5.67	5.80	6.33	5.78	5.23	6.34
	pTGI	4.71	5.43	4.99	4.93	5.52	5.77	5.15	4.10	5.65
	pLC_{50}	<4	4.76	4.30	4.21	5.24	5.38	4.27	<4	5.06
7	pGI_{50}	6.43	6.75	6.81	6.53	6.81	6.78	6.45	6.30	6.88
	pTGI	5.27	6.44	6.52	5.79	6.54	6.50	5.88	5.34	6.56
	pLC_{50}	<4	6.13	6.24	4.54	5.55	6.21	5.37	<4	6.24
8	pGI_{50}	5.88	5.81	6.71	6.02	6.27	5.99	5.87	5.62	6.81
	pTGI	4.76	5.48	6.41	4.88	5.75	5.51	5.44	4.58	6.48
	pLC_{50}	<4	4.33	6.10	<4	4.80	5.03	5.00	<4	6.14
9	pGI_{50}	5.35	5.25	5.86	5.45	6.09	5.77	5.42	5.13	5.72
	pTGI	4.36	4.56	5.09	4.35	5.52	5.04	4.71	4.35	4.93
	pLC_{50}	<4	4.00	4.43	<4	5.00	<4	4.17	<4	4.28
10	pGI_{50}	5.56	5.87	6.48	5.72	6.30	6.42	5.70	5.61	6.49
	pTGI	4.79	5.36	5.90	5.01	5.73	5.81	5.03	5.10	5.86
	pLC_{50}	<4	4.58	5.36	4.07	5.36	5.33	4.30	4.25	5.16
11	pGI_{50}	6.46	5.86	6.60	5.87	6.55	6.62	6.09	5.86	6.59
	pTGI	5.28	5.51	6.29	5.51	5.91	5.65	5.52	5.38	5.89
	pLC_{50}	<4	5.17	5.96	5.15	5.43	5.27	5.19	4.87	5.10
12	pGI_{50}	6.78	5.81	6.24	5.91	6.61	6.59	6.42	5.78	6.39
	pTGI	6.20	5.52	5.74	5.43	6.15	5.97	5.83	5.38	5.78
	pLC_{50}	<4	5.23	5.32	4.88	5.59	5.47	5.40	4.95	5.28
13	pGI_{50}	6.30	6.32	6.70	5.91	6.75	6.82	6.02	5.97	6.35
	pTGI	4.89	5.67	6.43	5.29	6.46	6.46	5.63	5.06	5.66
	pLC_{50}	<4	5.06	6.17	4.56	6.17	6.11	5.24	<4	4.96
V	pGI_{50}	6.58	6.83	6.85	6.46	6.79	6.90	6.81	6.69	6.80
	pTGI	6.03	6.61	6.55	5.83	6.52	6.59	6.52	6.23	6.51
	pLC_{50}	<4	6.20	6.25	5.33	6.26	6.29	6.23	5.46	6.21
VI	pGI_{50}	6.78	7.11	7.45	6.93	7.10	7.25	7.09	7.05	7.09
	pTGI	6.19	6.81	7.01	6.47	6.83	6.94	6.78	6.68	6.81
	pLC_{50}	4.30	6.50	6.66	5.72	6.56	6.62	6.47	6.30	6.50

The analysis of the results reported in Table 5.1, showed that the most cytotoxic compound is **3**, bearing the spermidine chain; **7**, the spermine-like derivative, is the second most active compound, thus indicating a preference of the cancer cells for the natural polyamine carriers.
In compound related to **3** and **7**, the decrease of the number of methylenes between the inner nitrogen atoms, providing **1**, **5** and **6**, causes a decrease of the cytotoxic activity that is more pronounced in the spermine-like derivatives. The substituents on the aromatic ring are also able to influence the activity, in fact, compound **8**, bearing a 2,3,4-trimethoxy substituent on the phenyl ring, is less active than the omologue **7**; for that reason all the derivatives (except **8**) contain an *o*-methoxy substituent.
The methylation of the terminal nitrogen atom in **2** and **9** negatively influence the cytotoxicity of the NDI derivatives, probably because the presence of a terminal primary amine funcion is necessary for the PTS-mediated transport into the cell.
Compound **11**, in which the inner nitrogen atoms of spermine have been substituted with oxygen atoms in order to investigate their influence in the PTS-mediated internalization, shows a lower cytotoxic activity than the spermine derivative **7** but higher compared to the shorter derivatives **5** and **6**. This finding allows to hypothesize that the presence of the secondary amine functions does not influence the delivery through the PTS or the existence of another mechanism of action/transport for the oxygen-containing derivative. This latter hypothesis is confirmed by the fact that also **12** that does not incorporate in its structure a basic nitrogen atom, is quite active towards all the cancer cell lines tested: this NDI derivative cannot use the PTS to gain into the cell, so another expedient to enter the cells must be used.
All the synthesized derivatives do not show any selectivity towards a specific cancer cell line.
All the compounds, including **6** not selected by the NCI, have been tested to evaluate their ability to exploit the PTS to enter into the cells. For that purpose, previously the IC_{50} towards HL60 leukemia cells after 24 h has been assessed. As it can be seen from table 5.2, the results obtained are in line with the ones obtained from the NCI screening.
The most active compound is still **3**, with a cytotoxicity similar to the one exhibited by the lead compound **V**.
The same experiment has been repeated after pre-treatment of the cells with DFMO. DFMO is a polyamine synthesis inhibitor; therefore, the pre-treatment with DFMO leads to a decrease of the intercellular level of polyamines and increases the compounds' import from the external cellular environment. The results of the investigation are reported in table 5.2. Compounds **5-8**, bearing a tetramine group, exert more elevated cytotoxic activity against DFMO-treated cells with a decrease of IC_{50} values, unlike **3** and the reference compound. These results allow us to advance the hypothesis that PTS is involved in delivering **5-8** inside the cell and they are preferred by PTS instead of **3**, suggesting that at least three cationic heads are needed to interact with the transporter. These results confirm the robustness of the rational drug design.
To further validate the use of the PTS to gain into the cells, the same experiment was conducted in the presence of aminoguanidine, an inhibitor of the enzymes involved in the metabolism of natural polyamines (PAO). The results obtained are a little controversial. As reported in table 5.2, all the compounds except the lead compound **V** and the asymmetric NDI **11**, in which the inner nitrogen atoms are replaced with oxygen atoms, show a decrease in the cytotoxic activity in the presence of aminoguanidine. These results lead to the hypotesis that the polyamine chains are PAO substrates in the cell and that the cytotoxicity is due to the products deriving from their degradation. Compounds **V** and **11**, bearing no polyamine carriers, are not substrates for the PAO; for that reason, their IC_{50} is not correlated to the presence of the aminoguanidine.

Table 5.2. Cytotoxic activity (mg/ml) of compounds **1-13** towards HL-60 cells (column 2), after pre-treatment with DFMO (5 mM) (column 3) and after treatment with aminoguanidine (1 mM) (column 4).

Compound	HL-60	+ DFMO (5mM)	+ AG (1mM)
1	**7.45**	**8.77**	**19.00**
2	**n.d.**	**n.d.**	**n.d.**
3	**2.64**	**2.67**	**37.50**
4	**6.02**	**7.82**	**19.07**
5	**16.14**	**9.00 (-45%)**	**26.17**
6	**16.00**	**5.25 (-67%)**	**37.50**
7	**5.60**	**3.67 (-35%)**	**23.17**
8	**7.43**	**2.70 (-63%)**	**26.00**
9	**n.d.**	**n.d.**	**n.d.**
10	**n.d.**	**n.d.**	**n.d.**
11	**4.84**	**4.58**	**4.90**
12	**n.d.**	**n.d.**	**n.d.**
13	**n.d.**	**n.d.**	**n.d.**
V	**2.22**	**1.76**	**1.83**

We are currently waiting for compounds **2** and **9** to be tested: the results for these two derivatives should elucidate if the presence of a primary amine function is required to obtain the PTS recognition and further could give insight into the PAO-mediated catabolism. The terminal methyl group should avoid the PAO-mediated metabolism, so the IC_{50} for the derivatives should not change in presence of aminoguanidine.

All the compounds have also been tested for their ability to bind G-quadruplex structures using the Fluorescence Resonance Energy Transfer (FRET) melting technique. G-quadruplex and duplex DNA recognition by the synthesized compounds was evaluated through fluorescence quenching melting assay using a G-quadruplex folded sequence based on the human telomeric sequence (G4) and a 18-bp random double stranded DNA (dsDNA), in order to assess their quadruplex binding activity and selectivity. The results obtained are reported in table 5.3.

As emerged from figure 5.2, all the synthesized derivatives are able to significantly increase the tested Htel22 melting temperature in a concentration dependent manner. It emerged that the increment in the melting temperature was generally more intense for the G-quadruplex folded sequence than for the dsDNA template, thus indicating the presence of some kind of selectivity. However, on both substrates, the process appeared to reach saturation in the low micromolar range, which suggests a strong interaction with both DNA arrangements.

The most efficient G-quadruplex binder is **3** that causes an increment in the quadruplex melting temperature of 24.26 ºC and 29.30 ºC at 1 and 2.5 µM concentrations, respectively. At the lower concentration the derivative proves also to be selective, in fact the increasing in the melting temperature of the double stranded DNA is only 2.33 ºC. The selectivity is lost by increasing the dose. It is very interesting to note that the oxigen containing derivative **11** is still able to bind the quadruplex sequence, probably thanks to the presence of the primary amine function, more efficiently compared to duplex DNA. The presence of the oxigen atoms is able to influence the binding mode of this derivative, allowing the compound to display a high selectivity for the quadruplex form. Compound **13** does not present a polyamine chain, as a consequence it does not present any quadruplex stabilizing activity, while the NDI **12**,

possessing only a primary nitrogen atom, has a lower affinity for the quadruplex respect to the other polyamine conjugated NDIs, its behavior is very similar to the one displayed by **11.**

Table 5.3. Fluorescence quenching melting on dsDNA and G4 of compounds **1-13** and **V-VI** induced by 1 µM (black) and 2.5 µM (red) drug concentrations. Errors were 0.4 ºC.

Compound	Htel22	DsDNA
1	4.44 / 13.26	2.04 / 6.98
2	4.45/ 18.01	2.87 / 9.05
3	24.26 / 29.30	2.33 / 12.19
4	10.93 / 22.15	2.33 / 9.12
5	5.88 / 22.00	1.81 / 10.42
6	4.75 / 16.29	3.82 / 13.40
7	2.49 / 21.40	1.21 / 6.70
8	4.14 / 13.11	1.40 / 12.57
9	9.79 / 26.06	7.92 / 17.12
10	n.d.	n.d.
11	2.56 / 12.89	0.47 / 1.49
12	5.80 / 11.38	2.64 / 6.71
13	0.83 / 2.41	0.23 / 0.9
V	15.50	7.70
VI	20.50	8.40

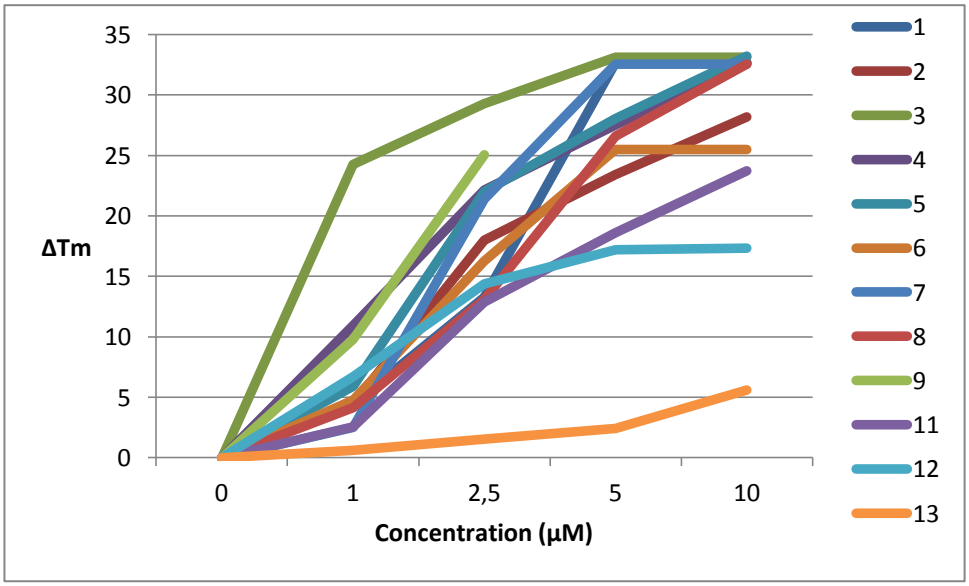

Figure 5.2. Variation of DNA (0.25 µM) thermal stability (ΔTm °C) produced by compounds **1-13** in 50 mM potassium buffer, pH 7.4, evaluated by fluorescence quenching melting experiments. Heating rate 1 °C/min. at increasing concentration of the NDIs derivatives on G-quadruplex folded telomeric sequence.

In general, it can be state that the trend showed is unusual: the introduction of additional charges does not increase the quadruplex binding affinity. The spermidine-derivatives **3** and **4** are in fact more active than the tetramine-derived compounds, thus indicating that the presence of an additional cationic group does not influence the binding. Among the lead compounds **V** and **VI**, the presence of the 2,3,4-trimethoxy substituent on the aromatic ring positively influences both the duplex and quadruplex stabilization. This phenomenon is not displayed in the NDI-polyamine conjugate series: compound **7** is a stronger binder than **8**, probably

because the presence of the polyamine chain is responsible for a different mode of interaction between the molecule and the DNAs.
In addition to G-quadruplexes, double stranded DNA represents a confirmed target for NDI, that have proved to be responsible for the modulation of the activity of DNA processing enzymes, thanks to the formation of NDI-DNA complexes. Thus, agarose electrophoresis has been performed to assess the DNA binding and the potential influence on Topo activity of these compounds.
The DNA binding activity was proved using the plasmid pBR322: the plasmid pBR322 results shifted in the gel by the presence of increasing concentrations of NDIs (Fig.5.3), proving the interaction of the ligands with the DNA; indeed, the binding causes a reduction of the net negative charge of the macromolecule and, eventually, an alteration of its hydrodynamic volumes. In particular, the derivative endowed with a major DNA-binding ability is **1**, followed by **4**, **3**, **V** and finally **VI** respectively. Again the triamine derivatives has demonstrated to be not only the most cytotoxic derivatives and the best quadruplex binders but also the best DNA interacting agents, thus allowing to consider them the most interesting molecules within the series.

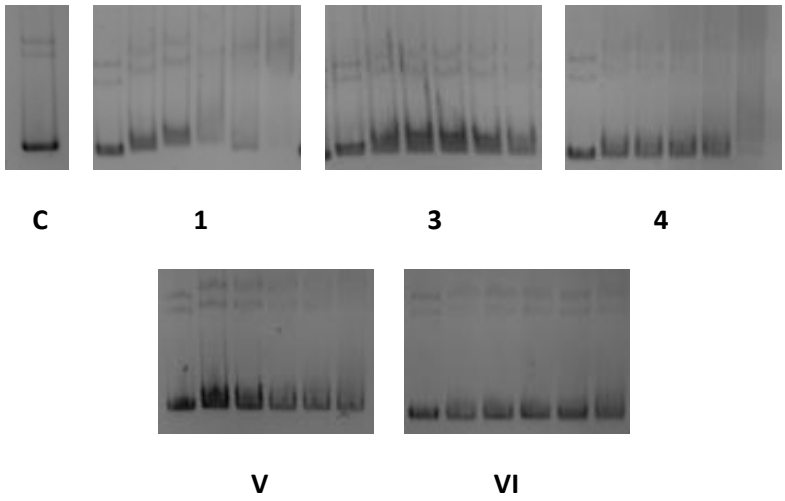

Figure 5.3. pBR322 DNA binding test: C (negative control) pBR322 alone and pBR322 incubated with **1, 3, 4**, **V**, **VI** at the concentrations of 1 (lane 1), 5 (lane 2), 10 (lane 3), 25 (lane 4), 50 (lane 5) and 100 (lane 6) µM.

The same compounds were used to verify the impairment of the ability of TAQ polymerase to duplicate a template. The efficiency in the interference respects perfectly the trend showed in the previous test. The concentrations inducing TAQ inhibition are reported in table 5.4. The new asymmetric derivatives are more active than the parent compounds **V** and **VI** towards the TAQ polimerase, thus confirming their ability to block the DNA replication, and compound **1** proved to be the best one within the series.

Table 5.4. TAQ and topoisomerase inhibition induced by compounds **1, 3, 4, 7, 10**, **V** and **VI**.

Compound	Taq inhibition	IC50 Topoisomerase
1	>0.25 µM	1.5 µM
3	>0.5 µM	8 µM
4	>0.5 µM	7 µM
7	nd	3 µM
10	nd	8.5 µM
V	>10 µM	18 µM
VI	>40 µM	12 µM

Compounds **1**, **3**, **4**, **7** and **10** and the lead compounds **V** and **VI** were also evaluated for the recombinant human DNA Topo IIα to verify whether they have any effect on its activity as Topo IIα inhibitors or poisons. Topo IIα is the target of widely used anticancer drugs (ie Etoposide, anthracyclines and Mitoxantrone), whose function is to avoid the DNA superhelical tension and knots, allowing replicative and transcriptional events.
It is possible to distinguish two different classes of topoisomerase IIα inhibitors: the poisons, able to stabilize the covalent DNA topoisomerase IIα complex, and catalytic inhibitors, agents acting on any other steps in the catalytic cycle.
In order to do this, after1 h incubation, the reaction mixture was added of 200 mM NaCl and 0.1% sodium dodecyl sulphate (SDS): the high ionic strength allows to break potential DNA-topoisomerase covalent adducts which would cause a reduction of the nucleic acid electrophoretic mobility, whereas the SDS remove the DNA-ligand interaction. As a result, variations on the electrophoretic run rely only on the activity of the enzyme before loading.
When the substrate is the supercoiled form of pBR322, topoisomerase induces its relaxation and thus produces a form with a reduced electrophoretic mobility.
Figure 5.4 shows that almost all the tested compounds interfere with topoisomerase activity in the low micromolar range, with **1** being the most effective and **3** the worst. That can be correlated to the higher quadruplex binding activity of **3.** Taken in account the last result, it is possible to hypothesize a potential selective DNA recognition process. All the new derivatives are more potent than **V** and **VI** in inhibiting the enzyme, probably due to the improvement in the DNA binding properties. The same compounds were tested in the telomerase IIα poisoning assay, but none of them produced inhibition up to 100 µM concentration (data not showed).

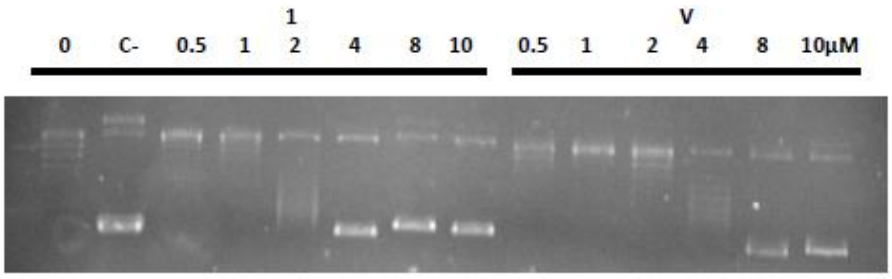

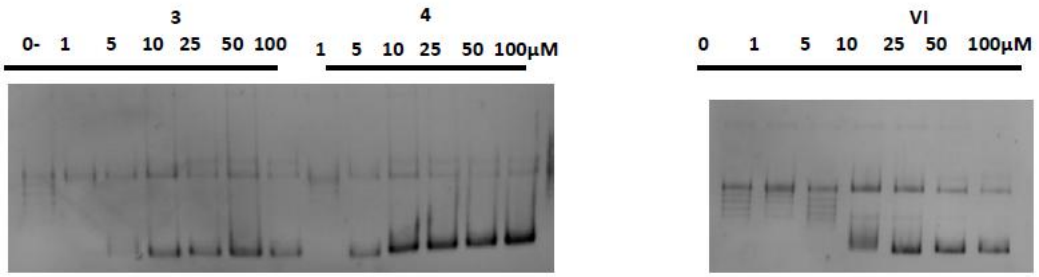

Figure 5.4. Effect of compounds **1**, **3**, **4**, **V** and **VI** on human topoisomerase IIα activity.

With the aim to characterize the conformational profile and binding mode for duplex and quadruplex DNAs, compound **3**, **7**, **8**, **11** and **VI** have been submitted to molecular modelling studies. Analysis of the ionization state showed that at pH 7.4 the form in which all the basic function are protonated was the most prevalent among all the ionizable states. Consequently, the conformational study has been carried out with these ionization forms by the Monte Carlo search. The docking simulations were performed using the available crystallographic structures from the Protein Data Bank (PDB). Docking models have been obtained with Autodock.

The free energy of the energetically most stable conformers towards quadruplex DNA, whose probability to exist is higher than 10%, was evaluated and are reported in Table 5.5, where ΔG is the free energy of complexation, dElectr is the electrostatic term, dVdW is the Van der Waals term and dGB/SA is the Gibbs Born Surface Area solvatation term, all expressed in kcal/mol.

Table 5.5. Details about the best pose of **3**, **7**, **8**, **11** and **VI** against the G-quadruplex target. ΔG is the free energy of complexation, dElectr is the electrostatic term, dVdW is the Van der Waals term and dGB/SA is the Gibbs Born Surface Area solvatation term, all expressed in kcal/mol.

Compound	Conformer	Position	ΔG	dVdW	dElectr	dGB/SA
3	30 (93,2%)	top	-51,2	-33,49	-1426,85	1409,11
7	10 (50,98%) 15 (37,21%)	top bottom	-54,3 -35,3	-34,78 -30,67	-1792,85 -1757,36	1773,33 1752,68
8	4 (100%)	top	-51,2	-29,23	-1927,33	1905,35
11	1 (99,99%)	bottom	-41,6	-26,59	-1033,72	1018,71
VI	10 (78,29%) 25 (21,69%)	top top	-45,4 -50,9	-55,95 -62,58	-841,75 -872,48	852,29 884,13

All the compounds are able to stack on the external G-quartet, at the top or at the bottom of the structure. From the free energy results, the best ligand is **3**, as reported also by the FRET assay. For the polyamine conjugates **3**, **7** and **8**, the most important term contributing to the stabilization is the electrostatic one that considers all the ionic interactions. From the results obtained it is possible to explain why the higher number of nitrogen atoms in **7** and **8** does not cause an increase in the quadruplex stabilization respect to **3**. The deriving higher electrostatic contribution is balanced by the solvatation term, thus explaining why **3**, whose solvatation term is a lot lower, is the best quadruplex ligand within the series. Compounds **11** and **VI**

possess a lower free energy term, thus their quadruplex stabilizing activity is lower respect to the polyamine conjugates.
The molecular recognition obtained in the docking simulations of the ligand **3** with the G-quadruplex DNA model is shown in Figure 5.5.

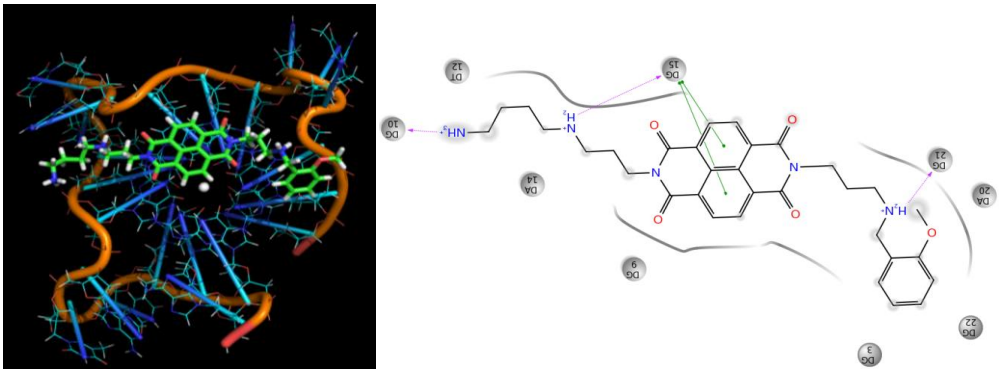

Figure 5.5. 3D representation of the best intercalative pose of compound **3** within the quadruplex DNA. The ligand and the DNA are respectively displayed as polytube and wireframe models. Positive ionizable target nitrogens are shown as blue features. b) 2D ligand representation with the main interaction features with the DNA duplex model. The intermolecular hydrogen bonds are represented by green dotted vectors.

In the complex the ligand fits the NDI core onto the DNA G-tetrads in top position by efficient end stacking interaction. All the ionized nitrogen atoms are able to donate hydrogen bonds, respectively to the phosphate groups of dG10, dG15 and dG21 (Fig. 5.5b).
Compound **7** is able to bind the quadruplex DNA both at the top and the bottom position where the 2:1 stoichiometry results in a sort of "sandwich-type interaction". The two binding modes have different features, as showed in figure 5.6. In this ternary complex the first bound ligand assumed a more relaxed conformation, fitting the NDI core onto the DNA G-tetrads in top position by efficient end stacking interaction. Only the benzylic nitrogen and the primary one are able to donate hydrogen bonds, respectively to the phosphate groups of dG19 and dG20 and dG22 (Fig. 5.6A). The second ligand recognized the G-tetrad in the bottom position by stacking of the NDI core, adapting itself in a semi-folded conformation (Fig. 5.6B). The side chains of this second ligand assumed a less extended conformation realizing different DNA interactions. In this case, only the secondary nitrogen atoms of the spermine chain establish hydrogen bonds with dG18 and dG17.

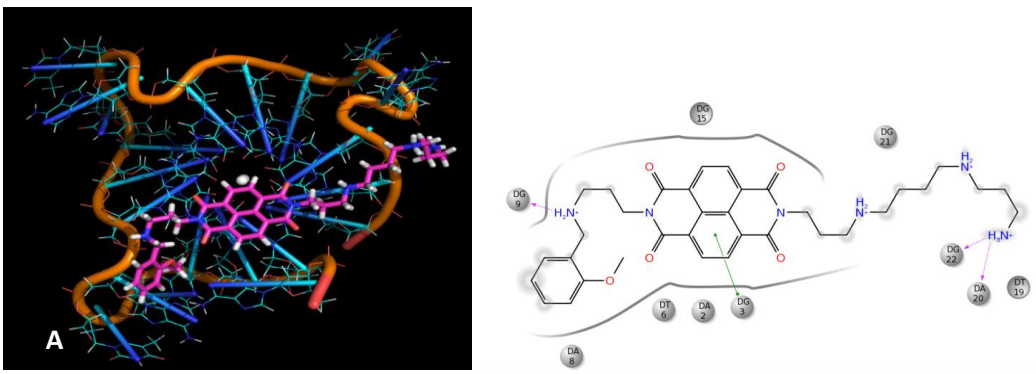

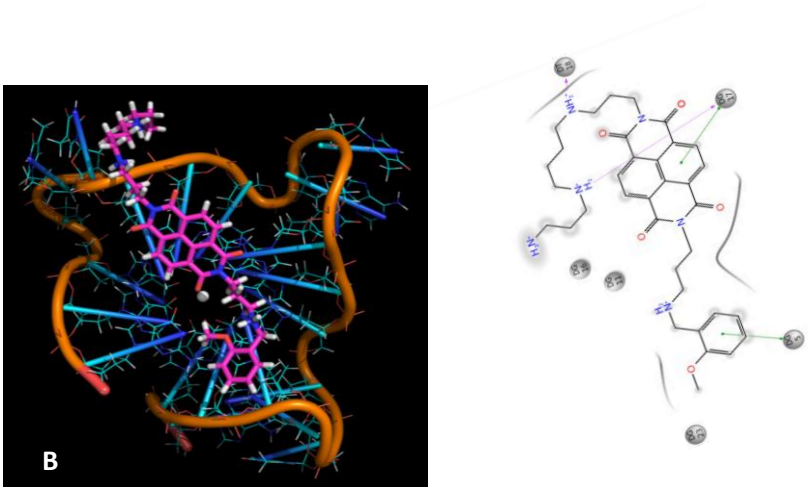

Figure 5.6. 3D and 2D representation of the best intercalative pose of compound **7** within the quadruplex DNA at the top (A) and bottom (B) positions.

The free energy of the energetically most stable conformers towards duplex DNA, whose probability to exist is higher than 10%, was evaluated and is reported in Table 5.6. Again all the polyamine conjugates are more effective in binding the DNA duplex in comparison to compound **VI**, being the electrostatic term the most important one. The latter is always balanced by a more important solvatation term. It is very interesting to note that the free energy for all the compounds towards duplex DNA is a lot higher respect to quadruplex DNA, thus confirming their optimal quadruplex targeting profile. Again, the more selective compound is **3**, for which the difference in the free energy of complexation between quadruplex and duplex DNA is of 4.1 Kcal/mol, the highest one among the tested compounds.

Table 5.6. Details about the best pose of **3**, **7**, **8**, **11** and **VI** against the DNA-duplex target. ΔG is the free energy of complexation, dElectr is the electrostatic term, dVdW is the Van der Waals term and dGB/SA is the Gibbs Born Surface Area solvatation term, all expressed in kcal/mol.

Compound	Conformer	ΔG	dVdW	dElectr	dGB/SA
3	12 (99,91 %)	-47,0	-26,27	-894,83	874,14
7	24 (98,93 %)	-43,9	-26,60	-1205,80	1188,54
8	40 (100%)	-51,9	-31,07	-1227,24	1206,40
11	8 (16,06%) 18 (13,66%) 43 (59,02%)	-39,1 -36,1 -37,8	-21,82 -27,21 -28,60	-671,32 -624,32 -630,48	654,00 615,39 621,23
VI	42 (17,88%) 47 (81,52%)	-42,7 -40,7	-36,85 -38,27	-556,69 -598,80	550,81 596,35

Within the series, compound **3** proved to be the most interesting one and was selected by NCI for *in vivo* studies, using the hollow fiber assay. First, the toxicity of the compound toward non tumored animal was assessed in order to define the concentration to use in the following study. Compound **3** shows no toxicity up to 6.25 mg/kg dose that can be defined as its Maximum Tolerated Dose. Taken that in consideration, the hollow fiber assay was performed

using a 2.4 mg/kg therapeutic intraperitoneal regimen on different tumors. In particular the cell lines used were: breast cancer (MDA-MB-231), non small cell lung cancer (NCI-H23, NCI-H522), colon cancer (SW-620, COLO205), melanoma (LOX IMVI, UACC-62, MDA-MB-435), ovarian cancer (OVCAR-3, OVCAR-5) and CNS cancer (U251, SF-295). Unfortunately **3** did not reach the minimum score necessary for additional test, so it was not further investigated.

5.4 Conclusion

In this work it has been demonstrated that the insertion of a polyamine chain on the **V** and **VI** scaffold allows increasing the quadruplex targeting profile and to exploit the PTS to enter into cancer cells. In particular, compound **3**, characterized by the spermidine chain and by 2-methoxy group on the aromatic ring, was the most potent within the new series and showed an interesting biological profile. In fact, it displayed pGI_{50} values around 7, demonstrating the mantenance of the cytotoxic activity towards multiple cancer lines, comparable with those of the lead compound **V**. Nevertheless, the mechanism of action of **3** was distinct from the one proved for **V**. Indeed, **3** showed the ability to tightly bind quadruplex DNA with high selectivity for this higher arrangement, differently from the lead compound. The molecular modeling studies explained that the lower solvatation term for the complex is the reason why the compound is a better G-quadruplex binder than the spermine NDI derivatives.
3 was able to inhibit Taq polymerase and topoisomerase; further studies aimed at veryfing wheter is responsible for the triggering of caspase cascade, downregulation of ERK 2 protein and to inhibition of ERKs phosphorylation, thus possessing the same biological profile of **V** are due to course.
Unfortunately, **3** was not able to exploit the polyamine transporter for the cell internalization, differently from the spermine-like derivatives; the mechanism that allows the compound to get into the cell is now under investigation.
These data, together with the fact that **3** was the only compound selected for the in vivo study by NCI, point out that the compound interacts with several targets involved in cancer development, therefore this study may represent a promising starting point for the development of new MTDLs hopefully useful for the cancer treatment.

5.5 Experimental section

5.5.1 Chemistry

All the synthesized compounds have a purity of at least 95% determined by elemental analysis. Uncorrected melting points were taken in glass capillary tubes on a Buchi SMP-20 apparatus. ESI-MS spectra were recorded on Perkin Elmer 297 and Waters ZQ 4000. ^{1}H NMR and ^{13}C NMR were recorded on Varian VRX 200 and 400 instruments. Chemical shifts are reported in parts per million (ppm) relative to peak of tetramethylsilane (TMS) and spin multiplicities are given as s (singlet), brs (broad singlet), d (doublet), t (triplet), q (quartet) or m (multiplet). IR spectral data were consistent with the assigned structures. From all new compounds satisfactory elemental analyses were obtained, confirming 95% purity. Chromatographic separations were performed on silica gel columns by flash (Kieselgel 40, 0.040 e 0.063 mm, Merck) column chromatography. Reactions were followed by thin layer chromatography (TLC) on Merck (0.25 mm) glass-packed precoated silica gel plates (60 F254) and then visualized in an iodine chamber or with a UV lamp.

Compounds **1-13** were synthesized following the general procedure developed by our research group as follows (see scheme 5.1, 5.2, 5.3 and 5.4).

General procedure for the synthesis of 40 and 41

A mixture of the appropriate diamine (5 eq) and aldehyde (1 eq) in toluene was refluxed in a DeanStark apparatus for 5 h. Following solvent removal, the residue was taken up in EtOH, $NaBH_4$ (8 eq) was added at 0 °C and the stirring was continued at r.t. for 16 h. The solvent was then removed and the residue was dissolved in CH_2Cl_2 and washed with brine. Removal of the dried solvent gave a residue that was purified by flash chromatography using as eluent a mixture of CH_2Cl_2/MeOH/33% aq. NH_4OH 8/2/0.1, providing the desired product **40** and **41**.

N1-(2-methoxybenzyl)propane-1,3-diamine (40). Yellow oil; 56% yield; ^{1}H NMR (200 MHz, $CDCl_3$) δ 1.65-1.67 (m, 2H), 2.03 (brs, 3H, exch D_2O), 2.55 (t, 2H, *J* = 6.4 Hz), 2.63-2.66 (m, 2H), 3.73 (s, 3H), 3.81(s, 2H), 6.90- 7.01(m, 2H), 7.09- 7.18 (m, 2H).

N1-(2,3,4-trimethoxybenzyl)propane-1,3-diamine (41). Yellow oil; 66% yield; ^{1}H NMR (200 MHz, $CDCl_3$) δ 1.67- 1.71 (m, 2H), 2.04 (brs, 3H, exch D_2O), 2.57 (t, 2H, *J* = 6.6 Hz), 2.66- 2.69 (m, 2H), 3.77 (s, 9H), 3.86 (s, 2H), 7.05- 7.12 (m, 2H).

General procedure for the synthesis of 47-57, 59 and 60

A mixture of the appropriate diamine **40** or **41** (1 eq), 1,4,5,8-naphthalene-tetracarbocylic dianhydride (1 eq) and the Boc-protected polyamine **23, 24, 27, 38, 39, 42-46, 18** or **58** (1 eq) in DMF was refluxed for 2 h. After cooling down, removal of the solvent gave a residue that was purified by flash chromatography using as eluent a mixture of toluene/CH_2Cl_2/MeOH/33% aq. NH_4OH 4/5/1/0.03 providing the desired products **47-57, 59** and **60**, respectively**.**

tert-butyl(3-((tert-butoxycarbonyl)amino)propyl)(3-(7-(3-((2-methoxybenzyl)amino) propyl)-1,3,6,8-tetraoxo-7,8-dihydrobenzo[lmn][3,8]phenanthrolin-2(1H,3H,6H)-yl)propyl)carbamate (47). Brown oil; 15% yield; ^{1}H NMR (400 MHz, $CDCl_3$) δ 1.43 (s, 18H), 1.62- 1.73 (m, 2H+1H exch D_2O), 1.95- 2.01 (m, 4H), 2.71 (t, 2H, *J* = 6.4 Hz), 3.10-3.12 (m, 2H), 3.30- 3.34 (m, 4H), 3.77 (s, 2H), 3.83 (s, 3H), 3.88- 4.30 (m, 4H), 4.76 (brs, 1H, exch D_2O), 6.83- 6.86 (t, 2H, *J* = 7.2 Hz), 7.17- 7.21 (m, 2H), 8.72- 8.26 (m, 4H).

tert-butyl(3-(7-(3-((2-methoxybenzyl)amino)propyl)-1,3,6,8-tetraoxo-7,8-dihydrobenzo [lmn][3,8]phenanthrolin-2(1H,3H,6H)-yl)propyl)(3-(methylamino)propyl)carbamate (48). Yellow oil; 16% yield; ^{1}H NMR (400 MHz, $CDCl_3$) δ 1.42 (s, 9H), 1.96- 2.01 (m, 6H), 2.59 (s, 3H), 2.73 (t, 2H, *J* = 6.8 Hz), 2.85- 2.88 (m, 2H), 3.23- 3.35 (m, 4H), 3.80 (s, 2H), 3.82 (s, 3H), 4.17 (t, 2H, *J* = 7.6 Hz), 4.26 (t, 2H, *J* = 7.2 Hz), 6.81- 6.83 (m, 2H), 7.18- 7.24 (m, 3H), 8.72 (s, 4H).

tert-butyl (4-((3-(7-(3-((2-methoxybenzyl)amino)propyl)-1,3,6,8-tetraoxo-7,8-dihydro benzo[lmn][3,8]phenanthrolin-2(1H,3H,6H)-yl)propyl)amino)butyl)carbamate (49). Yellow oil, 19% yield; ^{1}H NMR (400 MHz, $CDCl_3$) δ 1.43 (s, 9H), 1.52- 1.56 (m, 4H), 1.95-2.02 (m, 4H), 2.06 (brs, 1H, exch D_2O), 2.63- 2.67 (m, 6H), 2.71- 2.75 (m, 2H), 3.12 (brs, 1H, exch D_2O), 3.79 (s, 2H), 3.84 (s, 3H), 4.29 (t, 4H, *J* = 7.0 Hz), 4.89 (brs, 1H, exch D_2O), 6.84 (t, 2H, *J* = 7.4 Hz), 7.19 (t, 2H, *J* = 6.8 Hz), 8.73 (d, 4H, *J* = 7.2 Hz); ^{13}C NMR (100MHz, $CDCl_3$) δ 27.16, 27.78, 28.15, 28.40, 29.65, 38.82, 39.03, 40.37, 46.44, 46.95, 48.96, 49.27, 55.21, 78.92, 110.12, 120.27, 126.43, 126.62, 127.97, 128.13, 129.74, 130.86, 130.93, 156.01, 157.54, 162.80, 162.88.

tert-butyl (3-((4-(7-(3-((2-methoxybenzyl)amino)propyl)-1,3,6,8-tetraoxo-7,8-dihydro benzo[lmn][3,8]phenanthrolin-2(1H,3H,6H)-yl)butyl)amino)propyl)carbamate (50). Yellow oil; 15% yield; ^{1}H NMR (400 MHz, $CDCl_3$) δ 1.42 (s, 9H), 1.64-1.73 (m, 4H), 1.78-

1.85 (m, 2H), 1.95-2.02 (m, 2H), 2.3 (brs, 1H, exch D_2O), 2.70-2.75 (m, 6H), 3.20-3.22 (m, 2H), 3.79 (s, 2H), 3.84 (s, 3H), 4.22 (t, 2H, *J* = 7.6 Hz), 4.29 (t, 2H, *J* = 6.4 Hz), 5.15 (brs, 1H exch D_2O), 6.84 (t, 2H, *J* = 7.2 Hz), 7.19 (t, 2H, *J* = 6.8 Hz), 8.73 (s, 4H). ^{13}C NMR (100MHz, $CDCl_3$) δ 25.72, 26.96, 28.16, 28.38, 29.51, 38.88, 39.03, 40.50, 46.44, 47.37, 48.95, 49.14, 55.20, 78.99, 120.27, 126.46, 126.57, 128.00, 128.13, 129.74, 130.84, 130.88, 156.19, 157.55, 162.80.

tert-butyl (2-((tert-butoxycarbonyl)(2-((tert-butoxycarbonyl)amino)ethyl)amino)ethyl)(3-(7-(3-((2-methoxybenzyl)amino)propyl)-1,3,6,8-tetraoxo-7,8-dihydrobenzo[lmn][3,8]phenanthrolin-2(1H,3H,6H)-yl)propyl)carbamate (51). Brown oil; 16% yield; NMR (200 MHz, $CDCl_3$) δ 1.46 (s, 27H), 1.66 (brs, 1H, exch D_2O), 1.89- 1.98 (m, 6H), 2.69- 2.76 (t, 2H, *J* = 6.8 Hz), 2.88- 3.26 (m, 10H), 3.78 (s, 2H), 3.84 (s, 3H), 4.20-4.32 (m, 4H), 5.12 (brs, 1H, exch D_2O), 6.82 (t, 2H, *J* = 7.0 Hz), 7.17 (t, 2H, *J* = 6.3 Hz), 8.74 (s, 4H).

tert-butyl (3-((tert-butoxycarbonyl)(3-((tert-butoxycarbonyl)amino)propyl)amino)propyl)(3-(7-(3-((2-methoxybenzyl)amino)propyl)-1,3,6,8-tetraoxo-7,8-dihydrobenzo[lmn][3,8]phenanthrolin-2(1H,3H,6H)-yl)propyl)carbamate (52). Brown oil; 20% yield; NMR (400 MHz, $CDCl_3$) δ 1.44 (s, 27H), 1.66-1.99 (m, 8H), 2.73 (t, 2H, *J* = 6.8 Hz), 3.18-3.34 (m, 10H), 3.79 (s, 2H), 3.84 (s, 3H), 4.21 (t, 2H, *J* = 7.4 Hz), 4.29 (t, 2H, *J* = 7 Hz), 6.85 (t, 2H, *J* = 7.4 Hz), 7.19 (t, 2H, *J* = 7Hz), 8.74 (s, 4H).

tert-butyl (4-((tert-butoxycarbonyl)(3-((tert-butoxycarbonyl)amino)propyl)amino)butyl)(3-(7-(3-((2-methoxybenzyl)amino)propyl)-1,3,6,8-tetraoxo-7,8-dihydrobenzo[lmn][3,8]phenanthrolin-2(1H,3H,6H)-yl)propyl)carbamate (53). Brown oil; 30% yield; ; ^{1}H NMR (400 MHz, $CDCl_3$) δ 1.26- 2.01 (m, 37H+1H exch D_2O), 2.74 (t, 2H, *J* = 6.8 Hz), 3.09- 3.25 (m, 10H), 3.81(s, 3H), 3.84 (s, 2H), 4.21(t, 2H, *J* = 7.2 Hz), 4.29 (t, 2H, *J* = 7.2 Hz), 5.16 (brs, 1H, exch D_2O), 6.85 (t, 2H, *J* = 7.6 Hz), 7.18-7.22 (m, 2H), 8.76 (s, 4H). ^{13}CNMR (100MHz, $CDCl_3$) δ 19.96, 25.68, 27.29, 28.08, 37.42, 38.66, 38.96, 43.78, 44.18, 44.94, 46.35, 46.66, 48.88, 50.31, 55.16, 78.77, 79.37, 90.54, 107.02, 110.07, 120.22, 126.38, 126.53, 126.54, 127.86, 128.10, 129.70, 130.79 130.84, 155.38, 157.49, 162.64, 162.72.

tert-butyl (4-((tert-butoxycarbonyl)(3-((tert-butoxycarbonyl)amino)propyl)amino)butyl)(3-(1,3,6,8-tetraoxo-7-(3-((2,3,4-trimethoxybenzyl)amino)propyl)-7,8-dihydrobenzo[lmn][3,8]phenanthrolin-2(1H,3H,6H)-yl)propyl)carbamate (54). Brown oil; 16% yield; ^{1}H NMR (400 MHz, $CDCl_3$) δ 1.43 (s, 27H), 1.45- 1.52 (m, 4H), 1.94- 1.99 (m, 4H+1H exch D_2O), 2.74 (t, 2H, *J* = 6.8 Hz), 3.08- 3.31 (m, 10H), 3.73 (s, 2H), 3.84 (s, 9H), 4.21(t, 2H, *J* = 7.0 Hz), 4.29 (t, 2H, *J* = 7.2 Hz), 5.16 (brs, 1H, exch D_2O), 6.57(d, 2H, *J* = 8.4 Hz), 6.92 (d, 2H, *J* = 8.4 Hz), 8.74 (s, 4H). ^{13}C NMR (100MHz, $CDCl_3$) δ 25.69, 28.23,28.40, 38.71, 39.04, 46.53, 48.56, 55.93, 60.68, 61.01, 79.38, 106.89, 123.93, 126.05, 126.45, 126.62, 128.95, 130.85, 130.90, 142.04, 152.97, 152.69, 162.77.

tert-butyl (4-((tert-butoxycarbonyl)(3-(methylamino)propyl)amino)butyl)(3-(7-(3-((2-methoxybenzyl)amino)propyl)-1,3,6,8-tetraoxo-7,8-dihydrobenzo[lmn][3,8]phenanthrolin-2(1H,3H,6H)-yl)propyl)carbamate (55). Yellow oil; 23% yield; ^{1}H NMR (400 MHz, $CDCl_3$) δ 1.43 (s, 18H), 1.48- 1.52 (m, 6H), 1.97- 2.01 (m, 4H), 2.58 (s, 3H), 2.73 (t, 2H, *J* = 6.8), 2.77- 2.79 (t, 2H), 3.09- 3.27 (m, 8H), 3.80 (s, 2H), 3.83 (m, 3H), 4.15- 4.19 (m, 2H), 4.28 (t, 2H, *J* = 6.8 Hz), 6.82- 6.86 (m, 2H), 7.17- 7.21 (m, 2H), 8.74 (s, 4H).

tert-butyl (4-((tert-butoxycarbonyl)(3-((tert-butoxycarbonyl)amino)propyl)amino) butyl)(3-(7-(3-((2-methoxybenzyl)amino)propyl)-1,3,6,8-tetraoxo-7,8-dihydrobenzo[lmn][3,8]phenanthrolin-2(1H,3H,6H)-yl)propyl)carbamate (56). Yellow oil; 23% yield; ^{1}H NMR (400 MHz, $CDCl_3$) δ 1.44-1.56 (m, 27H+6H), 2.04-2.08 (m, 4H), 2.74-2.81 (m, 6H),

3.15-3.18 (m, 8H), 3.85 (s, 2H), 3.87 (s, 3H), 4.30-4.32 (m, 4H), 6.84-6.91 (m, 2H), 7.19-7.28 (m, 2H), 8.75 (s, 4H).

tert-butyl (3-(4-(3-(7-(3-((2-methoxybenzyl)amino)propyl)-1,3,6,8-tetraoxo-7,8-dihydrobenzo[lmn][3,8]phenanthrolin-2(1H,3H,6H)-yl)propoxy)butoxy)propyl)carbamate (57). Brown oil; 26% yield; ^{1}H NMR (400 MHz, $CDCl_3$) δ 1.41 (s, 9H), 1.53- 1.54 (m, 4H), 1.70- 1.72 (m, 2H), 1.89 (brs, 1H, exch D_2O), 1.93- 2.03 (m, 4H), 2.70 (t, 2H, *J* = 6.8 Hz), 3.17- 3.19 (m, 2H), 3.19- 3.33 (m, 2H), 3.34- 3.44 (m, 4H), 3.54 (t, 2H, *J* = 6.0 Hz), 3.76 (s, 2H), 3.81 (s, 3H), 4.25- 4.31 (m, 4H), 4.99 (brs, 1H, exch D_2O), 6.81 (t, 2H, *J* = 8.0 Hz), 7.16 (t, 2H, *J* = 6.2 Hz), 8.69 (s, 4H).^{13}C NMR (100MHz, $CDCl_3$) δ 26.36, 26.39, 28.22, 28.27, 28.41, 28.69, 38.68, 39.08, 46.52, 49.03, 55.20, 68.67, 69.16, 70.60, 70.71, 77.36, 110.12, 120.27, 126.55, 126.59, 126.62, 128.06, 128.18, 129.67, 130.82, 130.85,155.98, 157.60, 162.60, 162.84.

tert-butyl (3-(7-(3-((2-methoxybenzyl)amino)propyl)-1,3,6,8-tetraoxo-7,8-dihydrobenzo[lmn][3,8]phenanthrolin-2(1H,3H,6H)-yl)propyl)carbamate (59). Yellow oil, 16% yield; ^{1}H NMR (400 MHz, $CDCl_3$) δ 1.44(s, 9H), 1.94- 1.97 (m, 4H), 2.72 (t, 2H, *J* = 7.0 Hz), 3.18- 3.19 (m, 2H), 3.77 (s, 2H), 3.82 (s, 3H), 4.29 (t, 4H, *J* = 6.2 Hz).

2-ethyl-7-(3-((2-methoxybenzyl)amino)propyl)benzo[lmn][3,8]phenanthroline-1,3,6,8(2H,7H)-tetraone (60). Brown solid; 24 % yield; ; ^{1}H NMR (400 MHz, $CDCl_3$) δ 1.35 (t, 2H, *J* = 7.0 Hz), 1.98- 2.02 (m, 2H), 2.74 (t, 2H, *J* = 7.2 Hz), 3.81 (s, 2H), 3.83 (s, 3H), 4.26- 4.28 (m, 4H), 6.82- 6.84 (m, 2H), 7.19- 7.20 (m, 2H), 8,73 (s, 4H).

General procedure for the synthesis of 1-12

A solution of **43-52** or **55** in MeOH and HCl 3M was stirred overnight at r.t. Following solvent removal, the residue was washed with Et_2O. The resulting solid was filtered and dried to afford **1-12**, respectively, as hydrochloride salt.

2-(3-((3-aminopropyl)amino)propyl)-7-(3-((2-methoxybenzyl)amino)propyl)benzo[lmn][3,8]phenanthroline-1,3,6,8(2H,7H)-tetraone hydrocloride salt (1). Orange solid; quantitative yield; m.p. >250 °C; ^{1}H NMR (400 MHz, D_2O) δ 2.09-2.21 (m, 6H), 3.12-3.25 (m, 8H), 3.89 (s, 3H), 4.16-4-24 (m, 4H), 4.27 (s, 2H), 6.87 (t, 1H, *J* = 7.4 Hz), 7.21 (d, 1H, *J* = 8.4 Hz), 7.28-7.33 (m, 2H), 8.42-8.48 (m, 4H); ^{13}C NMR (100MHz, D_2O) δ 23.70, 23.77, 24.29, 36.61, 36.68, 44.09, 44.725, 45.50, 55.58, 11.01, 117.99, 120.69, 125.04, 125.21, 130.95, 131.60, 157.59, 162.97, 163.00; MS (ESI) m/z = 280 $(M+2H)^{2+}$.

2-(3-((2-methoxybenzyl)amino)propyl)-7-(3-((3-(methylamino)propyl)amino) propyl)benzo[lmn][3,8]phenanthroline-1,3,6,8(2H,7H)-tetraone hydrocloride (2). Yellow solid, quantitative yield; m.p. >250 °C; ^{1}H NMR (400 MHz, D_2O) δ 2.16- 2.19 (m, 6H), 2.76 (s, 3H), 3.15- 3.25 (m, 8H), 3.89 (s, 3H), 4.20- 4.26 (m, 4H), 4.28 (m, 2H), 6.86 (t, 1H, *J* = 7.4Hz), 7.02 (d, 1H, *J* = 8Hz), 7.30- 7.34 (m, 2H), 8.50-8.57 (m, 4H). ^{13}C NMR (100MHz, D_2O) δ 23.46, 23.98, 24.20, 32.76, 43.08, 43.99, 44.50, 45.44, 45.72, 46.67, 55.39, 63.51, 111.06, 118.13, 120.76, 125.46, 125.60, 130.95, 131.56, 157.70, 163.59. MS (ESI) m/z = 287 $(M+2H)^{2+}$.

2-(3-((4-aminobutyl)amino)propyl)-7-(3-((2-methoxybenzyl)amino)propyl)benzo [lmn][3,8]phenanthroline-1,3,6,8(2H,7H)-tetraone hydrocloride (3). Brown solid; quantitative yield; m.p. >250 °C; ^{1}H NMR (400 MHz, D_2O) δ 1.62- 1.67 (m, 4H), 2.00- 2.04 (m, 4H), 2.91 (t, 2H, *J* = 7.0 Hz), 2.97- 3.01(m, 4H), 3.07 (t, 2H, *J* = 7.6 Hz), 3.74 (s, 3H), 4.03- 4.10 (m, 4H), 4.13 (s, 2H), 6.69-6.73 (m, 1H), 6.87 (d, 1H, *J* = 7.6 Hz), 7.13- 7.19 (m, 2H), 8.34- 8.37 (m, 4H); ^{13}C NMR (100MHz, D_2O) δ 22.70, 23.85, 23.96, 24.18, 37.60, 37.80,

38.76, 44.03, 45.25, 46.57, 46.98, 55.41, 110.10, 118.03, 120.70, 125.10, 125.17, 125.33, 130.91, 131.53, 157.60, 163.16; MS (ESI) m/z = 287 $(M+2H)^{2+}$.

2-(4-((3-aminopropyl)amino)butyl)-7-(3-((2-methoxybenzyl)amino)propyl)benzo[lmn][3,8]phenanthroline-1,3,6,8(2H,7H)-tetraone hydrocloride (4). Brown solid, quantitative yield, m.p. . >250 °C; ^{1}H NMR (400 MHz, D_2O) δ 1.84-1.85 (m, 4H), 2.12-2.15 (m, 2H), 2.21-2.15 (m, 2H), 3.11-3.20 (m, 8H), 3.90 (s, 3H), 4.18-4.14 (m, 2H), 4.21 (t, 2H, *J* = 6.4Hz), 4.30 (s, 2H), 6.87 (t, 1H, *J* = 7.4Hz), 7.03 (d, 1H, *J* = 8Hz), 7.29-7.35 (m, 2H), 8.49-8.50 (m, 4H). ^{13}C NMR (100MHz, D_2O) δ 23.16, 23.71, 24.00, 24.18, 36.53, 37.62, 40.09, 44.04, 44.47, 46.67, 47.29, 55.41, 111.07, 118.13, 120.76, 125.16, 125.49, 130.83, 130.94, 131.58, 157.69, 163.20, 163.37; MS (ESI) m/z = 287 $(M+2H)^{2+}$.

2-(3-((2-((3-aminopropyl)amino)ethyl)amino)propyl)-7-(3-((2-methoxybenzyl)amino)propyl)benzo[lmn][3,8]phenanthroline-1,3,6,8(2H,7H)-tetraone hydrocloride (5). Orange solid, quantitative yield; m.p. >250 °C; ^{1}H NMR (400 MHz, D_2O) δ 2.16- 2.22 (m, 6H), 3.11-3.18 (m, 4H), 3.27-3.34 (m, 4H), 3.57 (s, 4H), 3.90 (s, 3H), 4.17 (t, 2H, *J* = 6.4 Hz), 4.21 (t, 2H, *J* = 7.0 Hz), 4.28 (s, 2H), 6.87-6.89 (m, 1H), 7.01 (d, 1H, *J* =7.6 Hz), 7.30- 7.33 (m, 2H), 8.38-8.44 (m, 4H); ^{13}C NMR (100MHz, D_2O) δ 23.66, 23.99, 24.23, 36.39, 37.57, 37.71, 43.28, 43.31, 43.95, 45.08, 45.96, 46.65, 55.38, 111.07, 118.13, 120.77, 125.44, 125.64, 131.01, 131.57, 157.17, 163.61; MS (ESI) m/z = 302 $(M+2H)^{2+}$.

2-(3-((3-((3-aminopropyl)amino)propyl)amino)propyl)-7-(3-((2-methoxybenzyl)amino)propyl)benzo[lmn][3,8]phenanthroline-1,3,6,8(2H,7H)-tetraone hydrocloride (6). Brown solid, quantitative yield; m.p. >250 °C; ^{1}H NMR (400 MHz, D_2O) δ 2.09- 2.19 (m, 8H), 3.11-3.25 (m, 12H), 3.28 (s, 3H), 4.17-4.25 (m, 4H), 4.26 (s, 2H), 6.86 (t,1H, *J* = 7.4 Hz), 7.01 (d, 1H, *J* = 8.4 Hz), 7.28- 7.32 (m, 2H), 8.45 (m, 4H). ^{13}C NMR (100MHz, D_2O) δ 22.58, 22.64, 23.67, 23.98, 24.22, 36.45, 37.56, 43.99, 44.51, 44.56, 44.65, 45.49, 46.69, 55.39, 111.07, 118.14, 120.77, 125.62, 130.99, 131.56, 157.71, 163.60; MS (ESI) m/z = 309 $(M+2H)^{2+}$.

2-(3-((4-((3-aminopropyl)amino)butyl)amino)propyl)-7-(3-((2-methoxybenzyl)amino)propyl)benzo[lmn][3,8]phenanthroline-1,3,6,8(2H,7H)-tetraone hydrocloride (7). Brown solid, quantitative yield; m.p. >250 °C; ^{1}H NMR (400 MHz, D_2O) δ 1.82- 1.84 (m, 4H), 2.01-2.22 (m, 6H), 3.11- 3.25 (m, 12H), 3.90 (s, 3H), 4.20- 4.29 (m, 4H), 4.29 (s, 2H), 6.87 (t, 1H, *J* = 7.0 Hz), 7.03 (d, 1H, *J* = 8.0 Hz), 7.29-7.34 (m, 2H), 8.54-8.60 (s, 4H); ^{13}C NMR (100MHz, D_2O) δ 22.80, 22.79, 23.71, 24.04, 24.26, 24.78, 34.56, 36.58, 36.67, 36.97, 37.67, 37.87, 44.09, 44.53, 45.33, 46.58, 47.01, 55.49, 111.05, 118.08, 120.76, 125.08, 125.11, 125.16, 125.31, 130.95, 131.60, 157.65, 163.11, 163.16, 163.27; MS (ESI) m/z = 315 $(M+2H)^{2+}$.

2-(3-((4-((3-aminopropyl)amino)butyl)amino)propyl)-7-(3-((2,3,4-trimethoxybenzyl)amino)propyl)benzo[lmn][3,8]phenanthroline-1,3,6,8(2H,7H)-tetraone hydrocloride (8). Brown solid, quantitative yield, m.p.>250 °C; ^{1}H NMR (400 MHz, D_2O) δ 1.82- 1.84 (m, 4H), 2.11 (m, 6H), 3.10-3.21 (m, 12H), 3.69 (s, 3H), 3.74 (s, 3H), 3.81 (s, 3H), 4.18-4.23 (m, 4H), 4.24 (s, 2H), 6.74 (d, 1H, *J* = 8.8 Hz), 7.12 (d, 1H, *J* = 8.8 Hz), 8.44 (m, 4H) ; ^{13}C NMR (100MHz, D_2O) δ 22.75, 23.68, 23.99, 24.22, 36.49, 37.57, 37.78, 43.71, 44.49, 45.31, 45.86, 49.97, 60.75, 61.26, 107.98, 116.04, 125.45, 125.49, 125.65, 126.72, 130.96, 140.75, 151.76, 154.43, 163.57, 163.59; MS (ESI) m/z = 345 $(M+2H)^{2+}$.

2-(3-((2-methoxybenzyl)amino)propyl)-7-(3-((4-((3-(methylamino)propyl) amino)butyl) amino)propyl)benzo[lmn][3,8]phenanthroline-1,3,6,8(2H,7H)-tetraone hydrocloride (9). Brown solid, quantitative yield, m.p. >250 °C; ^{1}H NMR (400 MHz, D_2O) δ 1.81- 1.83 (m, 4H), 2.10- 2.18 (m, 6H), 2.76 (s, 3H), 3.93- 3.25 (m, 10H), 3.90 (s, 3H), 4.22- 4.28 (m, 4H), 4.29 (s, 2H), 6.86 (t, 1H, *J* = 7.2 Hz), 7.02 (d, 1H, *J* = 7.6 Hz), 7.26-7.34 (m, 2H), 8.66-8.72 (m, 4H) ; ^{13}C NMR (100 MHz, D_2O) δ 22.44, 22.73, 22.75, 23.99, 24.21, 32.75, 44.02, 44.39, 45.30, 45.71, 46.68, 46.97, 55.40, 111.07, 118.13, 120.77, 125.44, 125.59, 130.97, 131.57, 157.70, 163.56; MS (ESI) m/z = 643 $(M+H)^{+}$.

2-(3-((4-((4-aminobutyl)amino)butyl)amino)propyl)-7-(3-((2-methoxybenzyl)amino) propyl)benzo[lmn][3,8]phenanthroline-1,3,6,8(2H,7H)-tetraone (10). Brown solid, quantitative yield, m.p. >250 °C; ^{1}H NMR (400 MHz, D_2O) δ 1.78-1.83 (m, 8H), 2.17 (m, 4H), 3.06-3.19 (m, 12H), 3.89 (s, 3H), 4.10 (m, 4H), 4.27 (s, 2H), 6.82 (t, 1H, *J* = 7.2 Hz), 6.96 (d, 1H, *J* = 8.4 Hz), 7.25-7.28 (m, 2H), 8.45-8.46 (m, 4H); ^{13}C NMR (100MHz, D_2O) δ 20.72, 22.68, 22.77, 23.85, 24.23, 34.54, 38.78, 45.29, 46.62, 46.81, 48.90, 49.20, 125.29, 125.46, 130.96, 157.63, 163.39. MS (ESI) m/z = 322 $(M+2H)^{2+}$.

2-(3-(4-(3-aminopropoxy)butoxy)propyl)-7-(3-((2-methoxybenzyl)amino)propyl) benzo[lmn][3,8]phenanthroline-1,3,6,8(2H,7H)-tetraone hydrocloride (11). Orange solid, quantitative yield; m.p. . 189.6 °C; ^{1}H NMR (400 MHz, D_2O) δ 1.48- 1.89 (m, 4H), 1.89- 1.95 (m, 4H), 1.99- 2.07 (m, 2H), 3.06 (t, 2H, *J* = 7.2 Hz), 3.12 (t, 2H, *J* = 8.0 Hz), 3.40- 3.48 (m, 4H), 3.54- 3.61 (m, 4H), 3.89 (s, 3H), 4.09 (t, 2H, *J* = 6.4 Hz), 4.17 (t, 2H, *J* = 6.6 Hz), 4.28 (s, 2H), 6.86 (t, 1H, *J* = 7.4 Hz), 7.01 (d, 1H, *J* = 7.6 Hz), 7.29- 7.32 (m, 2H), 8.35-8.42 (m, 4H) ; ^{13}C NMR (100 MHz, D_2O) δ 23.94, 25.22, 26.50, 26.99, 37.38, 43.96, 46.40, 55.40, 67.51, 68.02, 70.21, 70.31, 110.91, 117.97, 120.59, 124.63, 124.92, 130.60, 130.78, 131.49, 157.58, 162.29, 162.73; MS (ESI) m/z = 645 $(M+H)^{+}$.

2-(3-aminopropyl)-7-(3-((2-methoxybenzyl)amino)propyl)benzo[lmn][3,8]phenanthroline -1,3,6,8(2H,7H)-tetraone hydrocloride (12). Yellow solid, quantitative yield, m.p. >250 °C; ^{1}H NMR (400 MHz, D_2O) δ 2.10- 2.16 (m, 4H). 3.08- 3.15 (m, 4H), 3.87 (m, 3H), 4.14- 4.22 (m, 4H), 4.25 (s, 2H), 6.83 (t, 1H, *J* = 7.4 Hz), 6.99 (d, 2H, *J* = 8.4 Hz), 7.26-7.30 (m, 2H), 8.44-8.49 (m, 4H); ^{13}C NMR (100MHz, D_2O) δ 23.96, 25.30, 37.21, 37.59, 37.60, 37.78, 44.00, 46.55, 55.37, 110.96, 118.02, 120.68, 125.05, 125.13, 130.90, 131.51, 157.59, 163.14. MS (ESI) m/z = 501 $(M+H)^{+}$.

Synthesis of compound 13

61 (115 mg, 0.243 mmol) was dissolved in the minimum amount of Et_2O. Et_2O saturated with HCl (1 ml) was slowly added to the solution and the precipitate was filtered and washed with Et_2O (3 x 3 ml). **13** was obtained as a brown solid.

2-ethyl-7-(3-((2-methoxybenzyl)amino)propyl)benzo[lmn][3,8]phenanthroline-1,3,6,8 (2H,7H)-tetraone hydrocloride (13). Brown solid, quantitative yield, m.p.> >250 °C; ^{1}H NMR (400 MHz, D_2O) δ 1.12 (t, 3H, *J* = 7.2 Hz), 2.01- 2.05 (m, 4H), 3.00 (t, 2H, *J* = 7.4 Hz), 3.75 (s, 3H), 3.84- 3.89 (m, 2H), 4.02 (t, 2H, *J* = 6.2 Hz), 4.13 (s, 2H), 6.73 (t, 1H, *J* = 7.4 Hz), 6.87 (d, 1H, *J* = 8.4 Hz), 7.15- 7.19 (m, 2H), 8.15 (s, 4H). ^{13}C NMR (100MHz, D_2O) δ 15.65, 26.74, 36.45, 45.51, 46.43, 54.77, 109.87, 117.37, 120.16, 123.79, 125.63, 130.25, 130.98, 155.83, 160.16. MS (ESI) m/z = 472 $(M+H)^{+}$.

General Procedure for the synthesis of 14 and 15

To a cooled solution (0 °C) of the appropriate aminoalcohol (0.8 eq) was added dropwise ethyltrifluoroacetate (1 eq) and the resulting mixture was stirred at r.t. for 1 h. After the consumption of the starting material, the mixture was dried under vacuum and the product obtained was used without further purification.

2,2,2-trifluoro-N-(3-hydroxypropyl)acetamide (14). Yellow oil, quantitative yield; ^{1}H NMR (400 MHz, $CDCl_3$) δ 1.70-1.78 (m, 2H), 3.18 (t, 2H, *J* = 5.1 Hz), 3.69 (brs, 1H, exch D_2O), 3.52 (t, 2H, *J* = 4.8 Hz), 8.74 (brs, 1H, exch D_2O).

2,2,2-trifluoro-N-(4-hydroxybutyl)acetamide (15). Yellow oil, quantitative yield; ^{1}H NMR (200 MHz, $CDCl_3$) δ 1.53-1.66 (m, 4H), 3.31 (t, 2H, *J* = 10.0 Hz), 3.65 (t, 2H, *J* = 7.2 Hz), 3.79 (brs, 1H, exch D_2O), 8.02 (brs, 1H, exch D_2O).

General Procedure for the synthesis of 16 and 17

To a cooled solution of **14/15** (1 eq) in CH_2Cl_2 were added NEt_3 (2 eq), a catalytic amount of DMAP and tosyl chloride (1.2 eq). The reaction mixture was stirred at r.t. overnight. Removal of the dried solvent gave a residue that was purified by flash chromatography using as eluent a mixture of EtOAc/petroleum ether 6/3, providing the desired products **16** and **17**.

3-(2,2,2-trifluoroacetamido)propyl 4-methylbenzenesulfonate (16). Yellow solid, 55% yield; ^{1}H NMR (400 MHz, $CDCl_3$) δ 1.94-2.00 (m, 2H), 2.46 (s, 3H), 3.45-3.50 (m, 2H), 4.11 (t, 2H, *J* = 5.6 Hz), 7.36-7.38 (m, 2H), 7.78-7.80 (m, 2H).

4-(2,2,2-trifluoroacetamido)butyl 4-methylbenzenesulfonate (17). Yellow solid, 60% yield; ^{1}H NMR (400 MHz, $CDCl_3$) δ 1.60-1.71 (m, 4H), 2.38 (s, 3H), 3.24- 3.27 (m, 2H), 4.02 (t, 2H, *J* = 6.8 Hz), 7.29-7.33 (m, 2H), 7.68- 7.63 (m, 2H).

General Procedure for the synthesis of 18 and 19

The appropriate diamine (10 eq) was dissolved in CH_2Cl_2, a solution of Boc_2O (1 eq) was added slowly in 20 minutes. Stirring was continued for 16 h at r.t**.** Removal of the solvent gave residue that was dissolved in CH_2Cl_2 and washed with brine. The organic fraction was dried over Na_2SO_4 providing the desired products **18** and **19.**

tert-butyl (3-aminopropyl)carbamate (18). Yellow oil; 72% yield; ^{1}H NMR (400 MHz, $CDCl_3$) δ 1.40 (s, 9H), 1.80-1.85 (m, 2H) 2.00 (brs, 2H, exch D_2O), 2.61-2.68 (m, 2H), 2.90-2.98 (m, 2H), 5.90 (brs, 1H, exch D_2O).

tert-butyl (4-aminobutyl)carbamate (19). Yellow oil; 60% yield; ^{1} H NMR (400 MHz, $CDCl_3$) δ 1.38 (s, 9H), 1.52-1.59 (m, 4H) 2.34 (brs, 2H, exch D_2O), 2.72-2.79 (m, 2H), 3.19-3.24 (m, 2H), 5.95 (brs, 1H, exch D_2O).

General Procedure for the synthesis of 20-22 and 26

To a cooled solution (0°C) of **16** or **17** (1 eq) in THF was added a solution of **18, 19** or **25** (1.5 eq) in THF. The reaction mixture was stirred for 1 h at 0 °C and then for 16 h at r.t. Removal of the solvent gave a crude product that was purified by flash chromatography using as eluent a mixture of CH_2Cl_2/MeOH/33% aq. NH_4OH 9/1/0.05, providing the desired products **20-22** and **26**.

tert-butyl (4-((3-(2,2,2-trifluoroacetamido)propyl)amino)butyl)carbamate (20). Yellow oil, 35%yield; ^{1}H NMR (400 MHz, $CDCl_3$) δ 1.44 (s, 9H), 1.52-1.54 (m, 4H), 1.72-1.75 (m, 2H), 2.62-2.65 (m, 2H), 2.82-2.85 (m, 2H), 3.11 (m, 2H), 3.46-3.49 (m, 2H). ^{13}C NMR (100MHz, $CDCl_3$) δ 27.10, 27.31, 28.00, 39.31, 40.23, 47.78, 48.79, 49.49, 78.66, 111.51(CF_3), 114.36 (CF_3), 117.21 (CF_3), 120.06 (CF_3), 156.02 ($COCF_3$), 156.13 ($COCF_3$), 156.43($COCF_3$), 156.79 ($COCF_3$), 157.52.

tert-butyl (3-((4-(2,2,2-trifluoroacetamido)butyl)amino)propyl)carbamate (21). Yellow oil, 47% yield; ^{1}H NMR (400 MHz, $CDCl_3$) δ 1.41 (s, 9H), 1.54-1.68 (m, 6H), 2.64 (t, 4H, *J* = 6.8 Hz), 3.07 (t, 2H, *J* = 6.4 Hz), 3.27-3.30 (m, 2H). ^{13}C NMR (100MHz, $CDCl_3$) δ 25.70, 26.15, 26.43, 27.45, 28.77, 37.49, 39.06, 39.19, 78.53, 111.89 (CF_3), 114.74 (CF_3), 117.58 (CF_3), 120.43 (CF_3), 156.96 ($COCF_3$), 157,21 ($COCF_3$), 157.32 ($COCF_3$), 157.69 ($COCF_3$), 158.05.

tert-butyl (4-((4-(2,2,2-trifluoroacetamido)butyl)amino)butyl)carbamate (22). Yellow oil, 27% yield; ^{1}H NMR (400 MHz, $CDCl_3$) δ 1.37 (s, 9H), 1.46-1.47 (m, 4H), 1.55-1.62 (m, 4H), 2.56-2.63 (m, 4H), 3.05 (brs, 2H, exch D_2O + m, 2H), 3.34- 3.26(m, 2H), 4.79 (brs, 1H, exch D_2O).

tert-butyl(4-((tert-butoxycarbonyl)amino)butyl)(4-((3-(2,2,2-trifluoroacetamido)propyl) amino) butyl)carbamate (26). Yellow oil, 27% yield; ^{1}H NMR (400 MHz, $CDCl_3$) δ 1.40 (s,

18H), 1.46-1.56 (m, 8H), 1.62-1.63 (m, 2H), 1.79-1.80 (m, 2H), 2.93-2.94 (m, 2H), 3.09-3.10 (m, 6H), 3.43-3.47 (m, 2H).

General Procedure for the synthesis of 23 and 24

To a stirred solution of **20** or **21** in MeOH was added slowly a solution of NaOH 40% p/p . The reaction mixture was allowed to stir at r.t. for 16 h. After removal of the solvent, the residual was taken up with CH_2Cl_2 and washed with brine. The organic layer was dried to obtain the desired products **23** and **24**.

tert-butyl (4-((3-aminopropyl)amino)butyl)carbamate (23). Yellow oil, 87% yield, ^{1}H NMR (400 MHz, D_2O) δ 1.28 (s, 9H), 1.32- 1.35 (m, 4H), 1.44- 1.52 (m, 2H), 2.41- 2.52 (m, 6H), 2.93- 2.94 (m, 2H).

tert-butyl (3-((4-aminobutyl)amino)propyl)carbamate (24). Yellow oil, 64% yield; ^{1}H NMR (400 MHz, D_2O) δ 1.30 (s, 9H), 1.39-1.41 (m, 4H), 1.53-1.58 (m, 2H), 2.49-2.61 (m, 6H), 2.97-2.99 (t, 2H, *J* = 6.8 Hz). ^{13}C NMR (100MHz, D_2O) δ 22.91, 23.52, 24.46, 25.60, 27.36, 38.48, 44.78, 46.51, 80.79, 157,90.

General Procedure for the synthesis of 25 and 27

To a solution of **22** or **26** (1 eq) in MeOH was added a solution of Boc_2O (1eq) in MeOH. The solution was stirred for 16 h at r.t., then NaOH 40% p/p was added. The stirring was continued for 12 h at r.t., then the solvent was removed and the residue obtained was purified by flash chromatography eluting with a mixture of CH_2Cl_2/MeOH/33% aq.NH_4OH 9/1/0.1, to give the desire product **25** and **27.**

tert-butyl (4-aminobutyl)(4-((tert-butoxycarbonyl)amino)butyl)carbamate (25). Yellow oil, 51% yield; ^{1}H NMR (400 MHz, $CDCl_3$) δ 1.41 (s, 18H), 1.52-1.53 (m, 6H), 2.18-2.20 (m, 2H), 2.63-2.77 (m, 2H), 3.08-319 (m, 6H), 4.83 (brs, 1H, exch D_2O).

tert-butyl(4-((3-aminopropyl)(tert-butoxycarbonyl)amino)butyl)(4 ((tertbutoxycarbonyl)amino)butyl)carbamate (27). Yellow oil, 31% yield; ^{1}H NMR (400 MHz, $CDCl_3$) δ 1.42-1.51 (m, 35H), 1.58-1.65 (m, 2H), 2.67-2.70 (t, 2H, *J* = 6.6 Hz), 3.09-3.25 (m, 10H), 4.67 (brs, 1H, exch D_2O).

General Procedure for the synthesis of 30 and 31

To a solution of **28** or **29** (5 eq) in toluene was added benzaldheyde (1 eq). The resulting mixture was refluxed for 5 h. The solvent was removed and the residue was taken up with ethanol. $NaBH_4$ (3 eq) was added and the solution was stirred for 16 h at r.t. After evaporation of the solvent, the crude product was dissolved in CH_2Cl_2 and washed with brine (1x10 ml). The organic phase was dried over Na_2SO_4, evaporated and purified by flash chromatography using as eluent a mixture of CH_2Cl_2/MeOH/33% aq.NH_4OH 9/1/0.1, providing the desired products **30/31**.

tert-butyl (3-aminopropyl)(3-(benzylamino)propyl)carbamate (30). Yellow oil; 80% yield; ^{1}H NMR (400 MHz, $CDCl_3$) δ 1.41 (s, 9H), 1.74- 1.77 (m, 4H), 2.61- 2.65 (m, 2H), 2.73-2.78 (m, 2H), 3.13 (brs, 3H, exch D_20), 3.21- 3.27 (m, 4H), 3.81 (s, 2H), 7.29- 7.32 (m, 5H).

tert-butyl (4-((3-aminopropyl)(tert-butoxycarbonyl)amino)butyl)(3-(benzylamino) propyl)carbamate (31). Yellow oil, quantitative yield; ^{1}H NMR (400 MHz, $CDCl_3$) δ 1.44 (s, 18H), 1.62- 1.64 (m, 4H), 1.69- 1.78 (m, 4H), 2.59 (t, 2H, *J* = 6.8 Hz), 2.66 (t, 2H; *J* = 6.6 Hz), 3.13- 3.22 (m, 8H), 3.75 (s, 2H), 7.27- 7.29 (m, 5H).

General Procedure for the synthesis of 32 and 33

To a stirred solution of **30** or **31** (1 eq) in MeOH, NEt_3 (1 eq) and ethyltrifluoroacetate (1 eq) were added. The stirring was continued for 16 h at r.t. The solvent was removed and the crude product was purified purified by flash chromatography using as eluent a mixture of

CH_2Cl_2/MeOH/33% aq. NH_4OH 9/1/0.05, providing the desired products **32** and **33,** respectively.

tert-butyl (3-(benzylamino)propyl)(3-(2,2,2-trifluoroacetamido)propyl)carbamate (32). Yellow oil, 72% yield; ^{1}H NMR (400 MHz, $CDCl_3$) δ 1.42 (s, 9H), 1.69- 1.73 (m, 4H), 2.61 (t, 2H, *J* = 6.8 Hz), 3.18- 3.20 (m, 2H), 3.27- 3,29 (m, 4H), 3.76 (s, 2H), 7.29-7.31 (m, 5H).

tert-butyl (3-(benzylamino)propyl)(4-((tert-butoxycarbonyl)(3-(2,2,2-trifluoroacetamido) propyl)amino)butyl)carbamate (33). Yellow oil, 92% yield; ^{1}H NMR (400 MHz, $CDCl_3$) δ 1.44 (s, 18H), 1.46- 1.48 (m, 4H), 1.67- 1.70 (m, 4H), 2.62 (t, 2H, *J* = 7.0 Hz), 3.11- 3.14 (m, 4H), 3.27- 3.31 (m, 4H), 3.78 (s, 2H), 7.30- 7.32 (m, 5H).

General Procedure for the synthesis of 34 and 35

To a stirred solution of **32** or **33** (1 eq) in THF, NEt_3 (1 eq) and methyl iodide (1.5 eq) were added and the resulting mixture was stirred for 24 h at r.t. The solvent was removed under vacuum and the crude product was purified by flash chromatography using as eluent a mixture of CH_2Cl_2/MeOH/33% aq. NH_4OH 9/1/0.04, providing the desired products **34** and **35**, respectively.

tert-butyl(3-(benzyl(methyl)amino)propyl)(3-(2,2,2-trifluoroacetamido)propyl) carbamate (34). Yellow oil, 66% yield; ; ^{1}H NMR (400 MHz, $CDCl_3$) δ 1.44 (s, 9H), 1.58- 1.64 (m, 6H), 2.20 (s, 3H), 2.22- 2.23 (m, 2H), 3.26- 3.27 (m, 4H), 3.42 (s, 2H), 7.31- 7.33 (m, 5H).

tert-butyl (3-(benzyl(methyl)amino)propyl)(4-((tert-butoxycarbonyl)(3-(2,2,2-trifluoroacetamido)propyl)amino)butyl)carbamate (35). Yellow oil, 30% yield; ^{1}H NMR (400 MHz, $CDCl_3$) δ 1.41 (s, 18H), 1.43- 1.46 (m, 4H), 1.65- 1.67 (m, 4H), 2.17 (s, 3H), 2.37- 2.39 (m, 2H), 3.13- 3.15 (m, 6H), 3.26- 3.29 (m, 4H), 3.46 (s, 2H), 7.27- 7.29 (m, 5H).

General Procedure for the synthesis of 36 and **37**

To a stirred solution of **34** or **35** in MeOH was added a solution of NaOH 40% p/p. The resulting mixture was allowed to stir for 16 h at r.t. After removal of the solvent, the residue was dissolved in CH_2Cl_2 and was washed with water. The organic layer was dried over Na_2SO_4, providing the desire products **36** and **37**, respectively.

tert-butyl (3-aminopropyl)(3-(benzyl(methyl)amino)propyl)carbamate (36). Yellow oil, 88% yield; ^{1}H NMR (400 MHz, $CDCl_3$) δ 1.43 (s, 9H), 1.61- 1.64 (m, 2H), 1.71- 1.74 (m, 2H), 1.75 (brs, 1H, exch D_20), 2.16 (s, 3H), 2.34 (t, 2H, *J* = 7.2 Hz), 2.67 (t, 2H, *J* = 6.6 Hz), 3.16- 3.19 (m, 4H), 3.46 (s, 2H), 7.28- 7.31 (m, 5H).

tert-butyl (4-((3-aminopropyl)(tert-butoxycarbonyl)amino)butyl)(3-(benzyl(methyl) amino)propyl)carbamate (37). Yellow solid, 92 % yield; ^{1}H NMR (400 MHz, $CDCl_3$) δ 1.41 (s, 18H), 1.45- 1.46 (m, 4H), 1.68- 1.71 (m, 4H), 2.15 (s, 3H), 2.33 (t, 2H, *J* = 6.0 Hz),2.73- 2.75 (m, 2H), 3.00- 3.03 (m, 4H), 3.12- 3.15 (m, 4H), 3.44 (s, 2H), 7.21- 7.27 (m, 5H).

General Procedure for the synthesis of 38 and 39

To a stirred solution of **36** or **37** dissolved in MeOH, the catalyst was added and the reaction mixture was stirred for 5 h at r.t. under H_2 flow. After the consumption of the starting material, the solution was filtered in order to remove the catalyst and the solution was dried under vacuum. The crude product was purified by flash chromatography using as eluent a mixture of CH_2Cl_2/MeOH/33% aq. NH_4OH 8/2/0.2, providing the desired products **38** and **39**, respectively.

tert-butyl (3-aminopropyl)(3-(methylamino)propyl)carbamate (38). Yellow oil, 68% yield; ^{1}H NMR (400 MHz, $CDCl_3$) δ 1.40 (s, 9H), 1.61- 1.69 (m, 4H), 1.72 (brs, 1H, exch D_2O), 2.38 (s, 3H), 2.56 (t, 2H, *J* = 6.6 Hz), 2.67 (t, 2H, *J* = 6.6 Hz), 3.16- 3.23 (m, 4H).

tert-butyl(3-aminopropyl)(4-((tert-butoxycarbonyl)(3-(methylamino)propyl)amino) butyl)carbamate (39). Yellow oil, 76% yield; ; ^{1}H NMR (400 MHz, $CDCl_3$) δ 1.42 (s, 18H), 1.45- 1.47 (m, 4H), 1.60- 1.63 (m, 2H), 1.64- 1.66 (m, 2H), 1.94 (brs, 3H, exch D_20), 2.41(s, 3H), 2.54- 2.56 (m, 2H), 2.66 (t, 2H, *J* = 6.6 Hz), 3.14- 3.22 (m, 8H).

5.5.2 Biophysical Evaluation

5.5.2.1 Fluorescence Resonance Energy Transfer (FRET)

Fluorescence melting curves were determined in a Roche Light Cycler (lecc 470 nm, lemm 520 nm) in LiP buffer (10 mM LiOH, 50 mM KCl, pH 7.4 with H_3PO_4). Increasing ligands concentrations were added to 0.25 mM final concentration of a labeled human telomeric sequence (50-Dabcyl-AGGGTTAGGGTTAGGGTTAGGGTFAM 30 Eurogentec, Belgium). Before scan acquisition the reaction mixture was first denatured and annealed. Then, samples were maintained at 30 ºC for 5 min before being slowly heated to 95 ºC (1 ºC/min) and annealed at a rate of 1 ºC/min. When double stranded DNA was used, dsUP (50-FAM-ACTATTCCCGGGTAATGA) and dsDOWN (TCATTACCCGGGAATAGT-Dabcyl 30) were mixed at equimolar concentrations, heated to 95 ºC for 5 min, and then cooled to rt overnight before use. Recordings were taken during both the annealing and melting steps. Tm values were determined from the first derivatives of the melting profiles using the Roche Light Cycler software. Each curve was repeated at least three times and errors were 0.4 ºC.

5.5.3 Biology

5.5.3.1 Growth inhibitory activity

The screening is a two-stage process, beginning with the evaluation of all compounds against the 60 cell lines at a single dose of 10 µM. The output from the single dose screen is reported as a mean graph and is available for analysis by the COMPARE program. Compounds which exhibit significant growth inhibition are evaluated against the 60 cell panel at five concentration levels.

The human tumor cell lines of the cancer screening panel are grown in RPMI 1640 medium containing 5% fetal bovine serum and 2 mM L-glutamine. For a typical screening experiment, cells are inoculated into 96 well microtiter plates in 100 µL at plating densities ranging from 5,000 to 40,000 cells/well depending on the doubling time of individual cell lines. After cell inoculation, the microtiter plates are incubated at 37° C, 5 % CO_2, 95 % air and 100 % relative humidity for 24 h prior to addition of experimental drugs.

After 24 h, two plates of each cell line are fixed in situ with TCA, to represent a measurement of the cell population for each cell line at the time of drug addition (Tz). Experimental drugs are solubilized in dimethyl sulfoxide at 400-fold the desired final maximum test concentration and stored frozen prior to use. At the time of drug addition, an aliquot of frozen concentrate is thawed and diluted to twice the desired final maximum test concentration with complete medium containing 50 µg/ml Gentamicin. Additional four, 10-fold or ½ log serial dilutions are made to provide a total of five drug concentrations plus control. Aliquots of 100 µl of these different drug dilutions are added to the appropriate microtiter wells already containing 100 µl of medium, resulting in the required final drug concentrations.

Following drug addition, the plates are incubated for an additional 48 h at 37 °C, 5 % CO_2, 95 % air, and 100 % relative humidity. For adherent cells, the assay is terminated by the addition of cold TCA. Cells are fixed in situ by the gentle addition of 50 µl of cold 50 % (w/v) TCA (final concentration, 10 % TCA) and incubated for 60 minutes at 4 °C. The supernatant is discarded, and the plates are washed five times with tap water and air dried. Sulforhodamine B (SRB) solution (100 µl) at 0.4 % (w/v) in 1 % acetic acid is added to each well, and plates are incubated for 10 minutes at r.t. After staining, unbound dye is removed by washing five times with 1% acetic acid and the plates are air dried. Bound stain is subsequently solubilized with 10 mM trizma base, and the absorbance is read on an automated plate reader at a wavelength of 515 nm. For suspension cells, the methodology is the same except that the assay is terminated by fixing settled cells at the bottom of the wells by gently adding 50 µl of 80% TCA (final concentration, 16% TCA). Using the seven absorbance measurements [time zero, (Tz), control growth, (C), and test growth in the presence of drug at the five concentration levels (Ti)], the percentage growth is calculated at each of the drug concentrations levels. Percentage growth inhibition is calculated as:

[(Ti-Tz)/(C-Tz)] x 100 for concentrations for which Ti>/=Tz

[(Ti-Tz)/Tz] x 100 for concentrations for which Ti<Tz.

Three dose response parameters are calculated for each experimental agent. Growth inhibition of 50% (GI_{50}) is calculated from [(Ti-Tz)/(C-Tz)] x 100 = 50, which is the drug concentration resulting in a 50% reduction in the net protein increase (as measured by SRB staining) in control cells during the drug incubation. The drug concentration resulting in total growth inhibition (TGI) is calculated from Ti = Tz. The LC_{50} (concentration of drug resulting in a 50% reduction in the measured protein at the end of the drug treatment as compared to that at the beginning) indicating a net loss of cells following treatment is calculated from [(Ti-Tz)/Tz] x 100 = -50. Values are calculated for each of these three parameters if the level of activity is reached; however, if the effect is not reached or is exceeded, the value for that parameter is expressed as greater or less than the maximum or minimum concentration tested.

5.5.3.2 Hollow fiber assay

A standard panel of 12 tumor cell lines are used for the routine hollow fiber screening of the *in vitro* actives. These include NCI-H23, NCI-H522, MDA-MB-231, MDA-MB-435, SW-620, COLO 205, LOX, UACC-62, OVCAR-3, OVCAR-5, U251 and SF-295. In addition, alternate lines can be used for specialized testing of compounds on a nonroutine basis. The cell lines are cultivated in RPMI-1640 containing 10% FBS and 2 mM glutamine. On the day preceeding hollow fiber preparation, the cells are given a supplementation of fresh medium to maintain log phase growth. For fiber preparation, the cells are harvested by standard trypsinization technique and resuspended at the desired cell density (2^{-10} x 10^6 cells/ml). The cell suspension is flushed into 1 mm (internal diameter) polyvinylidene fluoride hollow fibers with a molecular weight exclusion of 500000 Da. The hollow fibers are heat-sealed at 2 cm intervals and the samples generated from these seals are placed into tissue culture medium and incubated at 37 ºC in 5% CO_2 for 24 to 48 hours prior to implantation. A total of 3 different tumor lines are prepared for each experiment so that each mouse receives 3 intraperitoneal implants (1 of each tumor line) and 3 subcutaneous implants (1 of each tumor line). On the day of implantation, samples of each tumor cell line preparation are quantitated for viable cell mass by a stable endpoint MTT assay so that the time zero cell mass is known. Mice are treated with experimental agents starting on day 3 or 4 following fiber implantation and continuing daily for 4 days. Each agent is administered by intraperitoneal injection at 2 dose levels. The doses are based on the maximum tolerated dose (MTD) determined during prior acute toxicity testing. The fibers are collected from the mice on the day following the fourth

compound treatment and subjected to the stable endpoint MTT assay. The optical density of each sample is determined spectrophotometrically at 540 nm and the mean of each treatment group is calculated. The percent net growth for each cell line in each treatment group is calculated and compared to the percent net growth in the vehicle treated controls. A 50% or greater reduction in percent net growth in the treated samples compared to the vehicle control samples is considered a positive result. Each positive result is given a score of 2 and all of the scores are totaled for a given compound. The maximum possible score for an agent is 96 (12 cell lines X 2 sites X 2 dose levels X 2 [score]). A compound is considered for xenograft testing if it has a combined ip + sc score of 20 or greater, a sc score of 8 or greater, or produces cell kill of any cell line at either dose level evaluated. This scoring system has been validated by DCTDC statisticians in CTEP to represent a level of detection expected to score current "standard" agents as active.

Chapter 6. An epigenetic-genetic approach: targeting HDAC with naphthalene diimide derivatives

6.1 Drug design

As described previously, one of the main targets for the development of new antitumor agents is the DNA and among the different class of drugs able to interact with this target, a very important one is the class of the intercalating agents. Among these, NDIs are able to interact with the DNA intercalating in double helix. The molecules characterized by this planar aromatic can recognize the DNA when it is in the form of a double helix and when it forms supramolecular aggregates as in the case of the G-quadruplex structures. My research group is engaged in the design and synthesis of new anticancer agents with NDI structure, able to stabilize the G-quadruplex DNA and block the action of the enzyme telomerase. In particular compound **3,** designed as NDI-polyamine conjugate, is the one that showed the most interesting biological profile.

Since cancer is a multifactorial disease, we tried to improve the activity of compound **3** through the insertion of other functional groups endowed with antitumor activity, capable to interact with other targets involved in the pathology. Recently one of the target which has aroused considerable interest in cancer chemotherapy is HDAC. Numerous types of HDACIs are currently in clinical trials for the treatment of various forms of tumors and the FDA has approved the use of SAHA (Fig. 3.8) and of FK228 (Fig. 3.15) for the treatment of cutaneous T-cell cancer. A very interesting HDACi is Scriptaid: this compound, which was identified through a High-Throughput Transcriptional Screening of a library of over 16 thousand compounds, contains a hydroxamic acid moiety distanced by a five methylene chain from the NI core (Fig 3.10).

On this basis, we thought to synthesize compounds **1a-5a** combining the main chemical features of compound **3** and Scriptaid (Fig. 6.1). These derivatives, characterized by different polyamine chains, were designed and synthesized with the goal of obtaining molecules capable of:

- bind G-quadruplex DNA and inhibit the activity of telomerase;
- inhibit HDAC;
- selectively target cancer cells through interaction with the PTS.

The rationale for the design of a single chemical entity able to simultaneously interact with DNA and with HDAC derived from studies conducted by different research groups. First, it must be considered that the deacetylated DNA is non-covalently associated with histone proteins; HDACIs, by inducing iperacetylation of histone proteins complexed with DNA, increase the accessibility of the DNA and consequently the antitumor activity of molecules capable of binding the macromolecule. A study by Marks et al. demonstrated that the administration of a HDACi (SAHA) before a Topo II inhibitor (Etoposide), potentiates the cytotoxic activity of the latter, through a synergistic effect not drug-specific.[257] A second study has provided the rationale for combining in one molecule the hydroxamic acid moiety and the intercalating core. This study has shown that molecules derived from the fusion of a Topo II inhibitor (Daunomycin) and a HDACi (SAHA), are more active than the Topo II inhibitor alone, highlighting that it is not essential that the hydroxamic acid is administered before the drug acting on DNA, to exert its action.[258]

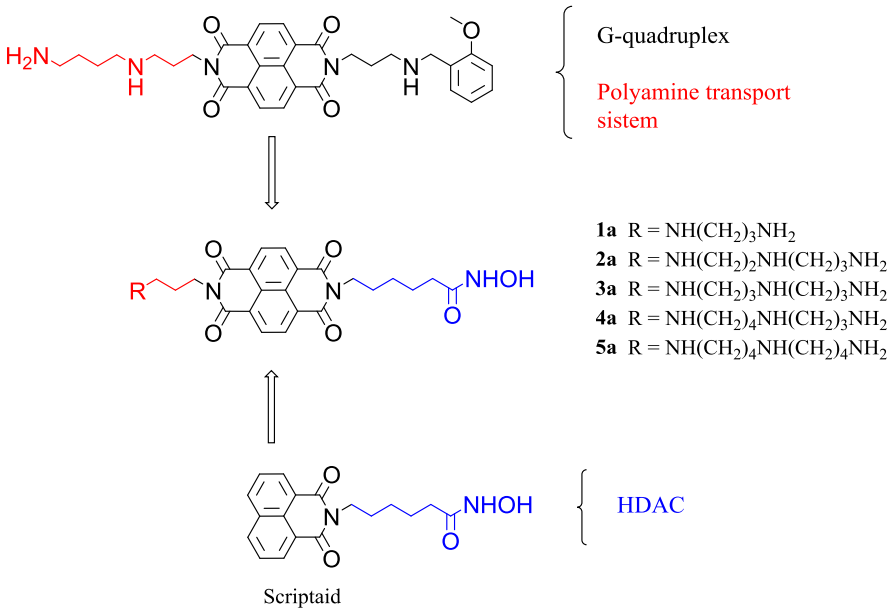

Figure 6.1 Drug design of compounds **1a-5a**.

As cancer results from a combination of epigenetic and genetic aberrations, a combination of therapeutic approaches could be very useful. Thus, combining epigenetic pharmacophores with both conventional cytotoxic agent in one molecule might be an important clinical avenue to explore, combining an epigenetic-genetic approach within a singular molecular entity.
The synthesized compounds **1a-5a** have different polyamine chains: these differ both in the number of atoms of nitrogen and in the number of methylene units separating them; with the aim to identify the correct molecular architecture for the interaction with the PTS, the DNA and the HDAC. Furthermore, the presence of various amino groups protonated at physiological pH can increase the affinity towards DNA and HDAC.

6.2 Methods

6.2.1 Chemistry

Compounds **1a-5a** were synthesized according to Scheme 6.1.
The procedure for the preparation of the polyamine chains **42-45** and **27** has already been described in Chapter 5.
The synthesized polyamines **42-45** and **27** were condensed with NTCDA and aminocaproic acid, thus obtaining the asymmetric derivatives **6a-11a** in which the carboxylic function was transformed in a protected hydroxamic acid one using NH_2OTHP. The final acid hydrolysis allowed the removal of all the protecting groups, leading to the formation of the final products **1a-5a**.

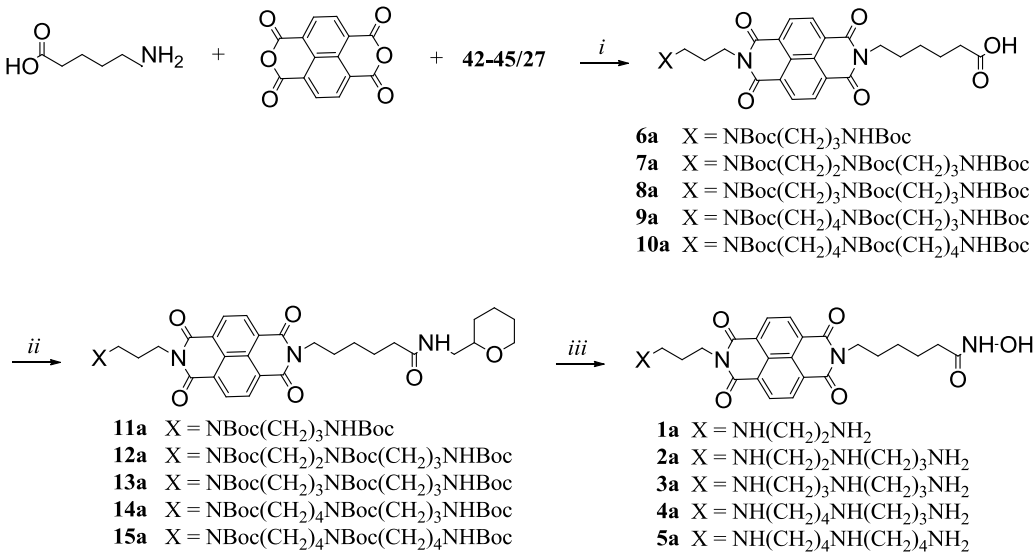

Scheme 6.1. (*i*) DMF, reflux, 2 h; (*ii*) O-(Tetrahydro-2H-pyran-2-yl)hydroxylamine, EDCI, HOBT, CH_2Cl_2, r.t., 5 h; (*iii*) HCl 4M in dioxane, CH_2Cl_2, r.t., 5 h**.**

6.2.2 Biophysical Evaluation

The G-quadruplex binding ability of compounds **1a**-**5a** was assessed by Fluorescence Resonance Energy Transfer (FRET) melting technique. Values are expressed as the melting temperature difference between the nucleotide with drug and the negative control (ΔTm).

6.2.3 Biology

Derivatives **1a**-**5a** were tested for their ability to inhibit HDAC in HL-60 leukemia cell line. Values are showed as the concentration required to the activity of the enzyme by 50% (IC_{50}). The antiproliferative activity has been evaluated by the MTT short-term cytotoxicity assay. Values are showed as the concentration required to inhibit cell growth by 50% (IC_{50}).
The compounds HDAC inhibitory activity was also tested in an isoenzyme mixture, while the ability to increase the histone acetylation levels for **3a** was investigated through Western Blotting.

6.3 Results and discussion

The prepared hydroxamic acids were examined for their HDAC inhibiting properties. For this purpose, the compounds were tested using a HDAC isoenzyme mixture purified from HeLa cervical carcinoma nuclei, containing at least HDAC isoenzymes 1, 2, 3, 5, and 8. Scriptaid was used as reference compound.
The results reported in Table 6.1 show that all the NDI derivatives are better HDACIs compared to the lead compound Scriptaid. The most active compound within the serie proved to be **3a**, a lower spermine derivative, but it is not possible to describe any trend for the inhibition properties linked to the nature of the polyamine chain.

Table 6.1. IC_{50} values towards a HDAC isoenzyme mixture of **1a-5a** and Scriptaid.

Compound	IC50 dose [μM]
Scriptaid	0.61
1a	0.47
2a	0.56
3a	0.42
4a	0.58
5a	0.61

To further assess the HDAC inhibitory activity, the compounds were also tested using a 5 μM concentarion in a cell based assay, using a panel of cancer cell lines, with the aim to assess their inhibitory activity in a more complex sistem (Fig. 6.2). TSA was used as a reference compound. Again, all the synthesized compounds proved to be less active than TSA (used in a concentration of 0.2 μM because of its high cytotoxic activity) but more active than the lead compound Scriptaid. The compounds were not active towards MCF7 cells, so this cell line was excluded from further studies. Among the NDI derivatives, the best one proved again to be **3a**, together with **5a**, so the biological profile of the two compounds was further investigated.

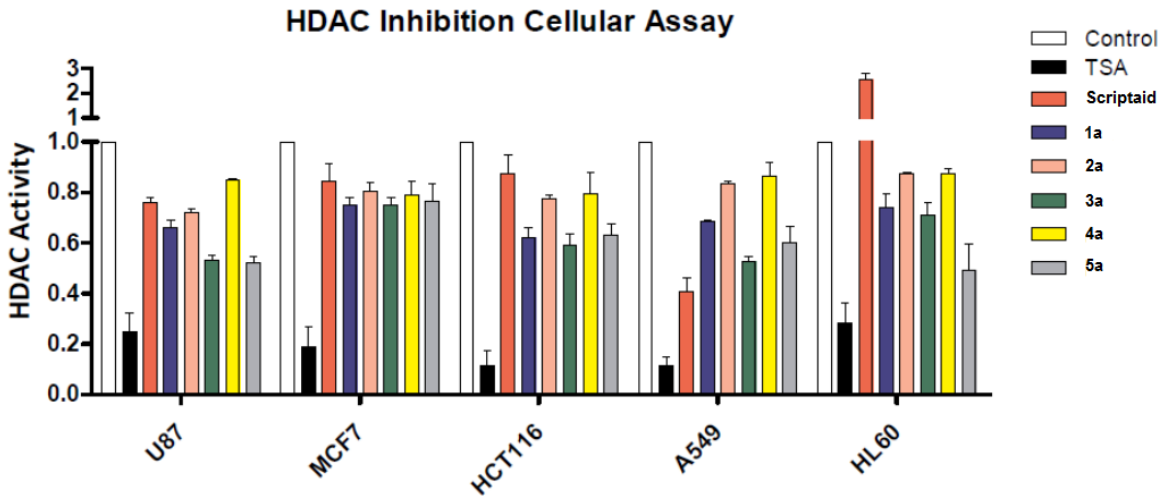

Figure 6.2. HDAC inhibitory activity of compounds **1a-5a** (5 μM) in comparison with Scriptaid (5 μM) and TSA (0.2 μM).

The antiproliferative activity of **3a** and **5a** was evaluated in all the cancer cell lines tested (except MCF7) using a concentration of 5 μM and including the polyamine conjugates in order to define if the introduction of the hydroxamic acid moiety causes any increase in the cytotoxic activity of the derivatives (Fig. 6.3). The hydroxamic acid containing NDIs were more active than the precursors;

The higher antiproliferative activity may be due to an additional mechanism of action for the new derivatives, i.e. HDAC inhibition, in addition to an increased DNA accessibility.

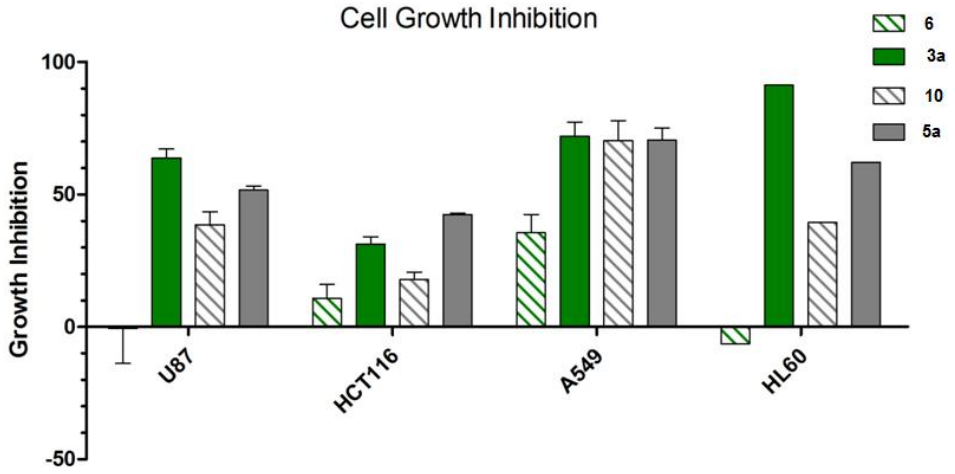

Figure 6.3. Antiproliferative activity of compounds **3a** and **5a** in comparison with the homologous polyamine conjugates **6** and **10**. The concentrations used for the assay was 5 μM.

The assessment of the degree of the histone acetylation after treatment with compound **3a** and Scriptaid, was done in U87 cancer cells and IMR90 lung cells in presence and absence of DFMO (Fig. 6.4). While Scriptaid is able to increase the acetylation level in all the cell lines, both in presence and absence of DFMO; compound **3a** is able to target selectively the U87 cells and the increase in the hystone acetylation level can be well seen only in presence of DFMO. This results clearly indicate that, differently from Scriptaid, the polyamine-hydroxamic acid conjugate exerts its action selectively towards the cancer cells and, considering that their activity is higher in presence of DFMO, they can exploit the PTS to enter into the cells.

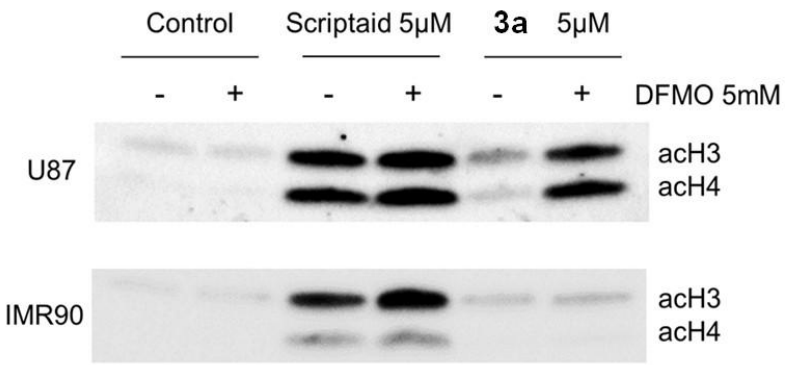

Figure 6.4. Modification of histone acetylation level induced by **3a** and Scriptaid and evaluation of the tubulin acetylation after the treatment with **3a** and Scriptaid at 5 μM in U87 and IMR90 cell lines in presence and absence of 5 mM DFMO.

All the compounds have also been tested for their ability to bind G-quadruplex structures using the Fluorescence Resonance Energy Transfer (FRET) melting technique. G-quadruplex and duplex DNA recognition of the synthesized compounds was evaluated by fluorescence

quenching melting assay using a G-quadruplex folded sequence based on the human telomeric sequence (G4) and a 18-bp random double stranded DNA (dsDNA), in order to assess their quadruplex binding activity and selectivity. The results obtained are reported in table 6.2.

Table 6.2. Fluorescence quenching melting on dsDNA and G4 of compounds **1a-5a** induced by 1 (black) and 2.5 (red) μM drug concentrations. Errors were 0.4ºC.

Compound	Htel22	DsDNA
1a	**0.75 / 7.76**	**0.09 / 3.44**
2a	**3.54 / 14.48**	**1.49 / 8.47**
3a	**4.00 / 10.93**	**3.17 / 8.01**
4a	**2.71 / 6.33**	**1.4 / 3.26**
5a	**6.86 / 20.43**	**3.26 / 13.96**

The compounds proved to be quadruplex ligands as good as the polyamine-conjugate precursors (except the good quadruplex binder **3**), thus indicating that the presence of the hydroxamic acid moiety does not influence the interaction with the DNA. Interestingly, the quadruplex targeting profile of the new derivatives follows the trend reported in the previous series: in the spermine-like derivatives, the quadruplex stabilization increases by lowering the number of the methylene groups within the inner nitrogen atoms. Among the NDI based HDACis, the best one proved to be **5a**, the higher spermine omologue but unfortunately, all the compounds display a poor selectivity: all of them are able to bind the quadruplex and the duplex DNA almost at the same extent.

All the synthesized derivatives are able to significantly increase the tested Htel22 melting temperature in a concentration dependent manner (Fig. 6.5). Using **5a** on both substrates the process appeared to reach saturation in the low micromolar range, suggesting a strong interaction with both DNA arrangements.

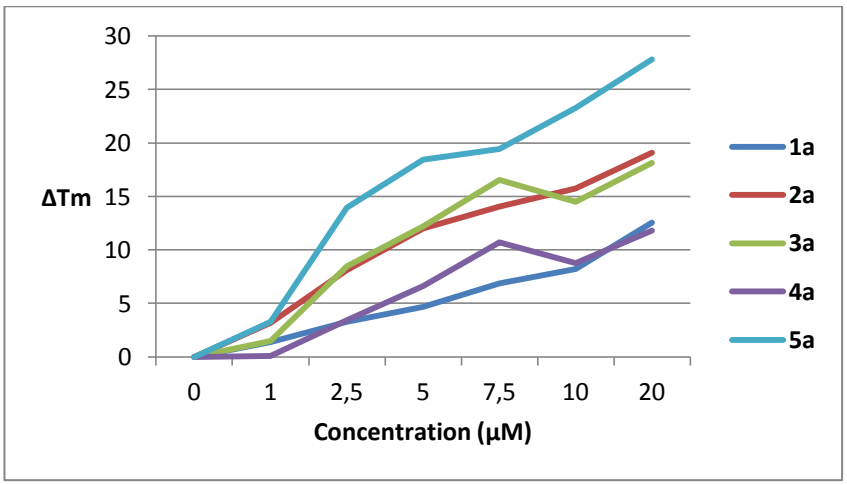

Figure 6.5. Variation of DNA (0.25 μM) thermal stability (ΔTm °C) produced by tested ligands in 50 mM potassium buffer, pH 7.4, evaluated by fluorescence quenching melting experiments. Heating rate 1 °C/min. at increasing concentration of the NDIs derivatives on G-quadruplex folded telomeric sequence.

6.4 Conclusions

This study allowed us to discover new MTDLs endowed with additional biological activities respect to the NDI-polyamine conjugates, i.e. the ability to inhibit HDAC enzymes, as potential anticancer agents.

All the synthesized compounds displayed a HDAC inhibitory activity in the submicromolar range against a HDAC isoenzyme mixture, proving to possess a better biological profile than the lead compound Scriptaid. In particular, compounds **3a** and **5a** emerged as the most potent of the series, showing the ability to halve the HDAC activity in different cancer cell lines at 5 μM concentration.

Furthermore, **3a** and **5a** were able to induce higher growth inhibition levels in the same cancer cell lines respect to the homologous NDI-polyamine conjugates, thus underlying the presence of additional mechanisms responsible for the cytotoxic activity, probably linked to the HDAC inhibition properties.

Moreover, the lower spermine derivative **3a** caused a higher level of histone acetylation than the lead compound Scriptaid and it was found that it was responsible for the increase in histone acetylation selectively in cancer cells. This effect was more evident in presence of DFMO, thus indicating the ability of the derivative to target selectively the cancer cells by means of the PTS.

All together, these data point out that **3a** inhibits HDAC enzymes, thus increasing the anticancer potential of the NDI-based MTDLs. Further studies are currently going on in order to assess if the compounds display some kind of isoform selectivity and to further investigate other possible mechanisms of action, concurring to their cytotoxic activity.

6.5 Experimental section

6.5.1 Chemistry

For the experimental procedures see Chapter 5.5.1.

Compounds **1a- 5a** were synthesized following the general procedure developed by our research group as follows (see scheme 6.1).

General procedure for the synthesis of 1a-5a.

To a cooled solution (0 °C) of the appropriate compound **29a/33a** (1 eq) in CH_2Cl_2 (3 ml) was added dropwise HCl 4M in dioxane. The reaction mixture was stirred for 5 h at r.t., and the precipitated formed was filtered under vacuum and was washed with Et_2O. The solid was dried to obtain **1a-5a**, as hydrochloride salts.

6-(7-(3-((3-aminopropyl)amino)propyl)-1,3,6,8-tetraoxo-7,8-dihydrobenzo[lmn][3,8]phenanthrolin-2(1H,3H,6H)-yl)-N-hydroxyhexanamide hydrocloride (1a). Yellow solid: quantitative yield; mp >250 °C; ^{1}H NMR (400 MHz, D_2O) δ 1.31-1.32 (m, 2H), 1.56-1.57 (m, 4H), 1.95-2.11 (m, 6H), 3.01 (t, 2H, *J* = 7.8 Hz), 3.07-3.14 (m, 4H), 3.84 (t, 2H, *J* = 7.6 Hz), 4.09 (t, 2H, *J* = 6.2 Hz), 8.23-8.30 (m, 4H); ^{13}C NMR (D_2O, 100 MHz): δ 27.10, 28.39, 29.33, 30.01, 47.17, 48.16, 76.78, 77.11, 77.43, 124.91, 125.05, 125.15, 126.50, 126.66, 126.87, 140.56, 165.98; ESI-MS (m/z): 510 $[M+H]^+$.

6-(7-(3-((2-((3-aminopropyl)amino)ethyl)amino)propyl)-1,3,6,8-tetraoxo-7,8-dihydrobenzo[lmn][3,8]phenanthrolin-2(1H,3H,6H)-yl)-N-hydroxyhexanamide hydrocloride (2a). Yellow solid: quantitative yield; mp >250 °C; ^{1}H NMR (400 MHz, D_2O) δ 1.44-1.48 (m, 2H), 1.71-1.74 (m, 4H), 2.14-2.27 (m, 6H), 3.16 (t, 2H, *J* = 7.8 Hz), 3.28-3.36 (m, 4H), 3.56 (s, 4H), 4.07 (m, 2H), 4.30 (m, 2H), 8.84-8.57 (m, 4H); ^{13}C NMR (D_2O, 100

MHz): δ 23.67, 24.25, 24.51, 25.58, 36.39, 43.11, 45.10, 45.98, 125.41, 125.61, 130.81, 131.02, 142.82, 148.46, 163.30, 163.60; ESI-MS (m/z): 553 $[M+H]^+$.

6-(7-(3-((3-((3-aminopropyl)amino)propyl)amino)propyl)-1,3,6,8-tetraoxo-7,8-dihydrobenzo[lmn][3,8]phenanthrolin-2(1H,3H,6H)-yl)-N-hydroxyhexanamide hydrocloride (3a): Yellow solid: quantitative yield; mp >250 °C; ^{1}H NMR (400 MHz, D_2O) δ 1.46 (m, 2H), 1.73 (m, 4H), 2.13-2.25 (m, 8H), 3.12-3.27 (m, 10H), 4.09 (m, 2H), 4.29 (t, 2H, *J* = 6 Hz), 8.58-8.61 (m, 4H); ^{13}C NMR (D_2O, 100 MHz): δ 22.64, 23.38, 24.21, 24.52, 25.60, 26.65, 36.45, 37.80, 40.65, 44.54, 44.66, 45.47, 124.89, 125.03, 125.16, 125.27, 130.71, 130.94, 162.84, 163.17; ESI-MS (m/z): 567 $[M+H]^+$.

6-(7-(3-((4-((3-aminopropyl)amino)butyl)amino)propyl)-1,3,6,8-tetraoxo-7,8-dihydrobenzo[lmn][3,8]phenanthrolin-2(1H,3H,6H)-yl)-N-hydroxyhexanamide hydrocloride (4a). Yellow solid: quantitative yield; mp < 250°C; ^{1}H NMR (400 MHz, D_2O) δ 1.43-1.47 (m, 2H), 1.69-1.74 (m, 4H), 1.85-1.86 (m, 4H), 2.11-2.28 (m, 6H), 3.12-3.29 (m, 10H), 3.93-3.95 (m, 2H), 4.23 (t, 2H, *J* = 6.4 Hz), 8.29-8.32 (m, 2H), 8.38-8.41 (m, 2H); ^{13}C NMR (D_2O, 100 MHz): δ 22.81, 23.70, 23.90, 24.29, 24.64, 25.77, 26.79, 32.22, 33.55, 36.58, 37.92, 40.59, 44.55, 45.34, 47.03, 124.57, 124.75, 124.94, 130.62, 130.88, 162.14, 162.24, 162.68, 172.54, 177.89; ESI-MS (m/z): 581 $[M+H]^+$.

6-(7-(3-((4-((4-aminobutyl)amino)butyl)amino)propyl)-1,3,6,8-tetraoxo-7,8-dihydrobenzo[lmn][3,8]phenanthrolin-2(1H,3H,6H)-yl)-N-hydroxyhexanamide hydrocloride (5a). Yellow solid: quantitative yield; mp >250 °C; ; ^{1}H NMR (400 MHz, D_2O) δ 1.45-1.49 (m, 2H), 1.66-1.87 (m, 10H), 2.11-2.23 (m, 2H), 2.38-2.49 (m, 2H), 3.02-3.08 (m, 4H), 3.11-3.24 (m, 6H), 3.35-3.36 (m, 2H), 4.01-4.13 (m, 2H), 4.24-4.37 (m, 2H), 8.59-8.70 (m, 4H); ^{13}C NMR (D_2O, 100 MHz): δ 22.78, 23.54, 23.76, 24.37, 24.55, 25.61, 26.66, 32.10, 33.42, 34.54, 36.97, 37.62, 40.74, 44.60, 45.00, 47.20, 124.20, 124.68, 124.89, 130.38, 130.77, 162.02, 162.32, 162.74; ESI-MS (m/z): 595 $[M+H]^+$.

General synthesis of 6a-10a.

To a solution of **42-45/27** (1 eq) in DMF (10 ml) were added NTCDA (1 eq) and aminocaproic acid (1 eq). The solution was refluxed at 160 °C for 2 h. The solvent was removed and the crude product was purified by gradient flash chromatography using as a eluent a mixture of EtOAc/petroleum ether 6/4 first and then CH_2Cl_2/MeOH 9.5/0.5, to give the desire product **6a/10a.**

6-(7-(3-((tert-butoxycarbonyl)(3-((tert-butoxycarbonyl)amino)propyl)amino)propyl)-1,3,6,8-tetraoxo-7,8-dihydrobenzo[lmn][3,8]phenanthrolin-2(1H,3H,6H)-yl)hexanoic acid (6a). Yellow oil: 56% yield; ^{1}H NMR (400 MHz, $CDCl_3$) δ = 1.30-1.32 (m, 2H), 1.44 (s, 18H), 1.64-1.73 (m, 6H), 2.01-2.18 (m, 2H), 2.41-2.42 (m, 2H), 3.08-3.09 (m, 2H), 3.36-3.38 (m, 4H), 4.14-4.24 (m, 4H), 8.79 (s, 4H).

6-(7-(9,12-bis(tert-butoxycarbonyl)-2,2-dimethyl-4-oxo-3-oxa-5,9,12-triazapentadecan-15-yl)-1,3,6,8-tetraoxo-7,8-dihydrobenzo[lmn][3,8]phenanthrolin-2(1H,3H,6H)-yl)hexanoic acid (7a). Yellow oil: 35% yield; ^{1}H NMR (400 MHz, $CDCl_3$) δ 1.41-1.48 (m, 27H), 1.66-1.76 (m, 8H), 1.95-1.97 (m, 2H), 2.33-2.36 (m, 2H), 3.06-3.07 (m, 2H), 3.20-3.29 (m, 8H), 4.16-4.17 (m, 4H), 5.38 (brs, 1H, exch D_2O), 8.70 (s, 4H).

6-(7-(9,13-bis(tert-butoxycarbonyl)-2,2-dimethyl-4-oxo-3-oxa-5,9,13-triazahexadecan-16-yl)-1,3,6,8-tetraoxo-7,8-dihydrobenzo[lmn][3,8]phenanthrolin-2(1H,3H,6H)-yl)hexanoic acid (8a). Yellow oil: 25% yield; ^{1}H NMR (400 MHz, $CDCl_3$) δ 1.38-1.39 (m, 29H), 1.62-1.76 (m, 8H), 1.91-1.99 (m, 2H), 2.28-2.32 (m, 2H), 2.32-3.33 (m, 10H), 4.12-4.15 (t, 4H, *J* = 6.6 Hz), 5.353 (brs, 1H, exch D_2O), 8.67-8.68 (m, 4H).

6-(7-(9,14-bis(tert-butoxycarbonyl)-2,2-dimethyl-4-oxo-3-oxa-5,9,14-triazaheptadecan-17-yl)-1,3,6,8-tetraoxo-7,8-dihydrobenzo[lmn][3,8]phenanthrolin-2(1H,3H,6H)-

yl)hexanoic acid (9a). Yellow oil: : 45% yield; ^{1}H NMR (400 MHz, $CDCl_3$) δ 1.42 (s, 27H), 1.44-1.50 (m, 6H), 1.69-1.82 (m, 6H), 1.96- 1.99 (m, 2H), 2.38-2.43 (m, 2H), 3.09-3.36 (m, 10H), 4.21-4.19 (m, 4H), 5.38 (brs, 1H, exch D_2O), 8.77 (s, 4H).

6-(7-(10,15-bis(tert-butoxycarbonyl)-2,2-dimethyl-4-oxo-3-oxa-5,10,15-triazaoctadecan-18-yl)-1,3,6,8-tetraoxo-7,8-dihydrobenzo[lmn][3,8]phenanthrolin-2(1H,3H,6H)-yl)hexanoic acid (10a). Yellow oil: 25% yield; ^{1}H NMR (400 MHz, $CDCl_3$) δ 1.24-1.29 (m, 27H), 1.42-1.76 (m, 14H), 1.94-1.97 (m, 2H), 2.25-2.40 (m, 2H), 3.05-3.19 (m, 10H), 4.16-4.23 (m, 4H), 4.67 (brs, 1H, exch D_2O), 8.74 (s, 4H).

General procedure for the synthesis of 11a-15a.

Compound **6a-10a** (1 eq) was dissolved in CH_2Cl_2 (10 ml) and EDCI (2eq), HOBT (1 eq) were added. After 1 h, O-(Tetrahydro-2H-pyran-2-yl)hydroxylamine (1.2 eq) was added and the resulting solution was stirred at r.t. for 5 h. The solvent was removed and the residue was purified by flash chromatography eluting with a mixture of EtOAc/petroleum ether 8/2, to give the desire product **11a/15a.**

tert-butyl (3-((tert-butoxycarbonyl)amino)propyl)(3-(1,3,6,8-tetraoxo-7-(6-oxo-6-(((tetrahydro-2H-pyran-2-yl)oxy)amino)hexyl)-7,8-dihydrobenzo[lmn][3,8] phenanthrolin-2(1H,3H,6H)-yl)propyl)carbamate (11a). Yellow oil: 71% yield; ^{1}H NMR (400 MHz, $CDCl_3$) δ 1.26-1.27 (m, 2H), 1.41 (m, 20H), 1.69-1.78 (m, 12H), 1.99-2.01 (m, 2H), 3.05-3.07 (m, 2H), 3.30-3.34 (m, 4H), 3.61-3.66 (m, 1H), 3.95-3.98 (m, 1H), 4.15-4.21 (m, 4H), 4.95-4.96 (m, 1H), 5.23 (brs, 1H, exch D_2O), 8.73 (s, 4H).

tert-butyl (2-((tert-butoxycarbonyl)(3-((tert-butoxycarbonyl)amino)propyl)amino) ethyl)(3-(1,3,6,8-tetraoxo-7-(6-oxo-6-(((tetrahydro-2H-pyran-2-yl)oxy)amino)hexyl)-7,8-dihydrobenzo[lmn][3,8]phenanthrolin-2(1H,3H,6H)-yl)propyl)carbamate (12a). Yellow oil: 89% yield; ^{1}H NMR (400 MHz, $CDCl_3$) δ 1.45 (s, 27H), 1.51- 1.81 (m, 14H), 2.00-2.01 (m, 2H), 2.18-2.19 (m, 2H), 3.11-3.12 (m, 2H), 3.33-3.34 (m, 8H), 3.62-3.67 (m, 1H), 3.95-3.96 (m, 1H), 4.20-4.24 (t, 4H, *J* = 7.4 Hz), 4.95-4.96 (m, 1H), 8.77 (s, 4H).

tert-butyl (3-((tert-butoxycarbonyl)(3-((tert-butoxycarbonyl)amino)propyl)amino) propyl)(3-(1,3,6,8-tetraoxo-7-(6-oxo-6-(((tetrahydro-2H-pyran-2-yl)oxy)amino)hexyl)-7,8-dihydrobenzo[lmn][3,8]phenanthrolin-2(1H,3H,6H)-yl)propyl)carbamate (13a). Yellow oil: 55% yield; ^{1}H NMR (400 MHz, $CDCl_3$) δ 1.38-1.47 (s, 27H + m, 2H), 1.53-1.76 (m, 14H), 1.90-1.99 (m, 2H), 2.11-2.15 (m, 2H), 3.04-3.29 (m, 10H), 3.54-3.57 (m, 1H), 3.87-3.89 (m, 1H), 4.09-4.17 (m, 4H), 4.87-4.88 (m, 1H), 8.68 (s, 4H).

tert-butyl (4-((tert-butoxycarbonyl)(3-((tert-butoxycarbonyl)amino)propyl)amino) butyl)(3-(1,3,6,8-tetraoxo-7-(6-oxo-6-(((tetrahydro-2H-pyran-2-yl)oxy)amino)hexyl)-7,8-dihydrobenzo[lmn][3,8]phenanthrolin-2(1H,3H,6H)-yl)propyl)carbamate (14a). Yellow oil: 64% yield; ^{1}H NMR (400 MHz, $CDCl_3$) δ 1.38-1.61 (s, 27H + m, 11H), 1.67-1.74 (m, 7H), 1.87-1.99 (m, 2H), 2.12-2.13 (m, 2H), 3.04-3.35 (m, 10H), 3.54-3.61 (m, 1H), 3.88-3.90 (m, 1H), 4.12-4.86 (m, 4H), 4.87-4.88 (m, 1H), 5.25 (brs, 1H exch D_2O), 8.69 (s, 4H).

tert-butyl (4-((tert-butoxycarbonyl)(4-((tert-butoxycarbonyl)amino)butyl)amino) butyl)(3-(1,3,6,8-tetraoxo-7-(6-oxo-6-(((tetrahydro-2H-pyran-2-yl)oxy)amino)hexyl)-7,8-dihydrobenzo[lmn][3,8]phenanthrolin-2(1H,3H,6H)-yl)propyl)carbamate (15a). Yellow oil: : 51% yield; ^{1}H NMR (400 MHz, $CDCl_3$) δ 1.41-1.56 (s, 27H + m, 16H), 1.74-1.77 (m, 7H), 1.92-1.94 (m, 2H), 2.17-2.18 (m, 2H), 3.09-3.14 (m, 6H), 3.20-3.21 (m, 1H), 3.34-3.37 (m, 2H), 3.90-3.93 (m, 1H), 4.17-4.19 (m, 4H), 4.90-4.91 (m, 1H), 8.73 (s, 4H).

6.5.2 Biophysical Evaluation

6.5.2.1 Fluorescence Resonance Energy Transfer (FRET)

The FRET experiments were conducted as freported in Chapter 5.5.2.1.

Chapter 7. Macrocyclic naphthalene diimide derivatives as potential G-quadruplex ligands

7.1 Drug design

In the previous chapters it has been highlighted that the design and synthesis of new anticancer agents is one of the most active areas in the pharmaceutical research field but that, despite the progress of knowledge on this disease, cancer remains one of the main causes of death worldwide. The development of new anticancer agents must necessarily take into account the problems of current drug therapies, first of all, the lack of an adequate selectivity of action, for which the drugs are not able to distinguish cancer cells from healthy ones determining the onset of numerous side effects. As described previously, one of the main targets for the development of new antitumor agents is the DNA and in this context different classes of molecules belonging to the category of intercalating agents have been designed.

In the last years G-quadruplex structures have been identified and characterized, they proved to be an excellent target for a more innovative anticancer therapy, because of their localization in the telomeric ends and in the regulatory regions of several genes whose involvement in cancer is, to date, fully confirmed. G-quadruplexes are proposed, moreover, as discriminating elements between tumor cells and healthy cells, thereafter selective ligands towards these structures could have a potentially antitumor action free from side effects. For that reason in the last decades the search for selective G-quadruplex ligands has involved many researchers and has provided promising results.

My research group have been engaged in the design and synthesis of new anticancer agents based on a naphthalene diimide structure since several years. Among the various molecules synthesized, the symmetric naphthalene diimide derivative **V** (Fig. 2.19) has shown the most interesting biological profile: it has a good cytotoxic activity against a panel of 60 cell lines in studies conducted at the National Cancer Institute (NCI) and, among different mechanism of actions demonstrated, it exploits its activity through the binding to the G-quadruplex DNA, even though its selectivity towards this target is not so high compared to duplex DNA. With the aim to improve its binding ability and its selectivity, we tried to include the NDI core into a macrocyclic structure. As extensively discussed in the previous chapters, macrocyclic structures are particularly interesting for the design of G-quadruplex ligands, despite the synthetic accessibility of these compounds limits their achievement. This class of compound is very interesting because, on one hand, they have low affinity for the duplex DNA and, on the other, they can interact optimally with the external G-quartet of G-quadruplexes.

A very important feature for G-quadruplex binders is the aromaticity, that is essential in order to achieve high affinity for this secondary structure of DNA. Their aromatic surface has to be greater than a normal intercalator, in order to improve the stacking interactions with the large surface area characteristic of the G-quartet. However to increase the affinity and reach the selectivity towards the G-quadruplex at the expense of duplex DNA, additional interactions with the grooves are needed. For this purpose it is possible to exploit the electrostatic interactions between the positive charges of basic functions, protonated at physiological pH, and the phosphate groups of the DNA backbone. The presence of positive charges, in addition, contributes favorably to the water solubility of the compound, balancing the lipophilicity of the aromatic fragment.

Among G-quadruplex ligands, a well known macrocyclic one is BOQ1 containing two quinacridine cores linked with polyamine chains (Fig. 2.29). BOQ1 is an example of how the

macrocyclization can be a useful strategy in the design of new quadruplex binders: the macrocyclic bis-quinacridine binds G-quadruplex in a stronger and more specific way than the opened monomer MOQ2 (F21T stabilization ΔTm: BOQ1 = 28 °C, MOQ2 = 10 °C).[171]
Based on all these observations, the aim of this project was to design and synthesize the macrocyclic derivatives **1b-5b**, by stiffening the structure of compound **V** into a macrocycle (Fig. 7.1).

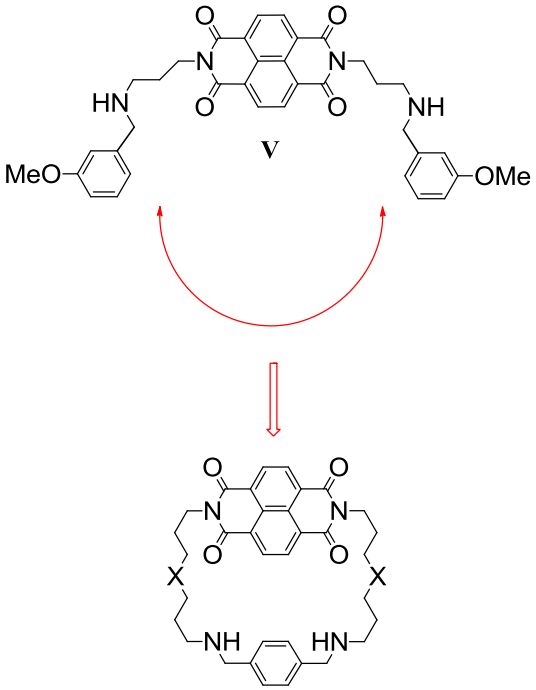

1b X = $NH(CH_2)_2NH$
2b X = $NH(CH_2)_3NH$
3b X = $NH(CH_2)_4NH$
4b X = NH
5b X = $O(CH_2)_4O$

Figure 7.1. Drug design of compounds **1b-5b**.

In the design of the new derivatives we have considered two critical elements in order to optimize the interaction with G-quadruplex: the number of nitrogen atoms of the polyamine linker, that determines the number of interactions that can be established with the DNA backbone, and the length of the methylene chains between them, which define the size of the macrocycle. The series of macrocycles **1b-4b** was obtained using spermine and nor-spermidine as linkers and by varying the distance between the inner nitrogen atoms. Moreover, compound **5b** was synthesized, where the two inner nitrogen atoms of the spermine linkers of **3b** have been replaced with oxygen atoms, in order to assess the importance of the positive charges in the quadruplex-stabilization process and to define which is the driving force in the interaction.

7.2 Methods

7.2.1 Chemistry

Compound **1b-4b** have been synthesized following the procedure reported in Scheme 7.1. The appropriate polyamines **6b-9b** were protected at the secondary amine functions with di-tertbutyl-dicarbonate to give the intermediates **10b-13b**, following a literature procedure.[274] **10b-13b** underwent to the protection of one of the primary amine function as trifluroacetic amide, obtaining **14b-17b**. The protected polyamines were then condensed with NTCDA to give the NDIs **18b-21b** that, after the removal of the protecting group of the primary amine through basic hydrolysis, were reacted with terephthalaldehyde to give the corresponding Schiff bases. These latter were reduced using sodium borohydride to give the macrocyclic derivatives **26b-29b**. The removal of the last protecting groups through acid hydrolysis allowed obtaining the desire final compounds **1b-4b** as hydrocloride salts.

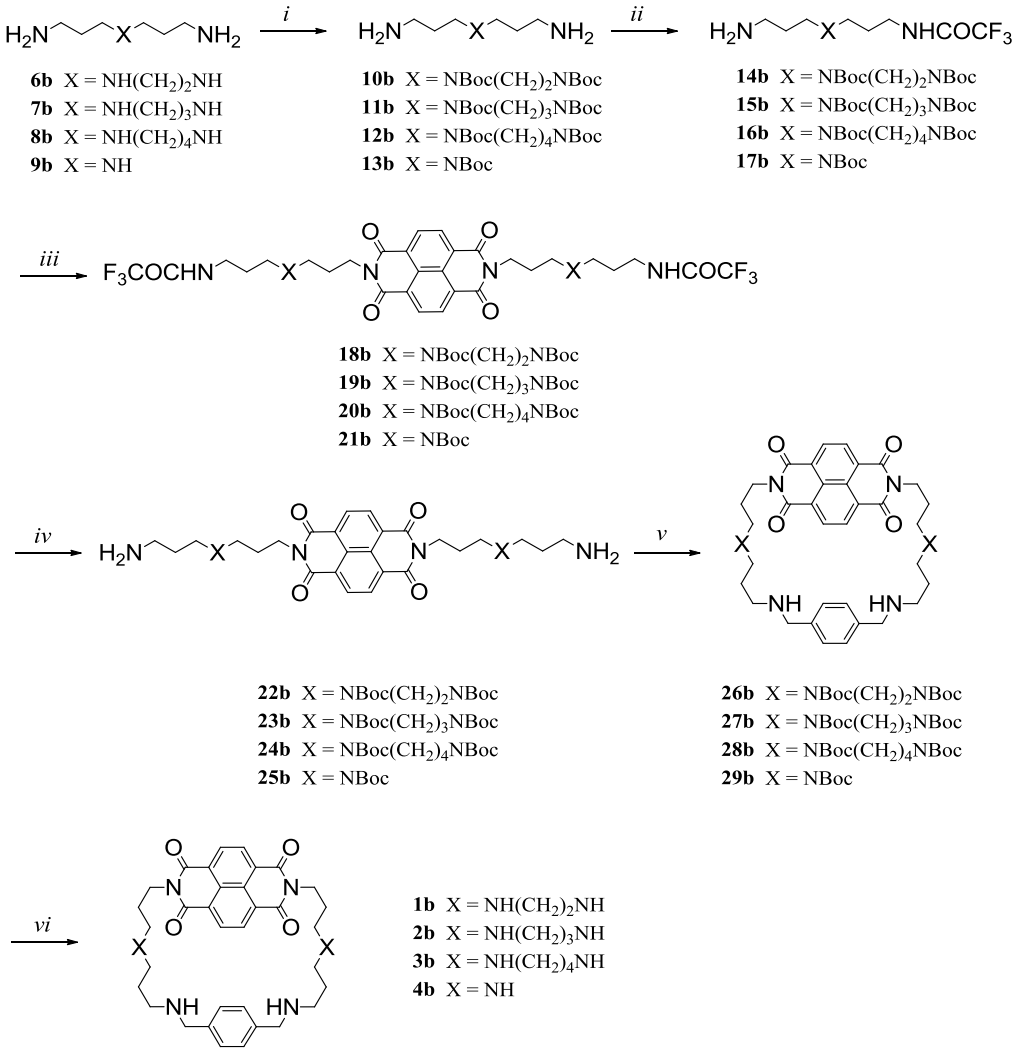

Scheme 7.1. (*i*) a) CF_3COOEt, MeOH, -78 °C, 30 min; b) Boc_2O, MeOH, r.t., 16 h; c) NaOH 40%, H_2O, r.t., 20 h; (*ii*) CF_3COOEt, MeOH, r.t., 16 h; (*iii*) NTCDA, DMF, reflux, 2 h; (*iv*) K_2CO_3, MeOH, H_2O, reflux, 2 h; (*v*) a) terephthalaldehyde, EtOH, r.t., 72 h; b) $NaBH_4$, r.t., 16 h; (*vi*) HCl 3N, r.t., 16 h.

Compound **5b** has been obtained as reported in Scheme 7.2.
The appropriate polyamine was monoprotected using di-tertbutyl-dicarbonate to give intermediate **30b** that was further condensed with NTCDA to give the NDI derivative **31b**. The acid hydrolysis using HCl 3N allowed obtaining **32b** with free primary amine functions. Intermediate **32b** was reacted with terephthalaldehyde to give the Schiff base that, after reduction with sodium borohydride, led to the final compound **5b**, that was then transformed in the corresponding hydrochloride salt in order to obtain a derivative easier to handle.

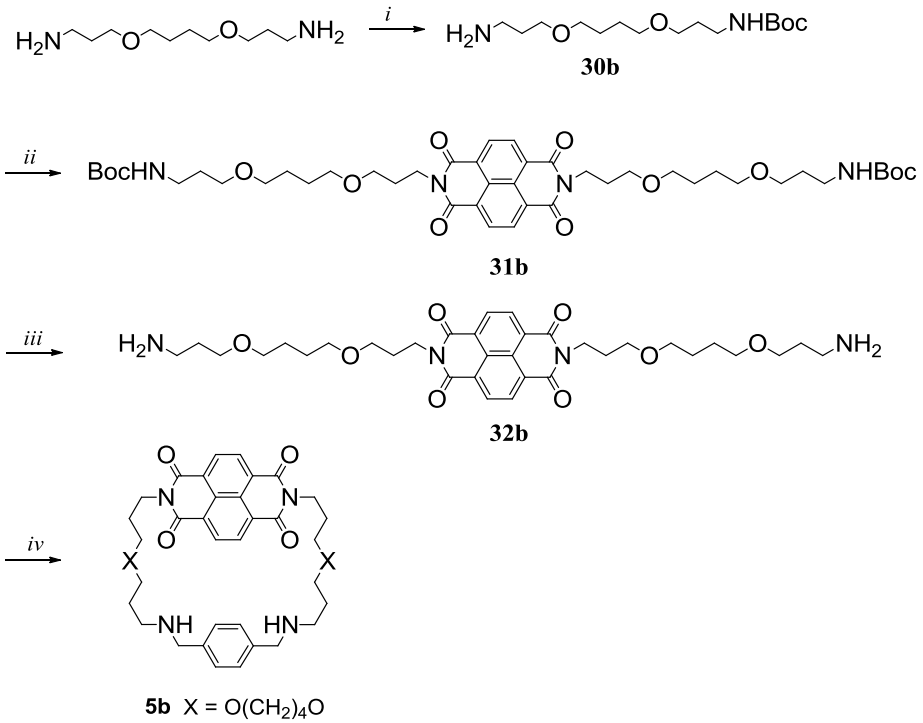

Scheme 7.2. (*i*) Boc_2O, CH_2Cl_2, r.t., 16 h; (*ii*) NTCDA, DMF, reflux, 2 h; (*iii*) HCl 3N, r.t., 16 h; (*iv*) a) terephtalaldehyde, EtOH, r.t., 72 h; b) $NaBH_4$, r.t., 16 h.

7.2.2 Biophysical Evaluation

The G-quadruplex binding ability of compounds **1b**-**5b** was assessed by Fluorescence Resonance Energy Transfer (FRET) melting technique. Values are expressed as the melting temperature difference between the nucleotide with the drug and the negative control (ΔTm).

7.2.3 Biology

All the synthesized derivatives were tested for *in vitro* antiproliferative activity in a panel of cancer cell lines. The antiproliferative activity has been evaluated by the Sulforhodamine B short-term cytotoxicity assay (SRB). Values are showed as the concentration required to inhibit cell growth by 50% (IC_{50}). Telomerase inhibitory activities of **2** and **3** were determined using the TRAP-LIG assay, a modified telomere repeat amplification protocol that ensures that there is no carryover of ligand into the second PCR step of the assay.[123]

7.2.4. Computational studies

With the aim to investigate the binding mode of **2b** and **5b** for duplex and G-quadruplex DNA, docking simulation were performed using the available crystallographic structures from the Protein Data Bank (PDB).

7.3 Results and discussion

Compounds **1b-5b** were firstly evaluated through Fluorescence Resonance Energy Transfer (FRET) melting technique in order to assess their ability to interact with G-quadruplex DNA and their selectivity for this kind of DNA *vs* duplex DNA compared to **V**. The quadruplex sequences used for the screening are F21T (telomeric) and the promoter region of c-kit2. Tloop is a DNA-duplex sequence used as control. The results are reported in table 7.1.
With the exception of **5b,** that was indeed designed as a "negative control", all the spermine and norspermidine-like synthesized compounds have proved to be very good G-quadruplex ligands. All the ΔTm values are near 20 ºC at 1 µM or 2 µM concentrations. Compound **V** is a worse binder, with a ΔTm of only 9.9 ºC at 1 µM, thus demonstrating the validity of the rational basis of the project.

Table 7.1. ΔTm values (°C) for FRET analyses of compounds **1b-5b** and **V** at 1 µM (black) and at 2 µM (red) concentrations with a series of G-rich sequences: hTel (F21T), c-kit2, Tloop (duplex DNA). Esds are from triplicate measurements and average 0.3 °C.

	F21T	c-kit2	Tloop
1b	**18.9/26.7**	**14.3/25**	**1.2/7.8**
2b	**22.1/28.6**	**15.1/28**	**3.3/15.2**
3b	**26.8/31.9**	**33.1/39.9**	**8.6/27**
4b	**12.6/18.8**	**12.2/19.6**	**1.4/5.2**
5b	**0.4/5**	**0/4.5**	**0.2/0.4**
V	**9.9/17.3**	**7.4/19.6**	**2.2/8.4**

As a general trend, the quadruplex stabilization increases by increasing the number of charges, probably due to a stronger interaction with the DNA backbone. A very interesting point is that the open analogue **V** is not selective: it displays activity towards both duplex and quadruplex DNAs, with a selectivity index between F21T and Tloop of 4.5. The macrocyclic derivatives **1b-4b** are instead more selective for quadruplex DNA, interacting from 3- to 15-fold less with duplex DNA. The less selective compound is **3b**, endowed with a selectivity index of only 3, but with a much promising binding activity towards G-quadruplex respect to **V**. In particular the best G-quadruplex ligands are **2b** and **3b**, with ΔTm values of 22.1 ºC and 26.8 ºC respectively at 1 µM, reaching 28.6 ºC and 31.9 ºC respectively at 2 µM. It is also worth notice that the ΔTm values obtained for those two compounds are very similar to the values reported in literature for BOQ1 (ΔTm = 28 ºC at 1 µM) and Tlomestatin (ΔTm = 22.8 ºC at 1 µM), well known G-quadruplex binders. The reduction of the number of methylenes between the inner nitrogen atoms is correlated with a decreasing in the quadruplex binding activity. As already pointed out the ΔTm for **2b** is lower than for **3b**, furthermore compound **1b**, with a linker made up only by two methylenes, proved to be the worst one in the spermine-like series but the derivative with the higher selectivity for quadruplex over duplex DNA.

Elimination of two nitrogen atoms from **3b** leads to **4b** which has far less affinity for G-quadruplex (ΔTm = 12.6 °C at 1 μM) underlying the requirement of nitrogen atoms for the correct interaction with the target.

We have designed compound **5b** in order to assess the importance of the secondary basic functions for the interaction with the quadruplex DNA. From the results in Table 7.1, it is possible to state that the replacement of the inner nitrogens of **3b** with oxygen atoms abolishes the DNA-binding ability (ΔTm = 0.4 °C at 1 μM): this finding suggests that **3b**, likely due to its ionized state higher than **5b**, can establish with the DNA stronger electrostatic interactions, this explaining why the latter derivative loses every kind of activity towards both quadruplex and duplex DNAs.

As already mentioned, G-quadruplex binders are very interesting since they can hinder gene transcription by binding to the quadruplex sequences located in the promoter regions of human oncogenes. c-kit is an important oncogene encoding for tyrosine kinase receptor and represents an attractive target in the treatment of gastrointestinal tumors. Two quadruplex sequences (c-kit1 and c-kit2) in the kit promoter have been identified and, recently, Gunaratnam et al. have reported about a NDI-based derivative able to stabilize the kit2 quadruplex with significantly higher ΔTm values than for the kit1. For this reason, we decide to evaluate also our NDI-based macrocycles towards the c-kit2 G-quadruplex sequence.

With the exception of **5b**, the stabilizing activity of the spermine and spermidine-like derivatives follows the same pattern observed for the telomeric sequence; **3b** shows the highest stabilizing activity (ΔTm = 33.1 °C at 1 μM, ΔTm = 39.9 °C at 2 μM) while a linear decrease of the affinity is observed, again, by lowering the length of the chain between the two inner nitrogen atoms, eliminating one nitrogen atom from each side chain and replacing the nitrogen with oxygen atoms (**5b**, ΔTm = 0 °C at 1 μM).

From the data obtained, the most interesting compound seems to be **2b**, endowed with good binding properties and good selectivity, while **3b** has proved to be the best ligand, even though is not a very selective one.

As shown in Fig. 7.2, reporting the FRET melting curve for compound **2b** with the F21T and c-kit2 quadruplex sequences at all the different concentrations tested (0.1-5 μM), it is possible to observe for both the targets a significant increase in the melting temperature, especially at higher concentration (4 and 5 μM). The compound is able to induce a ΔTm around 40°C, that is the maximum that can be detected by the assay, thus confirming its optimal quadruplex targeting profile.

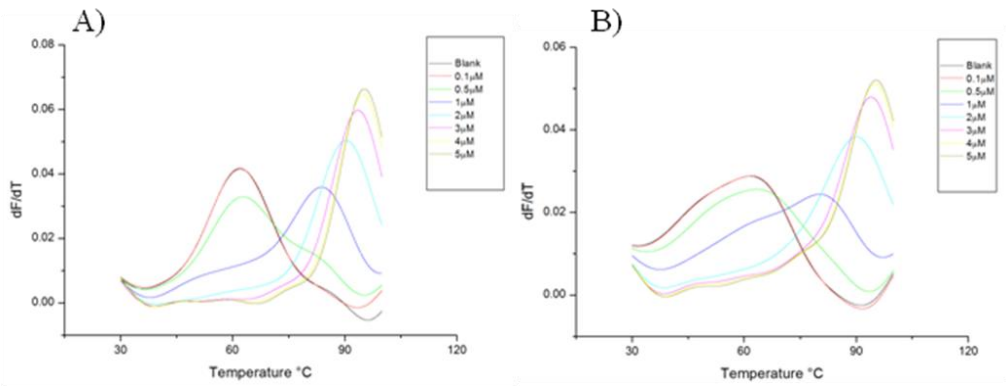

Figure 7.2. FRET melting curve for compound **2b** at different ligand concentrations with A) h-tel F21T quadruplex sequence and B) c-kit2 promoter quadruplex sequences.

In order to investigate the validity of the FRET data in *in vitro* assay, we decided to evaluate the telomerase inhibitory activity of the compounds that exhibit a higher quadruplex stabilizing activity, for that reason the ability to inhibit telomerase of compounds **2b** and **3b** was assessed in MIAPaCa-2 cells, using the modified TRAP-LIG assay, a modified TRAP assay that assures that there is no carryover of the ligand during the PCR process and that is able to give more reliable results (Fig. 7.3). None of the compounds tested is active towards telomerase, in fact it is not possible to see any change in the products of telomerase-mediated telomere elongation up to 50 μM concentration of each compound. This finding agrees with the data reported by Neidle at al. that have demonstrated that some NDI derivatives lack of telomerase activity, despite their ability to induce a very high increase in the melting temperature of the telomeric sequence in the FRET assay. Taking into account that FRET melting studies prove the ability of these derivatives to induce G-quadruplex stabilization, it is very likely that the compounds act via poly-targeting of G-rich oncogene promoter regions, while telomerase does not seem to be the obvious target, as judged by the lack of change in the elongation product gel ladders. Further, the TRAP assay determines activity of telomerase from a cellular protein extract *in vitro*, and not telomerase activity in cells. Lowered telomerase activity may be the consequence of downregulation of hTERT expression through G-quadruplex stabilization in the promoter region of the hTERT gene. As a consequence long term growth inhibition study has to be performed in order to assess if the compounds are able to decrease telomerase activity in the cells by acting at the hTERT promoter level.

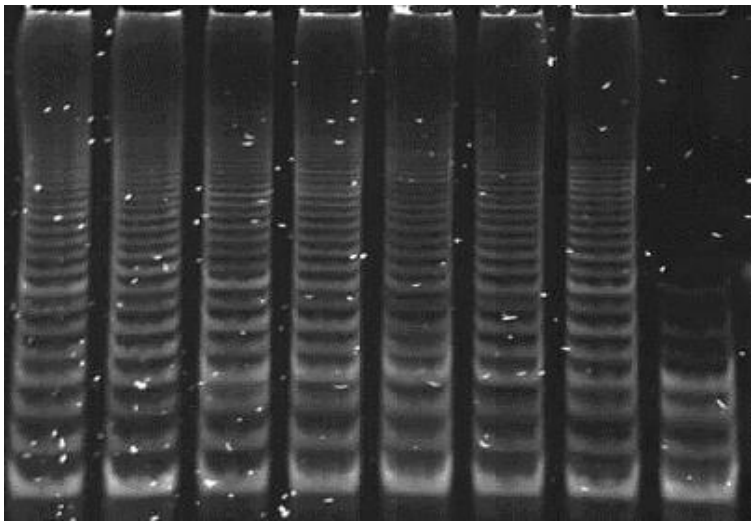

Figure 7.3. Gel showing telomerase activity in MIAPaCa-2 cells treated with compounds **2b** at increasing concentrations. Compound concentrations are indicated. n.c., negative control (line 8); p.c., positive control of untreated cells (with telomerase but no ligand, line 1), increasing concentrations from 1 μM to 50 μM (lines 2-7).

Preliminary biological evaluation has been obtained by the SRB assay. The cell growth inhibition ability of all the macrocyclic derivatives and **V** has been assessed in a panel of cancer cell lines comprising: A549 (lung), MCF7 (breast), MIAPaca-2 (pancreatic), Panc1 (pancreatic), ALT (alternative lengthening of telomeres cancer cells) and W138 (human fibroblast) (Table 7.2).

All the synthesized compounds display a promising cytotoxic activity in the submicromolar and nanomolar range; although none of them is as active as the lead compound **V**.
Further, the cytotoxic activities seem to follow an inverse pattern compared with the result obtained in *in vitro* assays. In particular, taking into account the spermine- and spermidine-derived compounds, the worst G-quadruplex stabilizing agent **4b** is the most active in cell-based assay showing an IC_{50} in submicrolar- or low micromolar range in all five cancer cell lines without showing any cell-type selectivity. On the other hand, the most active compound **3b** in *in vitro* assays is the less active in cell-based assays.

Table 7.2. Short-term 96 h IC_{50} values (in μM) for compounds **1b-5b** and **V** in a cancer cell line panel, comprising MCF7 (breast), A549 (lung cancer), MIAPaCa-2/Panc1 (pancreatic cancer), ALT (Alternative Lengthening of Telomeres) and WI38 (lung fibroblast) cell lines. Esds average 0.25 μM.

	A549	MCF7	MIAPaca-2	Panc1	ALT	WI38
1b	**5.21**	**5.47**	**0.747**	**1.02**	**3.26**	**6.09**
2b	**4.61**	**19.13**	**8.62**	**8.20**	**>25**	**>25**
3b	**10.4**	**>25**	**19.3**	**13.6**	**14.85**	**>25**
4b	**0.951**	**0.834**	**0.389**	**0.386**	**1.00**	**1.29**
5b	**0.488**	**1.178**	**1.01**	**0.627**	**1.09**	**2.86**
V	**0.203**	**0.301**	**0.190**	**0.350**	**0.249**	**0.425**

From the results obtained it is possible to describe a general trend: within the macrocyclic derivatives the cytotoxic activity decreases by enhancing the molecular weight and the number of charges. We have hypothesized that this trend is due to the lower internalization into the cells of the heaviest compounds; in fact, thanks to Lipinski's rules of five, it is well known that features like the molecular weight and the number of hydrogen bonding donors and acceptors can influence the pharmacokinetic profile of a drug. It is, indeed, well known that G-quadruplex-binders do not present, in most of cases, favorable drug-like properties (i.e. molecular weight, etc). Further, highly charged molecules, such as polyamine-based compounds, have several difficulties to cross the cellular lipid bilayers. These derivatives may use an active polyamines transport system PTS to gain into the cells that has proved to be promiscuous, carrier-mediated, pH-dependent and saturable. Despite plenty of polyamine conjugates delivered through the PTS have been reported so far, it is hard to hypothesize that the structures of the new macrocycles fulfil the structural demands of the system because of their high molecular weight and the lack of primary basic functions.
All the newly synthesized derivatives are less active than **V** towards all the cell lines tested but they are more selective for the cancer cell lines respect to the normal fibroblasts (WI38), which are severely affected by compound **V** with an IC_{50} of 425 nM. This effect does not seem to be due to the quadruplex over duplex DNA selectivity, in fact compound **5b**, not endowed with any quadruplex binding activity, is one of the less cytotoxic compound towards the normal fibroblasts together with **1b**.
Among the macrocyclic series, compound **5b** proved to be the most powerful one despite its almost absent DNA-binding activity: that can be due to the insurgence of multiple different mechanisms of action, while **4b** is the most cytotoxic derivative between the spermine and spermidine-like series.
More studies have to be performed in order to understand how our derivatives can get into the cell and their mechanisms of action. Indeed, polyamine-based compounds are able to interact with a multitude of biochemical targets and exert cytotoxic activity through several

mechanisms: macrocyclic-polyamines are reported to display toxic effects by, for instance, depleting cellular ATP and interfering with enzymes of involved in the polyamines biosynthetic pathway.

With the aim to characterize the conformational profile and binding mode for duplex and quadruplex DNAs, compound **2b** has been submitted to molecular modelling studies. Analysis of the ionization state showed that at pH 7.4 the tetracationic form, with two protonated secondary basic functions in each spermine chain, was the most prevalent among all the ionizable states. Consequently, the conformational study has been carried out with this ionization form. Firstly, the conformational degrees of freedom of **2b** have been explored, in particular 3000 conformations were generated by means of the Monte Carlo method. The total number of conformers found within 5 kcal/mol above the global minimum was equal to 56. The plot reported in Fig. 7.3 shows the potential energy (kcal/mol) calculated for each conformer.

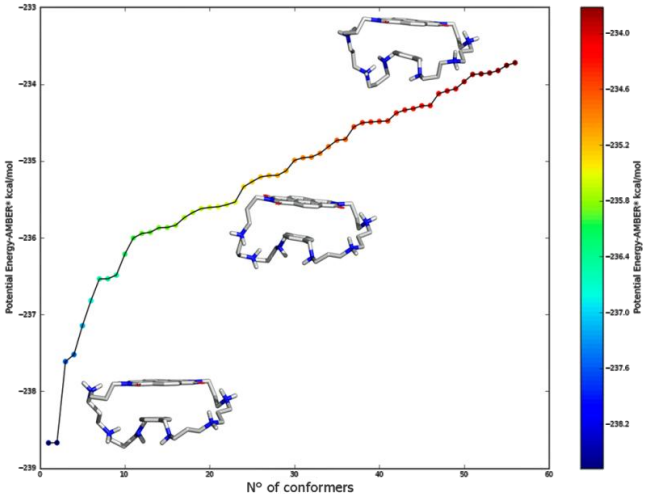

Figure 7.3. Potential Energy scatter plot of the 56 conformers of compound **2b** found in the conformational search. Non polar hydrogen atoms are omitted for clarity.

The energetically most stable conformer of **2b**, shown in Fig. 7.3, ($E_{potential}$ = -238.672 kcal/mol) has been submitted to docking calculations. Concerning the duplex DNA, the lowest energy binding conformation of **2b** (ΔG = -27.18 kcal/mol) was found to recognize the minor groove of the DNA (Fig. 7.4A). Our design strategy has proved to be correct: **2b** is not capable of intercalating between the base pair of the duplex DNA because of steric reason. The steric hindrance of the spermine-like side chains, in fact, prevents the intercalation within the guanine-cytosine region and is mostly involved in electrostatic interactions with the negative counterpart of the phosphate backbone as reported graphically in the Poisson-Boltzmann electrostatic potential surface area (Fig. 7.4B). In addition, the formation of two H-bond interactions with the C5 residue contributes to the binding affinity.

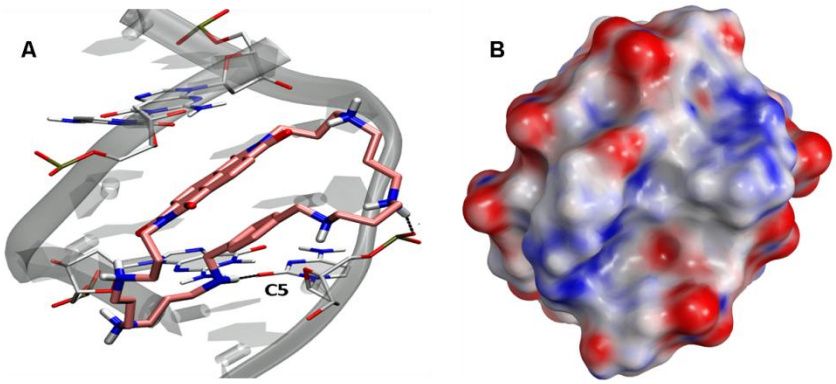

Fig. 7.4. A) Binding mode of compound 2b against the duplex DNA and the involved hydrogen bond interactions. Compound 2b is represented as pink licorice while the duplex DNA in transparent gray ribbon. Hydrogen bonds are depicted as dashed black lines. B) The Poisson-Boltzmann electrostatic potential surface area computed using Maestro ver. 9.7, red and blue colours are respectively related to negative and positive areas.

Surprisingly, in the case of the quadruplex DNA, although NDIs are well known to stack with the external G-quartets of the quadruplex structures, the most energetically stable (ΔG = -63.69 kcal/mol) and populated (Boltzmann's probability of distribution equal to 98.95%) binding conformation of **2b** has been found to be into the groove, close to the G21-G3-G22 residues (Fig. 7.5A). The presence of the protonated nitrogen atoms allows the electrostatic term to be the main driving force in the interaction. This observation is again supported graphically in Fig. 7.5B. These results indicate minor contributions of Van der Waals and H-bond terms, always coherent toward a better G-quadruplex recognition. This binding mode allows us to explain the not excellent selectivity for quadruplex over duplex DNA: the groove binding is allowed in both the DNA structures, thereby preventing the exclusive interaction with the quadruplexes.

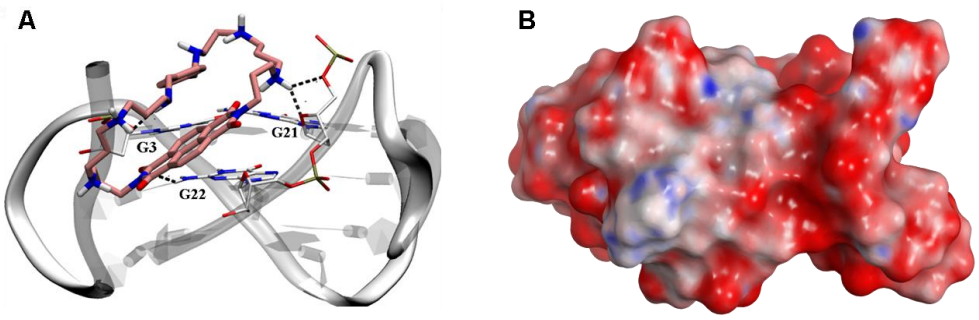

Fig. 7.5.A) Docking best pose of compound 2b against quadruplex DNA and the involved hydrogen bond interactions. The compound b2 is represented as pink licorice while the quadruplex DNA in white ribbon. Hydrogen bonds are depicted as dashed black lines. B) The Poisson-Boltzmann electrostatic potential surface area computed using Maestro ver. 9.7.

The same computational protocol has been used to model the interaction of **5b** with the same sequences as shown in figure 7.6A and B. As it can be seen from the structure, in this case the binding is mainly guided by stacking interactions and by the formation of hydrogen bond with

the phosphate of the skeleton of the loop. As regard the duplex DNA, the steric hindrance again does not allow the intercalation within the base pairs and the interaction happens with the groove of the DNA, but in this case the presence of only two protonated nitrogen atoms prevents the onset of a strong connection.

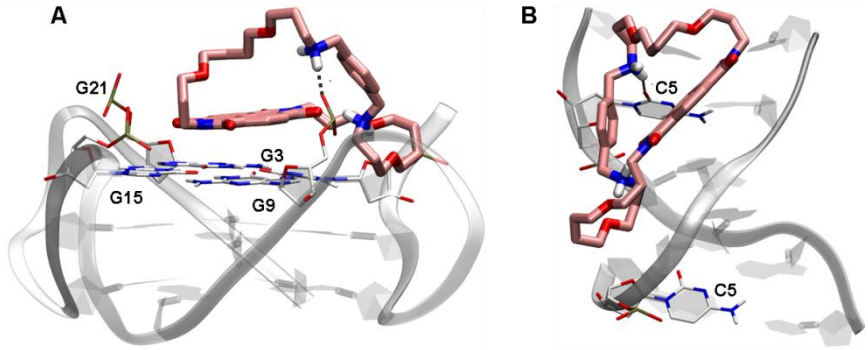

Figure 7.6. Docking best pose computed for compound **5b** against A) G-quadruplex and B) duplex DNA.

7.4 Conclusion

In this work it has been demonstrated that the transformation of a linear structure into a macrocyclic one produces a great enhancement in quadruplex binding activity and selectivity. In particular compounds **2b** and **3b** proved the ability to induce a very high quadruplex stabilization with ΔTm values of 22.1 ºC and 26.8 ºC at 1 µM respectively. This makes them the best G-quadruplex binders within the series, with an affinity comparable to Telomestatin.

The lack of quadruplex selectivity shown by the open derivative **V** strongly suggests that the macrocyclic structure is a minimal requirement for these NDI derivatives. The absence of quadruplex binding activity displayed by compound **5b** indicates that also the presence of protonable basic functions is necessary for the interaction with the DNA, both in duplex and quadruplex form.

Molecular modelling studies were performed and, coherently with experimental data, compound **2b** was found to be highly selective in the G-quadruplex topology respect to duplex. A deeper evaluation of the non-covalent bond interactions, pointed out that the four protonated aliphatic secondary amine groups of the spermine-like side chains were the most involved part of the designed macrocyclic NDI in the quadruplex recognition. Hence, the electrostatic term resulted as the main driving force in the binding process although even H-bond interactions can discriminate between the quadruplex/duplex selectivity.

The cytotoxic activities of these derivatives displayed an unexpected trend, not correlated with the *in vitro* data. All the derivatives possessed a high cytotoxic activity in the submicro- and nanomolar range, but the most cytotoxic compounds are **1b** and **5b**, i.e. the worst quadruplex binders. We have hypothesized that is due to the lower internalization of the heavier and most protonated compounds into the cells. The smaller and less charged derivatives proved to be more active in inhibiting the growth of cancer cells, probably due to their better pharmacokinetic profiles. The druglikeness has always been an issue in the G-quadruplex ligand field and these results confirm that trend. The good *in vitro* and cellular activities suggest that appropriate modifications aiming at enhancing drug-like features should result in an enhanced biological activity.

7.5 Experimental section

7.5.1 Chemistry

For the experimental procedures see Chapter 5.5.1.
Compounds **1b-5b** were synthesized following the general procedure developed by our research group as follows (see scheme 7.1 and 7.2).

General procedure for the synthesis of 1b-4b.
To a cooled solution (0 °C) of the appropriate compound **26b-29b** (1 eq) in MeOH was added dropwise HCl 3N. The reaction mixture was stirred at r.t. for 16 h, and then the solvent was removed in vacuum. The residue was taken up with H_2O and washed three times with ether. The aqueous phase was evaporated in vacuum to obtain **1b-4b**, as hydrochloride salts.
(1b). Yellow solid: quantitative yield; mp >250 °C; ^{1}H NMR (400 MHz, D_2O) δ 2.12.- 2.28 (m, 8H), 3.15- 3.29 (m, 12H), 3.47- 3.54 (m, 8H), 4.30 (s, 4H), 4.33 (t, 4H, *J* = 6 Hz), 7.54 (s, 4H), 8.74 (s, 4H); ^{13}C NMR (100MHz, D_2O) δ 22.47, 24.49, 37.44, 42.57, 42.67, 43.39, 44.66, 45.55, 50.36, 121.80, 126.76, 130.67, 131.16, 131.51, 164.13; MS (ESI) m/z = 683 $(M+H)^+$.
(2b). Yellow solid: quantitative yield; mp >250 °C; ^{1}H NMR (400 MHz, D_2O)) δ 2.11- 2.14 (m, 8H), 2.17- 2.22 (m, 4H), 3.13- 3.20 (m, 20H), 4.30 (s, 4H), 4.32 (t, 4H, *J* = 6 Hz), 7.56 (s, 4H), 8.74 (s, 4H); 13C NMR (100MHz, D2O) δ 22.37, 24.21, 37.30, 43.56, 44.26, 44.30, 44.38, 45.06, 50.53, 126.16, 126.22, 130.72, 131.14, 131.73, 164.64; MS (ESI) m/z = 356 $(M+2H)^{+2}$.
(3b). Yellow solid: 92% yield; mp > 250°C; ^{1}H NMR (400 MHz, D_2O) δ 1.76- 1.77 (m, 8H), 2.07- 2.21 (m, 8H), 3.01- 3.26 (m, 20H), 4.29- 4.78 (m, 8H), 7.55 (s, 4H), 8.60 (s, 4H); ^{13}C NMR (100MHz, D_2O) δ 19.82, 22.34, 22.43, 24.40, 37.48, 43.56, 44.08, 44.95, 46.54, 50.41, 53.66, 125.98, 130.68, 131.10, 131.63, 135.73, 164.41; MS (ESI) m/z = 370 $(M+2H)+^2$.
(4b). Yellow solid: quantitative yield; mp >250 °C; ; ^{1}H NMR (400 MHz, D_2O) δ 2.08- 2.20 (m, 8H), 3.03- 3.22 (m, 12H), 4.24 (s, 4H), 4.35 (t, 4H, *J* = 5.8 Hz), 7.47 (s, 4H), 8.62 (s, 4H); ^{13}C NMR (100MHz, D_2O) δ 21.81, 24.09, 37.05, 43.83, 44.03, 44.19, 50.56, 125.75, 125.86, 130.59, 131.19, 131.74, 164.16; MS (ESI) m/z = 597 $(M+H)^+$.

General procedure for the synthesis of 5b and 26b-29b.
The appropriate precursor **32b** and **22b-25b** (1 eq) was dissolved in EtOH (10^4 eq) and 3Å molecular sieves were added to the solution. A solution of terephthalaldehyde (1eq) in EtOH (10^4 eq) was added dropwise within 72 h. Then $NaBH_4$ (1eq) was added to the solution and the stirring was continued for 16 h at r.t. The solvent was evaporated, the residue was taken up with CH_2Cl_2 and washed with brine. The organic phase was dried and evaporated under vacuum, the residue was purified by flash chromatography eluting with a mixture of CH_2Cl_2/MeOH/33% aq.NH_4OH 9/1/0.03 to give **5b and 26b-29b,** respectively. **5b** was then dissolved in Et_2O and treated with Et_2O saturated with HCl, in order to obtain **5b** as dihydrocloride salt.
(5b) Free base. Yellow solid: 23% yield; ^{1}H NMR (200 MHz, $CDCl_3$) δ 1.26- 1.31 (m, 8H), 1.71- 1.77 (m, 4H), 2.01- 2.07 (m, 4H), 2.71 (t, 4H, *J* = 6 Hz), 2.83 (brs, 2H, exch D_2O), 3.11- 3.57 (m, 16H), 3.78 (s, 4H), 4.34 (t, 4H, *J* = 6 Hz), 7.29 (s, 4H), 8.71 (s, 4H).
(5b) Hydrochloride salt. Pink solid: quantitative yield; mp > 250°C; ^{1}H NMR (400 MHz, D_2O) δ 1.15- 1.18 (m, 8H), 1.86- 1.89 (m, 4H), 1.98- 2.01 (m, 4H), 3.06- 3.10 (m, 4H), 3.14- 3.17 (m, 4H), 3.28- 3.31 (m, 4H), 3.40- 3.43 (m, 4H), 3.58- 3.61 (m, 4H), 3.20- 3.23 (m, 8H), 7.51 (s, 4H), 8.40 (s, 4H); ^{13}C NMR (100 MHz, D_2O) δ 25.13, 25.21, 25.35, 26.78, 39.06, 45.01, 50.06, 67.61, 68.99, 70.24, 70.31, 125.30, 125.51, 130.45, 131.06, 132.01, 163.30. MS (ESI) *m/z* 743 $(M+H)^+$.

tetra-tert-butyl 11,13,16,18-tetraoxo-11,12,13,16,17,18-hexahydro-5,8,12,16,20,23-hexaaza-1(2,7)-benzo[lmn][3,8]phenanthrolina-14(1,4)-benzenacyclo- hexacosaphane-5,8,20,23-tetracarboxylate (26b). Yellow oil: 31% yield; ^{1}H NMR (400 MHz, $CDCl_3$) δ 1.23- 1.43 (m, 36H), 1.60 (brs, 2H, exch D_2O), 1.69- 1.73 (m, 4H), 1.96- 1.99 (m, 4H), 2.56- 2.59 (m, 4H), 3.23- 3.32 (m, 16H), 3.68 (s, 4H), 4.20 (t, 4H, *J* = 6 Hz), 7.17 (s, 4H), 8.57 (s, 4H).

tetra-tert-butyl 11,13,16,18-tetraoxo-11,12,13,16,17,18-hexahydro-5,9,13,17,21,25-hexaaza-1(2,7)-benzo[lmn][3,8]phenanthrolina-15(1,4)-benzenacycloocta cosaphane-5,9,21,25-tetracarboxylate (27b). Yellow oil: 18% yield; ^{1}H NMR (400 MHz, $CDCl_3$) δ 1.23- 1.43 (m, 36H), 1.78- 1.97 (m, 12H), 2.69- 2.74 (m, 4H), 3.17- 3.31 (m, 16H), 3.80 (s, 4H), 4.20 (t, 4H, *J* = 8 Hz), 7.37 (s, 4H), 8.64 (s, 4H).

tetra-tert-butyl 11,13,16,18-tetraoxo-11,12,13,16,17,18-hexahydro-5,10,14,18,22,27-hexaaza-1(2,7)-benzo[lmn][3,8]phenanthrolina-16(1,4)-benzenacyclo- triacontaphane-5,10,22,27-tetracarboxylate (28b). Yellow oil: 34% yield; ^{1}H NMR (400 MHz, $CDCl_3$) δ 1.36- 1.42 (m, 36H), 1.49- 1.57 (m, 8H), 1.81- 1.87 (m, 4H), 1.91-1.98 (m, 4H), 2.68- 2.71 (m, 4H), 3.14- 3.28 (m, 16H), 3.81 (s, 4H), 4.19 (t, 4H, *J* = 6 Hz), 7.40 (s, 4H), 8.69 (s, 4H).

di-tert-butyl 11,13,16,18-tetraoxo-11,12,13,16,17,18-hexahydro-5,9,13,17-tetraaza-1(2,7)-benzo[lmn][3,8]phenanthrolina-11(1,4)-benzenacycloicosaphane-5,17-dicarboxylate (29b). Yellow oil: 26% yield; ^{1}H NMR (400 MHz, $CDCl_3$) δ 1.39- 1.48 (m, 22H), 2.00- 2.03 (m, 4H), 2.44- 2.49 (m, 4H), 3.14- 3.17 (m, 4H), 3.25- 3.29 (m, 4H), 4.09 (s, 4H), 4.27- 4.31 (m, 4H), 6.94 (s, 4H), 8.71 (s, 4H).

General procedure for the synthesis of 10b-13b.

A solution of the appropriate polyamine **6b-9b** (1 eq) in MeOH (30 ml) was cooled to -78 °C and ethyl trifluoroacetate (2 eq) was added dropwise within 30 minutes. The stirring solution was allowed to r.t. and a solution of Boc_2O (2 eq for **6b-8b**, 1 eq for **9b**) in MeOH was added dropwise. The reaction mixture was stirred at r.t. for 16 h, then a solution of NaOH 40% was added and the stirring was continued for other 20 h. The solvent was evaporated under vacuum and the residue was taken up with H_2O and extracted with CH_2Cl_2. The organix layers, dried and evaporated, were purified by flash chromatography eluting with a mixture of CH_2Cl_2/MeOH/33% aq.NH_4OH 8/2/0.2 to give **10b-13b,** respectively.

di-tert-butyl ethane-1,2-diylbis((3-aminopropyl)carbamate) (10b). Yellow oil: 80% yield; ^{1}H NMR (400 MHz, $CDCl_3$) δ 1.38 (s, 18H), 1.79-1.88 (m, 4H), 2.70-2.28 (m, 4H), 2.89- 2.96 (m, 4H), 3.17 (s, 4H).

di-tert-butyl propane-1,3-diylbis((3-aminopropyl)carbamate) (11b). Yellow oil: 87% yield; ^{1}H NMR (400 MHz, $CDCl_3$) δ 1.42 (s, 18H), 1.70- 1.79 (m, 4H), 1.85- 1.92 (m, 2H), 2.50- 2.61 (m, 4H), 2.96 (t, 4H, *J* = 7.4 Hz), 3.12- 3.18 (m, 4H).

di-tert-butyl butane-1,4-diylbis((3-aminopropyl)carbamate) (12b). Yellow oil: 92% yield; ^{1}H NMR (400 MHz, $CDCl_3$) δ 1.45- 1.47 (m, 18H), 1.48- 1.53 (m, 4H), 1.79- 1.85 (m, 4H), 2.55- 2.63 (m, 4H), 3.01- 3.15 (m, 8H).

tert-butyl bis(3-aminopropyl)carbamate (13b). Yellow oil: 90% yield; ; ^{1}H NMR (400 MHz, $CDCl_3$) δ 1.38 (s, 9H), 1.79- 1.92 (m, 4H), 2.55- 2.63 (m, 4H), 3.01 (t, 4H, *J* = 7.2 Hz).

General procedure for the synthesis of 14b-17b.

The appropriate compound **10b-13b** (3 eq) was dissolved in MeOH and ethyl trifluoroacetate (1 eq) was added dropwise. The solution was allowed to stir for 16 h at r.t., then the reaction mixture was evaporated and the residue was purified by flash chromatography eluting with a mixture of CH_2Cl_2/MeOH/33% aq.NH_4OH 9/1/0.1 to give **14b-17b, respectively**.

tert-butyl (3-aminopropyl)(2-((tert-butoxycarbonyl)(3-(2,2,2-trifluoroacetamido) propyl)amino)ethyl)carbamate (14b). Yellow oil: 93% yield; ^{1}H NMR (400 MHz, $CDCl_3$) δ

1.42- 1.43 (s, 18H), 1.61- 1.68 (m, 4H), 1.77 (brs, 2H, exch D_2O), 2.66 (t, 2H, *J* = 6 Hz), 3.23- 3.26 (m, 10H), 8.12 (brs, 1H, exch D_2O).

tert-butyl (3-aminopropyl)(3-((tert-butoxycarbonyl)(3-(2,2,2-trifluoroacetamido) propyl)amino)propyl)carbamate (15b). Yellow oil: 83% yield; ^{1}H NMR (400 MHz, $CDCl_3$) δ 1.44- 1.45 (s, 18H), 1.65- 1.76 (m, 6H), 1.94 (brs, 2H, exch D_2O), 2.70 (t, 2H, *J* = 6 Hz), 3.13- 3.19 (m, 4H), 3.29- 3.36 (m, 6H), 8.15 (brs, 1H, exch D_2O).

tert-butyl(3-aminopropyl)(4-((tert-butoxycarbonyl)(3-(2,2,2trifluoroacetamido) propyl)amino)butyl)carbamate (16b). Yellow oil: 74% yield; ^{1}H NMR (200 MHz, $CDCl_3$) δ 1.34- 1.59 (s, 18 H), 1.60- 1.81 (m, 6H), 2.65- 2.85 (m, 2H), 2.86- 3.08 (m, 2H), 3.08- 3.40 (m, 10H).

tert-butyl (3-aminopropyl)(3-(2,2,2-trifluoroacetamido)propyl)carbamate (17b). Yellow oil: 98% yield; ^{1}H NMR (400 MHz, $CDCl_3$) δ 1.41-1.44 (s, 9H), 1.63- 1.68 (m 4H), 1.75 (brs, 2H, exch D_2O), 3.20 (t, 2H, *J* = 6 Hz), 3.28- 3.29 (m, 4H), 3.42- 3.47 (m, 2H), 8.17 (brs, 1H, exch D_2O).

General procedure for the synthesis of 18b-21b and 31b.

To a solution of **14b-17b and 31b** (2 eq) in DMF was added NTCDA (1eq). The reaction mixture was refluxed for about 2 h, until the reagents were consumed. Following solvent removal, the residue was purified by flash chromatography eluting with a mixture of petroleum ether/EtOAc 5/5 to give the desire products **18b-21b** and **31b**, respectively.

di-tert-butyl ((1,3,6,8-tetraoxo-1,3,6,8-tetrahydrobenzo[lmn][3,8]phenanthroline-2,7-diyl)bis(propane-3,1-diyl))bis((2-((tert-butoxycarbonyl)(3-(2,2,2-trifluoroaceta- mido) propyl)amino)ethyl)carbamate) (18b). Brown oil: 16% yield; ^{1}H NMR (400 MHz, $CDCl_3$) δ 1.41- 1.44 (m, 36H), 1.70- 1.76 (m, 4H), 1.97- 2.01 (m, 4H), 3.24- 3.31 (m, 20H), 4,18- 4.20 (m, 4H), 8.74 (s, 4H).

di-tert-butyl ((1,3,6,8-tetraoxo-1,3,6,8-tetrahydrobenzo[lmn][3,8]phenanthroline-2,7-diyl)bis(propane-3,1-diyl))bis((3-((tert-butoxycarbonyl)(3-(2,2,2-trifluoroaceta-mido)propyl)amino)propyl)carbamate) (19b). Brown oil: 43% yield; ^{1}H NMR (400 MHz, $CDCl_3$) δ 1.30- 1.40 (m, 36H), 1.64- 1.69 (m, 4H), 1,71- 1.74 (m, 4H), 1.89- 1.94 (m, 4H), 3.10- 3.25 (m, 20H), 4.12 (t, 4H, *J* = 8 Hz), 8.11 (brs, 2H), 8.66 (s, 4H).

di-tert-butyl ((1,3,6,8-tetraoxo-1,3,6,8-tetrahydrobenzo[lmn][3,8]phenanthroline-2,7-diyl)bis(propane-3,1-diyl))bis((4-((tert-butoxycarbonyl)(3-(2,2,2-trifluoroaceta-mido)propyl)amino)butyl)carbamate) (20b). Brown oil: 50% yield; ^{1}H NMR (400 MHz, $CDCl_3$) δ 1.24- 1.44 (m, 36H), 1.45- 1.51 (m, 8H), 1.67- 1.70 (m, 4H), 1.96- 1.99 (m, 4H), 3.15- 3.18 (m, 4H), 3.24- 3.30 (m, 16H), 4.19- 4.21 (m, 4H), 8.74 (s, 4H).

di-tert-butyl ((1,3,6,8-tetraoxo-1,3,6,8-tetrahydrobenzo[lmn][3,8]phenanthroline-2,7-diyl)bis(propane-3,1-diyl))bis((3-(2,2,2-trifluoroacetamido)propyl)carbamate) (21b). Yellow oil: 47% yield; ^{1}H NMR (400 MHz, $CDCl_3$) δ 1.44 (s, 18H), 1.74- 1.78 (m, 4H), 1.96- 2.03 (m, 4H), 3.35- 3.37 (m, 12H), 4.20 (t, 4H, *J* = 8 Hz), 8.13 (brs, 2H), 8.76 (s, 4H).

tert-butyl (2- (4- (3- (7- (2,2-dimethyl-4-oxo-3,9,14-trioxa-5-azaheptadecan-17-yl)-1,3,6,8-tetraoxo-3,6,7,8-tetrahydrobenzo[lmn][3,8]phenanthrolin-2(1H)-yl) ropoxy) butoxy)ethyl)carbamate (31b). Brown oil: 90% yield; ^{1}H NMR (400 MHz, $CDCl_3$) δ 1.41 (s, 18H), 1.52- 1.54 (m, 4H), 1.69- 1.72 (m, 8H), 1.99- 2.03 (m, 4H), 3.17- 3.18 (m, 4H), 3.31- 3.34 (m, 4H), 3.38- 3.44 (m, 8H), 3.52- 3.55 (m, 4H), 4.29 (t. 4H, *J* = 6 Hz), 4.90 (brs, 2H, exch D_2O), 8.71 (s, 4H).

General procedure for the synthesis of 22b-25b.

The appropriate compound **18b-21b** (1 eq) was dissolved in a mixture of MeOH/H_2O (10:1 ratio) and to the resulting solution was added K_2CO_3 (10 eq). The reaction mixture was refluxed for 2 h, then the solvent was removed and the residue was taken up with H_2O and

extracted with CH_2Cl_2. The organic phase was dried and evaporated in vacuum, the residue was purified by flash chromatography eluting with a mixture of CH_2Cl_2/MeOH/33% aq.NH_4OH 8/2/0.2 to give **22b-25b, respectively**.

di-tert-butyl ((1,3,6,8-tetraoxo-1,3,6,8-tetrahydrobenzo[lmn][3,8]phenanthroline-2,7-diyl)bis(propane-3,1-diyl))bis((2-((3-aminopropyl)(tert-butoxycarbonyl)amino) ethyl)carbamate) (22b). Brown oil: 44% yield; ^{1}H NMR (400 MHz, $CDCl_3$) δ 1.49 (s, 36H), 1.72- 1.90 (m, 4H), 1.96- 2.00 (m, 4H), 3.68- 3.87 (m, 4H), 3.32- 3.33 (m, 16H), 4.21- 4.25 (m, 4H), 8.75 (s, 4H).

di-tert-butyl ((1,3,6,8-tetraoxo-1,3,6,8-tetrahydrobenzo[lmn][3,8]phenanthroline-2,7-diyl)bis(propane-3,1-diyl))bis((3-((3-aminopropyl)(tert-butoxycarbonyl)amino) propyl)carbamate) (23b). Brown oil: 63% yield; ^{1}H NMR (400 MHz, $CDCl_3$) δ 1.42- 1.44 (m, 36H), 1.79-1.81 (m, 8H), 1.96- 1.97 (m, 4H), 2.87- 2,94 (m, 4H), 3.16- 3.23 (m, 8H), 3.24-3.33 (m, 8H), 4. 20 (t, 4H, *J* = 8 Hz), 8.76 (s, 4H).

di-tert-butyl ((1,3,6,8-tetraoxo-1,3,6,8-tetrahydrobenzo[lmn][3,8]phenanthroline-2,7-diyl)bis(propane-3,1-diyl))bis((4-((3-aminopropyl)(tert-butoxycarbonyl) amino) butyl)carbamate) (24b). Brown oil: 61% yield; ^{1}H NMR (400 MHz, $CDCl_3$) δ 1.37- 1.40 (m, 36H), 1.44- 1.49 (m, 12H), 1.95- 2.01 (m, 4H), 2.93- 3.01 (m, 4H), 3.20- 3.51 (m, 16H), 4.18 (m, 4H), 8.83 (s, 4H).

di-tert-butyl ((1,3,6,8-tetraoxo-1,3,6,8-tetrahydrobenzo[lmn][3,8]phenanthroline-2,7-diyl)bis(propane-3,1-diyl))bis((3-aminopropyl)carbamate) (25b). Yellow oil: 60% yield; ^{1}H NMR (400 MHz, $CDCl_3$) δ 1.42 (s, 18H), 1.62- 1.80 (m, 4H), 1.95- 1.99 (m, 4H), 2.77-2.80 (m, 4H), 3.13- 3.29 (m, 8H), 4.16- 4.21 (m, 4H), 8.72 (s, 4H).

Synthesis of compound 30b

The appropriate polyamine (10 eq) was dissolved in CH_2Cl_2,a solution of Boc_2O (1 eq) in CH_2Cl_2 was added slowly dropwise. The reaction mixture was allowed to stir at r.t. for 16 h. The solvent was removed under vacuum, the residue was taken up with H_2O and extracted with CH_2Cl_2. The organic phase was dried over Na_2SO_4 and evaporated to obtain the desire product **30b**.

tert-butyl (3-(4-(3-aminopropoxy)butoxy)propyl)carbamate (30b). Yellow oil: 93% yield; ^{1}H NMR (400 MHz, $CDCl_3$) δ 1.44 (s, 9H), 1.62-1.77 (m, 8H), 2.77- 2.81 (m, 2H), 3.20- 3.21 (m, 2H), 3.40- 3.50 (m, 8H), 5.21 (brs, 1H, exch $D_2$0).

Synthesis of compound 32b

To a stirring solution of **30b** (1 eq) in MeOH, HCl 3N was added dropwise at 0° C. The stirring was continued for 16 h. The solvent was removed, the residue was taken up with H_2O and washed with Et_2O; the aqueous phase was basified with NaOH and the resulting solution was extracted with CH_2Cl_2. The organic phase was dried over Na_2SO_4 and dried to obtain the desire product **32b**.

tert-butyl (3-(4-(3-(7-(3-(4-(3-aminopropoxy)butoxy)propyl)-1,3,6,8-tetraoxo-7,8-dihydrobenzo[lmn][3,8]phenanthrolin-2(1H,3H,6H)-yl)propoxy)butoxy)propyl)carbamate (32b). Yellow oil: 88% yield; ^{1}H NMR (400 MHz, $CDCl_3$) δ 1.48- 1.51 (m, 8H), 1.71- 1.73 (m, 4H), 2.00- 2.03 (m, 4H), 2.81- 2.83 (m, 4H), 3.31 (t, 4H, *J* = 5.8 Hz), 3.37 (t, 4H, *J* = 5.8 Hz), 3.44 (t, 4H, *J* = 6.4 Hz), 3.54 (m, 4H, *J* = 6.0 Hz), 4.30 (t, 4H, *J* = 7.0 Hz), 8.74 (s, 4H).

7.5.2 Biophysical Evaluation

7.5.2.1 Fluorescence Resonance Energy Transfer (FRET)

The following oligonucleotide sequences, all purchased from Eurofins, were used: F21T: (5‟-FAM-GGG TTA GGG TTA GGG TTA GGG-TAMRA-3‟), c-kit2 (5‟-FAM-CCC GGG CGG GCG CGA GGG AGG GGA GG-TAMRA-3‟), T-Loop: (5‟-FAM-TAT AGC TATA TTT TTT TATA GCT ATA-TAMRA-3‟). TAMRA (6-carboxytetramethylrhodamine) is the acceptor fluorophore, and FAM (6-carboxyfluorescein) is the donor fluorophore. From 20 μM stock solutions, 400 nM solutions in FRET buffer (60 mM potassium cacodylate pH 7.4) were prepared. The nucleotides were annealed by heating the samples to 90 °C for 10 min and allowing them to cool down to RT within 4 h. 10 mM solutions of the compounds in deionised water were prepared and diluted to double of the required concentrations with FRET buffer. In RT-PCR 96 well plates (MJ Research, Waltham, MA), each well was loaded with 50 μL of nucleotide solution and 50 μL of drug solution. Drug concentrations of 0.1, 0.2, 0.5, 1, 2, 5 and 10 μM were used, and every drug concentration was repeated 3 times. Measurements were made on a DNA Engine Opticon (MJ Research) with excitation at 450 – 495 nm and detection at 515 – 545 nm. The flourescence was read at intervals of 0.5 °C over the range 30 – 100 °C. Before each reading the temperature was held constant for 30 s. The raw data were processed using Origin (Version 7.0, OriginLab Corp.). The graphs were smoothed using a 10-point running average and normalized. The melting temperatures were obtained by determining the maxima of the first derivative of the smooth melting curves. The value ΔT is the melting temperature difference between the nucleotide with drug and the negative control.

7.5.3 Biology

7.5.3.1 Cell Culture

The cell lines ALT, MCF7, A549, MIA-Paca-2, Panc-1 (European Collection of Cell Cultures) and WI38 (American Type Culture Collection) were maintained in monolayer culture in 75 cm2 flasks (TPP, Switzerland) under a humidified 5 % CO_2 atmosphere at 37 °C. For the cell line A549, the medium Dulbecco's MEM (GIBCO 21969, Invitrogen, UK) supplemented with L-glutamine (2 mM, GIBCO 25030, Invitrogen, UK), essential amino acids (1 %, GIBCO 11140, Invitrogen, UK), and foetal calf serum (10 %, S1810, Biosera, UK) was used. For MIAPa-Ca-2 and Panc-1, Dulbecco's MEM, supplemented with L-glutamine (2 mM) and foetal calf serum (10 %) was used. The medium MEM (M2279, Sigma, UK) with added L-glutamine (2 mM), essential amino acids (1 %) and foetal calf serum (10 %) was used for the cell lines WI38, MCF7 and ALT. To passage the cells, they were washed with PBS (GIBCO 14040, Invitrogen, UK), treated with trypsine (GIBCO 25300, Invitrogen, UK), and re-seeded into fresh medium, resulting in an initial cell density of approximately $1x10^4$ cells/mL medium. Cells were counted using a Neubauer haemocytometer (Assistant, Germany) by microscopy or a MacsQuant flow cytometer (Miltenyi Biotech, Germany) on a suspension of cells obtained by washing with PBS, trypsinisation, centrifugation at 8 °C at 8000 rpm for 3 minutes, and re-suspension in fresh medium.

7.5.3.2 Sulforhodamine B (SRB) short-term cytotoxicity assay

The cells were counted and diluted to the required concentration in 20 mL medium. For the cell lines A549, Panc-1 and MIA-Pa-Ca-2, 2000 cells with 160 μL media were seeded into each well of a 96 well plate (Nunc, Denmark). For WI38, 6000 cells per well, while for MCF7, 4000 cells per well were used due to their higher doubling time. After incubation for 24 hours, the compounds to be tested, dissolved in 40 μL of medium, were added at different

concentrations, and the cells incubated for 96 hours. The medium was then removed and the cells fixed by incubation with TCA (10 %, Sigma-Aldrich, UK) in water for 30 min. After removal of the TCA, the cells were washed with deionised water 5 times and dried at 60 °C for 1 h. Cells were then incubated with SRB (80 µL, 0.4 % in 1 % acetic acid, Acros Organics, UK) for 15 min at r.t. The SRB was removed, the wells washed with 1 % acetic acid (200 µL), and dried at 60 °C for 1 h. Tris-base (100 µL, 10 mM, Acros Organics, UK) solution was added to each well, and the plates were gently shaken for 5 min. The absorbance at 540 nm was measured with a plate reader (Spectrostar Omega, BMG Labtech, Germany). The data were normalised to the value of 100 for the control experiment (untreated cells), and the IC_{50} values were obtained by interpolation from a plot done with Origin (Version 7.0, OriginLab Corp.), as the concentration leading to an absorbance intensity of 50%.

7.5.3.3 Telomerase repeat amplification protocol (TRAP) assay

Pelleted cells were lysed in RIPA lysis buffer (1x) containing protease cocktail inhibitors, PMSF and sodium orthovanadate (Santa Cruz Biotechnology) according to manufacturer's instruction. Total protein concentration was determined using the Pierce BCA protein assay kit according to manufacturer's instructions. Protein extract from MIA-Pa-Ca-2 cells treated with the compound was incubated with master mix containing the TS forward primer (0.1 µg of 5'-AAT CCG TCG AGC AGA GTT-3'), TRAP buffer (20 mM Tris-HCl [pH 8.3], 68 mM KCl, 1.5 mM MgCl2, 1 mM EGTA, 0.05 % v/v Tween-20), bovine serum albumin (0.05 µg), and dNTPs (125 µM each), protein extract (1000 ng/sample) diluted in lysis buffer (10 mM Tris-HCl, pH 7.5, 1 mM MgCl2, 1 mM EGTA, 0.5 % CHAPS, 10 % glycerol, 5 mM ß-mercaptoethanol, 0.1 mM AEBSF). The telomerase elongation step was carried out for 10 min at 30 °C, followed by 94 °C for 5 min and a final maintenance of the mixture at 20 °C. Elongated products were purified using the QIAquick nucleotide purification kit (Qiagen) according to the manufacturer's instructions. The purified samples were freeze-dried and then redissolved in PCR-grade water at r.t. prior to the amplification step. Purified telomerase extended samples were then subject to PCR amplification. For this, a second PCR master mix was prepared consisting of ACX reverse primer (1 µM, 5'-GCG CGG [CTTACC]3 CTA ACC-3'), TS forward primer (0.1 µg, 5'-AAT CCG TCG AGC AGA GTT-3'), TRAP buffer, BSA (5 µg), 0.5 mM dNTPs, and 2 U of TAQ polymerase (RedHot, ABgene, Surrey, UK). An aliquot of 10 µL of the master mix was added to the purified telomerase extended samples and amplified for 35 cycles of 94 °C for 30 s, at 61 °C for 1 min, and at 72 °C for 1 min. Samples were separated on a 12 % PAGE and visualised with SYBR green (Sigma Aldrich, UK) staining. Gels were quantified using a gel scanner and gene tool software (Sygene, Cambridge, UK). Intensity data were obtained by scanning and integrating the total intensity of each PCR product ladder in the denaturing gels. Drug treated samples were normalised against positive control containing untreated protein only. All samples were corrected for background by subtracting the fluorescence reading of the negative control.

7.5.4 Molecular Modeling

The molecular modeling studies were performed using different computational methods. The ionization state was analyzed by the LigPrep program ver. 2.9. The conformational analysis of compound **2** and **8** was performed by the Monte Carlo search as implemented in MacroModel, generating 3000 conformations and energy minimizing them by the AMBER* force field with the united atom notation and the GB/SA water salvation model. Docking experiments were carried out with Autodock 4.2 (AD4) software package. Full energy optimizations of DNA complexes with the compounds were carried out in the same conditions used for the conformational search of the isolated compounds. , docking calculations have been performed

using X-Ray experimental models of a 6 bp DNA duplex (PDB code: 1Z3F) complexed with the anticancer agent ellipticine, and the h-Tel sequence of the bimolecular quadruplex d(TAGGGTTAGGGT) (PDB code: 3CDM) co-crystallized with a tetrasubstituted naphthalene-diimide.

Chapter 8. Trisubstituted naphthalene diimides as G-quadruplex binding agents

8.1 Drug design

Pathways exhibiting differential activity in cancer cells compared to healthy cells are attractive targets for therapeutic intervention. Because of its overexpression in cancer cells, telomerase has been validated as an interesting target with the aim to obtain new anticancer entities endowed with as limited as possible side effects. As described before, one strategy to target telomere maintenance is the development of G-quadruplex ligands and, among different structures investigated until now, the NDI scaffold is very suitable for the design of new G-quadruplex binders. This nucleus possesses a π-acidic core, able to perform π-π stacking interactions with the external G-tetrads and, when it is functionalized with four side chains bearing amine end groups, has the potential to interact with the grooves at the sides of the G-quadruplexes, as demonstrated by X-ray crystallography.
Neidle and coworkers described a series of tetrasubstituted NDIs with high affinity for human telomeric DNA, endowed with high potency for growth inhibition in a panel of cancer cell lines, concomitant with telomerase inhibition. Among them, the most promising compound is Endamine, a derivative containing two N-methyl-piperazine and two morpholine end group side arms, that has shown exceptional potency in a panel of pancreatic cancer cell lines, with IC_{50} values in the low nanomolar range. This compound has also been tested in *in vivo* models with very good results.
Starting from these premises, the aim of this project was to synthesize new potent G-quadruplex ligands with improved antiproliferative activity, better pharmacokinetics properties (according to Lipinski's rule of five) and lower toxicity to normal cells than Endamine, in order to increase the uptake into the cells and limit the side effects.
Lipinski's rule of five is used to predict the druglikeness or determine if a chemical compound with a certain pharmacological or biological activity has properties suitable to make it an oral drug. The rule describes molecular properties that have proved to be important for the ADME (absorption, distribution, metabolism and excretion) profile in the humans. Following Lipinski's rules, a chemical compound can become a drug only if:

- its molecular mass is less than 500 Daltons;
- it does not contain more than 5 hydrogen bond donors;
- it does not contain more than 10 hydrogen bond acceptors;
- it has a LogP (octanol-water partition coefficient) lower than 5.

Endamine does not comply some of the rules, mainly because of the presence of the side chains and large end groups that add weight to the NDI nucleus, leading to a molecular weight of 831 g/mol. Furthermore, Lipinski's rules state that no more than 10H-bond acceptors and 5H-bond donors should be present in a drug molecule. The amount of H-bond donors and H–acceptors depends on the protonation state of the N-methyl-piperazine moieties, but in the best scenario of a single protonation of only one N-methyl-piperazine group, both requirements would not be obeyed in Endamine. Another requirement is an octanol/water partition coefficient logP below 5, sadly the hydrosolubility of the N-methylpiperazinyl compound is expected to be high.

In order to solve these issues, we synthesized a series of trisubstituted NDIs starting from Endamine as lead compound (Fig. 8.1). From SAR studies done before, it is known that the two morpholine end-group as diimide side arms are very important for the quadruplex stabilization, so we decide to delete one of the two N-methyl-piperazine chains, in order to obtain trisubstituted NDIs.

This kind of compounds retains in part the selectivity for quadruplex over duplex DNA and, thanks to this strategy, we are able to decrease the molecular weight, the number of hydrogen bond acceptors and the logP. All the synthesized compounds have a molecular weight around 600 g/mol, and two or three H-bond acceptors less than the lead compound. In order to perform some SAR studies, the *N*-methyl-piperazine substituent in the bay position has been changed with other different basic groups, such as pyrrolidine, pyridine, morpholine, diethylamine and piperidine, and, considering that the length of the side chains determines how deeply the end groups can reach into the grooves, different lengths have been chosen to study the influence in the binding to the nucleic acid. With the aim to assess whether the presence of protonable end groups at the end of the side chains are essential for the activity of the NDI derivatives, compounds with phenol and tetrahydrofuran end groups, which are not likely to be protonated, were synthesised.

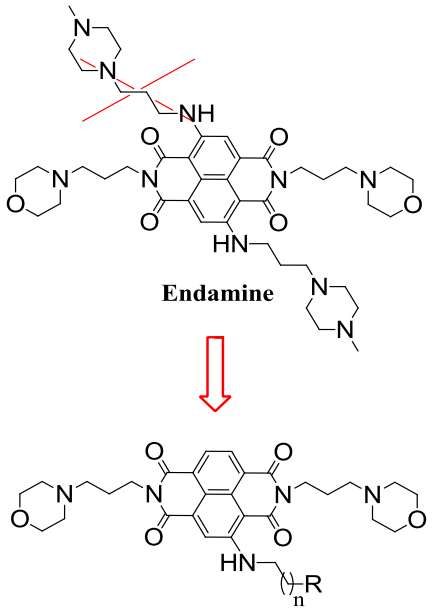

1c n = 2 R = N-Me-piperazine
2c n = 1 R = N-Me-piperazine
3c n = 1 R = pyrrolidine
4c n = 1 R = pyridine
5c n = 3 R = pyrrolidine
6c n = 1 R = piperidine
7c n = 1 R = morpholine
8c n = 1 R = tetrahydrofuran
9c n = 1 R = diethylamine
10c n = 1 R = phenol

Figure 8.1. Drug design of the trisubstituted-NDI derivatives.

Apart for groove binding, the function of the end groups of the side chains of NDIs is to give the molecules drug-like features such as solubility and high cellular uptake. All the basic groups introduced on the bay position in this series, after protonation, feature high hydrosolubility which is a desired effect, as the compounds are required to function in an aqueous environment.

8.2 Methods

8.2.1 Chemistry

Compounds **1c-10c** were synthesized according to Scheme 8.1.

The 2-monobromonaphthalene-1,4,5,8-tetracarboxylic dianhydride **11c** was obtained by reacting NTCDA with 5,5-dimethyldibromohidantoyn in sulphuric acid, to give intermediate **11c**.

3-morpholinopropylamine was condensed with **11c** in acetic acid to obtain the disubstituted naphthalene diimide **12c**.

Finally, such compound was treated with different amines in *N*-methylpyrrolidone (NMP) to obtain the final products **1c-10c.**

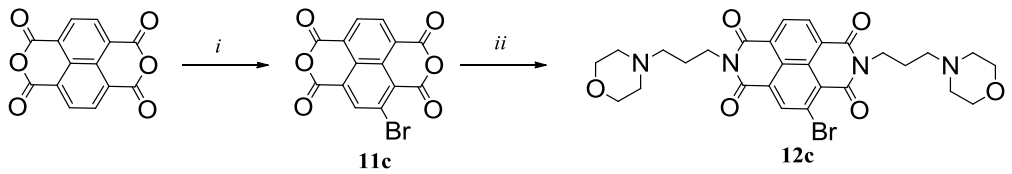

1c n = 2 R = N-Me-piperazine
2c n = 1 R = N-Me-piperazine
3c n = 1 R = pyrrolidine
4c n = 1 R = pyridine
5c n = 3 R = pyrrolidine
6c n = 1 R = piperidine
7c n = 1 R = morpholine
8c n = 1 R = tetrahydrofuran
9c n = 1 R = diethylamine
10c n = 1 R = phenol

Scheme 8.1. (*i*) 5,5-dimethyl-1,3-dibromohydantoin, H_2SO_4, 80 ^oC, 72 h; (*ii*) 3-morpholinopropylamine, acetic acid, microwave, 130 ^oC, 30 min; (*iii*) amine, NMP, microwave, 125 ^oC, 30 min.for **1c-9c** / amine, NEt_3, NMP, microwave, 125 ^oC, 30 min. for **10c**.

8.2.2 Biophysical Evaluation

The G-quadruplex binding ability of compounds **1c-10c** was assessed by Fluorescence Resonance Energy Transfer (FRET) melting technique. Values are expressed as the melting temperature difference between the nucleotide with drug and the negative control (ΔTm).

8.2.3 Biology

Derivatives were tested for *in vitro* antiproliferative activity in a panel of cancer cell lines. The antiproliferative activity has been evaluated by the Sulforhodamine B short-term cytotoxicity assay (SRB). Values are showed as the concentration required to inhibit cell growth by 50% (IC_{50}). The cytotoxic activity of **3c** was also evaluated through long-term growth inhibition study, where a fixed number of cells is incubated with the ligand at sub-cytotoxic concentrations over several weeks, and the number of population doublings is monitored

compared to untreated cells. A decrease in cell growth is attributed to senescence caused by the compound and the senescence was evaluated using the senescence staining protocol.
Telomerase activity was determined using the TRAP-LIG assay, a modified telomere repeat amplification protocol that ensures that there is no carryover of ligand into the second PCR step of the assay.
Alteration in gene expression induced by **3c** were investigated through immunoblotting while the cell localization was studied through confocal microscopy.
Compound **3c** was also tested to assess its microsomal metabolic stability compared to Verapamil, in order to determine its stability in the presence of human liver microsomes, and the plasma protein binding compared to Warfarin.

8.2.4 *In vivo* studies

Derivative **3c** was tested for *in vivo* antiproliferative activity in CD1 nude mice carrying a subcutaneous xenograft of the pancreatic tumour cell line MIA PaCa-2 ($5x10^6$ cells in the right flank) grown with Matrigel. The study was conducted in comparison to Endamine and Gemcitabine. The study, aside from determining the therapeutic potential of the drug compared to the lead compound and the main drug used for the treatment of pancreatic adenocarcinoma, allowed to determine roughly the time required for the localisation of **3c** in the tumor by fluorescent imaging (IVIS) and to assess the expression of apoptosis markers (caspase 3 and Bcl-2 family proteins) by histology.
First *in vivo* studies has required maximum tolerated dose (MTD) studies in order to assess whether the therapeutic window is wide enough for efficient inhibition of the target at non-toxic compound concentrations.

8.3 Results and discussion

The present project required a process of the optimization of the reaction conditions for all the steps of the synthetic process. The previous synthetic route was conducted starting from NTCDA that was reacted with dibromoisocyanuric acid (DBI) leading to the mono- and dibromo NDAs key intermediates, followed by the introduction of the amine chains at the imide and bay positions, in the order. The synthesis proceeded without any purification until the last step, leading to a very complex mixture that needed to be purified at least twice with preparative HPLC to obtain the desire products in a very low yield (less than 10%) (see yield for compounds **1c-2c/4c-8c**).[142] The critical passage in the previously reported synthetic scheme was the preparation of monobrominated NDA precursor **11c**, the criticality is due to the low solubility of **11c** that does not allow any kind of purification at this stage and any evaluation of the amount of monobromo derivative obtained. Purification can be performed only after the N-N' imidation reaction, due to the great enhancement of solubility assured by the introduction of the basic morpholino side chains. Lately a paper was published suggesting the use of 5,5-dimethyl-1,3-dibromohydantoin (DBH) as a useful agent for the regioselective bromination of NTCDA,[276] so we tried to apply this more efficient and convenient method to our synthesis in order to reach our purposes (Scheme 8.1). We performed the reaction using the procedure reported in literature, which involved first the treatment of NTCDA with DBH (0.55 eq) in H_2SO_4 at r.t. for 12 h. After crushing the reaction mixture into ice and filtering, the precipitate containing a mixture of nobromo-, mono- and dibrominated NDAs underwent to the N-N' imidation reaction with 3-morpholinopropyalmine (2 eq) in acetic acid at 125 ºC for 30 minutes under microwave irradiation to give the NDI intermediates. The purification of the obtained reaction mixture allowed us to afford the monobrominated NDI **12c** in 12% yield and

the dibrominated NDI in 3% yield. The main isolated product was the NDI without any bromine atom on the core, deriving from the unreacted starting material after the first step. The separation of the three products obtained, characterized by a very similar Rf, is very challenging but it has been achieved either through preparative HPLC, column chromatography or with the support of a Biotage apparatus.
We tried to improve the reaction conditions by changing the equivalent of brominating agent, the reaction time and temperature of the first step and maintaining unchanged the conditions of the N-N' imidation reaction. The results of our investigation are reported in Table 8.1.

Table 8.1. Reaction condition tested for the synthesis of intermediate **11c**. All the reactions were carried out using conc. H_2SO_4 as solvent.

DBH	**Reaction Conditions**	Yield % **12c**	Yield % dibrominated NDI
A) 0.55 equiv	r.t., 12h	12	3
B) 0.55 equiv	r.t., 72h	16	5
C) 0.55 equiv	80°, 24h	21	2
D) 0.55 equiv	80°, 48h	26	5
E) 0.55 equiv	80°, 72h	35	6
F) 1.0 equiv	80°, 24h	28	13
G) 1.0 equiv	80°, 48h	22	33
H) 1.5 equiv	50°, 10h	26	25

At first, we began the reaction conditions optimization process maintaining fixed the amount of brominating agent and increasing either the temperature and the reaction time: up to 72 h at r.t. yields of 16% for **12c** and 5% for the dibrominated NDI were reached, with concomitant high amounts of the no-bromoderivative deriving from the unreacted NTCDA. With the aim to reduce the amount of unreacted NTCDA in the first step, the reaction temperature was increased up to 80 ºC. As reported in Table 8.1, the amount of the mono- and dibrominated NDIs obtained increases with the reaction time, from 21% to 35% and from 2% to 6% respectively. In this case, the amount of the non brominated NDI is lower than before (around 20%) but that product was found together with other side products, including the partially opened ring one. In order to push higher the yield of the desired intermediate, the equivalent of brominating agent used were increased from 0.55 to 1 and finally to 1.5. The use of 1 equivalent of DBH, after 24 h at 80 ºC, afforded **12c** in 28% yield and the dibrominated NDI in 13% yield. Up to 48 h, the amount of the latter overcomes the one of **12c** with a yield of 33% versus 22%, respectively. Our last attempt has involved the use of 1.5 equivalents of DBH at 80 ºC for 10 h, leading to 26% yield for **12c**, with the presence of a high ratio of side products.
The best conditions to get the monobrominated intermediate **12c** have proved to be the use of 0.55 equivalent of brominating agent at 80 ºC for 72 h. Because of the complexity of the reaction mixture derived from our previous approach, there was no possibility to purify the final compounds using other methods than preparative HPLC. That procedure had to be repeated twice and only a little quantity of the crude mixture could be purified in a single purification because of the complications in the scale-up process, leading to a big loss of final

products and time. Thanks to the isolation of the intermediate **12c**, the reaction mixture after the last reaction resulted a lot less complex, thus it was possible to purify **3c** through column chromatography with a 75% yield.

Compounds **1c-10c** were firstly evaluated through Fluorescence Resonance Energy Transfer (FRET) melting technique in order to define their ability to stabilize G-quadruplex DNA. The sequences used for the screening are F21T (telomeric), promoter region of HSP90A and HSP90B, promoter region of Kras and promoter region of Bcl-2. Tloop is a duplex DNA sequence used as control. We also ran FRET competition experiments in which the affinity for the telomeric sequence was evaluated in the presence of increasing concentrations of duplex DNA. Together, these experiments enabled us to assess the selectivity of the ligands for quadruplex versus duplex DNA. The results in Table 8.2 show that the compounds bearing a basic substituent on the planar core are the most active towards G-quadruplex structures. As it can be seen compounds **6c, 8c** and **10c**, bearing respectively a pyridine, a tetrahydrofuran and a phenol group, present lower stabilizing activities compared to the others in the FRET assay. All the other compounds are able to stabilize G-quadruplex DNA almost at the same extent, but they are worse binder considering the tetrasubstituted lead compound Endamine. NDI compounds with the same end group and different length of the side chains in the bay position (i.e, compound **1c** and **2c**, **3c** and **5c**) displayed differences in the stabilization of various G-quadruplex sequences; that may be due to interactions of the side chains with different phosphates in the grooves of the G-quadruplexes. Generally it can be state that the stabilization of telomeric G-quadruplex DNA increases slightly by increasing the side chain length, while the stabilization of duplex DNA and G-quadruplexes induced in the Kras promoter is approximately the same or diminishes by increasing the length of the side chain.

The trisubstituted NDIs produce high stabilization of Bcl-2 and Hsp90A promoters, thus suggesting possible mechanisms of action for these derivatives.

All the compounds have proved a similar trend in the competition assay: the selectivity for the telomeric DNA is maintained up to 1:10, but when the concentration of the duplex DNA increase up to 100, the selectivity is lost. This can be explained by assuming that the target of the serie of the trisubstituted NDIs is not the telomeric DNA but one of the other oncogenic promoters.

Table 8.2.: ΔTm values (°C) for FRET analyses of compounds **1-10** and Endamine at 1μM concentrations with a series of G-rich sequences: hTel (F21T), Hsp90A, Hsp90B (Heat Shock Protein 90), Kras21, Kras32, Bcl-2, Tloop (duplex DNA). Esds are from triplicate measurements and average 0.3 °C. Calf Thymus (CT) competition data is shown in % retention of ΔTm .(*) indicates concentration of 5μM instead of 1μM.

	F21T	Hsp90A	Hsp90B	Kras21	Kras32	Bcl-2	Tloop	CT 1:1	CT 1:10	CT 1:100	CT 1:150
1c	14.3	19.8	16.5	9.8	6.1	15.8	0.8	100	100	39.1	19.2
2c	12.3	18.1	15.0	11.0	6.1	21.2	0.4	100	100	17.2	0
3c	11.8	15.7	12.7	11.0	9.6	13.3	0.6	100	100	4.2	0
4c	<2	2.5	<2	3.0	1.5	2.8	0	100*	100*	93.0*	83.5*
5c	15.9	20.6	16.9	11.7	6.6	16.1	0.2	100	100	24.1	8.2
6c	9.8	9.1	8.7	4.8	2.2	5.9	0.6	100*	100*	90.6*	45.4*
7c	1.4	3.9	6.8	3.4	1.2	4.2	0	100*	100*	88.4*	71*
8c	<2	2.7	4.5	0.7	0.2	2.4	0	100*	100*	83.5*	61.0*
9c	9	15.7	13.8	6.1	3.0	10.0	0.1	100*	100*	78.8*	40.6*
10c	6.0	11.0	9.4	2.4	1.5	5.8	1.5	100*	100*	96.5*	81.8*
Endamine	26.6	33.1	28.6	22.5	19.8	26.4	4.9	100	100	n/a	n/a

Preliminary biological evaluation has been obtained by the SRB assay. The cell growth inhibition ability of compounds **1c-10c** has been assayed in a panel of cancer cell lines comprising: A549 (lung), MCF-7 (breast), MIA Paca2 (pancreatic), Panc1 (pancreatic), ALT (alternative lengthening of telomeres cancer cells) and WI38 (human fibroblast) (Table 8.3).
All the compounds tested, except **10c**, displayed sub-micromolar activity in all the cancer cell lines used. In particular, it is very important to underline that all the derivatives show some kind of selectivity: the citotoxicity is higher towards the pancreatic cancer cell lines Panc1 and MIA PaCa2. Even **10c**, that is not endowed with high cytotoxic activity, has an IC_{50} of about 200 nM towards the pancreatic cancer cell lines.

Table 8.3. Short-term 96 hr IC_{50} values (in μM) for compounds **1c-10c** and Endamine in a cancer cell line panel, comprising MCF7 (breast), A549 (lung cancer), MIA PaCa2/Panc1 (pancreatic cancer), ALT (Alternative Lengthening of Telomeres) and WI38 (lung fibroblast) cell lines. Esds average 0.25 μM.

	A549	MCF7	MIAPaCa2	Panc1	ALT	WI38
1c	**0.067**	**0.357**	**0.059**	**0.045**	**0.224**	**1.83**
2c	**0.086**	**0.316**	**0.048**	**0.046**	**0.085**	**1.49**
3c	**0.024**	**0.159**	**0.012**	**0.022**	**0.093**	**1.19**
4c	**0.130**	**1.070**	**0.220**	**0.340**	**1.29**	**2.24**
5c	**0.026**	**0.222**	**0.036**	**0.033**	**0.089**	**1.22**
6c	**0.198**	**1.110**	**0.108**	**0.084**	**0.535**	**5.33**
7c	**0.146**	**1.03**	**0.139**	**0.808**	**0.71**	**1.88**
8c	**0.825**	**3.33**	**1.085**	**0.999**	**2.67**	**5.53**
9c	**0.092**	**1.538**	**0.059**	**0.163**	**0.451**	**1.65**
10c	**2.18**	**>25**	**0.206**	**0.220**	**10.874**	**17.65**
Endamine	**0.019**	**0.070**	**0.011**	**0.003**	**0.063**	**0.230**

It is also important to notice that, differently from the lead compound Endamine, the selectivity of these compounds for the cancer cell lines is improved: their activity *vs* WI38 cells, that are normal fibroblast, is much lower respect to the antiproliferative activity towards the cancer cells. The trisubstituted derivatives display more than 100 fold selectivity for these cell lines over the normal fibroblast cell line. Among the compounds, the best one proved to be **3c**, with an IC_{50} of 12 and 22 nM *vs* MIAPaCa2 and Panc1 respectively.
Considering that the most common mutation able to determine resistance to the current drug treatments in pancreatic cancer is the Kras mutation, all the derivatives were tested to assess their cytotoxicity against DT6606 and TB32047 mouse cancer cell lines together with Endamine and Gemcitabine. These two cytotipes own their unique features: more specifically DT6606 is a cancer cell line characterized by mutation in the Kras gene, while TB32047 is a cancer cell line with mutation in both Kras and p53 genes. The results of this investigation are reported in Table 8.4.
All the compounds display a lower cytotoxic activity for the mouse cancer cells compared to the human ones. That can be related to the deep differences between the two cytotypes. Endamine still remains the most active molecule within the NDI derivatives, with an IC_{50} of 310 and 295 nM and respectively for the two cancer cell lines. Gemcitabine proved to be very potent as well, with IC_{50} of 39 and 15 nM respectively.
Except for the abnormal change in the activity of compound **4c**, that in the normal cancer cell lines is not the most toxic derivative, from this study we obtained the usual trend, i.e. the pyrrolidine derivative **3c** seems to be the more active towards the two new cancer cell lines tested.

Table 8.4. Short-term 96 hr IC_{50} values (in μM) for compounds **1c-10c** and Endamine in DT6606 and TB32047 mouse cancer cell lines. Esds average 0.25 μM.

Compound	DT6606	TB32047
1c	**0.530**	**0.877**
2c	**0.947**	**0.316**
3c	**0.590**	**0.646**
4c	**0.363**	**0.343**
5c	**0.840**	**0.498**
6c	**8.499**	**6.095**
7c	**0.613**	**0.762**
8c	**5.890**	**5.040**
9c	**1.130**	**0.796**
10c	**>25**	**>25**
Endamine	**0.310**	**0.295**
Gemcitabine	**0.039**	**0.015**

In order to further investigate the biological activity of the most interesting derivative **3c**, long term growth inhibition study was performed using the target compound and Gemcitabine as control in MIA Paca2 and TB32047 cancer cell lines at different sub-cytotoxic concentrations (Figure 8.2). Cellular response to cytotoxic agents is often different in long-term exposures where cells tend to circumvent the cytotoxicity assault by triggering alternative biochemical pathways leading to development of drug-resistance. Thus, it was important to compare both short-term and long-term studies.

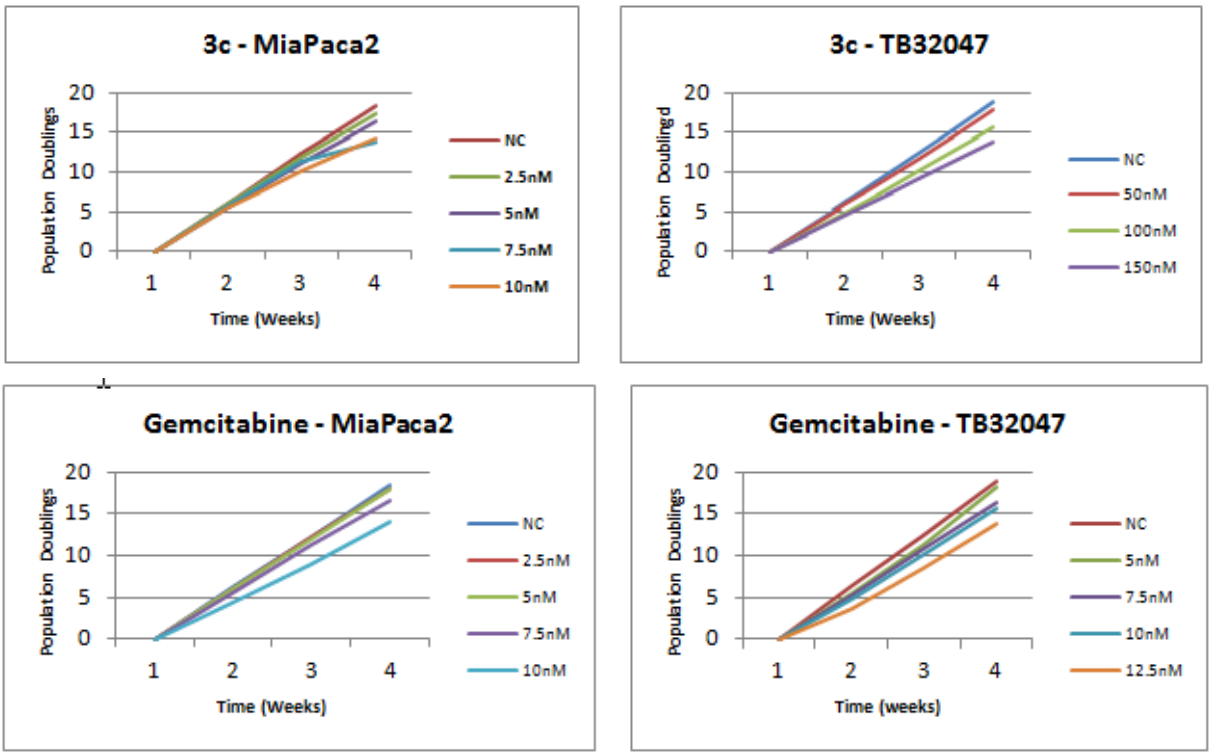

Figure 8.2. Long-term study: graphs representing the "population doubling" vs time, showing **3c** and in comparison to Gemcitabine effects on MiaPaca2 and TB32047 cell lines.

In all cases, proliferation of treated cells is decreased compared to untreated cells; in most cases, a delayed growth inhibition is observed only after two weeks, which implies that senescence caused by the compound is in part of a replicative nature. In most cases, proliferation decreased further after the second and third week, which indicates induction of senescence caused by the NDIs, which can be both replicative and stress-induced. In the long-term study using the human pancreatic cancer cell line MIA PaCa2, **3c** produces a reduction in the population doubling at the end of four weeks. When the higher concentration of **3c** (10 nM) is applied to the cells, the population doubling at the end of the cycle is 19.28 compared to 23.94 in the vehicle control, corresponding to an inhibition of 19.5%. Even exposing the cells at lower concentrations of **3c** (2.5 nM, 5 nM and 7.5 nM), cell growth decreases (PD = 22.69; PD = 21.91; PD = 21.97), comparing to the vehicle control (PD = 23.94) at the end of four week treatment. However, the highest dose of **3c** (10 nM) is the most effective. The Gemcitabine long term exposure at the highest concentration (10 nM) causes a population doubling of 19.06, corresponding to an inhibition of 20.4%. Also in this case the drug produces a decrease in cell growth using the lower concentrations (2.5 nM, 5 nM and 7.5 nM), with PD = 23.56; PD = 23.31; PD = 22.12 respectively.

In the long-term study of mouse cancer cell line TB32047, the effects of **3c** are very different depending on the concentration used: besides a reduction in the population doublings at the end of four weeks for all the concentrations tested, the long-term study shows a significant reduction in the number of cells treated with the highest concentrations (200 nM and 300 nM) after as little as seven days, that compromises the continuation of the study for these concentrations. Mouse cells treated with **3c** at 200 nM and 300 nM show significant changes in the population and morphology: fewer cells observed in the flask as well as rounded shape, and floating (dead) cells with some other cells in light orange colour, unveiling an apoptosis state. For the cells underwent to a 150 nM treatment with **3c**, the population doubling was 16.99 comparing to 25.38 in the vehicle control, with an inhibition of 33.1%. The Gemcitabine effect for the higher concentration used (12.5 nM) causes a population doubling of 15.55, corresponding to an inhibition of 38.8% of the cell viability.

MIA PaCa2 and TB32047 cells from long-term study were assessed for senescence at the end of each week of treatment with **3c** and Gemcitabine. The trend showed in both cell lines incubated with **3c** is the increment of the blue stain along with the increase in drug concentration (Fig. 8.3).

Also the morphology of both cells lines changed during the incubation with **3c**. The changes are more obvious in MiaPaCa2 cell line because of the features of this cancer cell line (as shown in the vehicle control) that presents rounded cells, making it possible to observe changes easily. The morphology of the cells incubated with drug became flattened and bigger in size and their ratio of nucleus to cytoplasm also increases, indicating senescence.

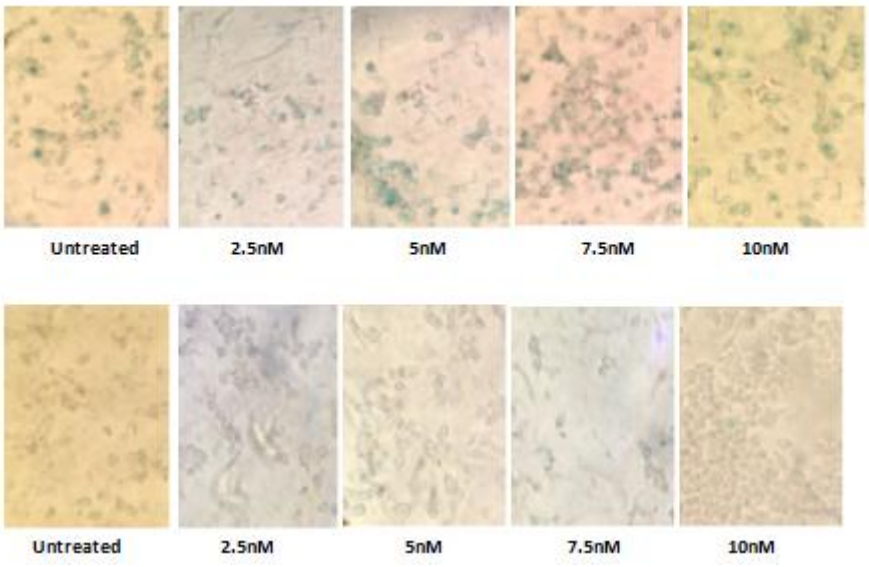

Figure 8.3. Top) Senescence-associated β-galactosidase (SA-βgal) activity in MiaPaCa2 cell line incubated with different concentrations of **3c**, after 2 weeks of incubation. Untreated is the positive control for SA-βgal activity. With increment of drug concentration, the amount of cells with SA-βgal activity increases (200X magnification). Bottom) Effect of **3c** on morphology of MiaPaCa2 cell line (4th week): untreated – no change observed; treated cells featured changes in shape and size, becoming flattened and bigger (200X magnification).

The telomerase inhibitory activity all the trisubstituted NDIs was assessed in MIA PaCa2 cells, using the modified TRAP-LIG assay (Fig. 8.4). No change in the products of telomerase-mediated telomere elongation are apparent at up to 50 μM of each compound, indicating that all the final compounds lack of telomerase inhibitory activity, at least at the dosage levels producing growth inhibitory effects.

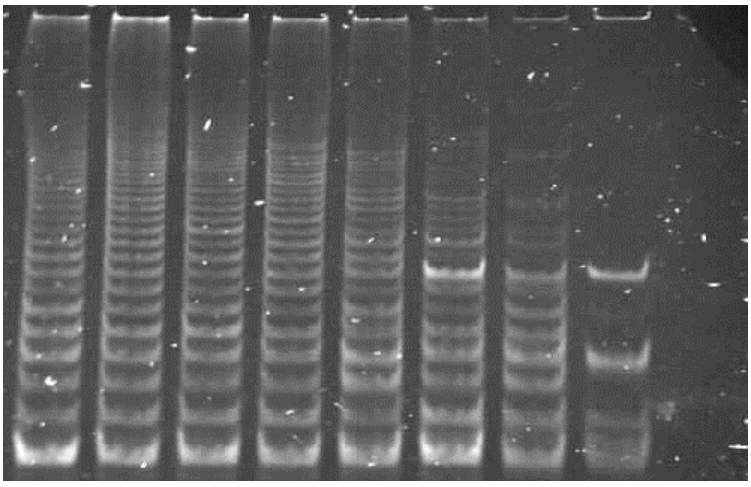

Figure 8.4. Gel showing telomerase activity in MIA PaCa2 cells treated with compounds **3c** at increasing concentrations. Compound concentrations are indicated. Neg, negative control (n.c.); Pos, positive control of untreated cells (with telomerase but no ligand, p.c.).

These results are in agreement with the previous one obtained for Endamine, that showed no inhibition as well, but it is in contrast with the data reported for other tetrasubstituted NDIs. In view of the potent antiproliferative activity of compounds **1c-10c**, their inactivity in the MIAPaCa2 cell line against telomerase at concentration levels that produce inhibition of cancer cell growth suggests a more complex mode of action in this line, probably involving the control of the transcription of the major human genes.

Immunoblotting was used to verify if the most interesting compound **3c** was able to modify the expression of specific proteins involved in cell cycle regulation. In particular, considering that Endamine has displayed activity towards Bcl-2, the same protein was used to test **3c**. No decrement in the bands was found in the western blot gels, indicating that Bcl-2 is not the main target. Furthermore, epidermal growth factor receptor (EGFR) was also a protein of interest, since its overexpression is correlated with disease progression and resistance to chemotherapy. Thus, the same technique was applied to screen this protein. However, as shown in Fig. 8.5, the expression of EGFR was very similar at all time points, which can lead to some different conclusions: (*i*) until the time points tested, no significant change in the expression of EGFR was apparent, due to the fact that the drug needs more time to display its action; (*ii*) the concentration of **3c** was not sufficient to induce changes in the expression of EGFR or (*iii*) the mechanism of action of **3c** does not interfere with the expression of EGFR.

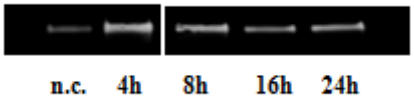

Figure 8.5. Western blots for EGFR protein in MIA paca2 cells (line 1), and MIA paca2 cells incubated with **3c** (20 nM) for 4 h (line2), 8 h (line 3), 16 h (line 4) and 24 h (line5).

Assessment of cellular uptake and location of anticancer agents inside the cell can provide information on whether compounds are able to reach their targets. Drug candidates must be able to enter and be sustained in cells, and compounds exerting their actions through the stabilization of G-quadruplexes located in telomeres or in the promoter regions of genes must enter the nucleus, where chromosomes are located. NDI compounds have fluorescent properties, which can be used for their visualisation in cells by confocal microscopy.

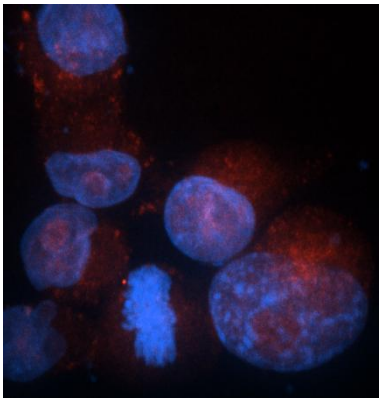

Figure 8.6. Cell uptake detection using confocal microscopy: **3c** (red) is mainly localized in the nucleus (blue) after 60 minutes exposure at 25 nM.

Confocal microscopy images of MIAPaca-2 cells incubated with **3c** at 25 nM concentration showed that the compound is taken up into cells and localize mainly in the nucleus after 60 minutes (Fig. 8.6).

Based on the previous observations, compound **3c** was selected as the lead compound for the *in vivo* studies. Compound **3c** and Endamine were tested *in vivo* using MIA Paca2 tumor transplant models in order to compare their efficacy. Gemcitabine was also included in the study and used as positive control, considering that is the drug mainly used for the treatment of pancreatic adenocarcinoma.

As the first *in vivo* experiment of a novel compound, the MTD must be determined, which is stated in the units mg of compound per kg of body weight. With that purpose, the drug was administered to mice on a regular schedule at slowly increasing doses starting from a dose of 10 mg/kg. When the toxic concentration is approached, animals show weight loss. For Endamine the MTD is 30mg/kg, while **3c** has proved to be a safer compound, with a MTD of 45mg/kg. This data allow to state that **3c** is endowed with a much higher therapeutic window compared to the parent compound. The initial MTD study showed that for Endamine the safe therapeutic dose was 15mg/kg given as a single i.v. injection. In order to compare the results from the study this dose was used for the parent compound and also for **3c**. A lower dose (10mg/kg) was also selected for compound **3c**, in order to assess if the derivative was more active than Endamine, while for Gemcitabine the dose used was of 15mg/kg, as reported in literature.

The study was carried on for 24 days in which the different groups underwent to a cycle of two intravenous injection per week. After 24 days the tumor growth inhibition rates of each group were calculated and the results are showed in Figure 8.7.

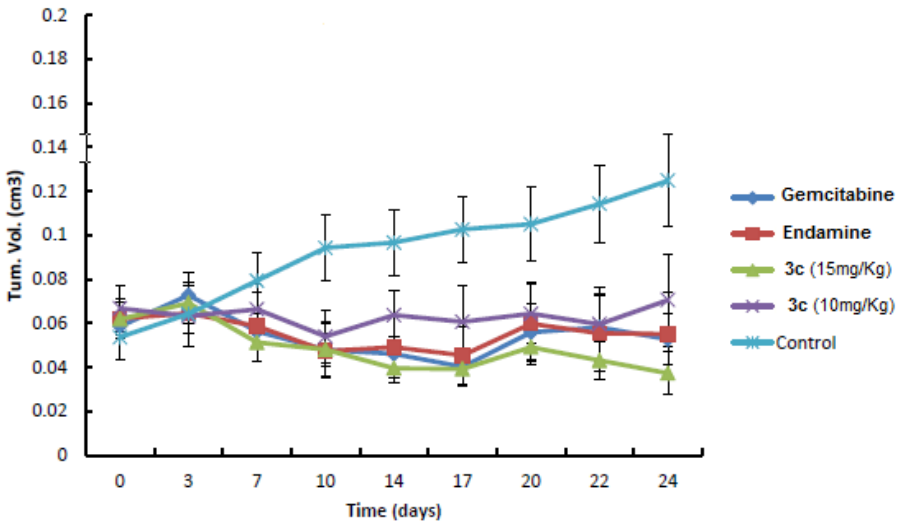

Figure 8.7. Plot of the changes in averaged tumour volume during the therapeutic xenograft experiments using **3c**, Endamine and Gemcitabine, for the control group of mice compared to groups dosed with 10 and 15 mg/kg respectively, administered twice weekly for 24 days in a pancreatic MIA PaCa2 xenograft model (8 injections).

As deductible from the plot, all the drugs are active in the *in vivo* model, in fact the tumor growth rates in mice treated with **3c**, Endamine and Gemcitabine were dramatically decreased. It is possible to state that the antitumor effect of **3c** at a dose of 15mg/Kg is stronger compared to those expressed by Endamine and Gemcitabine at the same dose. Lowering the dose of the

trisubstituted derivative from 15mg/kg to 10mg/kg leads to a strong decreasing of the antitumor activity. Compound **3c** is able to cause remission of the tumor and that makes it a possible drug candidate.

After stopping the injections, the different groups were allowed to live in order to evaluate the presence of any long term effect caused by the drugs and to find out if the re-growth of tumours occurs. The mice not anymore dosed were observed for 42 additional days and the results of this prolonged study are reported (Fig. 8.8).

After stopping the injection of the drugs, all the groups have shown a re-growth of the tumor mass, but this trend is more evident for groups treated with Endamine, Gemcitabine and **3c** at the lower dose (10mg/kg). In mice treated with **3c** at the higher dose, the tumor does not restart growing until 30 days after the last injection, thus indicating that the drug possesses some long term effect. From the results of the prolonged studies, **3c** appears to be the best candidate for the treatment of the disease, taking ito account also its long term effects. After 66 days all the mice belonging to the different groups were culled and the tumors were frozen. Treated and untreated samples of the tumors, as well as some non-tumour material, are currently undergoing to the histology studies.

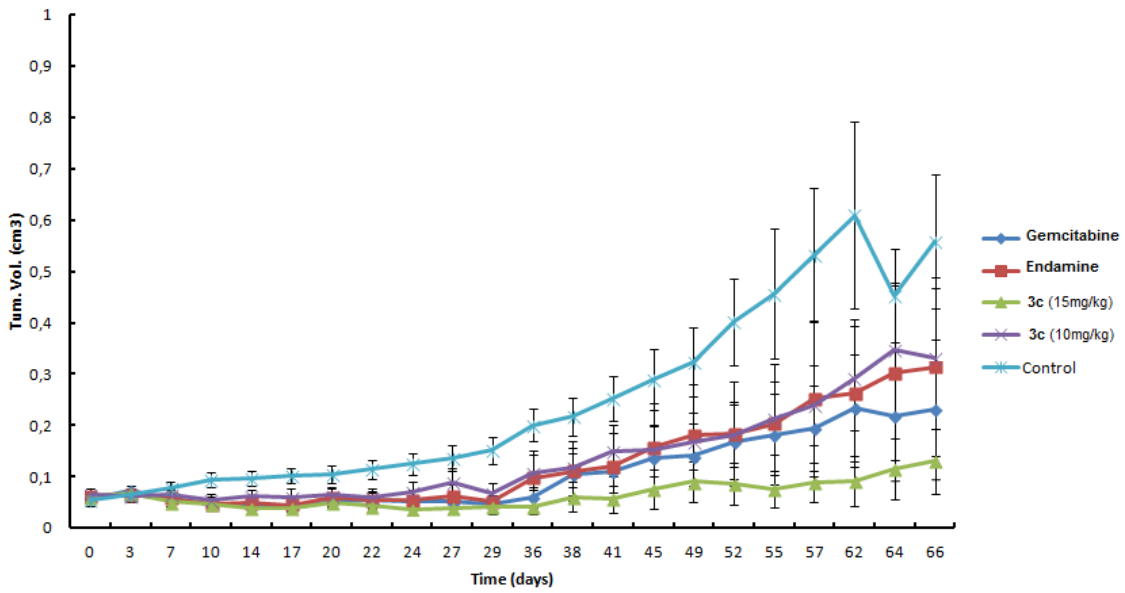

Figure 8.8. Plot of the changes in averaged tumour volume during the therapeutic xenograft experiments using **3c**, Endamine and Gemcitabine, for the control group of mice compared to groups dosed with 10 and 15 mg/kg respectively, in a pancreatic MIA PaCa2 xenograft model after 66 days (injections stopped on day 24).

The fluorescent properties of compound **3c** and Endamine were utilised for *in vivo* fluorescence imaging. This technique is highly sensitive and has the advantage over confocal microscopy that no washing steps are involved which could rinse out the compound. The imaging method allows location of the fluorescent compounds in the animal, and in excised organs.

Compound **3c** and Endamine were visualised thanks to their fluorescence in animals treated at 15mg/kg i.v. after 24 h. As it can be seen from figure 8.9, the *in vivo* imaging shows that both **3c** and Endamine localise in the tumor even though the tumor was better defined by this imaging modality with Endamine, whereas untreated animals only showed very low

autofluorescence. The fluorescence intensity is also maintained up to 72 h after the injection, thus indicating that both the molecules have a long period of retention in a living organism.

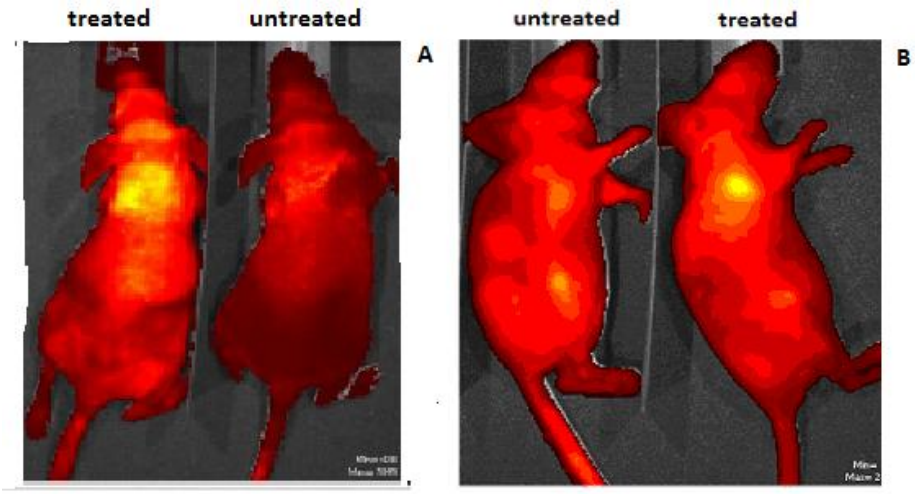

Figure 8.9. *In vivo* spectral fluorescence imaging of compound **3c** (**A**) and Endamine (**B**) 24 h after i.v. injection of 15mg/kg.

The liver is the most important site of drug metabolism in the body, approximately 60% of marketed compounds are cleared by hepatic CYP-mediated metabolism. The assessment of the half life of a drug is very important to decide if the compound possesses a druglike pharmacokinetic profile. The evaluation of the metabolic profile of **3c** was carried out using Verapamil, which is known to be quinckly metabolized by the human liver microsomes, as positive control. The microsome turnover and the amount of non metabolized compound were evaluated after 15, 30 and 60 minutes and the results of the investigation are reported in Fig. 8.10.

The results obtained attest that **3c** is a quite stable drug, the microsomal turnover is less than 40% after 60 minutes, much lower compared to the value obtained for Verapamil. The half life calculated for **3c** is of 122.23 minutes.

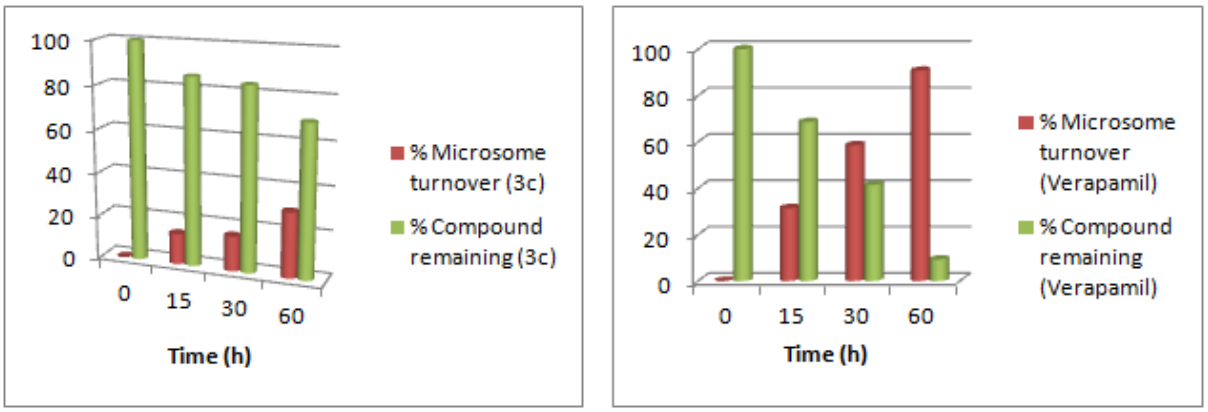

Figure 8.10. Human microsomal turnover of Verapamil and compound **3c** and % of compound remaining in the blood stream at different times of Verapamil and compound **3c**.

The binding of a drug to plasma proteins is a major determinant of drug distribution, it has a very important effect on drug dynamics since only the free (unbound) drug interacts with the target. Also the halflife of a compound is strictly correlated with its protein binding activity, that does not have to be too long but either too short. The evaluation of plasma binding properties for **3c** compared to Warfarin, a drug well known for its strong interaction with the proteins present in the plasma, has showed that only the 70% of the drug is bound to the latters, while the 30% of the compound is free. On the other hand Warfarin is present in 99.64% in the bound form (Fig. 8.11).
Many of the top 100 most prescribed drugs have greater than 98% protein binding, so the result obtained for compound **3c**, even if not perfect, can be considered very promising.

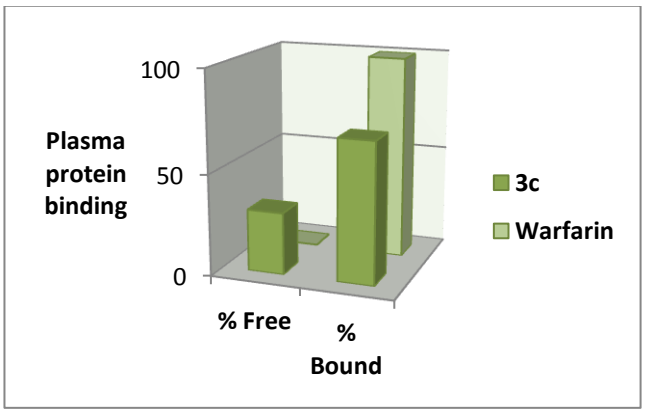

Figure 8.11. The plasma protein binding properties of **3c** compared to Warfarin.

8.4 Conclusion

This project has involved the synthesis of Endamine-related compounds, in order to improve the pharmacokinetics and anticancer profile of the lead compound. In particular, it was demonstrated that the removal of one of the bay substituents did not cause a great loss of the cytotoxic activity in the members of the new serie. Compound **3c**, bearing a pyrrolidine end-group and a chain made up of two methylenes, proved to be the most potent compound, showing growth inhibition ability in a panel of cancer cell line, similar to the one proven by the parent compound Endamine. In particular, it was the most potent inhibitor of cell growth in MIAPaca2 and Panc1 pancreatic cancer cell lines, where it showed IC_{50} values of 12 and 22 nM, respectively. Furthermore, compound **3c** displayed an interesting biological profile characterized by a 100-fold selectivity for pancreatic cancer cells respect to normal fibroblasts. Compound **3c** was also able to interact with the G-quadruplex formed in telomeres and oncogenic promoter regions at 1μM concentration with high ΔTm values, even if the loss of one basic chain caused a reduction of the G-quadruplex stabilizing activity respect to Endamine. The lack of quadruplex binding activity showed by compounds **6c**, **8c** and **10c** in this series, strongly suggests that a basic group is a minimal requirement for the NDI derivatives. The results obtained from the competition assay suggest that the target of this compound was not the telomeric G-quadruplex DNA but more likely some quadruplex structures in the oncogenic promoters. This hypothesis was confirmed by the lack of activity of **3c** towards telomerase through the telomerase repeat amplification protocol assay.
Compounds **3c** will be further investigated to better clarify its mechanism(s) of action.

The evaluation of the *in vivo* anticancer activity of **3c** in a xenograft model of pancreatic cancer proved that **3c** is more effective than Endamine and Gemcitabine for the treatment of the disease. The animals dosed with **3c** displayed a block in the tumor growth and a regression, that persisted also after the interruption of the treatment thus indicating the presence of some long term effect. *In vivo* fluorescence imaging showed the ability of the compound to localize selectively in the tumor mass, moreover compound **3c** presented a good miscrosomal stability and poor protein binding activity compared to most of the commercial drug, thus validating its good pharmacokinetic profile.
All this features make compound **3c** a good candidate for the treatment of pancreatic adenocarcinoma, that is still one of the most deadly form of cancer.

8.5 Experimental section

8.5.1 Chemistry

All chemicals, reagents and solvents were purchased from Sigma-Aldrich, Alfa Aesar, Lancaster Synthesis and Fluorochem (UK) and used without further purification. Solvents were supplied by VWR and Fisher scientific. Column chromatography was performed using BDH silica gel (BDH 153325P). HPLC analysis was carried out with a Gilson apparatus combining a 322 PUMP and an Agilent 1100 SERIES detector, using a C18 5µ (100 x 4.6 mm) column (41622271 (W), YMC, Japan), at a flow of 1 mL/min. Preparative HPLC was carried out with a Gilson apparatus combining a 322 PUMP and a UV/VIS-155 detector with detection at 280 nm, using a C18 5µ (100 x 20 mm) column (201022272) (W), YMC, Japan, at a flow of 20 mL/min. Water and MeOH with 0.1 % formic acid were used as solvents for HPLC. For the purification of compounds **1c-3c**, the following method was used: 100 % aqueous for 5 min after injection, gradually decreased to 60 % aqueous over 25 min. For compounds **12c**, the following method was used: 100% aqueous for 2 min after injection, gradually decreased to 20% aqueous over 17 minutes. For the HPLC purity analysis of compounds **1c-3c**, the method used was: 100 % aqueous for 5 min after injection, to 60 % aqueous over 18 min as well as 100 % aqueous for 5 min after injection, to 60 % aqueous over 43 min. Purity for final compounds was greater than 95% (HPLC, 280 nm). NMR spectra were recorded at 400 MHz or 500 MHz on a Bruker spectrometer. NMR spectra were analyzed with MestReC 4.5.6.0 with chemical shifts using TMS as a standard (δ = 0 ppm). NMR multiplicity abbreviations are s (singlet), bs (broad singlet), d (doublet), t (triplet), q (quartet), 5q (quintet), and m (multiplet). Coupling constants J are reported as observed in Hertz (Hz). High Resolution Mass spectra (HRMS) were measured on a Micromass Q-TTOF Ultima Global tandem mass spectrometer run under electrospray ionisation (ESI), and processed using the MassLab 3.2 software. Compounds **1c-10c** were prepared according to the optimized procedure reported in Scheme 8.1.

Synthesis of compound 11c.
Naphthalene dianhydride (0.150 g, 0.56 mmol) was slurried in H_2SO_4 (1.5 ml) and the suspension obtained was stirred for 5 min at r.t. to allow the complete dissolution. DBH was added slowly over a period of 1 h and the round bottom flask was tightly stopped to avoid the escape of bromine from the reaction mixture. The solution was stirred at 80 ºC for 72 h and then poured onto ice (30 ml). The yellow solid that formed was filtered, washed with water (2 x 10 ml) and dried under vacuum, yielding **11c**, that was used without further purification.

Synthesis of compound 12c.

2-monobromonaphthalene-1,4,5,8-tetracarboxylic dianhydride **11c** (0.58 mmol, 1 eq) and 3-morpholinopropylamine (1.76 mmol, 2 eq) were suspended in acetic acid (3 ml). The reaction was performed under microwave irradiation at 125 ºC for 30 minutes. After having been cooled to rt the solvent was removed and purified through by preparative HPLC or column chromatography using as eluent a mixture of CH_2Cl_2/MeOH 96/4 to give the desire compound **11c**.

4-bromo-2,7-bis(3-morpholinopropyl)benzo[lmn][3,8]phenanthroline-1,3,6,8(2H,7H)-tetraone (12c). Brown solid. ^{1}H NMR ($CDCl_3$) δ 1.95-1.97 9m, 4H), 2.40-2.43 (m, 8H), 2.52-2.53 (m, 4H), 3.51-3.54 (m, 8H), 4.28-4.33 (q, 4H), 8.77 (d, 1H, *J* = 8 Hz), 8.82 (d, 1H, *J* = 7.6 Hz), 8.935 (s, 1H). ^{13}C NMR (100 MHz, CDCl3, TMS) δ 29.3, 29.7, 31.2, 38.1, 53.5, 56.4, 56.5, 59.5, 66.9, 126.0, 126.1, 126.7, 126.9, 128.6, 130.6, 130.8, 131.6, 138.4, 161.1, 161.8, 161.9, 162.5. HRMS (ES^+) calculated $C_{28}H_{31}BrN_4O_6$ $[M+H]^+$ 600.1543. found: 600.1536.

General procedure for the synthesis of 1c-9c.

12c (1 eq), the appropriate amine (2 eq) and NMP were suspended in a microwave vessel. The tube was sealed with a rubber cup and heated to 125 ºC for 30 minutes under microwave irradiation. After solvent removal, the crude mixture was purified by preparative HPLC or through column chromatography to give the desire product **1c-9c.**

4-((3-(4-methylpiperazin-1-yl)propyl)amino)-2,7-bis(3-morpholinopropyl)benzo[lmn][3,8]phenanthroline-1,3,6,8(2H,7H)-tetraone (1c). Red oil, yield 31% from 1-(3-aminopropyl)-4-methylpiperazine as starting material; purified through preparative HPLC; ^{1}H NMR (400 MHz, $CDCl_3$) δ 1.99- 2.09 (m, 6H), 2.62- 2.80 (m, 17H), 3.01 (m, 8H), 3.68-3.76 (m, 10H), 4.20- 4.26 (m, 4H), 8.23 (s, 1H), 8.31 (d, 1H, *J* = 7.6 Hz), 8.61 (d, 1H, *J* = 7.6 Hz), 10.16 (t, 1H, exch D_20, *J* = 5.8 Hz). ^{13}C NMR (100MHz, $CDCl_3$) δ 23.7, 23.9, 38.2, 38.8, 41.1, 43.3, 50.2, 52.5, 52.7, 53.1, 54.6, 55.7, 65.5, 65.7, 99.9, 119.4, 119.8, 123.4, 124.6, 126.1, 127.9, 129.5, 131.4, 152.3, 163.0, 163.3, 166.0, 166.4. HRMS (ES^+) calculated for $(M+H)^+$ $C_{36}H_{49}N_7O_6$ 676.3823, found 676.3825.

4-((2-(4-methylpiperazin-1-yl)ethyl)amino)-2,7-bis(3-morpholinopropyl)benzo[lmn][3,8]phenanthroline-1,3,6,8(2H,7H)-tetraone (2c). Red oil, yield 12% from 2-(4-methylpiperazin-yl)ethylamine as starting material; purified through preparative HPLC; ^{1}H NMR (400 MHz, $CDCl_3$) δ 1.96-2.02 (m, 4H), 2.53-2.68 (m, 21H), 3.03-3.05 (m, 4H), 3.62 (t, 4H, *J* = 4.6 Hz), 3.67-3.72 (m, 6H), 4.23-4.28 (m, 4H), 8.21 (s, 1H), 8.34 (d, 1H, *J* = 7.6 Hz), 8.64 (d, 1H, *J* = 8 Hz), 10.28 (t, 1H, exch D_20, *J* = 4.8 Hz); ^{13}C NMR (100MHz, $CDCl_3$) δ 24.0, 38.3, 39.1, 40.2, 43.7, 50.4, 52.9, 53.1, 53.6, 55.8, 56.0, 56.0, 66.0, 66.3, 100.3, 119.5, 120.0, 123.6, 124.6, 126.3, 128.0, 129.5, 131.4, 152.1, 163.0, 163.1, 163.3, 165.9. HRMS (ES^+) calculated for $(M+H)^+$ $C_{35}H_{47}N_7O_6$ 662.3680, found 662.3666.

2,7-bis(3-morpholinopropyl)-4-((2-(pyrrolidin-1-yl)ethyl)amino)benzo[lmn][3,8]phenanthroline-1,3,6,8(2H,7H)-tetraone (3c). Red oil, yield 75% from 1-(3-aminoethyl)pyrrolidine as starting material; purified through column chromatography using as eluent a mixture of CH_2Cl_2/MeOH/34% aq. NH_4OH 9.5/0.5/0.03; ^{1}H NMR (400 MHz, $CDCl_3$) δ 1.85-1.92 (m, 4h), 1.93-1.95 (m, 4H), 2.42-2.53 (m, 12H), 2.67-2.68 (m, 4H), 2.93 (t, 2H, *J* = 6.6 Hz), 3.56 (t, 4H, *J* = 4.8 Hz), 3.61 (t, 4H, *J* = 4.6 Hz), 3.60-3.73 (m, 2H), 4.23-4.29 (m, 4H), 8.21 (s, 1H), 8.32 (d, 1H, *J* =7.6Hz), 8.62 (d, 1H, *J* = 8 Hz), 10.25 (t, 1H, exch D_20, *J* = 4.2 Hz). ^{13}CNMR (100MHz, $CDCl_3$) δ 23.7, 24.4, 24.6, 38.7, 39.3, 42.4, 53.5, 54.2, 54.7, 56.4, 56.5, 66.9, 66.9, 100.1, 119.3, 119.9, 123.6, 124.3, 126.1, 127.8, 129.4, 131.2, 152.1, 163.0, 163.1, 163.4, 165.9. HRMS (ES^+) calculated for $(M+H)^+$ $C_{34}H_{44}N_6O_6$ 633.3389, found 633.3401.

2,7-bis(3-morpholinopropyl)-4-((2-(pyridin-2-yl)ethyl)amino)benzo[lmn][3,8]phenanthroline-1,3,6,8(2H,7H)-tetraone (4c). Red oil, yield 20% from 2-(2-pyridinyl)ethanamine as starting material; purified through preparative HPLC; ^{1}H NMR (400 MHz, $CDCl_3$) δ 1.90-1.96 (m, 4H), 2.49-2.58 (m, 12H), 3.22 (t, 2H, *J* = 7 Hz), 3.57 (t, 4H, *J* = 4.6 Hz), 3.62 (t, 4H, *J* = 4.6 Hz), 3.97-4.02 (m, 2H), 4.16-4.20 (m, 4H), 7.11-7.15 (m, 1H), 7.29-7.27 (m, 1H), 7.57-7.61 (d, 1H, *J* = 7.8 Hz), 8.20 (s, 1H), 8.26 (d, 1H, *J* = 8 Hz), 8.56 (d, 2H, *J* = 8 Hz), 10.21 (t, 1H, exch D_20, *J* = 5.6 Hz); ^{13}C NMR (100MHz, $CDCl_3$) δ 24.2, 37.7, 38.6, 39.2, 42.8, 53.1, 53.3, 56.2, 66.5, 66.5, 100.1, 119.8, 121.9, 123.5, 123.6, 124.5, 126.2, 127.9, 129.5, 131.3, 136.8, 149.7, 151.9, 152.2, 157.8, 163.0, 163.1, 163.4, 166.1. HRMS (ES^+) calculated for $(M+H)^+$ $C_{35}H_{40}N_6O_6$ 641.3090, found 641.3088.

2,7-bis(3-morpholinopropyl)-4-((4-(pyrrolidin-1-yl)butyl)amino)benzo[lmn][3,8]phenanthroline-1,3,6,8(2H,7H)-tetraone (5c). Red oil, yield 15% from 4-(1-pyrrolidinyl)-1-butylamine as starting material; purified through preparative HPLC; ^{1}H NMR (400 MHz, $CDCl_3$) δ 1.94-2.11 (m, 12H), 2.59-2.77 (m, 12H), 3.14 (t, 2H, *J* = 7.8 Hz), 3.28-3.29 (m, 4H), 3.63-3.70 (m, 6H), 3.76 (t, 4H, *J* = 4.6 Hz), 4.23-4.27 (m, 4H), 8.17 (s, 1H), 8.34 (d, 1H, *J* = 8 Hz), 8.64 (d, 1H, *J* = 8 Hz), 10.10 (t, 1H, exch D_20, *J* = 5.4 Hz); ^{13}C NMR (100MHz, $CDCl_3$) δ 23.2, 23.4, 23.7, 23.8, 26.7, 38.3, 38.9, 42.4, 52.7, 52.8, 53.3, 54.7, 55.8, 55.9, 65.7, 65.9, 100.2, 119.5, 119.5, 123.6, 124.7, 126.3, 128.1, 129.5, 131.4, 152.3, 162.9, 163.1, 163.4, 166.2. HRMS (ES^+) calculated for $(M+H)^+$ $C_{36}H_{48}N_6O_6$ 661.3713, found 661.3713.

2,7-bis(3-morpholinopropyl)-4-((2-(piperidin-1-yl)ethyl)amino)benzo[lmn][3,8]phenanthroline-1,3,6,8(2H,7H)-tetraone (6c). Red oil, yield 12% from 1-(2-aminoethyl)piperidine as starting material; purified through preparative HPLC; ^{1}H NMR (400 MHz, $CDCl_3$) δ 1.57-1.60 (m, 2H), 1.69-1.75 (m, 4H), 1.95-2.00 (m, 4H), 2.51-2.68 (m, 16H), 2.87 (t, 2H, *J* = 6.4 Hz), 3.61 (t, 4H, *J* = 4.6 Hz), 3.67 (t, 4H, *J* = 4.6 Hz), 3.76-3.80 (m, 2H), 4.22-4.28 (m, 4H), 8.18 (s, 1H), 8.31 (d, 1H, *J* = 7.6 Hz), 8.61 (d, 1H, *J* = 8 Hz), 10.24 (t, 1H, exch D_20, *J* = 5 Hz); ^{13}C NMR (100MHz, $CDCl_3$) δ23.8, 24.2, 25.2, 38.5, 39.2, 39.9, 53.1, 53.2, 54.3, 56.2, 56.8, 66.4, 66.5, 100.3, 199.5, 119.9, 123.6, 124.5, 126.2, 127.9, 129.5, 131.2, 152.0, 162.9, 163.1, 163.4, 165.9. HRMS (ES^+) calculated for $(M+H)^+$ $C_{35}H_{46}N_6O_6$ 647.3566, found 647.3557.

4-((2-morpholinoethyl)amino)-2,7-bis(3-morpholinopropyl)benzo[lmn][3,8]phenanthroline-1,3,6,8(2H,7H)-tetraone (7c). Red oil, yield 7% from 4-(2-aminoethyl)morpholine as starting material; purified through column chromatography using as eluent a mixture of CH_2Cl_2/MeOH 9/1; ^{1}H NMR (400 MHz, $CDCl_3$) δ 1.92-1.96 (m, 4H), 2.42-45 (m, 8H), 2.49-2.54 (m, 4H), 2.59 (t, 4H, *J* = 4.4 Hz), 2.80 (t, 2H, *J* = 6 Hz), 3.56 (m, 4H, *J* = 4.4 Hz), 3.62 (t, 4H, *J* = 4.4 Hz), 3.66-3.70 (m, 2H), 3.78 (t, 4H, *J* = 4.4 Hz), 4.23-4.30 (m, 4H), 8.21 (s, 1H), 8.33 (d, 1H, *J* = 7.6 Hz), 8.64 (d, 1H, *J* = 8 Hz), 10.34 (t, 1H, exch D_20, *J* = 4.8 Hz); ^{13}C NMR (100MHz, $CDCl_3$) δ 24.4, 24.6, 38.7, 39.4, 40.1, 53.5, 53.6, 56.4, 56.5, 56.8, 66.93, 66.96, 66.99, 100.3, 119.5, 120.0, 123.7, 124.5, 126.2, 127.9, 129.5, 131.2, 152.1, 163.1, 163.5, 165.9. HRMS (ES^+) calculated for $(M+H)^+$ $C_{34}H_{44}N_6O_7$ 649.3376, found 649.3350.

2,7-bis(3-morpholinopropyl)-4-(((tetrahydrofuran-2-yl)methyl)amino)benzo[lmn][3,8]phenanthroline-1,3,6,8(2H,7H)-tetraone (8c). Red oil, yield 23% from tetrahydrofurfurylamine as starting material; purified through column chromatography using as eluent a mixture of CH_2Cl_2/MeOH 9.5/0.5; ^{1}H NMR (400 MHz, $CDCl_3$) δ 1.26-1.28 (m, 4H), 1.71-1.78 (m, 6H), 1.94-2.05 (m, 2H), 2.12-2.51 (m, 10H), 3.56-3.57 (m, 4H), 3.62-3.64 (m, 4H), 3.74-3.78 (m, 1H), 3.84-3.87 (m, 1H), 3.97-4.00 (m, 1H), 4.24-4.28 (m, 4H), 8.27 (s, 1H), 8.34 (d, 1H, *J* = 7.6 Hz), 8.65 (d, 1H, *J* = 7.6 Hz), 10.34 (t, 1H, exch D_20, *J* = 4.8 Hz); ^{13}C NMR (100MHz, $CDCl_3$) δ 24.4, 24.6, 25.9, 38.8, 39.4, 47.3,

53.6, 56.4, 56.5, 66.94, 66.97, 68.6, 100.2, 119.5, 120.0, 123.7, 124.5, 126.2, 127.9, 129.5, 131.2, 152.5, 163.1, 163.4, 166.2. HRMS (ES^+) calculated for $(M+H)^+$ $C_{33}H_{41}N_5O_7$ 620.3096, found 620.3084.

4-((2-(dimethylamino)ethyl)amino)-2,7-bis(3-morpholinopropyl)benzo[lmn][3,8]phenanthroline-1,3,6,8(2H,7H)-tetraone (9c). Red oil, yield 59% from N,N-dimethylenediamine as starting material; purified through column chromatography using as eluent a mixture of CH_2Cl_2/MeOH/34% aq. NH_4OH 9.5/0.5/0.03; ^1H NMR (400 MHz, $CDCl_3$) δ 1.11 (t, 6H, *J* = 7 Hz), 1.46-1.47 (m, 4H), 1.90-2.53 (m, 12H), 2.64-2.69 (m, 4H), 2.86 (t, 2H, *J* = 6.2 Hz), 3.56-3.57 (m, 4H), 3.61-3.65 (m, 6H), 4.23-4.30 (m, 4H), 8.21 (s, 1H), 8.31 (d, 1H, *J* = 7.6 Hz), 8.62 (d, 1H, *J* = 8 Hz), 10.27 (t, 1H, exch D_20, *J* = 5 Hz); ^{13}C NMR (100MHz, $CDCl_3$) δ 11.8, 24.4, 24.5, 38.6, 39.3, 47.1, 51.6, 53.5, 53.6, 56.5, 66.9, 100.1, 119.4, 120.2, 123.7, 124.3, 126.1, 127.8, 129.6, 131.2, 152.1, 163.12, 163.16, 163.5, 165.9. HRMS (ES^+) calculated for $(M+H)^+$ $C_{34}H_{46}N_6O_6$ 635.3552, found 635.3557.

Synthesis of compound 10c.

Compound **12c** (1 eq), tyramine hydrocloride (2 eq), NEt_3 (2 eq) and NMP were suspended in a microwave vessel. The tube was sealed with a rubber cup and heated to 130 ºC for 30 minutes under microwave irradiation. After solvent removal, the crude mixture was purified through column chromatography using as eluent a mixture of CH_2Cl_2/MeOH/34% aq. NH_4OH 9.5/0.5/0.02.

4-((4-hydroxyphenethyl)amino)-2,7-bis(3-morpholinopropyl)benzo[lmn][3,8]phenanthroline-1,3,6,8(2H,7H)-tetraone (10c). Red oil, yield 37% from tyramine hydrocloride as starting material; ^1H NMR (400 MHz, DMSO) δ 1.75-1.82 (m, 4H), 2.31-2.43 (m, 12H), 2.91 (t, 2H, *J* = 6.6 Hz), 3.41-3.44 (m, 8H), 3.9-3.71 (m, 2H), 4.02 (m, 4H), 6.72 (d, 2H, *J* = 8.4 Hz), 7.15 (d, 2H, *J* = 8 Hz), 7.84 (s, 1H), 8.02 (d, 1H, *J* = 8 Hz), 8.30 (d, 1H, *J* = 8 Hz), 9.86 (brs, 1H, exch D_20); ^{13}C NMR (100MHz, $CDCl_3$) δ 29.9, 30.9, 38.4, 38.9, 44.5, 53.4, 53.5, 56.2, 56.4, 66.5, 66.7, 94.4, 100.1, 116.1, 119.4, 120.2, 123.5, 124.5, 126.2, 129.0, 130.2, 131.3, 155.4, 162.9, 163.1, 163.5, 165.8. HRMS (ES^+) calculated for $(M+H)^+$ $C_{36}H_{41}N_5O_7$ 656.3074, found 656.3084.

8.5.2 Biophysical Evaluation

8.5.2.1 Fluorescence Resonance Energy Transfer (FRET)

The FRET experiments were conducted as reported in Chapter 7.5.2.1.

The following oligonucleotide sequences, all purchased from Eurofins, were used: F21T: (5‟-FAM-GGG TTA GGG TTA GGG TTA GGG-TAMRA-3‟), HSP90a: (5‟-FAM- GGG-CCA AAG GGA AGG GGT GGG-TAMRA-3‟), HSP90b: (5‟-FAM-GGGCGG GCC AAA GGG AAG GGG-TAMRA-3‟), Kras21 (5‟- FAM-AGG GCG GTG TGG GAA GAG GGA-TAMRA-3‟), Kras32 (5‟-FAM -AGG GCG GTG TGG GAA GAG GGA AGA GGG GGA GG- TAMRA-3‟), Bcl-2 (5‟-FAM-GGG CGC GGG AGG AAG GGG GCG GG-TAMRA-3‟), T-Loop: (5‟-FAM-TAT AGC TATA TTT TTT TATA GCT ATA-TAMRA-3‟).

8.5.2 Biology

8.5.2.1 Cell Culture

Cell culturing was conducted using the condition reported in Chapter 7.5.2.1.

For cell lines DT6606 and TB32047 the medium Dulbeccos MEM (GIBCO 21969, Invitrogen, UK) supplemented with L-glutamine (2 mM, GIBCO 25030, Invitrogen, UK), essential amino acids (1 %, GIBCO 11140, Invitrogen, UK), and foetal calf serum (10 %, S1810, Biosera, UK) was used.

8.5.2.2 Sulforhodamine B (SRB) short-term cytotoxicity assay

The SRB assay was as reported in Chapter 8.5.2.2.
For cell lines DT6606 and TB32047 4000cells per well were used.

8.5.2.3 Long term growth inhibition study

After counting, $3x10^4$ cells were seeded in 10 mL of medium containing the compound to be tested in a 75 cm^2 flask and incubated for 7 days. The cells were then harvested and counted. $3x10^4$ of the cells were re-seeded, and the process was repeated for another week. Population doublings were calculated using the formula

$$N_f = N_0\, 2^{pd}$$
$$pd = \log(N_f/N_0)/\log 2$$

where N_0 is the number of cells at the time of seeding ($3x10^4$), N_f is the number of cells at the time of counting, and pd is the number of population doublings.

8.5.2.4 Senescence staining

Staining for senescene associated β-galactosidase was carried out following the protocol from the supplier (Cell Signaling Technology, Inc., Beverly, MA).$1x10^5$ cells obtained from the long term studies were seeded in 35 mm 6-well plates (Nunc A/S) in 2 mL medium and incubated overnight. The medium was then removed, the cells washed, fixed with formaldehyde (2%) and glutaraldehyde (0.2%) in PBS for 15 min, and washed twice more. 1 mL of a staining solution (citric acid/sodium phosphate (40 mM), pH 6.0, NaCl (0.15 M), MgCl2 (2 mM), potassium ferrocyanide (5 mM), potassium ferricyanide (5mM),
X-gal (1mg/mL, 5-bromo-4-chloro-3-indolyl-βD-galactopyranoside)) was added to each well. The cells were incubated overnight and examined by light microscopy (magnification 200x) for the characteristic senescence-associated blue stain.

8.5.2.5 Telomerase repeat amplification protocol (TRAP) assay

The TRAp assay was conducted as reported in Chapter 7.5.3.3.

8.5.2.6 Immunoblotting

Total protein from samples was loaded onto pre-cast SDS-PAGE gels (Bio Rad) and transferred onto a nitrocellulose membrane (Invitrogen), and the membranes were probed with primary antibodies against bcl-2 and EGFR(Santa Cruz Biotechnology). Following incubation with the appropriate secondary antibodies, the membranes were visualised with the horseradish peroxidase luminescent visualisation system (National Diagnostics).

8.5.2.7 Visualization of the compound through confocal microscopy

MIA PaCa2 cells were grown on cover slips as for the cell uptake studies. After the cells had attached to the cover slips, they were incubated with the compouns (1 μM) and etoposide (30 μM) for 24 h. They were then washed with PBS, and fixed with fomaldehyde (2 % in PBS) for 10 min at r.t. Cells were permeabilised with triton x (0.1 % in PBS, Sigma Aldrich, UK) for 5

min at r.t., and washed with blocking buffer (3 % BSA, Sigma Aldrich, UK, and 0.05 % triton x in PBS). They were incubated with phospho-histone H2A.X (Ser139)(20E3) rabbit mAb alexa fluor 488 conjugate (1:67 dilution in PBS, 9719, Cell Signaling, USA) for 1 h and subsequently washed with PBS. Some samples were also incubated with DAPI (1:5000 dilution of a 2 mg/mL solution in PBS, Sigma Aldrich, UK) for 5 min and washed with PBS. Cover slips were mounted as described in chapter 6.4.2, and analysed by confocal microscopy on a LSM 710 META confocal microscope (Zeiss, Germany) with a planapochromat 40 x /1.3 Oil DIC M27 oil submersion lens. 6.6.2.2) Fluorescence in situ hybridisation (FISH) and 3D micr

8.5.2.8 Microsomal metabolic stability

Compound **3c** (3 μM) was incubated with pooled liver microsomes. Test compound was incubated at 5 times points over the course of a 45 min experiment and the test compound was analysed by LC-MS/MS. Pooled human liver microsomes and pooled mouse liver microsomes, 0.1M phosphate buffer pH 7.4 and compound **3c** were preincubated at 37° C prior to the addition of NADPH to initiate the reaction.. A control incubation is included for each compound tested where 0.1M phosphate buffer pH7.4 is added instead of NADPH. Two control compounds are included with each species. Compound **3c** was incubated for 0, 5, 15, 30 and 60 min. The control was incubated for 60 min only. The reaction was stopped by transferring 25 μL of incubate to 50 μL of MeOH at the appropriate time points. The terminated plates were centrifuged at 2500 rpm for 20 min at 4° C to precipitate the protein. Following protein precipitation, the supernatants were analysed using LC-MS/MS.

8.5.2.9 Assessment of plasma binding properties

Compound **3c** (5 μM) was prepared both in 100% species specific plasma and buffer. The experiment was performed using equilibrium dialysis with the two compartments separated by a semi-permeable membrane (molecular weight cut off (MWCO) ~ 8000). The plasma solution was added to one side of the membrane in an equilibrium dialysis system while the buffer solution (PBS) was added to the other side. The system was allowed to reach equilibrium at 37 °C and incubated for 4 h. After incubation, samples from both plasma (bound) chamber and the buffer (free) chamber were taken and placed into separate microcentrifuge for analysis. The samples were matrix-matched. Acetonitrile containing internal standard was added to all samples. The samples were centrifuged and the supernatant was analysed by UHPLC-TOF MS for parent compound. Results are expressed as either % of free compound and % of bound compound.

8.5.3 In vivo studies

8.5.3.1 Determination of the maximum tolerated dose (MTD)

Compound **3c** was dissolved in saline and administered intravenous to the CD1 mice (n = 2). Body weight was recorded daily and the animals were observed for clinical symptoms. The starting dose of 10 μg/kg was increased step-wise in order to determine the MTD.

8.5.3.2 Therapy study

The CD1 mice used were inoculated with SC $5x10^6$ Mia Paca2 cells in the right flank (unsupplemented RPMI + Matrigel). After waiting for to establish subcutaneously (approx. 11 days) and measuring the size of the tumours weekly until they reach a mean size of 0.05 cm^3. At this stage of the development of the tumours, mice are ready to begin the therapy study.

Mice were re-grouped to to form five therapeutic groups constituted of eight mice each, carrying approximately 0.05 cm^3 average of the tumour size per group.
The following doses of Endamine, **3c** and Gemcitabine were administered by IV.
Group 1: 8 mice treated with 15 mg/Kg of Gemcitabine twice weekly dose.
Group 2: 8 mice treated with 15 mg/Kg of Endamine twice weekly dose
Group 3: 8 mice treated with 10 mg/Kg of **3c** twice weekly dose.
Group 4: 8 mice treated with 15 mg/Kg of **3c** twice weekly dose.
Group 5: 8 control mice treated with only saline twice weekly.
The therapy study must be finished if tumours ulcerate; reach a size of 1.5 cm^3 or a weight loss of 10-20% of the initial body weight is observed.

8.5.3.3 Imaging studies

Mice from groups A, B and C will be monitored to determine Endamine and **3** accumulation within the tumor *in vivo* by fluorescent imaging (IVIS) following drug injection at: 30min, 1h, 2h, 4 h and 8 h then mice will be held till 24 h time point to be culled with the histology groups.
Group A: 2 mice treated with 15 mg/Kg single dose of Endamine
Group B: 2 mice treated with 10 mg/Kg single dose of **3c**
Group C: 2 mice treated with 15 mg/Kg single dose of **3c**

8.4.3.4 Histology study

To assess apoptosis markers and their colocalisation with drugs (Endamine and **3c**) mice of group A-D will be culled after 24 h and group E at 48 h time point following drugs' injection. Tumors will be harvested and snap-frozen (N_2 liquid). 10 µm sections will be cut from tumors and stained with anti-activated caspase3 and anti-BCL-2 family proteins.
Liver, kidneys, heart, lungs, spleen, colon and brain will be harvested from mice of therapeutic groups (1 to 5) and snap-frozen for pathology analysis.
Group A: 2 mice treated with 15 mg/Kg single dose of Endamine
Group B: 2 mice treated with 10 mg/Kg single dose of **3c**
Group C: 2 mice treated with 15 mg/Kg single dose of **3c**
Group D: 2 control mice treated with saline only twice

Abbreviations

ADMET: absorption, distribution, metabolism, excretion, toxicity
ADP: adenosine diphospate
AF-2: activation function-2 domain
APC: Adenomatous Polyposis Coli
AQ: antraquinone
Asp: aspartic acid
BA: butyric acid
BP: base pair
CAP: capping group
CBI: cyclobisintercalator family
CD: circular dichroism
CDK: cyclin-dependent kinase
CHAP: cyclic hydroxamic-acid containing peptide
CTBP: C-terminal-binding protein
CTCL: cutaneous cell T lymphoma
DAT: dissociates activities of telomerase
DFMO: difluoromthylornithine
DNA: Deoxyribonucleic acid
DNMT: methyltransferase protein
dNTPs: deoxynucleotides triphosphates
EGFRi: epiderma growth factor receptor inhibitor
ER: estrogen nuclear receptor
FAD: flavin-adenine dinucleotide
FO: fluorenones
FRET: Fluorescence resonance energy transfer
GIST: gastrointestinal stromal tumours
HAT: histone acetyltransferase
HDAC: histone deacetylase
HDACi: histone deacetylase inhibitor
HIF: hypoxia inducible factors
HP1: heterochromatin protein 1
hTER: telomere reverse transcriptase
hTR: telomere RNA component
ICAM1: adhesion molecule-1
IFD: 'insertion in fingers' domain
KB: kilo base
LSD: lysine demethylase
MAO: monoamino oxidase
MBDs: methyl-binding protein
MCM: multiple-compound medication
MM: multiple mieloma
MMT: multiple-medication therapy
MTDL: multi-target directed ligand
NAD: nicotinamide adenine dinucleotide
NCI: National Cancer Institute
NDI: naphthalene diimides
NHE: nuclease hypersensitivity element

NI: naphthalene imides
NMR: nuclear magnetic resonance
NSCLC: non-small cell lung carcinoma
NTCDA: 1,4,5,8-Naphthalenetetracarboxylic dianhydride
ODC: ornithine decarboxylase
PAO: poliamminoossidase
PAO: polyamino oxidase
PAT: polyamine transporters
PBA: phenylbutyric acid
PTS: polyamine transport system
RAP: repeat addition processivity
ROS: reactive oxigen species
r.t.: room temperature
SAHA: Vorinostat
SAM-DC: S-adenosylmethionine decarboxylase
SAR : structure activity relationship
SMA: spinal muscolar atrophy
TBP2: TATA-binding protein 2
TEN: essential N-terminal domain
TeRRA: telomeric ribonucleoprotein complex
TNFR-1: tumor necrosis factor receptor 1
TRAIL: TNF related apoptosis inducing ligand
TRBD: telomerase RNA-binding domain
Trx: thioredoxin
TSA: thricostatin A
VEGF: vascular endothelial growth factor
VPA: valproic acid
ZBG: zinc binding group

Bibliography

1. Siegel, R.; Naishadham, D.; A., J. *CA: a cancer journal for clinicians* **2012,** *62*, 10.
2. Cooper M.G. *The cell, a Molecular Approach 2000*.
3. N., S. *Japanese journal of clinical oncology* **2010,** *40*, 855.
4. J.A., K.; M.P., F.; Z., L. *Journal hematological oncology* ***2009,*** *2*, 2.
5. Cavalli, A.; Bolognesi, M. L.; Minarini, A.; Rosini, M.; Tumiatti, V.; Recanatini, M.; Melchiorre, C. *Journal of Medicinal Chemistry* **2008,** *51*, 347.
6. Hartman, J. L.; Garvik, B.; Hartwell, L. *Science* **2001,** *291*, 1001.
7. Morphy, R.; Z., R. *Journal of Medicinal Chemistry* **2005,** *48*, 6523.
8. Rask-Andersen, M.; Almén, M. S.; Schiöth, H. B. *Nat. Rev. Drug Discovery* **2011,** *10*, 579.
9. Kola, l. s. p. w. s. q. o. q. g. l.; Landis, J. *Nature Review Drug Discovery* **2004,** *3*, 711.
10. Morphy, R.; Rankovic, Z. *Drug Discovery Today* **2007,** *12*, 156.
11. Zhang, Y. M.; Cockerill, S.; Guntrip, S. B.; Rusnak, D.; Smith, K.; Vanderwall, D.; Wood, E.; Lackey, K. *Bioorganic & Medicinal Chemistry Letters* **2004,** *14*, 111.
12. Karaman, M. W.; Herrgard, S.; Treiber, D. K.; Gallant, P.; Atteridge, C. E.; Campbell, B. T.; Chan, K. W.; Ciceri, P.; Davis, M. I.; Edeen, P. T.; Faraoni, R.; Floyd, M.; Hunt, J. P.; Lockhart, D. J.; Milanov, Z. V.; Morrison, M. J.; Pallares, G.; Patel, H. K.; Pritchard, S.; Wodicka, L. M.; Zarrinkar, P. P. *Nature Biotechnology* **2008,** *26*, 127.
13. Siegel, R.; Naishadham, J.; Jemal, A. *Cancer statistics* **2013,** *63*, 11.
14. Hassan, M. M.; Bondy, M. L.; Wolff, R. A.; Abbruzzese, J. L.; Vauthey, J. N.; Pisters, P. W.; Evans, D. B.; Khan, R.; Chou, T. H.; Lenzi, R.; Jiao, L.; Li, D. *Am J Gastroenterol* **2007,** *102*, 2696.
15. Hassan, M. M.; Bondy, M. L.; Wolff, R. A.; Abbruzzese, J. L.; Vauthey, J. N.; Pisters, P. W.; Evans, D. B.; Khan, R.; Chou, T. H.; Lenzi, R.; Jiao, L.; Li, D. *Am J Gastroenterol.* **2007,** *102*, 2696.
16. Jaffee, E. M.; Hruban, R. H.; Canto, M.; Kern, S. E. *Cancer Cell* **2002,** *2*, 25.
17. Tersmette, A. C.; Petersen, G. M.; Offerhaus, G. J.; Falatko, F. C.; Brune, K. A.; Goggins, M.; Rozenblum, E.; Wilentz, R. E.; Yeo, C. J.; Cameron, J. L.; Kern, S. E.; Hruban, R. H. *Clin Cancer Res.* **2001,** *7*, 738.
18. Korc, M.; Chandrasekar, B.; Yamanaka, Y.; Friess, H.; Buchier, M.; Beger, H. G. *J Clin Invest* **1992,** *90*, 1352.
19. Watanabe, M.; Nobuta, A.; Tanaka, J.; Asaka, M. *Int J Cancer* **1996,** *67*, 264.
20. Yang, S. *Genes Dev* **2011,** *25*.
21. Bar-Sagi, D. *Science* **1986,** *233*, 1061.
22. Ying, H. *Cell* **2012,** *149*, 656.
23. McWilliams, R. R.; Wieben, E. D.; Rabe, K. G.; Pedersen, K. S.; Wu, Y.; Sicotte, H.; G.M., P. *Eur J Hum Genet.* **2011,** *19*, 471.
24. Jones, S.; Zhang, X.; Parsons, D.; Lin, J. C.; Leary R.J., A. P., Mankoo P., Carter H., Kamiyama H., Jimeno A., Hong S.M., Fu B., Lin M.T., Calhoun E.S., Kamiyama M., Walter K., Nikolskaya T., Nikolsky Y., Hartigan J., Smith D.R., Hidalgo M., Leach S.D., Klein A.P., Jaffee E.M., Goggins M., Maitra A., Iacobuzio-Donahue C., Eshleman J.R., Kern S.E., Hruban R.H., Karchin .R, Papadopoulos N., Parmigiani G., Vogelstein B., Velculescu V.E., Kinzler K.W.
25. Massagué, J.; Blain, S. W.; Lo, R. S. *Cell* **2000,** *103*, 295.
26. Tempero, M. A.; Arnoletti, J. P.; Behrman, S. W.; Ben-Josef, E.; Benson, A. B.; Casper, E. S.; Cohen, S. J.; Czito, B.; Ellenhorn, J. D.; Hawkins, W. G.; Herman, J.; Hoffman, J. P.; Ko, A.; Komanduri, S.; Koong, A.; Ma, W. W.; Malafa, M. P.; Merchant, N. B.; Mulvihill, S. J.; Muscarella, P.; Nakakura, E. K.; Obando, J.; Pitman, M. B.; Sasson, A. R.; Tally, A.; Thayer, S. P.; Whiting, S.; Wolff, R. A.; Wolpin, B. M.; Freedman-Cass, D. A.; Shead, D. A.; Networks, N. C. C. *J Natl Compr Canc Netw* **2012,** *10*, 703.
27. Moore, M. J.; Goldstein, D.; Hamm, J.; Figer, A.; Hecht, J. R.; Gallinger, S.; Au, H. J.; Murawa, P.; Walde, D.; Wolff, R. A.; Campos, D.; Lim, R.; Ding, K.; Clark, G.; Voskoglou-

Nomikos, T.; Ptasynski, M.; Parulekar, W.; Group, N. C. I. o. C. C. T. *J Clin Oncol* **2007,** *25*, 1960.
28.Shay, J. W.; Wright, W. E. *Nat Rev Drug Discov* **2006,** *5*, 577.
29.Dodson, L. F.; Hawkins, W. G.; Goedegebuure, P. *Immunotherapy* **2011,** *3*, 517.
30.Hegde, S.; Schmidt, M.; Doherty, A. *Annual Report Medicinal Chemistry* **2005,** *40*, 443.
31.LERMAN, L. S. *J Mol Biol* **1961,** *3*, 18.
32.Palchaudhuri, R.; Hergenrother, P. J. *Curr Opin Biotechnol* **2007,** *18*, 497.
33.Li, S.; Cooper, V. R.; Thonhauser, T.; Lundqvist, B. I.; Langreth, D. C. *J Phys Chem B* **2009,** *113*, 11166.
34.Sebestík, J.; Hlavácek, J.; Stibor, I. *Curr Protein Pept Sci* **2007,** *8*, 471.
35.Goodell, J. R.; Ougolkov, A. V.; Hiasa, H.; Kaur, H.; Remmel, R.; Billadeau, D. D.; Ferguson, D. M. *J Med Chem* **2008,** *51*, 179.
36.Roche, V. F. *Foye's Principles of Medicinal Chemistry*.
37.Sen, D.; Gilbert, W. *Nature* **1988,** *334*, 364.
38.Lipps, H. J.; Rhodes, D. *Trends Cell Biol* **2009,** *19*, 414.
39.Wheelhouse, R. T.; Jennings, S. A.; Phillips, V. A.; Pletsas, D.; Murphy, P. M.; Garbett, N. C.; Chaires, J. B.; Jenkins, T. C. *J Med Chem* **2006,** *49*, 5187.
40.Burge, S.; Parkinson, G. N.; Hazel, P.; Todd, A. K.; Neidle, S. *Nucleic Acids Res* **2006,** *34*, 5402.
41.Moon, I. K.; Jarstfer, M. B. *Front Biosci* **2007,** *12*, 4595.
42.Huppert, J. L.; Balasubramanian, S. *Nucleic Acids Res* **2005,** *33*, 2908.
43.Huppert, J. L.; Balasubramanian, S. *Nucleic Acids Res* **2007,** *35*, 406.
44.Neidle, S. *Curr Opin Struct Biol* **2009,** *19*, 239.
45.Shklover, J.; Weisman-Shomer, P.; Yafe, A.; Fry, M. *Nucleic Acids Res* **2010,** *38*, 2369.
46.Qin, Y.; Hurley, L. H. *Biochimie* **2008,** *90*, 1149.
47.Bochman, M. L.; Paeschke, K.; Zakian, V. A. *Nat Rev Genet* **2012,** *13*, 770.
48.Eddy, J.; Maizels, N. *Nucleic Acids Res* **2006,** *34*, 3887.
49.Sun, D.; Hurley, L. H. *J Med Chem* **2009,** *52*, 2863.
50.<st1:city w:st="on"><st1:place w:st="on">Gardner, L.; Lee, L.; Dang, C. *The c-Myc Oncogenic Transcription Factor, Encyclopedia of Cancer*.
51.Marcu, K. B.; Bossone, S. A.; Patel, A. J. *Annu Rev Biochem* **1992,** *61*, 809.
52.Balasubramanian, S.; Hurley, L. H.; Neidle, S. *Nat Rev Drug Discov* **2011,** *10*, 261.
53.Brooks, T. A.; Hurley, L. H. *Nat Rev Cancer* **2009,** *9*, 849.
54.Grand, C. L.; Powell, T. J.; Nagle, R. B.; Bearss, D. J.; Tye, D.; Gleason-Guzman, M.; Hurley, L. H. *Proc Natl Acad Sci U S A* **2004,** *101*, 6140.
55.Grand, C. L.; Han, H.; Muñoz, R. M.; Weitman, S.; Von Hoff, D. D.; Hurley, L. H.; Bearss, D. J. *Mol Cancer Ther* **2002,** *1*, 565.
56.Vliagoftis, H.; Worobec, A. S.; Metcalfe, D. D. *J Allergy Clin Immunol* **1997,** *100*, 435.
57.Sakurai, S.; Fukasawa, T.; Chong, J. M.; Tanaka, A.; Fukayama, M. *Jpn J Cancer Res* **1999,** *90*, 1321.
58.Tuveson, D. A.; Willis, N. A.; Jacks, T.; Griffin, J. D.; Singer, S.; Fletcher, C. D.; Fletcher, J. A.; Demetri, G. D. *Oncogene* **2001,** *20*, 5054.
59.Rankin, S.; Reszka, A. P.; Huppert, J.; Zloh, M.; Parkinson, G. N.; Todd, A. K.; Ladame, S.; Balasubramanian, S.; Neidle, S. *J Am Chem Soc* **2005,** *127*, 10584.
60.Fernando, H.; Reszka, A. P.; Huppert, J.; Ladame, S.; Rankin, S.; Venkitaraman, A. R.; Neidle, S.; Balasubramanian, S. *Biochemistry* **2006,** *45*, 7854.
61.Vogelstein, B.; Kinzler, K. W. *Nat Med* **2004,** *10*, 789.
62.Cogoi, S.; Xodo, L. E. *Nucleic Acids Res* **2006,** *34*, 2536.
63.Desoize, B. *Anticancer Res* **1994,** *14*, 2291.
64.Seto, M.; Jaeger, U.; Hockett, R. D.; Graninger, W.; Bennett, S.; Goldman, P.; Korsmeyer, S. J. *EMBO J* **1988,** *7*, 123.
65.Dai, J.; Dexheimer, T. S.; Chen, D.; Carver, M.; Ambrus, A.; Jones, R. A.; Yang, D. *J Am Chem Soc* **2006,** *128*, 1096.

66.Agrawal, P.; Lin, C.; Mathad, R. I.; Carver, M.; Yang, D. *J Am Chem Soc* **2014,** *136*, 1750.
67.Dexheimer, T. S.; Sun, D.; Hurley, L. H. *J Am Chem Soc* **2006,** *128*, 5404.
68.Palm, W.; de Lange, T. *Annu Rev Genet* **2008,** *42*, 301.
69.Oganesian, L.; Bryan, T. M. *Bioessays* **2007,** *29*, 155.
70.Baumann, P.; Cech, T. R. *Science* **2001,** *292*, 1171.
71.Li, B.; Oestreich, S.; de Lange, T. *Cell* **2000,** *101*, 471.
72.Bianchi, A.; Smith, S.; Chong, L.; Elias, P.; de Lange, T. *EMBO J* **1997,** *16*, 1785.
73.Celli, G. B.; de Lange, T. *Nat Cell Biol* **2005,** *7*, 712.
74.Wang, F.; Podell, E. R.; Zaug, A. J.; Yang, Y.; Baciu, P.; Cech, T. R.; Lei, M. *Nature* **2007,** *445*, 506.
75.Vizlin-Hodzic, D.; Ryme, J.; Simonsson, S.; Simonsson, T. *FASEB J* **2009,** *23*, 2587.
76.Luke, B.; Panza, A.; Redon, S.; Iglesias, N.; Li, Z.; Lingner, J. *Mol Cell* **2008,** *32*, 465.
77.Redon, S.; Reichenbach, P.; Lingner, J. *Nucleic Acids Res* **2010,** *38*, 5797.
78.Lundblad, V.; Szostak, J. W. *Cell* **1989,** *57*, 633.
79.Shay, J. W.; Zou, Y.; Hiyama, E.; Wright, W. E. *Hum Mol Genet* **2001,** *10*, 677.
80.Feng, J.; Funk, W. D.; Wang, S. S.; Weinrich, S. L.; Avilion, A. A.; Chiu, C. P.; Adams, R. R.; Chang, E.; Allsopp, R. C.; Yu, J. *Science* **1995,** *269*, 1236.
81.Fu, D.; Collins, K. *Mol Cell* **2007,** *28*, 773.
82.Nakamura, T. M.; Cech, T. R. *Cell* **1998,** *92*, 587.
83.Hukezalie, K. R.; Wong, J. M. *FEBS J* **2013,** *280*, 3194.
84.Lai, C. K.; Mitchell, J. R.; Collins, K. *Mol Cell Biol* **2001,** *21*, 990.
85.Sealey, D. C.; Zheng, L.; Taboski, M. A.; Cruickshank, J.; Ikura, M.; Harrington, L. A. *Nucleic Acids Res* **2010,** *38*, 2019.
86.Armbruster, B. N.; Etheridge, K. T.; Broccoli, D.; Counter, C. M. *Mol Cell Biol* **2003,** *23*, 3237.
87.Lingner, J.; Hughes, T. R.; Shevchenko, A.; Mann, M.; Lundblad, V.; Cech, T. R. *Science* **1997,** *276*, 561.
88.Joyce, C. M.; Steitz, T. A. *Annu Rev Biochem* **1994,** *63*, 777.
89.Lue, N. F.; Lin, Y. C.; Mian, I. S. *Mol Cell Biol* **2003,** *23*, 8440.
90.Harrington, L.; Zhou, W.; McPhail, T.; Oulton, R.; Yeung, D. S.; Mar, V.; Bass, M. B.; Robinson, M. O. *Genes Dev* **1997,** *11*, 3109.
91.Gillis, A. J.; Schuller, A. P.; Skordalakes, E. *Nature* **2008,** *455*, 633.
92.Mitchell, M.; Gillis, A.; Futahashi, M.; Fujiwara, H.; Skordalakes, E. *Nat Struct Mol Biol* **2010,** *17*, 513.
93.Lue, N. F. *Bioessays* **2004,** *26*, 955.
94.Shay, J. W.; Bacchetti, S. *Eur J Cancer* **1997,** *33*, 787.
95.Mitchell, J. R.; Wood, E.; Collins, K. *Nature* **1999,** *402*, 551.
96.HAYFLICK, L.; MOORHEAD, P. S. *Exp Cell Res* **1961,** *25*, 585.
97.Bodnar, A. G.; Ouellette, M.; Frolkis, M.; Holt, S. E.; Chiu, C. P.; Morin, G. B.; Harley, C. B.; Shay, J. W.; Lichtsteiner, S.; Wright, W. E. *Science* **1998,** *279*, 349.
98.Yui, J.; Chiu, C. P.; Lansdorp, P. M. *Blood* **1998,** *91*, 3255.
99.Asai, A.; Oshima, Y.; Yamamoto, Y.; Uochi, T. A.; Kusaka, H.; Akinaga, S.; Yamashita, Y.; Pongracz, K.; Pruzan, R.; Wunder, E.; Piatyszek, M.; Li, S.; Chin, A. C.; Harley, C. B.; Gryaznov, S. *Cancer Res* **2003,** *63*, 3931.
100. Xu, Y.; He, K.; Goldkorn, A. *Clin Adv Hematol Oncol* **2011,** *9*, 442.
101. Joseph, I.; Tressler, R.; Bassett, E.; Harley, C.; Buseman, C. M.; Pattamatta, P.; Wright, W. E.; Shay, J. W.; Go, N. F. *Cancer Res* **2010,** *70*, 9494.
102. Li, S.; Rosenberg, J. E.; Donjacour, A. A.; Botchkina, I. L.; Hom, Y. K.; Cunha, G. R.; Blackburn, E. H. *Cancer Res* **2004,** *64*, 4833.
103. Bernhardt, S. L.; Gjertsen, M. K.; Trachsel, S.; Møller, M.; Eriksen, J. A.; Meo, M.; Buanes, T.; Gaudernack, G. *Br J Cancer* **2006,** *95*, 1474.
104. Harley, C. B. *Nat Rev Cancer* **2008,** *8*, 167.
105. Pitts, A. E.; Corey, D. R. *Proc Natl Acad Sci U S A* **1998,** *95*, 11549.

106. Zahler, A. M.; Williamson, J. R.; Cech, T. R.; Prescott, D. M. *Nature* **1991,** *350*, 718.
107. Neidle, S.; Parkinson, G. *Nat Rev Drug Discov* **2002,** *1*, 383.
108. Hemann, M. T.; Strong, M. A.; Hao, L. Y.; Greider, C. W. *Cell* **2001,** *107*, 67.
109. Neidle, S. *FEBS J* **2010,** *277*, 1118.
110. Ou, T. M.; Lu, Y. J.; Tan, J. H.; Huang, Z. S.; Wong, K. Y.; Gu, L. Q. *ChemMedChem* **2008,** *3*, 690.
111. Collie, G. W.; Parkinson, G. N. *Chem Soc Rev* **2011,** *40*, 5867.
112. Neidle, S.; Balasubramanian, S. *Quadruplex Nucleic Acid*; Cambridge: RSC publishing, 2006.
113. Monchaud, D.; Teulade-Fichou, M. P. *Org Biomol Chem* **2008,** *6*, 627.
114. Nielsen, M. C.; Ulven, T. *Curr Med Chem* **2010,** *17*, 3438.
115. Sun, D.; Thompson, B.; Cathers, B. E.; Salazar, M.; Kerwin, S. M.; Trent, J. O.; Jenkins, T. C.; Neidle, S.; Hurley, L. H. *J Med Chem* **1997,** *40*, 2113.
116. Perry, P. J.; Gowan, S. M.; Reszka, A. P.; Polucci, P.; Jenkins, T. C.; Kelland, L. R.; Neidle, S. *J Med Chem* **1998,** *41*, 3253.
117. Perry, P. J.; Reszka, A. P.; Wood, A. A.; Read, M. A.; Gowan, S. M.; Dosanjh, H. S.; Trent, J. O.; Jenkins, T. C.; Kelland, L. R.; Neidle, S. *J Med Chem* **1998,** *41*, 4873.
118. Perry, P. J.; Read, M. A.; Davies, R. T.; Gowan, S. M.; Reszka, A. P.; Wood, A. A.; Kelland, L. R.; Neidle, S. *J Med Chem* **1999,** *42*, 2679.
119. Read, M. A.; Wood, A. A.; Harrison, J. R.; Gowan, S. M.; Kelland, L. R.; Dosanjh, H. S.; Neidle, S. *J Med Chem* **1999,** *42*, 4538.
120. Read, M.; Harrison, R. J.; Romagnoli, B.; Tanious, F. A.; Gowan, S. H.; Reszka, A. P.; Wilson, W. D.; Kelland, L. R.; Neidle, S. *Proc Natl Acad Sci U S A* **2001,** *98*, 4844.
121. Harrison, R. J.; Cuesta, J.; Chessari, G.; Read, M. A.; Basra, S. K.; Reszka, A. P.; Morrell, J.; Gowan, S. M.; Incles, C. M.; Tanious, F. A.; Wilson, W. D.; Kelland, L. R.; Neidle, S. *J Med Chem* **2003,** *46*, 4463.
122. Moore, M. J.; Schultes, C. M.; Cuesta, J.; Cuenca, F.; Gunaratnam, M.; Tanious, F. A.; Wilson, W. D.; Neidle, S. *J Med Chem* **2006,** *49*, 582.
123. Reed, J.; Gunaratnam, M.; Beltran, M.; Reszka, A. P.; Vilar, R.; Neidle, S. *Anal Biochem* **2008,** *380*, 99.
124. Gowan, S. M.; Harrison, J. R.; Patterson, L.; Valenti, M.; Read, M. A.; Neidle, S.; Kelland, L. R. *Mol Pharmacol* **2002,** *61*, 1154.
125. Burger, A. M.; Dai, F.; Schultes, C. M.; Reszka, A. P.; Moore, M. J.; Double, J. A.; Neidle, S. *Cancer Res* **2005,** *65*, 1489.
126. Incles, C. M.; Schultes, C. M.; Kempski, H.; Koehler, H.; Kelland, L. R.; Neidle, S. *Mol Cancer Ther* **2004,** *3*, 1201.
127. Gunaratnam, M.; Greciano, O.; Martins, C.; Reszka, A. P.; Schultes, C. M.; Morjani, H.; Riou, J. F.; Neidle, S. *Biochem Pharmacol* **2007,** *74*, 679.
128. Martins, C.; Gunaratnam, M.; Stuart, J.; Makwana, V.; Greciano, O.; Reszka, A. P.; Kelland, L. R.; Neidle, S. *Bioorg Med Chem Lett* **2007,** *17*, 2293.
129. Perry, P. J.; Gowan, S. M.; Read, M. A.; Kelland, L. R.; Neidle, S. *Anticancer Drug Des* **1999,** *14*, 373.
130. Caprio, V.; Guyen, B.; Opoku-Boahen, Y.; Mann, J.; Gowan, S. M.; Kelland, L. M.; Read, M. A.; Neidle, S. *Bioorg Med Chem Lett* **2000,** *10*, 2063.
131. Guyen, B.; Schultes, C. M.; Hazel, P.; Mann, J.; Neidle, S. *Org Biomol Chem* **2004,** *2*, 981.
132. Zhou, J. M.; Zhu, X. F.; Lu, Y. J.; Deng, R.; Huang, Z. S.; Mei, Y. P.; Wang, Y.; Huang, W. L.; Liu, Z. C.; Gu, L. Q.; Zeng, Y. X. *Oncogene* **2006,** *25*, 503.
133. Zhou, J. L.; Lu, Y. J.; Ou, T. M.; Zhou, J. M.; Huang, Z. S.; Zhu, X. F.; Du, C. J.; Bu, X. Z.; Ma, L.; Gu, L. Q.; Li, Y. M.; Chan, A. S. *J Med Chem* **2005,** *48*, 7315.
134. Ou, T. M.; Lu, Y. J.; Zhang, C.; Huang, Z. S.; Wang, X. D.; Tan, J. H.; Chen, Y.; Ma, D. L.; Wong, K. Y.; Tang, J. C.; Chan, A. S.; Gu, L. Q. *J Med Chem* **2007,** *50*, 1465.

135. Mergny, J. L.; Lacroix, L.; Teulade-Fichou, M. P.; Hounsou, C.; Guittat, L.; Hoarau, M.; Arimondo, P. B.; Vigneron, J. P.; Lehn, J. M.; Riou, J. F.; Garestier, T.; Hélène, C. *Proc Natl Acad Sci U S A* **2001,** *98*, 3062.
136. Bertrand, H.; Bombard, S.; Monchaud, D.; Teulade-Fichou, M. P. *J Biol Inorg Chem* **2007,** *12*, 1003.
137. Rangan, A.; Fedoroff, O. Y.; Hurley, L. H. *J Biol Chem* **2001,** *276*, 4640.
138. Braña, M. F.; Castellano, J. M.; Roldán, C. M.; Santos, A.; Vázquez, D.; Jiménez, A. *Cancer Chemother Pharmacol* **1980,** *4*, 61.
139. Liu, Z. R.; Hecker, K. H.; Rill, R. L. *J Biomol Struct Dyn* **1996,** *14*, 331.
140. Tumiatti, V.; Milelli, A.; Minarini, A.; Micco, M.; Gasperi Campani, A.; Roncuzzi, L.; Baiocchi, D.; Marinello, J.; Capranico, G.; Zini, M.; Stefanelli, C.; Melchiorre, C. *J Med Chem* **2009,** *52*, 7873.
141. Milelli, A.; Tumiatti, V.; Micco, M.; Rosini, M.; Zuccari, G.; Raffaghello, L.; Bianchi, G.; Pistoia, V.; Fernando Díaz, J.; Pera, B.; Trigili, C.; Barasoain, I.; Musetti, C.; Toniolo, M.; Sissi, C.; Alcaro, S.; Moraca, F.; Zini, M.; Stefanelli, C.; Minarini, A. *Eur J Med Chem* **2012,** *57*, 417.
142. Cuenca, F.; Greciano, O.; Gunaratnam, M.; Haider, S.; Munnur, D.; Nanjunda, R.; Wilson, W. D.; Neidle, S. *Bioorg Med Chem Lett* **2008,** *18*, 1668.
143. Parkinson, G. N.; Lee, M. P.; Neidle, S. *Nature* **2002,** *417*, 876.
144. Hampel, S. M.; Sidibe, A.; Gunaratnam, M.; Riou, J. F.; Neidle, S. *Bioorg Med Chem Lett* **2010,** *20*, 6459.
145. Gunaratnam, M.; de la Fuente, M.; Hampel, S. M.; Todd, A. K.; Reszka, A. P.; Schätzlein, A.; Neidle, S. *Bioorg Med Chem* **2011,** *19*, 7151.
146. Mpima, S.; Ohnmacht, S. A.; Barletta, M.; Husby, J.; Pett, L. C.; Gunaratnam, M.; Hilton, S. T.; Neidle, S. *Bioorg Med Chem* **2013,** *21*, 6162.
147. Shin-ya, K.; Wierzba, K.; Matsuo, K.; Ohtani, T.; Yamada, Y.; Furihata, K.; Hayakawa, Y.; Seto, H. *J Am Chem Soc* **2001,** *123*, 1262.
148. Kim, M. Y.; Vankayalapati, H.; Shin-Ya, K.; Wierzba, K.; Hurley, L. H. *J Am Chem Soc* **2002,** *124*, 2098.
149. Pettersen, E. F.; Goddard, T. D.; Huang, C. C.; Couch, G. S.; Greenblatt, D. M.; Meng, E. C.; Ferrin, T. E. *J Comput Chem* **2004,** *25*, 1605.
150. Minhas, G. S.; Pilch, D. S.; Kerrigan, J. E.; LaVoie, E. J.; Rice, J. E. *Bioorg Med Chem Lett* **2006,** *16*, 3891.
151. Barbieri, C. M.; Srinivasan, A. R.; Rzuczek, S. G.; Rice, J. E.; LaVoie, E. J.; Pilch, D. S. *Nucleic Acids Res* **2007,** *35*, 3272.
152. Pilch, D. S.; Barbieri, C. M.; Rzuczek, S. G.; Lavoie, E. J.; Rice, J. E. *Biochimie* **2008,** *90*, 1233.
153. De Cian, A.; Guittat, L.; Shin-ya, K.; Riou, J. F.; Mergny, J. L. *Nucleic Acids Symp Ser (Oxf)* **2005**, 235.
154. Gunaratnam, M.; Swank, S.; Haider, S. M.; Galesa, K.; Reszka, A. P.; Beltran, M.; Cuenca, F.; Fletcher, J. A.; Neidle, S. *J Med Chem* **2009,** *52*, 3774.
155. Palumbo, S. L.; Ebbinghaus, S. W.; Hurley, L. H. *J Am Chem Soc* **2009,** *131*, 10878.
156. Wei, C.; Jia, G.; Yuan, J.; Feng, Z.; Li, C. *Biochemistry* **2006,** *45*, 6681.
157. Phan, A. T.; Kuryavyi, V.; Gaw, H. Y.; Patel, D. J. *Nat Chem Biol* **2005,** *1*, 167.
158. Parkinson, G. N.; Ghosh, R.; Neidle, S. *Biochemistry* **2007,** *46*, 2390.
159. Dixon, I. M.; Lopez, F.; Tejera, A. M.; Estève, J. P.; Blasco, M. A.; Pratviel, G.; Meunier, B. *J Am Chem Soc* **2007,** *129*, 1502.
160. Wang, P.; Ren, L.; He, H.; Liang, F.; Zhou, X.; Tan, Z. *Chembiochem* **2006,** *7*, 1155.
161. Ren, L.; Zhang, A.; Huang, J.; Wang, P.; Weng, X.; Zhang, L.; Liang, F.; Tan, Z.; Zhou, X. *Chembiochem* **2007,** *8*, 775.
162. Alzeer, J.; Vummidi, B. R.; Roth, P. J.; Luedtke, N. W. *Angew Chem Int Ed Engl* **2009,** *48*, 9362.
163. Li, Y.; Geyer, C. R.; Sen, D. *Biochemistry* **1996,** *35*, 6911.

164. Alberti, P.; Ren, J.; Teulade-Fichou, M. P.; Guittat, L.; Riou, J. F.; Chaires, J.; Hélène, C.; Vigneron, J. P.; Lehn, J. M.; Mergny, J. L. *J Biomol Struct Dyn* **2001,** *19*, 505.
165. Hounsou, C.; Guittat, L.; Monchaud, D.; Jourdan, M.; Saettel, N.; Mergny, J. L.; Teulade-Fichou, M. P. *ChemMedChem* **2007,** *2*, 655.
166. McGhee, J. D.; von Hippel, P. H. *J Mol Biol* **1974,** *86*, 469.
167. Gabelica, V.; Baker, E. S.; Teulade-Fichou, M. P.; De Pauw, E.; Bowers, M. T. *J Am Chem Soc* **2007,** *129*, 895.
168. Monchaud, D.; Granzhan, A.; Saettel, N.; Guédin, A.; Mergny, J. L.; Teulade-Fichou, M. P. *J Nucleic Acids* **2010,** *2010*.
169. Bahr, M.; Gabelica, V.; Granzhan, A.; Teulade-Fichou, M. P.; Weinhold, E. *Nucleic Acids Res* **2008,** *36*, 5000.
170. Granzhan, A.; Monchaud, D.; Saettel, N.; Guédin, A.; Mergny, J. L.; Teulade-Fichou, M. P. *J Nucleic Acids* **2010,** *2010*.
171. Kaiser, M.; De Cian, A.; Sainlos, M.; Renner, C.; Mergny, J. L.; Teulade-Fichou, M. P. *Org Biomol Chem* **2006,** *4*, 1049.
172. Albert, B. *Essential Cell Biology*; New York: Garland Science, 2009.
173. Felsenfeld, G.; Groudine, M. *Nature* **2003,** *421*, 448.
174. Bird, A. *Nature* **2007,** *447*, 396.
175. Reilly, C. M.; Regna, N.; Mishra, N. *Mol Med* **2011,** *17*, 417.
176. Feinberg, A. P.; Ohlsson, R.; Henikoff, S. *Nat Rev Genet* **2006,** *7*, 21.
177. Bjornsson, H. T.; Fallin, M. D.; Feinberg, A. P. *Trends Genet* **2004,** *20*, 350.
178. Jones, P. A.; Baylin, S. B. *Cell* **2007,** *128*, 683.
179. Johnstone, R. W. *Nat Rev Drug Discov* **2002,** *1*, 287.
180. Esteller, M. *Oncogene* **2002,** *21*, 5427.
181. Zhang, Y.; Fang, H.; Jiao, J.; Xu, W. *Curr Med Chem* **2008,** *15*, 2840.
182. Finnin, M. S.; Donigian, J. R.; Cohen, A.; Richon, V. M.; Rifkind, R. A.; Marks, P. A.; Breslow, R.; Pavletich, N. P. *Nature* **1999,** *401*, 188.
183. Dowling, D. P.; Gantt, S. L.; Gattis, S. G.; Fierke, C. A.; Christianson, D. W. *Biochemistry* **2008,** *47*, 13554.
184. Vannini, A.; Volpari, C.; Gallinari, P.; Jones, P.; Mattu, M.; Carfí, A.; De Francesco, R.; Steinkühler, C.; Di Marco, S. *EMBO Rep* **2007,** *8*, 879.
185. Nielsen, T. K.; Hildmann, C.; Dickmanns, A.; Schwienhorst, A.; Ficner, R. *J Mol Biol* **2005,** *354*, 107.
186. Lombardi, P. M.; Cole, K. E.; Dowling, D. P.; Christianson, D. W. *Curr Opin Struct Biol* **2011,** *21*, 735.
187. Passier, R.; Zeng, H.; Frey, N.; Naya, F. J.; Nicol, R. L.; McKinsey, T. A.; Overbeek, P.; Richardson, J. A.; Grant, S. R.; Olson, E. N. *J Clin Invest* **2000,** *105*, 1395.
188. Lu, J.; McKinsey, T. A.; Zhang, C. L.; Olson, E. N. *Mol Cell* **2000,** *6*, 233.
189. Zhang, C. L.; McKinsey, T. A.; Chang, S.; Antos, C. L.; Hill, J. A.; Olson, E. N. *Cell* **2002,** *110*, 479.
190. Chang, S.; McKinsey, T. A.; Zhang, C. L.; Richardson, J. A.; Hill, J. A.; Olson, E. N. *Mol Cell Biol* **2004,** *24*, 8467.
191. Vega, R. B.; Matsuda, K.; Oh, J.; Barbosa, A. C.; Yang, X.; Meadows, E.; McAnally, J.; Pomajzl, C.; Shelton, J. M.; Richardson, J. A.; Karsenty, G.; Olson, E. N. *Cell* **2004,** *119*, 555.
192. Fischle, W.; Dequiedt, F.; Hendzel, M. J.; Guenther, M. G.; Lazar, M. A.; Voelter, W.; Verdin, E. *Mol Cell* **2002,** *9*, 45.
193. Zhang, C. L.; McKinsey, T. A.; Olson, E. N. *Mol Cell Biol* **2002,** *22*, 7302.
194. Hubbert, C.; Guardiola, A.; Shao, R.; Kawaguchi, Y.; Ito, A.; Nixon, A.; Yoshida, M.; Wang, X. F.; Yao, T. P. *Nature* **2002,** *417*, 455.
195. Gao, L.; Cueto, M. A.; Asselbergs, F.; Atadja, P. *J Biol Chem* **2002,** *277*, 25748.
196. Ropero, S.; Esteller, M. *Mol Oncol* **2007,** *1*, 19.
197. Jones, P. L.; Veenstra, G. J.; Wade, P. A.; Vermaak, D.; Kass, S. U.; Landsberger, N.; Strouboulis, J.; Wolffe, A. P. *Nat Genet* **1998,** *19*, 187.

198. Espada, J.; Ballestar, E.; Fraga, M. F.; Villar-Garea, A.; Juarranz, A.; Stockert, J. C.; Robertson, K. D.; Fuks, F.; Esteller, M. *J Biol Chem* **2004,** *279*, 37175.
199. Bai, S.; Ghoshal, K.; Datta, J.; Majumder, S.; Yoon, S. O.; Jacob, S. T. *Mol Cell Biol* **2005,** *25*, 751.
200. Kawai, H.; Li, H.; Avraham, S.; Jiang, S.; Avraham, H. K. *Int J Cancer* **2003,** *107*, 353.
201. Gregoretti, I. V.; Lee, Y. M.; Goodson, H. V. *J Mol Biol* **2004,** *338*, 17.
202. Yang, X. J.; Seto, E. *Oncogene* **2007,** *26*, 5310.
203. Glozak, M. A.; Sengupta, N.; Zhang, X.; Seto, E. *Gene* **2005,** *363*, 15.
204. Gui, C. Y.; Ngo, L.; Xu, W. S.; Richon, V. M.; Marks, P. A. *Proc Natl Acad Sci U S A* **2004,** *101*, 1241.
205. Juan, L. J.; Shia, W. J.; Chen, M. H.; Yang, W. M.; Seto, E.; Lin, Y. S.; Wu, C. W. *J Biol Chem* **2000,** *275*, 20436.
206. Francisco, R.; Pérez-Perarnau, A.; Cortés, C.; Gil, J.; Tauler, A.; Ambrosio, S. *Cancer Lett* **2012,** *318*, 42.
207. Archer, S. Y.; Meng, S.; Shei, A.; Hodin, R. A. *Proc Natl Acad Sci U S A* **1998,** *95*, 6791.
208. Richon, V. M.; Sandhoff, T. W.; Rifkind, R. A.; Marks, P. A. *Proc Natl Acad Sci U S A* **2000,** *97*, 10014.
209. Hitomi, T.; Matsuzaki, Y.; Yokota, T.; Takaoka, Y.; Sakai, T. *FEBS Lett* **2003,** *554*, 347.
210. Nakata, S.; Yoshida, T.; Horinaka, M.; Shiraishi, T.; Wakada, M.; Sakai, T. *Oncogene* **2004,** *23*, 6261.
211. Ashkenazi, A. *Nat Rev Cancer* **2002,** *2*, 420.
212. Zhang, X. D.; Gillespie, S. K.; Borrow, J. M.; Hersey, P. *Mol Cancer Ther* **2004,** *3*, 425.
213. Xu, W. S.; Perez, G.; Ngo, L.; Gui, C. Y.; Marks, P. A. *Cancer Res* **2005,** *65*, 7832.
214. Shao, Y.; Gao, Z.; Marks, P. A.; Jiang, X. *Proc Natl Acad Sci U S A* **2004,** *101*, 18030.
215. Ruefli, A. A.; Ausserlechner, M. J.; Bernhard, D.; Sutton, V. R.; Tainton, K. M.; Kofler, R.; Smyth, M. J.; Johnstone, R. W. *Proc Natl Acad Sci U S A* **2001,** *98*, 10833.
216. Bali, P.; Pranpat, M.; Bradner, J.; Balasis, M.; Fiskus, W.; Guo, F.; Rocha, K.; Kumaraswamy, S.; Boyapalle, S.; Atadja, P.; Seto, E.; Bhalla, K. *J Biol Chem* **2005,** *280*, 26729.
217. Liang, D.; Kong, X.; Sang, N. *Cell Cycle* **2006,** *5*, 2430.
218. Deroanne, C. F.; Bonjean, K.; Servotte, S.; Devy, L.; Colige, A.; Clausse, N.; Blacher, S.; Verdin, E.; Foidart, J. M.; Nusgens, B. V.; Castronovo, V. *Oncogene* **2002,** *21*, 427.
219. Bieliauskas, A. V.; Pflum, M. K. *Chem Soc Rev* **2008,** *37*, 1402.
220. Bertrand, P. *Eur J Med Chem* **2010,** *45*, 2095.
221. Yoshida, M.; Hoshikawa, Y.; Koseki, K.; Mori, K.; Beppu, T. *J Antibiot (Tokyo)* **1990,** *43*, 1101.
222. Richon, V. M.; Emiliani, S.; Verdin, E.; Webb, Y.; Breslow, R.; Rifkind, R. A.; Marks, P. A. *Proc Natl Acad Sci U S A* **1998,** *95*, 3003.
223. Miller, T. A.; Witter, D. J.; Belvedere, S. *J Med Chem* **2003,** *46*, 5097.
224. Van Ommeslaeghe, K.; Elaut, G.; Brecx, V.; Papeleu, P.; Iterbeke, K.; Geerlings, P.; Tourwé, D.; Rogiers, V. *Bioorg Med Chem Lett* **2003,** *13*, 1861.
225. Kim, Y. B.; Lee, K. H.; Sugita, K.; Yoshida, M.; Horinouchi, S. *Oncogene* **1999,** *18*, 2461.
226. Su, G. H.; Sohn, T. A.; Ryu, B.; Kern, S. E. *Cancer Res* **2000,** *60*, 3137.
227. Jung, M.; Brosch, G.; Kölle, D.; Scherf, H.; Gerhäuser, C.; Loidl, P. *J Med Chem* **1999,** *42*, 4669.
228. Dai, Y.; Guo, Y.; Curtin, M. L.; Li, J.; Pease, L. J.; Guo, J.; Marcotte, P. A.; Glaser, K. B.; Davidsen, S. K.; Michaelides, M. R. *Bioorg Med Chem Lett* **2003,** *13*, 3817.
229. Lavoie, R.; Bouchain, G.; Frechette, S.; Woo, S. H.; Abou-Khalil, E.; Leit, S.; Fournel, M.; Yan, P. T.; Trachy-Bourget, M. C.; Beaulieu, C.; Li, Z.; Besterman, J.; Delorme, D. *Bioorg Med Chem Lett* **2001,** *11*, 2847.

230. Bouchain, G.; Leit, S.; Frechette, S.; Khalil, E. A.; Lavoie, R.; Moradei, O.; Woo, S. H.; Fournel, M.; Yan, P. T.; Kalita, A.; Trachy-Bourget, M. C.; Beaulieu, C.; Li, Z.; Robert, M. F.; MacLeod, A. R.; Besterman, J. M.; Delorme, D. *J Med Chem* **2003,** *46*, 820.
231. Komatsu, Y.; Tomizaki, K. Y.; Tsukamoto, M.; Kato, T.; Nishino, N.; Sato, S.; Yamori, T.; Tsuruo, T.; Furumai, R.; Yoshida, M.; Horinouchi, S.; Hayashi, H. *Cancer Res* **2001,** *61*, 4459.
232. Kijima, M.; Yoshida, M.; Sugita, K.; Horinouchi, S.; Beppu, T. *J Biol Chem* **1993,** *268*, 22429.
233. Mwakwari, S. C.; Patil, V.; Guerrant, W.; Oyelere, A. K. *Curr Top Med Chem* **2010,** *10*, 1423.
234. Closse, A.; Huguenin, R. *Helv Chim Acta* **1974,** *57*, 533.
235. Furumai, R.; Komatsu, Y.; Nishino, N.; Khochbin, S.; Yoshida, M.; Horinouchi, S. *Proc Natl Acad Sci U S A* **2001,** *98*, 87.
236. Darkin-Rattray, S. J.; Gurnett, A. M.; Myers, R. W.; Dulski, P. M.; Crumley, T. M.; Allocco, J. J.; Cannova, C.; Meinke, P. T.; Colletti, S. L.; Bednarek, M. A.; Singh, S. B.; Goetz, M. A.; Dombrowski, A. W.; Polishook, J. D.; Schmatz, D. M. *Proc Natl Acad Sci U S A* **1996,** *93*, 13143.
237. Colletti, S. L.; Myers, R. W.; Darkin-Rattray, S. J.; Gurnett, A. M.; Dulski, P. M.; Galuska, S.; Allocco, J. J.; Ayer, M. B.; Li, C.; Lim, J.; Crumley, T. M.; Cannova, C.; Schmatz, D. M.; Wyvratt, M. J.; Fisher, M. H.; Meinke, P. T. *Bioorg Med Chem Lett* **2001,** *11*, 107.
238. Sandor, V.; Bakke, S.; Robey, R. W.; Kang, M. H.; Blagosklonny, M. V.; Bender, J.; Brooks, R.; Piekarz, R. L.; Tucker, E.; Figg, W. D.; Chan, K. K.; Goldspiel, B.; Fojo, A. T.; Balcerzak, S. P.; Bates, S. E. *Clin Cancer Res* **2002,** *8*, 718.
239. Shigematsu, N.; Ueda, H.; Takase, S.; Tanaka, H.; Yamamoto, K.; Tada, T. *J Antibiot (Tokyo)* **1994,** *47*, 311.
240. Göttlicher, M.; Minucci, S.; Zhu, P.; Krämer, O. H.; Schimpf, A.; Giavara, S.; Sleeman, J. P.; Lo Coco, F.; Nervi, C.; Pelicci, P. G.; Heinzel, T. *EMBO J* **2001,** *20*, 6969.
241. Pearn, J. *Lancet* **1980,** *1*, 919.
242. Warrell, R. P.; He, L. Z.; Richon, V.; Calleja, E.; Pandolfi, P. P. *J Natl Cancer Inst* **1998,** *90*, 1621.
243. Nudelman, A.; Rephaeli, A. *J Med Chem* **2000,** *43*, 2962.
244. Suzuki, T.; Ando, T.; Tsuchiya, K.; Fukazawa, N.; Saito, A.; Mariko, Y.; Yamashita, T.; Nakanishi, O. *J Med Chem* **1999,** *42*, 3001.
245. el-Beltagi, H. M.; Martens, A. C.; Lelieveld, P.; Haroun, E. A.; Hagenbeek, A. *Cancer Res* **1993,** *53*, 3008.
246. Saito, A.; Yamashita, T.; Mariko, Y.; Nosaka, Y.; Tsuchiya, K.; Ando, T.; Suzuki, T.; Tsuruo, T.; Nakanishi, O. *Proc Natl Acad Sci U S A* **1999,** *96*, 4592.
247. Frey, R. R.; Wada, C. K.; Garland, R. B.; Curtin, M. L.; Michaelides, M. R.; Li, J.; Pease, L. J.; Glaser, K. B.; Marcotte, P. A.; Bouska, J. J.; Murphy, S. S.; Davidsen, S. K. *Bioorg Med Chem Lett* **2002,** *12*, 3443.
248. Christianson, D. W.; Lipscomb, W. N. *J Am Chem Soc* **1986,** *108*, 545.
249. Lee, M. J.; Kim, Y. S.; Kummar, S.; Giaccone, G.; Trepel, J. B. *Curr Opin Oncol* **2008,** *20*, 639.
250. Marchion, D. C.; Bicaku, E.; Daud, A. I.; Richon, V.; Sullivan, D. M.; Munster, P. N. *J Cell Biochem* **2004,** *92*, 223.
251. Friedmann, I.; Atmaca, A.; Chow, K. U.; Jäger, E.; Weidmann, E. *J Chemother* **2006,** *18*, 415.
252. Nimmanapalli, R.; Fuino, L.; Stobaugh, C.; Richon, V.; Bhalla, K. *Blood* **2003,** *101*, 3236.
253. Stiborová, M.; Eckschlager, T.; Poljaková, J.; Hraběta, J.; Adam, V.; Kizek, R.; Frei, E. *Curr Med Chem* **2012,** *19*, 4218.
254. Kurz, E. U.; Wilson, S. E.; Leader, K. B.; Sampey, B. P.; Allan, W. P.; Yalowich, J. C.; Kroll, D. J. *Mol Cancer Ther* **2001,** *1*, 121.
255. Valentini, A.; Gravina, P.; Federici, G.; Bernardini, S. *Cancer Biol Ther* **2007,** *6*, 185.

256. Hajji, N.; Wallenborg, K.; Vlachos, P.; Nyman, U.; Hermanson, O.; Joseph, B. *Oncogene* **2008,** *27*, 3134.
257. Zhang, C. Z.; Zhang, H. T.; Chen, G. G.; Lai, P. B. *Apoptosis* **2011,** *16*, 683.
258. Khan, S. B.; Maududi, T.; Barton, K.; Ayers, J.; Alkan, S. *Br J Haematol* **2004,** *125*, 156.
259. Kitazoe, K.; Abe, M.; Hiasa, M.; Oda, A.; Amou, H.; Harada, T.; Nakano, A.; Takeuchi, K.; Hashimoto, T.; Ozaki, S.; Matsumoto, T. *Int J Hematol* **2009,** *89*, 45.
260. Shen, J.; Huang, C.; Jiang, L.; Gao, F.; Wang, Z.; Zhang, Y.; Bai, J.; Zhou, H.; Chen, Q. *Biochem Pharmacol* **2007,** *73*, 1901.
261. Guerrant, W.; Patil, V.; Canzoneri, J. C.; Oyelere, A. K. *J Med Chem* **2012,** *55*, 1465.
262. Bettuzzi, S.; Davalli, P.; Astancolle, S.; Pinna, C.; Roncaglia, R.; Boraldi, F.; Tiozzo, R.; Sharrard, M.; Corti, A. *FEBS Lett* **1999,** *446*, 18.
263. Wallace, H. M.; Fraser, A. V.; Hughes, A. *Biochem J* **2003,** *376*, 1.
264. Belting, M.; Mani, K.; Jönsson, M.; Cheng, F.; Sandgren, S.; Jonsson, S.; Ding, K.; Delcros, J. G.; Fransson, L. A. *J Biol Chem* **2003,** *278*, 47181.
265. Soulet, D.; Gagnon, B.; Rivest, S.; Audette, M.; Poulin, R. *J Biol Chem* **2004,** *279*, 49355.
266. Volkow, N.; Goldman, S. S.; Flamm, E. S.; Cravioto, H.; Wolf, A. P.; Brodie, J. D. *Science* **1983,** *221*, 673.
267. Dallavalle, S.; Giannini, G.; Alloatti, D.; Casati, A.; Marastoni, E.; Musso, L.; Merlini, L.; Morini, G.; Penco, S.; Pisano, C.; Tinelli, S.; De Cesare, M.; Beretta, G. L.; Zunino, F. *J Med Chem* **2006,** *49*, 5177.
268. Wallace, H. M.; Keir, H. M. *Biochim Biophys Acta* **1981,** *676*, 25.
269. Holley, J. L.; Mather, A.; Wheelhouse, R. T.; Cullis, P. M.; Hartley, J. A.; Bingham, J. P.; Cohen, G. M. *Cancer Res* **1992,** *52*, 4190.
270. Phanstiel, O.; Price, H. L.; Wang, L.; Juusola, J.; Kline, M.; Shah, S. M. *J Org Chem* **2000,** *65*, 7710.
271. Wang, C.; Delcros, J. G.; Biggerstaff, J.; Phanstiel, O. *J Med Chem* **2003,** *46*, 2672.
272. Barret, J. M.; Kruczynski, A.; Vispé, S.; Annereau, J. P.; Brel, V.; Guminski, Y.; Delcros, J. G.; Lansiaux, A.; Guilbaud, N.; Imbert, T.; Bailly, C. *Cancer Res* **2008,** *68*, 9845.
273. Melchiorre, C.; Bolognesi, M. L.; Minarini, A.; Rosini, M.; Tumiatti, V. *J Med Chem* **2010,** *53*, 5906.
274. Wellendorph, P.; Jaroszewski, J. W.; Hansen, S. H.; Franzyk, H. *Eur J Med Chem* **2003,** *38*, 117.
275. Morrell, A.; Placzek, M. S.; Steffen, J. D.; Antony, S.; Agama, K.; Pommier, Y.; Cushman, M. *J Med Chem* **2007,** *50*, 2040.
276. Sasikumar, M.; Suseela, Y. V.; Govindaraju, T. *Asian Journal of Organic Chemistry* **2013,** *2*, 779.